The University Of Sheffield.

Phosphate-modified calcium aluminate cements

by

Mehul A. Chavda

A thesis submitted in partial fulfilment of the requirements for the degree of Doctor of Philosophy

University of Sheffield
Faculty of Engineering
Department of Materials Science and Engineering

Thesis Supervisors:

Dr. Hajime Kinoshita and Professor John L. Provis

2015

Abstract

The effect of phosphate modification on CAC hydration is poorly understood, and the investigation in this thesis focuses on the sodium phosphate modification of a commercially available calcium aluminate cement, examining the following : (i) the effect of modification upon the fresh state properties, (ii) long-term phase evolution, (iii) binding phase characterisation, and (iv) trials of aluminium encapsulation.

Formulations of CAC modified by sodium polyphosphate, sodium monophosphate and mixtures of these, in varying proportions, are investigated. ATR-FTIR and solution NMR are used to examine the chain length of phosphate ions in solution prior to mixing. Immediately after mixing the fresh state properties are investigated using isothermal calorimetry, to assess the effect of average phosphate chain length on the heat of hydration and thermal behaviour of pastes during the initial curing period.

The phase assemblage over the long term is examined by XRD and TGA up to a period of 180 days, elucidating trends in hydration behaviour with phosphate modification. This focuses upon assessment of the degree of conversion, identifying phosphate modifications which prolong the presence of metastable CAC hydrates for up to 180 days and also formulations that prevent any conventional phases forming at all and hence avoid conversion. Promising formulations with no conventional CAC hydrate formations are studied up to a period of 1050 days to confirm the longer-term stability of the alternate hydrates being formed. Characterisation of these samples after hydrothermal treatment showed the formation of hydroxyapatite, boehmite and a zeolite type phase.

The disordered binding phase of this system is further investigated using solid-state nuclear magnetic resonance (NMR) to probe the environments of the ^{31}P and ^{27}Al nuclei. Results from advanced REAPDOR NMR experiments, used to assess the interactions between these nuclei, are reported and confirm the presence of a disordered C-A-P-H type binding phase.

Results from trials of aluminium encapsulation are also reported, where corrosion is assessed by hydrogen evolution evaluation using mass spectroscopy and water displacement, differential scanning calorimetry, scanning electron microscopy, and mass loss measurements. Promising formulations with phosphate modification outperformed the neat CAC encapsulants in all experiments performed, considering both powder and plate aluminium. The series of formulations with polyphosphate to cement mass ratio of 0.4 are recommended for further investigation as waste encapsulants.

It was determined from the results of this study that altering the average phosphate ion chain length in solution prior to mixing can be used as a tool to tune the fresh state properties, including the heat of hydration and setting time. The kinetics of long term hydration and phase assemblage development maybe affected with the addition of sodium monophosphate, and radically altered away from conventional CAC hydration and instead the formation of an x-ray amorphous binding phase. This binding phase, optimal formulations, is shown to be stable in to a minimum of 1050 days with elevated compressive strength. NMR spectroscopy is used to positively verify the binding phase to be a calcium aluminium phosphate hydrate phase. Optimised phosphate modified CAC formulations are shown to outperform other conventionally used cementitious encapsulants, including OPC, OPC/BFS and neat CAC.

Declaration

Acknowledgements

The completion of this Ph.D. would not have been possible without the direction, support and patience of many people. In no particular order:

I would like to thank Dr. Hajime Kinoshita for initially suggesting this project, his support during the difficult initial months and his invaluable commitment to my progress as a researcher.

Heartfelt thanks go to Professor John L. Provis, who has motivated and instilled confidence throughout his supervision. The much-needed support given, especially during the final two years, has been far beyond what I could have imagined.

My thanks go to Dr. Susan Bernal, for her assistance in conducting experiments, data analysis, and most of all, warmth and emotional support during difficult times.

Thanks to my friends for their support and useful distractions throughout my residence in Sheffield, a place I consider a second home. My partner Voula, Hilmi, Silvia and also Mohsen, you have all made my experience in Sheffield memorable and it is not the same without you.

Many thanks to all members of the ISL group members, especially Oday, Rupert, Seddon, Kris, Sam and Laura.

Many thanks go to the technical and administrative staff in the Department of Materials Science & Engineering, especially Karen Burton, Bev Lane, Ben Palmer and Anne Newbould.

Most of all, thanks and love to my parents and brothers for unceasing moral and financial support, putting up with my absence during the later years, and never saying ‘no’.

Each of you has shaped my past, present and thus my future, for this I am eternally grateful.

Publications from the thesis

Journal publications

Chavda, M.A., Kinoshita, H. & Provis, J.L., **2014**. Phosphate modification of calcium aluminate cement to enhance stability for immobilisation of metallic wastes. *Advances in Applied Ceramics*, 113(8), pp.453–459.

Chavda, M.A. et al., **2015**. Identification of the hydrate gel phases present in phosphate-modified calcium aluminate binders. *Cement and Concrete Research*, 70, pp.21–28.

Conference proceedings

Chavda, M.A., Kinoshita, H. & Provis, J.L., 2012. Modification of a calcium aluminate cement system to prevent conversion to cubic hydrates and minimise corrosion of encapsulated aluminium metal. In 32st Cement and Concrete Science Conference. Belfast, pp. 207-211.

Chavda, M.A. et al., 2013. Hydration phases forming in sodium polyphosphate-modified calcium aluminate cement. In 33nd Cement and Concrete Science. Portsmouth..

Chavda, M.A. et al., 2013. An NMR study of the hydration phases of sodium polyphosphate-modified calcium aluminate cement. In 1st International Conference on the Chemistry of Construction Materials. Berlin.

Contents

List of figures

List of tables

Nomenclature

Conventional cement chemistry notation is used in this thesis to refer to oxides:

C – CaO A – Al_2O_3 S – SiO_2 H – H_2O F – Fe_2O_3 T – TiO_2

Materials

CAC	Calcium aluminate cement	HAC	High alumina cement
CPC	Calcium phosphate cement	PC	Portland cement
SCM	Supplementary cementitious material	MDF	Macro defect free
PFA	Pulverised fuel ash		
BFS	Blast furnace slag		

Experimental technique terms

XRD	X-ray diffractometry	ATR	Attenuated total reflectance
TGA	Thermogravimetric analysis	DTG	Derivative thermogravimetry
DSC	Differential scanning calorimetry		
SEM	Scanning electron microscopy	FTIR	Fourier transform infrared
NMR	Nuclear magnetic resonance	MAS	Magic angle spinning
CP	Cross polarisation	MS	Mass spectroscopy

Formulation notation

Sample names are indicative of their formulation and can be described by the general form “PpMm”, where P and M are the polyphosphate and monophosphate to cement clinker ratios, defined on a mass basis, respectively.

w/c	water to cement mass ratio

Other terms

C-A- H	Calcium aluminate hydrate	HA	Hydroxyapatite
PDF	Powder diffraction file	ILW	Intermediate level waste
C-A-P-H	Calcium aluminophosphate hydrate		

1 Introduction

Calcium aluminate cements (CACs), first developed approximately 200 years ago, present an alternative to the widely used Portland cement and present a number of advantageous properties for applications within severe conditions for which Portland cements are unsatisfactory. These applications are wide ranging including high temperature refractories, specialist structural materials, and components in biocomposite materials, and often CACs may be used in place of non-cementitious materials for many of these applications. The hydration chemistry of CACs is considerably different from that of Portland cements, precipitating a variety of calcium aluminate hydrates that are either thermodynamically metastable or stable. Over time there is a conversion process whereby the water-rich metastable hydrates dissolve to re-precipitate as the denser, less water-rich, thermodynamically stable hydrates. This conversion process can result in strength regression, dimensional instability and the liberation of free water; such consequences are unattractive for industrial adoption of this material for a number of applications. Notable well-publicised examples of failures of CAC structural materials in public buildings have driven research to examine the conversion of these materials, mitigating the consequences and also preventing it.

Phosphate modification of calcium aluminate cements, originally developed for geothermal well applications due to its high carbonation resistance and chemical stability in severe conditions, has been reported to radically alter the conventional CAC hydration chemistry and potentially avoid conversion. This subset of materials have been identified as suitable materials for a wide range of applications due to their interesting rheological properties in the fresh state, high bioresorptivity, high resistance to carbonation and high flexural strength in addition to maintaining the rapid setting and early strength development properties of neat CAC. More recently they have also been reported to be promising materials for toxic and radioactive waste encapsulation, the promise around the latter due to the lower pore solution pH of CAC matrices in comparison with that of the widely adopted Portland composite cement encapsulants. High pH environments found in materials based on Portland cement can

cause aggressive corrosion of aluminium metal, found in some waste streams earmarked for packaging by cement encapsulation, resulting in considerable volume changes and explosion risks due to the accumulation of hydrogen gas as a corrosion product. Maintaining a lower pH environment and the prevention of conversion liberating free water suggest that this system may be favourable for the encapsulation of aluminium metal containing wastes among other applications.

Whereas the Portland cement system benefits from a wealth of literature covering its fundamental hydration chemistry and applications focused research, literature for the CAC system is dwarfed in comparison, and this is the case even more so for phosphate-modified CAC. Hence if these materials are to be considered for adoption by industry a better understanding of the system and a greater body of available literature is required.

The investigation reported in this thesis examines the sodium phosphate modification of a commercially available calcium aluminate cement, the effect of modification upon the fresh state properties, long-term phase evolution, binding phase characterisation and initial trials of aluminium encapsulation.

Chapter 2 presents a literature review, which focuses upon the chemistry of the CAC clinker and hydration process, examines fresh state and long-term properties and identifies key applications. The conversion process itself, and methods to either mitigate the detrimental consequences or avoid conversion by modification of the hydration processes through chemical additions, are described. The development of phosphate-modified CACs is discussed and the body of literature available is discussed, with a focus upon the incoherence present surrounding the characterisation of the main binding phase. The significance of the system as a potential waste encapsulant is considered with reference to the requirements for packaging an intermediate level waste stream containing aluminium.

Chapter 3 outlines the sample synthesis protocols established to prepare, cast and cure slurries. The principles behind the analytical techniques used to characterise the samples, including specimen preconditioning and sample preparation steps, are explained in detail and where relevant parameters used are given. These techniques include isothermal calorimetry, X-ray diffractometry (XRD), thermogravimetric

analysis (TGA), Fourier transform infrared (FTIR) spectroscopy, nuclear magnetic resonance (NMR) spectroscopy, mass spectroscopy, and differential scanning calorimetry (DSC).

Results are presented in four chapters, with each chapter having its own self-contained discussion and conclusions sections. Chapter 4 is split into two parts, (i) and examination of the clinker and other precursor materials with an assessment of the speciation of the phosphate ions in solution prior to slurry preparation, and (ii) an examination of the fresh state properties of CAC formulations with either sodium polyphosphate or sodium monophosphate or both in varying ratios, by the Vicat method and by isothermal calorimetry. Formulations are described throughout this thesis using a sample name, which is a composite of the mass ratios of the polyphosphate and monophosphate to cement of the formulation, *P* and *M* respectively in the general sample name *P*p*M*m.

Chapter 5 looks at the long-term hydration of samples in each of the formulation series, 0p*x*m, 0.2p*x*m and 0.4p*x*m where *x* is in each case variable, assessing phase assemblages by XRD and TGA to determine the effects of phosphate modification upon hydration and effectiveness in preventing or hindering conversion. Of these samples the 0.4p0.05m sample was chosen for extended curing up to 1080 days and subjected to hydrothermal treatment and phase development was assessed.

Chapter 6 examines the binder phase in samples with a relatively high polyphosphate modification cured up to 360 days, with the aim of determining the aluminium-phosphorous interaction in the samples. These samples are characterised using XRD, TGA and advanced solid-state NMR techniques including cross polarisation magic angle spinning and rotational echo adiabatic passage double resonance (REAPDOR) to elucidate more information regarding the highly disordered binding phases found in such samples.

In Chapter 7, results from initial trials of encapsulated aluminium, in both powder and monolithic forms, are reported. The importance of using different techniques to measure the corrosion of powder and monolithic aluminium is examined. The assessment of degree of corrosion is made using a number of different techniques assessing the mass of encapsulated aluminium metal remaining in the sample by

differential thermal analysis, image analysis and by mass loss measurements; and the hydrogen being evolved by mass spectrometry and water displacement.

Chapter 8 summarises the conclusions drawn from each chapter and contains recommendations for further avenues of research stemming from the work contained in this thesis, and other necessary areas of study identified.

2 Literature review

2.1 Alternative cements

Since its first development, around 200 years ago, Portland cement (PC) has dominated as the material of choice when binding aggregates together to form concrete (Juenger et al. 2011). Portland cements consist of calcium silicates as the primary reactive phases, which upon reaction with water form amorphous calcium silicate hydrate and calcium hydroxide as principal hydrates that bind the particles together to form a hardened monolith (Scrivener et al. 1999). Good economic value, abundant precursor materials and versatility have maintained the high volume consumption of Portland cement derived materials and this is anticipated to continue, driven by infrastructure development demands in emerging markets (Juenger et al. 2011).

The development of nuclear power generation and its wide scale commercialisation in the UK has resulted in the accumulation of vast amounts of radioactive waste. These wastes, generated either through activation during service or contamination during decommissioning, categorised as either high, intermediate or low level depending on their activity. Currently in the UK cementation is the established preferred route for packaging of this waste, ensuring that the migration of the encapsulated radionuclides is minimised, followed by long-term storage in a geological disposal facility. At this time composite PC systems are the established preferred route for the encapsulation and packaging of this waste (Milestone 2006). However, the high pH environments of PC composite systems are likely to result in high levels of corrosion of reactive metals such as aluminium and magnesium, present in large quantities when considering ILW waste streams in the UK, and as such alternative systems require further investigation.

A greater departure from the conventional and familiar Portland cement material is the development of alternate binder chemistries, which aim to produce materials whose manufacturing routes have smaller environmental footprints whilst maintaining performances in the field which satisfy the benchmarks for their respective

applications. Four systems outlined by Juenger et al. (2011), being calcium aluminate cement, calcium sulphoaluminate cement, alkali-activated binders and supersulphated cement, have been identified as promising alternatives to PC. In many cases these alternative materials may outperform the conventional PC system, one such example being the rapid setting of calcium aluminate cements (CACs), which have been widely adopted as high performance repair materials and as a binder in refractory concrete applications (Scrivener et al. 1999). These alternative systems provide the added flexibility to develop blended and hybrid binders, take advantage of local raw material availability and provide a greater variety of cementitious materials to choose from, marking a departure away from a one size fits all PC based solution.

In comparison with PC chemistry, relatively little research has been conducted on these alternative systems, as such this presents one the largest barriers to their adoption for industrial application. The familiarity and understanding of the hydration of PC and performance resulted in a historically one-sided debate when identifying a cementing solution for applications ranging from infrastructure to waste cementation, the latter due to the relatively low pH of their pore solutions. However with a greater focus upon the performance requirements generated by increasingly demanding applications, there is considerably greater motivation to further investigate the alternatives to Portland cement.

2.2 Calcium aluminate cement

Calcium aluminate cement (CAC), previously commonly known as high alumina cement (HAC) (Bensted & Barnes 2002), is often considered to be the most important of non-Portland cements (Scrivener 2003). CAC, or ciment fondu, was commercially developed and patented in 1908 by Jules Bied from the Pavin de Lafarge Company in France (Bied 1908), building upon the work of Frémy who experimented with melts of alumina and lime in varying quantities (Bensted & Barnes 2002). Work in the early 1900s was motivated by a desire to develop cementitious material that was resistant to sulphate attack (Taylor 1990) especially for application in ground containing large quantities of gypsum and anhydrite (Hewlett 2004). The resulting material exhibited properties such as rapid hardening, early strength development, resistance to chemical attack and thermal shock (Scrivener 2003; Hewlett 2004), high heat of hydration

(Taylor 1990) and comparatively lower pore solution pH (Macias et al. 1996), for which they are well known. Some of these properties coupled with a high cost led these materials towards use in more specialised applications such as precursors for refractory concretes and in specialised construction applications (Hewlett 2004).

The necessity of rebuilding of civil infrastructure after World War I contributed to the initial industrial development of these materials (Gosselin 2009) which were introduced to the UK during the same period (Hewlett 2004).

The applications for CACs have varied over time, with the most common contemporary uses being the rapid repair of concrete structures, the binder in refractory concretes and in blended PC-CAC systems. The properties of CAC can change considerably as a function of time even after the initial period of hydration, known as conversion. One of the most fundamental properties in structural applications is strength, and this is particularly known to be affected by the conversion processes. Failures of CAC in structural applications in the UK between 1973-1974 (Neville 2009a); three notable examples in public buildings (two schools and a university) generated much public interest and media attention. This fuelled considerable re-evaluation of the use of CAC in the field by a number of committees and organisations, including the purpose-established Stone Committee (Neville & Brooks 1987) in the immediate aftermath of the failures in the 1970s and more recently the Concrete Society Committee, which both identified the requirement to account for the strength loss due to conversion in the design of structures (Scrivener 2003). A sizeable body of work in the literature followed the initial attention received from the publicised failures, both looking at assessing the conversion and also preventing/avoiding it.

2.2.1 Clinker mineralogy

CACs are manufactured by fusing mixtures of bauxite and limestone or chalk at 1450-1600°C in either open hearth furnaces or in the case of smaller scale production, electric arc furnaces (Taylor 1990; Hewlett 2004). The resulting clinker has an oxide composition dominated by aluminium and calcium. Figure 2-1 (a) shows the proportions of major oxides present in CAC clinker; with increasing alumina content a ‘whiter’ cement is obtained. Achieving higher alumina content requires either

additional processing or higher grade raw materials with fewer impurities, hence these grades of CAC tend to be considerably more expensive (Scrivener 2003), up to 5 times more costly than PC (Falzone et al. 2015). However these materials are better suited to refractory applications due to their higher melting temperatures, as seen in Figure 2-1 (b).

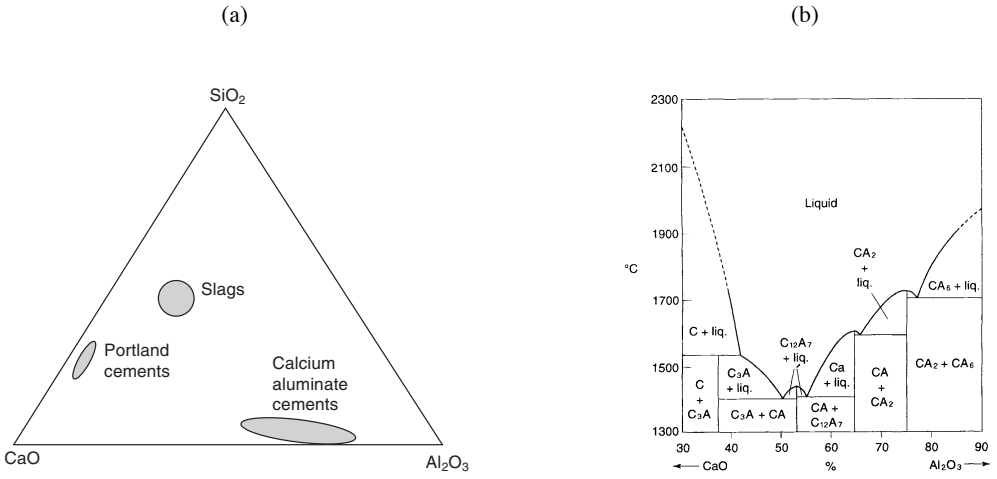

Figure 2-1 (a) Ternary phase diagram showing oxide composition of CACs (Scrivener 2003), and (b) CaO-Al_2O_3 phase diagram (Hewlett 2004).

As with most manufacturing processes involving alumina/aluminium there can be significant iron content, and the colour of the cement also depends heavily on the bauxite type using in the manufacturing process (Scrivener 2003). Iron oxides are reported to constitute in the region of 20 % of cements made with red bauxite (such as Ciment Fondu) and hence exhibit a dark brown to black colour (Scrivener 2003), whereas cements derived from white bauxite (such as Secar) contain considerable less (Kerneos Inc 2006) and are light grey in appearance.

The reactivity of the anhydrous calcium aluminates is dependent upon the lime to alumina ratio, with phases rich in lime, such as monocalcium aluminate, exhibiting significantly higher reactivity with water than alumina rich phases such as CA_2 and

CA_6[1], of which the latter is inert at ambient temperatures (Scrivener 2003). Hence major reactive phases of CAC are monocalcium aluminate ($CaAl_2O_4$, CA) and mayenite ($12CaO{\cdot}7Al_2O_3$, $C_{12}A_7$) (Scrivener 2003), however in clinkers with a higher alumina content calcium dialuminate (CA_2), calcium hexaluminate (CA_6), belite (C_2S) and corundum (α-A) may also be present (Taylor 1990). This thesis focuses upon an intermediate level CAC, with between 50-60% alumina content.

$C_{12}A_7$, the most reactive phase, has a cage like structure, which is capable of retaining small numbers of hydroxyl ions even at high temperatures. It has a cubic crystal structure (Hewlett 2004). This phase is responsible for the initiation of the setting of the cement due to its high reactivity, and as its content may heavily influence the setting period of the cement, its presence in the clinker content is heavily monitored and regulated (Scrivener 2003). This phase also exists in a non-crystalline form, which combined with the limited quantities present in the clinker often means it is very difficult to detect.

CA is the major reactive phase and can constitute 40-60% of the clinker (Scrivener 2003), its high reactivity with water contributes the rapid hardening and early strength development properties to CAC materials. Structurally, it is monoclinic (Christensen & Lehmann 1984), with aluminium atoms bound in tetrahedral co-ordination and calcium sitting in the cavities, with a co-ordination number of 9, Figure 2-2 (a). The structure is fully polymerised with a tetrahedral aluminate framework (Torréns-Martín et al. 2013). CA occurs as an interconnected three dimensional network running through the clinker particles, Figure 2-2 (b), hence its dissolution is not limited by the solubility of other less reactive phases in the particle (Scrivener 2003).

[1] Where CA_2 and CA_6 refer to monocalcium dialuminate ($CaO{\cdot}2Al_2O_3$) and monocalcium hexa-aluminate ($CaO{\cdot}6Al_2O_3$) respectively.

(a)

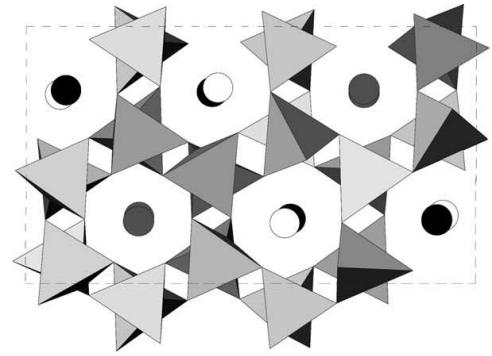

(b)

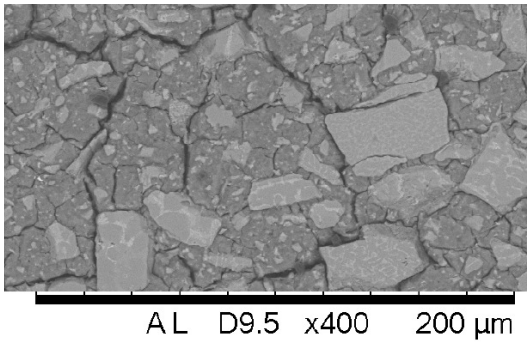

Figure 2-2 (a) Structure of CA (Prodjosantoso & Kennedy 2006), where tetrahedra are 4 co-ordinated aluminium atoms and circles denote calcium atoms, and (b) SEM micrograph showing CA streaking in unreacted cement grains .

Minor phases are also present in the clinker, and although their cumulative proportions may be large, they remain relatively unreactive especially at lower temperatures and earlier curing periods (Scrivener 2003). These phases include ferrite (C_4AF), perovskite ($CaTiO_3$, CT), gehlenite ($Ca_2Al(AlSiO_7)$, C_2AS) and spinel (MA). As a result they have a minimal or negligible role in the hydration reactions, however they may affect the phase precipitation under hydrothermal conditions or in the presence of additives and in hybrid binder systems.

Of these potential minor phases, belite and spinel occur in the intermediate alumina content CAC studied in this work in quantities below the detection limits of the techniques used to characterise the material, and so will be neglected. Gehlenite is one of the principal members of the melilite family, a group of sorosilicates with the general structure $A_2B(T_2O_7)$. In the case of gehlenite, the tetragonal structure consists of corner sharing alumina and silica tetrahedra (T_2O_7) forming sheets with aluminium and hosting 8-coordinated Ca^{2+} ions in between these layers (Taylor 1990).

The ferrite phase is an iron oxide substituted dicalcium aluminate type phase, (Bensted & Barnes 2002) which has a variable composition in the following range : $Ca_2(Al_xFe_{1-x})_2O_5$, where $0 < x < 0.7$ (Taylor 1990). It has an orthorhombic unit cell built up of layers of alternating corner sharing octahedra and tetrahedral chains, both holding the aluminium and iron atoms, with calcium atoms between the layers (Taylor 1990). Calcium titanate, also known as perovskite and having an orthorhombic crystal structure, is the least reactive of the phases found calcium aluminate cements with intermediate level alumina content. Composed of corner sharing titanium octahedra, it holds calcium within the cavity with coordination 12. Of the constituent phases of the clinker material, CT is the only which is non hydraulic.

2.2.2 Mechanism of reaction and products

2.2.2.1 Main phase hydration and conversion

The setting and hardening of CAC can be attributed to the hydration of the constituent clinker phases. This hydration process involves the dissolution of the reactive anhydrous clinker phases resulting in a solution holding a number of ionic species, the populations of which increase with increased clinker dissolution. Over time a supersaturation of the ions within the solution develops, which drives the precipitation of hydrated phases that are formed by the combination of the ions found in the solution. The precipitation of these phases results in a decrease in the concentrations of the ions in solution (depending on the phases precipitated), resulting in further dissolution of clinker phases, and possibly also of hydrate phases with high solubility. Precipitated phases, which have a larger solid volume, can result in the solidification and hardening of the cement by bridging the gap between the cement grains (Scrivener 2003) and forming a three dimensional network. Once the hydration process begins, water exists in a number of forms, including free water in pores and voids, adsorbed surface water, and structurally bound water in crystalline and gel phases.

There is a typical 325-400 $kJ \cdot kg^{-1}$ release of heat for CACs as a result of the hydration process, which is less than the total heat release for conventional Portland cements, however this is all released within the first 24 hours (Taylor 1990), whereas in the case of Portland cements the heat of hydration is released over a much longer period. Hence CAC materials are advantageous when considering hydration in low temperature environments (Bensted & Barnes 2002).

The hydration of calcium aluminate cement is well described in the literature with a wide variety of advanced techniques used to study it. These include ultrasonic testing (Chotard et al. 2001), acoustic emission testing (Chotard, Smith, et al. 2003), X-ray computed tomography (Chotard, Boncoeur, et al. 2003), NMR spectroscopy (Cong & Kirkpatrick 1993; Skibsted et al. 1993), and synchrotron energy-dispersive diffraction (Rashid & Turrillas 1997) in addition to more conventional techniques such as X-ray diffraction (Luz & Pandolfelli 2011; Guirado & Galí 2006) and thermal analysis (Bushnell-Watson & Sharp 1992; Das et al. 1996; Ramachandran et al. 2002; Pacewska & Nowacka 2014).

During hydration the main reactive phase, CA, containing tetrahedrally co-ordinated aluminium dissolves into solution, to give Ca^{2+} and $Al(OH)_4^-$ species (Scrivener 2003). These ions combine and precipitate out of the solution, with aluminium in precipitates largely being held in octahedral co-ordination (Skibsted et al. 1993; Müller et al. 1981; Müller et al. 1984). Various combinations of these ions are permissible, however depending on curing temperature and time some are more favourable than others, which is described well in Figure 2-3 adapted from Scrivener et al. (1999). This description of CAC hydration is valid for a low iron containing CAC, manufactured from white bauxite such as Secar 51, distributed by Kerneos.

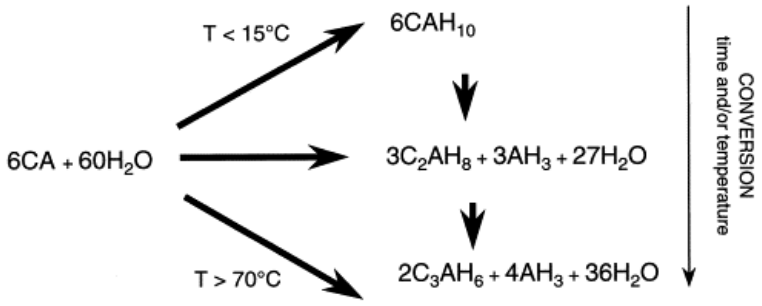

Figure 2-3 Hydration mechanism of CA (Scrivener et al. 1999)

In addition to a poorly crystalline aluminous gel, the precipitation of metastable hydrate phases dominates the phase assemblage of the during early hydration (Taylor 1990) at room temperature and below. These metastable phases, monocalcium aluminate decahydrate ($CaAl_2O_4 \cdot 10H_2O$, CAH_{10}) and dicalcium aluminate octahydrate ($Ca_2Al_2O_5 \cdot 8H_2O$, C_2AH_8), are shown in Figure 2-4 and **Error! Reference source not found.** respectively, and their respective needle-like and hexagonal platelet morphologies are held responsible for the high early strength exhibited by when curing at lower temperatures (Bensted & Barnes 2002). C_2AH_8 has been identified as existing as two polymorphs, α and β, with the former being the most common, and both acting as intermediates to initiate nucleation during conversion to C_3AH_6

(a)

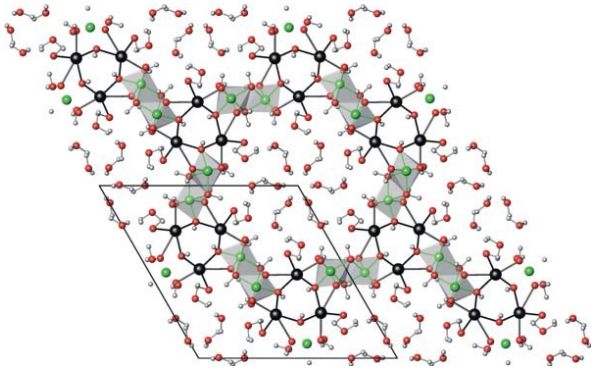

(b)

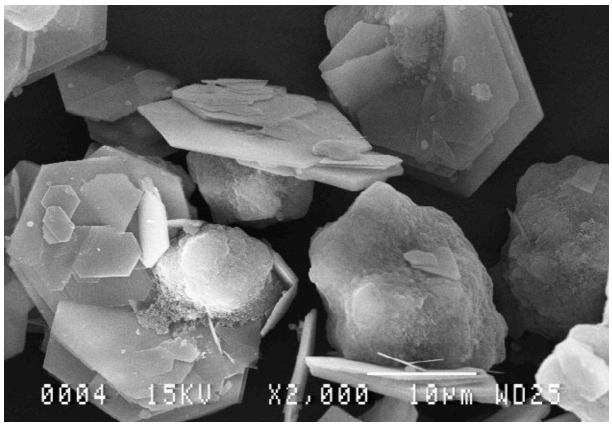

Figure 2-4 (a) Structure of CAH_{10} (Christensen et al. 2008) where black, red, green and grey spheres represent calcium, aluminium, oxygen and hydrogen atoms respectively, and (b) SEM micrograph of CAH_{10} hexagonal crystals (Parr 2008).

(a)

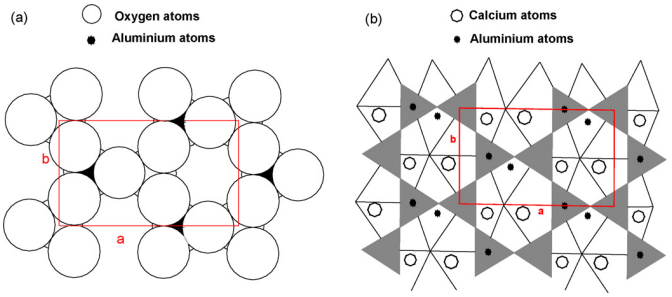

(b)

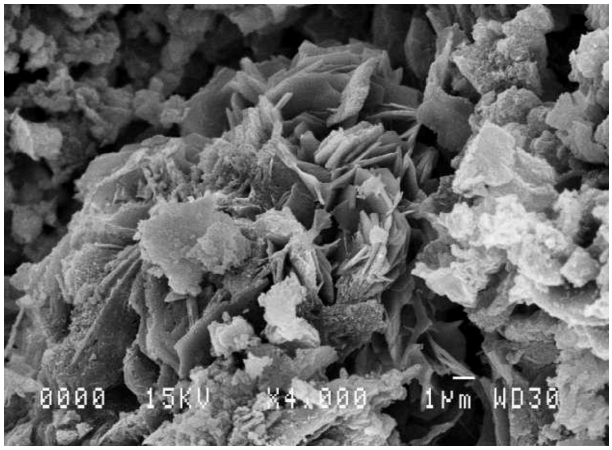

Figure 2-5 (a) Structure of C_2AH_8 (Ukrainczyk et al. 2007), and (b) SEM micrograph of C_2AH_8 hexagonal crystals (Parr 2008).

Both of these hydrate phases are preferentially precipitated at lower temperatures, are prone to having low long-range order, have hexagonal crystal structures and dehydrate below 200°C (Ramachandran et al. 2002; Hewlett 2004). Despite their precipitation lowering the Gibbs free energy of the system, they are not the most thermodynamically favoured reaction products, hence their characterisation as metastable. At elevated curing temperatures the direct precipitation of more thermodynamically stable phases is preferable and the formation of crystalline gibbsite ($Al(OH)_3$, AH_3) and silicon-free katoite hydrogarnet ($Ca_3Al_2(OH)_{12}$, C_3AH_6) can be observed, as indicated in Figure 2-3. Once these phases are present in the system they will continue to form even at temperatures not associated with their direct precipitation (Scrivener 2003).

Gibbsite formation occurs in two steps at ambient temperatures and can be slow, initially it is precipitated as AH_3 gel which crystallises into gibbsite over time (Hewlett 2004), and more rapidly at higher pH (McHardy 1971). The characterisation of this precursor gel phase is debated in the literature, with some researchers

suggesting it to be a hydrated alumina type phase (AH_n) (Skibsted et al. 1993; Fujii et al. 1986), and other publications (Bushnell-Watson & Sharp 1992; Francesc Guirado et al. 1998; Ramachandran et al. 2002) have proposed a calcium aluminium hydrate (C-A-H) type gel from which gibbsite may crystallise.

Gibbsite (γ-AH_3), an aluminium hydroxide, has a monoclinic crystal structure with hexagonal close packed layers. It has a number of polymorphs including bayerite (β-AH_3), nordstrandite and doyleite, with the largest differences being : (i) crystal structure, where the latter two are triclinic instead of monoclinic, and (ii) stacking of the AH_3 (Lookman et al. 1997). Of gibbsite and bayerite, only the former is commonly found in nature (McHardy 1971), however bayerite has been reported as a corrosion product of encapsulated aluminium metal in cement, albeit as an intermediate metastable phase with respect to eventual gibbsite formation (Setiadi et al. 2006)

C_3AH_6, the other stable hydrate, is a silicon-free hydrous garnet. Garnets have a general formula $X_3Y_2(SiO_4)_3$ where X is a divalent cation such as calcium, and Y is a trivalent cation such as aluminium. The hydrogrossular variety describes a calcium aluminium garnet series where the silicate is (partially or wholly) replaced with OH, $Ca_3Al_2(SiO_4)_{3-x}(OH)_{4x}$. Hydrogrossular structures where $1.5 \leq x \leq 3$ are known as katoite hydrogarnets (Nobes et al. 2000). C_3AH_6 generally precipitates with a cubic crystal structure and habit, and whose crystallites (in the hydrated CAC system) are found surrounded by a matrix of less crystalline gibbsite (Scrivener 2003). In addition to these three calcium aluminate aluminate hydrates, one with an even greater calcium to aluminium ratio, C_4AH_{13}, is reported for low alumina CACs at ambient temperatures (Bensted & Barnes 2002).

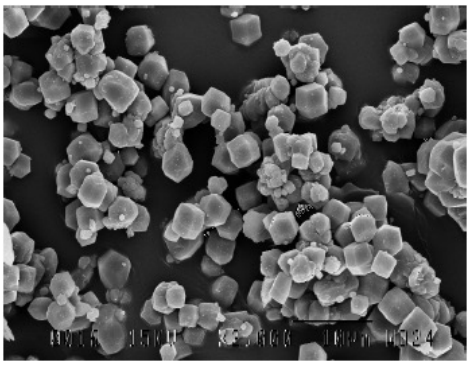

Figure 2-6 Micrograph of C_3AH_6 crystals, from Scrivener (2003).

In the absence of direct precipitation of the stable hydrate, the metastable phases eventually undergo a conversion process whereby they dissolve and re-precipitate as more stable phases via the reactions in Equations 2-1 to 2-4. The conversion process can manifest as a multistage process as described in each of the equations, where the two polymorphic forms of C_2AH_8 act as nucleating agents for the initial of precipitation of C_3AH_6 (Rashid et al. 1994), however it is possible to bypass this under the correct conditions. Regardless of the number of steps in the process the thermodynamic hierarchy must be followed: less stable precipitates must dissolve and result in the formation of more stable products. The dehydration temperatures of these phases, shown in Figure 2-7, are indicative of their rank in the conversion process. In addition there is a contribution to AH_3 formation by the conversion of the amorphous aluminous gel phase to crystalline gibbsite (Bensted & Barnes 2002).

$$CA + 10H \rightarrow CAH_{10}$$ Equation 2-1

$$2CA + 11H \rightarrow C_2AH_8 + AH_3$$ Equation 2-2

$$2CAH_{10} \rightarrow C_2AH_8 + AH_3 + 9H$$ Equation 2-3

$$3C_2AH_8 \rightarrow 2C_3AH_6 + AH_3 + 9H$$ Equation 2-4

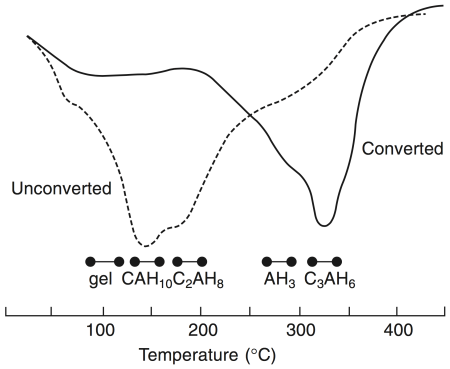

Figure 2-7 Schematic thermogravimetric plot showing typical dehydration temperatures of conventional CAC hydrates, figure taken from Scrivener (2003).

The kinetics of this thermodynamically inevitable conversion process (Scrivener et al. 1999) depends on a number of factors including the water to cement ratio (w/c), curing temperature, relative humidity and the dimensions of the cast cement (Taylor 1990; Scrivener 2003; Hewlett 2004). As a result of the rapid hydration reactions, larger volumes can result in self heating of the cement to temperatures of up to 70°C or more (Scrivener et al. 1999), driving either the direct precipitation of the stable hydrates or instant conversion.

The conversion process results in volume changes within the hardened material as a result of the difference in densities between the metastable and stable phases, shown in **Table 2-1**. When considering the hydration of pure CA, the total volume may reduce by up to 53% if the initial hydration product is CAH_{10}, or less with direct precipitation of C_2AH_8 and AH_3 (Taylor 1990). A net increase in porosity can be responsible for a considerable reduction in mechanical integrity of the monolith (Bushnell-Watson & Sharp 1992) and increased susceptibility to chemical attack (Scrivener 2003). A typical example of strength reduction due to conversion is shown in **Error! Reference source not found.**.

Table 2-1 Properties of some calcium aluminate phases (Scrivener 2003; Bensted & Barnes 2002; Taylor 1990; Ukrainczyk et al. 2007; Hewlett 2004)

Phase	Density ($kg \cdot m^{-3}$)	Combined water (%)	Aluminium coordination	Crystal system
CA_2	2910		4	Monoclinic
CA	2945		4	Monoclinic
$C_{12}A_7$	2680		4	Cubic
C_4AF	3700		4	Orthorhombic
C_2AS	2980		4	Tetragonal
CAH_{10}	1720	53	6	Hexagonal
C_2AH_8	1950	40	6	Hexagonal
C_3AH_6	2520	28	6	Cubic
γ-AH_3	2440	35	6	Monoclinic

The negative effects associated with conversion are more pronounced with increased water to cement ratio (Bensted & Barnes 2002), a higher water to cement ratio (w/c $\geq$0.7) provides more water and space facilitating significantly more metastable hydrate formation (Scrivener 2003). This is following by the large precipitation of metastable hydrates, filling the space initially occupied by the water resulting in a low solid density and porosity. With the onset of conversion there is a considerably greater solid volume reduction and porosity increase as a result of a larger volume of metastable phases converting to stable phases compared with formulations with a lower w/c that precipitate metastable hydrates at a slower rate in a smaller volume.

2.2.2.2 Minor phase hydration

The hydration behaviour of CA_2 and $C_{12}A_7$ is similar to that observed for CA. $C_{12}A_7$, as explained earlier, is considerably reactive as a result of its higher calcium to aluminium ratio, and at room temperature the formation of C_2AH_8 tends to dominate during precipitation, followed by conventional conversion to stable hydrates (Bensted & Barnes 2002). At elevated temperatures, as with CA, direct precipitation of stable

hydrates is observed, indeed all three of these calcium aluminates exhibit similar hydration behaviour, however their reactivities are all notably different.

The ferrite phase, C_4AF, although minor especially in CACs with a higher alumina content, has also been shown to hydrate as follows (Bensted & Barnes 2002), and generally reacts at a higher temperature regime (30-38°C):

$$C4AF + 16H \rightarrow C_4AFH_{16}$$ Equation 2-5

$$C_4AF + 22H \rightarrow C_2AFH_{20} + 2CH$$ Equation 2-6

The existence of CH (calcium hydroxide / portlandite) is brief in this system, as it dissolves to reprecipitate and contribute to the formation of CA hydrates (Bensted & Barnes 2002). Furthermore the C_4AF hydrate phases, both standard and calcium deficient, are formed in solid solution with C_2AH_8 and CAH_{10} respectively and hence are difficult to independently identify (Bensted & Barnes 2002). CH formation is also observed with calcium silicate hydrate (C-S-H) precipitation during the hydration of CAC clinkers containing belite (β-C_2S) (Bensted & Barnes 2002).

The hydration of gehlenite is also possible, however similar to the other minor phases it is very slow to form its hydrate phase, strätlingite (C_2ASH_8) via the following reaction :

$$C_2AS + 8H \rightarrow C_2ASH_8$$ Equation 2-7

The formation of strätlingite has also been observed in a number of modified CAC systems, both as a byproduct in the process of mitigating conversion (Ding et al. 1995) and as a corrosion product of encapsulated metals (Setiadi et al. 2004).

2.3 Mechanical and durability properties of CAC

2.3.1 Fresh state properties

The period of good workability of a cement material is dependent upon the setting time. Curing at temperatures between 25 – 30°C maximises the setting times for conventional CAC hydration (Taylor 1990). As discussed earlier in this chapter, this property may be tuned according to the mayenite content of the clinker. Due to the rapid nature of hydration once the process has been initiated by the mayenite, the energy imparted during mixing, either from a long mixing duration or from a high shear rate, can result in rapid acceleration of the setting and affect the viscosity of the slurry (Taylor 1990).

For the particular calcium aluminate cement used here, Secar 51, it is reported that the Vicat test indicated initial and final setting times of ≥ 160 min and ≤ 300 min respectively (Kerneos Inc 2006). Section 2.5.1 also summarises a number of typical additives which are used to accelerate and retard the rate of hydration and ultimately the setting times.

The intrinsic shrinkage properties of CAC materials compared to Portland cements would be comparable if both systems were hydrating at similar rates, however this is very rarely the case. As discussed, the CAC system hydrates much faster during the initial 36-72 hours proceeding mixing and thus exhibits far greater degrees of shrinkage during this period, as can be seen in Figure 2-8. As the shrinkage takes place over a shorter time period the symptoms of this process are more pronounced and can result in cracking of the cast monoliths (Scrivener 2003).

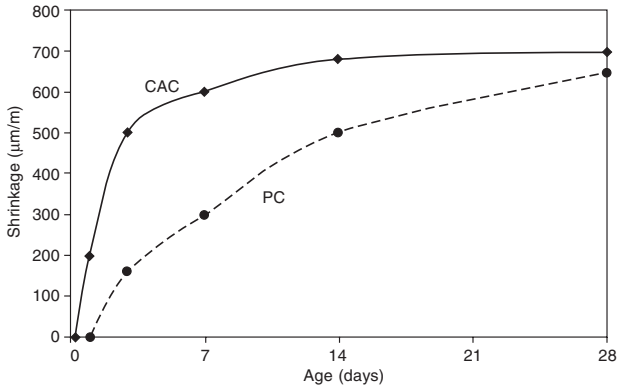

Figure 2-8 Shrinkage as a function of curing period for CAC and PC prisms (40 x 40 x 160 mm at 20°C and 50% RH). Figure taken from Scrivener (2003).

2.3.2 Mechanical properties

The early strength development of CAC is one of its key advantages over Portland cement. It has been reported that CAC concrete may have a useful strength within just 6 hours and a strength at 24 hours which is comparable to that of Portland cement after 28 days (Taylor 1990). However, the conversion process complicates the strength behaviour of CAC materials and as such special care must be given to their design, preparation and use. Standards such as EN 14647 (Comité Européen de Normalisation 2005) refer to correct use of CAC and indicate potential losses in strength as a result of conversion (Annex A of that standard), with the aim of reducing the disruptive consequences of conversion. The product data information provided by Kerneos Inc. (2006), for its product Secar 51, claims compressive strengths of 15.0 MPa and 53.8 MPa after 6 and 24 hours of curing respectively.

In addition to the conversion process, self-heating of the material after mixing (due to the rapid hydration rate and the specific heat of hydration for CAC materials) considerably affects the compressive strength properties of the material. Figure 2-9 shows a schematic of the strength as a function of curing time for these materials, a clear decrease in the strength can be seen for isothermally cured materials without self heating. This can be attributed to the start of the conversion process and is followed by the strength tending to a residual value, which it generally will maintain in the absence of the any degradation (Scrivener 2003). In the case of a more realistic service scenario, where there is self heating, temperatures may rise by tens of degrees, resulting in the early precipitation of stable hydrates and the conversion process

occurring over a longer duration, resulting in less of an impact on the compressive strength.

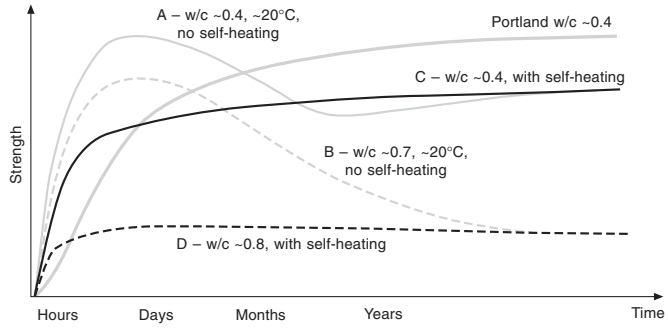

Figure 2-9 Compressive strength development in calcium aluminate cements, showing the effect of self heating (Scrivener 2003)

This is in agreement with a number of studies including an investigation by Kirca et al. (2006) who reported that the compressive strength of unmodified CAC increases during the initial period of hydration up to a peak value (ca. 100 MPa), after which it falls to a stable value. This peak value indicates where the conversion process begins, and it was found that with increasing curing temperatures it was reached quicker. Samples which were cured at 20°C for 28 days followed by higher temperatures exhibited decreasing strengths with increasing curing temperature, which can be attributed in part to the conversion process occurring over a shorter time period and hence affecting the morphology of the hydrogarnet crystals being precipitated (Taylor 1990). However, while the compressive strength of the cast CAC materials can be considerably affected by the conversion process, it has been reported that the tensile strength and toughness are not reduced to the same extent, and performance in these metrics may be comparable to Portland cement materials (Lamour et al. 2001). Other than preventing the conversion process via altering the hydration pathway, general advice to reduce the effects of conversion have focused about the use of low water to cement ratios in CAC materials for structural applications (Scrivener 2003; Bensted & Barnes 2002; Taylor 1990; Neville 2009a). As discussed in section 2.2.2.1, the initial water content determines the volume fraction occupied by metastable phases upon hydration. Hence it is important to limit this, such that the volume of material converting from metastable phases to hydrogarnet at any period is small, resulting in a

smaller volume changes at any one time and hence maintaining the structural integrity. Of course the free water liberated during this process continues to hydrate unreacted clinker material. Thus the rate of conversion process is limited and its consequences are mitigated.

2.3.3 Durability properties

2.3.3.1 Thermal resistance

The thermal properties of CAC based materials, either at high temperature for refractory applications or at very low temperatures for structural applications, give a competitive advantage over alternative cementing systems. The high heat of hydration enables the material to cure well in low temperature conditions, and despite the high self heating the system can accommodate thermally induced strain. This has been reported to be as a result of strain relaxation by creep promoted by conversion of the CAC (Scrivener 2003).

The refractory properties of CAC are well known and exploited in thermal processes where refractory linings are required. Bauxite derived CACs are commonly used in furnace hot face applications at temperatures up to 1350°C, whereas CACs with higher alumina contents may be used to produce concretes which can withstand temperatures up to 2000°C (Taylor 1990). As the composite system is heated, the CAC completes the conversion process to hydrogarnet, which is then followed by a complete dehydration of the system and recrystallization of the clinker type phases such as CA and $C_{12}A_7$ during which the compressive strength of the system is decreasing. However at higher temperatures a sintering type effect is seen where these clinker type phases bond with the aggregate, increasing the compressive strength and the abrasion resistance (Bensted & Barnes 2002). 'Low' temperature refractory applications commonly use crushed fire-brick as the aggregate, whereas higher temperature solutions are more likely to use pure alumina (Bensted & Barnes 2002). It must be noted that the aggregates used in these refractory concretes play an important role in determining the thermal resistance of the final product, which is not solely a product of the base cement.

2.3.3.2 Exposure to aggressive agents

Acidic agents induce an aggressive environment for cements, which are generally alkaline. In the case of Portland cements acid attack dissolves calcium hydroxide phases increasing the porosity of the cement. A developed symptom of acid attack can be the decalcification of the main binder phase, C-S-H gel, which may result in a loss mechanical integrity (Scrivener et al. 1999).

In the case of CAC systems, although acid attacks result in the leaching of calcium from the major binding calcium aluminate hydrate phases, thus increasing porosity, there is significant formation of the minor binding phase, alumina hydrate (poorly crystalline gel). This increased phase formation counteracts increases in porosity induced by the acid attack, protecting the cement from further degradation (Scrivener et al. 1999). Indeed the higher porosity of CAC (concrete especially) is able to accommodate more corrosion products (Neville 2009b). The alumina hydrate is stable at pH as low as 3.5, however below this it dissolves, which via uptake of protons neutralises the solution further.

CACs have been developed to be resilient against sulphate attack and hence have been reported (Bensted & Barnes 2002) to perform well in natural conditions and reasonably well within laboratory investigations. The primary reason for this resistance is the absence of $Ca(OH)_2$ from the hydration products (Neville & Brooks 1987). However, it has been shown that the surface layer of the cement is influential and its removal may result in increased damage from sulphate attack (Hewlett 2004).

Alkali-induced hydrolysis has been reported in the case of cements with a high water content (w/c > 0/8) and in the presence of CO_2 and a source of alkalis (Scrivener 2003). This poses a greater threat to CAC materials in comparison with PC based systems due to their much lower pH (Neville 2009b). The process results in the breakdown of the calcium aluminate hydrates to give calcite, an alkali aluminium hydroxide and water (Bensted & Barnes 2002), whereby the strength contributing phases of the mature hydrated CAC are broken down. The presence of alkalis during the main phase of hydration before the maturation can result in the acceleration of the conversion process (Bensted & Barnes 2002), potentially increasing the negative side-effects.

Limited investigations on the resilience of CAC to freeze-thaw is known, however it is clear from examples where CAC concretes have been used in cold climates that their behaviour shows little susceptibility to freeze-thaw damage (Scrivener 2003).

2.3.3.3 Corrosion of encapsulated metals

The encapsulation of metals by cementitous materials is commonplace, either to improve the mechanical properties in structural applications or indeed as a result of packaging metal containing wastes in a cementitious matrix. As with any composite system, the interface between the constituent component materials is integral to the mechanical performance of the final product.

The corrosion of cement-encapsulated steel has long been studied to maintain the strength benefits contributed to cement and concrete by steel reinforcement. Generally corrosion of steel is prevented by the formation of a passivation layer at pH values of between 12 and 13.5 (Ann et al. 2010). However in the presence of chloride ions, which is particularly likely in marine environments, this passivation layer is broken down by reacting with the chloride ions which reveals fresh steel prime for corrosion. It has been found that this passivation breakdown maybe mitigated by reduction of the chloride ions through the cement via the pore solution, and it has been reported (Ann & Cho 2014) that CAC has a higher binding capacity than Portland cement to precipitate chloride complexes from the pore solution hence blocking their supply to the encapsulated steel and resulting in lower levels of corrosion. The lower pH environment of the CAC seems to be less significant than its increased binding capacity for chloride ions (Goñi et al. 1991) via calcium chloroaluminate formation.

With the adoption of cementation as the method for the immobilisation for the majority of ILW in the UK (Wilding 1992), there has been concern regarding the corrosion of aluminium and magnesium, two common elemental components of intermediate level waste in the UK inventory. The corrosion of aluminium in cementitious matrices has been investigated from this perspective. As with steel there are optimum pH regimes within which aluminium and magnesium maintain their passivation layer. Figure 2-10 which shows the interaction between aluminium and water as a function of pH and electrochemical potential, indicates that the range of pH

4 to 9 maintains the passivation layer for this metal. Aluminium is amphoteric, corroding at both lower and higher pH values outside of the passivating regime.

The process by which encapsulated aluminium corrodes in a Portland cement matrix is shown in Figure 2-11. This process can be summarised by the dissolution of the existing alumina passivation layer, which exposes aluminium metal to corrosion. This generates aluminium hydroxide and hydrogen gas in addition to porosity generated by the dissolution of the passivating layer.

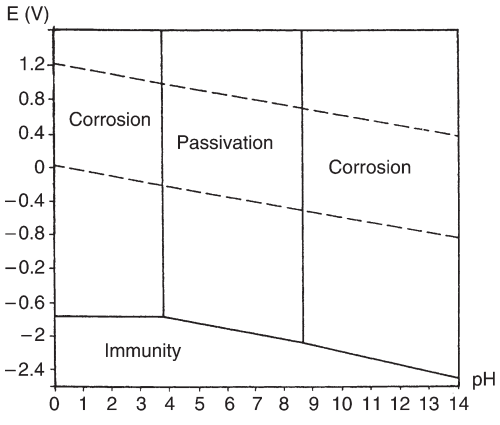

Figure 2-10 Pourbaix diagram for aluminium (Vargel 2004).

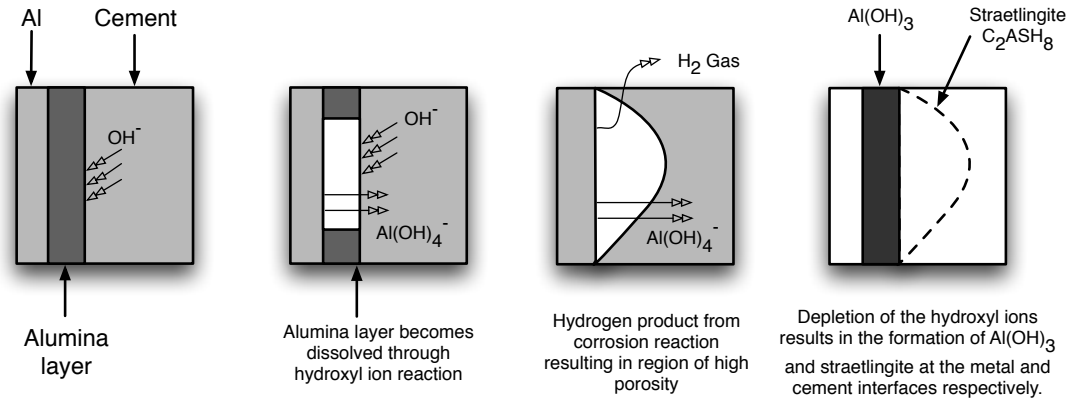

Figure 2-11 Schematic showing the breakdown of the alumina passivation layer and subsequent corrosion of aluminium within a Portland cement matrix (Setiadi 2006).

The formation of hydroxylaluminate ions as a corrosion product is described in Equation 2-8 and Equation 2-9, where the former describes the dissolution of the passivation layer and the latter describes the corrosion of the virgin aluminium in an

alkaline solution. These ions then precipitate out of solution to form an aluminium hydroxide, either bayerite or gibbsite depending on the conditions (McHardy 1971).

$$Al_2O_3 + 2OH^- + 3H_2O \rightarrow Al(OH)_4^-$$ Equation 2-8

$$Al + 2OH^- + 2H_2O \rightarrow Al(OH)_4^- + H_2$$ Equation 2-9

In the case of corrosion within an PC matrix there is migration of the aluminate ions towards the cement component of the reaction interface, which results in the precipitation of a calcium aluminosilicate hydrate, straetlingite (Setiadi et al. 2006), however with the limited quantity and reactivity of silica in conventional CAC hydration, the mechanism of corrosion is more unclear for systems other than PC.

Due to the reactive nature of aluminium in cement, there are few circumstances where aluminium is encapsulated in cement, hence there is little legacy literature outside of that produced for the nuclear industry. However notable studies examining reactive metal corrosion in the context of ILW streams or metal corrosion in CAC are shown in

Table 2-2. There are four prominent methods of determining corrosion at the laboratory scale which are observed for these investigations: (i) Resistance polarisation, where a three electrode system is arranged with the working electrode selected to be the corroding metal encapsulated in the cement; (ii) DSC, where the uncorroded material maybe quantified; (iii) water displacement, by collection of hydrogen gas corrosion products; and (iv) mass loss, where the mass lost as a result of corrosion is measured.

Table 2-2 Notable studies examining cement encapsulated metal corrosion in CAC binders or relevant to the radioactive waste context.

Binder System	Encapsulated metal	Corrosion assessment technique	Reference
CAC & PC concretes exposed to salt environments	Steel bar	Resistance polarisation	(Ann et al. 2010)
CAC/PC blends in salt solutions	Steel bar	Resistance polarisation	(Ann & Cho 2014)
PC & PC/BFS blends	Aluminium, magnesium, 316L stainless steel and 43A mild steel bars	DSC & qualitative	(Setiadi et al. 2003)
CAC exposed to salt environments and accelerated carbonation	Steel bar	Resistance polarisation	(Macias et al. 1996)
PC and CAC based systems including phosphate-modified CAC	Aluminium bar	Water displacement by hydrogen & DSC	(Kinoshita et al. 2013)
BFS/PC composites	High purity aluminium, 1050 aluminium, high purity magnesium	Qualitative: DSC, SEM, XRD	(Setiadi et al. 2006)
M-S-H cement [2]	1050 aluminium strip	Water displacement	(Zhang et al. 2012)
BFS/PC & PFA/PC blends with added anhydrite	Aluminium strips	Water displacement	(Collier 2010)
Magnesium phosphate cement & PC	Steel bar	Mass loss	(Yang et al. 2000)
PC + LiNO	Aluminium wire	Galvanic current	(Matsuo et al. 1995)

[2] Magnesium-silicate-hydrate cement, M-S-H cement.

2.4 Applications of CAC based materials

Applications of CAC based materials generally fall in to one of the following categories : (i) refractory materials (ii) specialist structural materials, (iii) biomaterials, and (iv) waste immobilisation/encapsulation matrix materials. Despite the applications of calcium aluminate cements being diverse, its selection as a refractory material is regarded as its single largest use (Scrivener 2003).

CAC concrete refractory applications were first introduced commercially during the 1920s and 30s, and then on a wider scale with the outbreak of World War II. CAC materials are used as binder agents in refractory castables as they contribute a rapid strength development of the green (unfired) material (Cardoso et al. 2004). A compromise between the ultimate refractoriness and the initial rate of hardening must be made, as those calcium aluminates which are less reactive (with water) and have a lower calcium to aluminium ratio generally have better refractory properties and higher melting points (Cardoso et al. 2004; Taylor 1990). In addition to hot face applications in furnaces for metals processing, these materials in conjunction with appropriate aggregates are also used to line fireflood and thermal recovery wells (Bensted & Barnes 2002).

In addition to being used as an additive in mixed/hybrid binder systems to improve properties and for use in specialist mortar applications (Scrivener 2003), CACs have also been suggested for some niche applications such as matrix materials for tape cast composite plates with high temperature fibres for thermostructural applications (Soro et al. 2006; El Hafiane et al. 2014).

Due to the higher manufacturing costs of CACs compared to other cements, they are generally only prescribed for highly demanding and specialised applications where other materials would not be suitable. These can include environments where a high chemical and abrasive resistance is required as in flooring materials for heavy industry manufacturing, and environments where there is exposure to acids such as breweries and industrial chemical plants (Scrivener 2003). As discussed in section 2.3.2, due to the effect of conversion upon the compressive strength and the loss of public confidence following high profile structural failures of CAC concretes, their use is now very limited in low temperature structural applications. In cases where the

self-heating during initial hydration provides an adequate bulk temperature for casting and hardening, such materials have seen service as structural materials in well drilling applications in the Arctic (Bensted & Barnes 2002). The phosphate-modified CAC system was initially developed by Sugama and co-workers for geothermal well applications, where resistance to carbonation and favourable hydrothermal hydration properties are required (Sugama & Carciello 1992).

The compatibility between calcium phosphates and calcium aluminates has spawned a number of bioceramic applications. These range from potential reinforcement of dental cements (Morejón-Alonso 2009) and CAC based endodontic cements (Oliveira et al. 2010) to composite orthopaedic cements (Roemhildt et al. 2006). The biocompatibility of acid-base interaction of phosphates and calcium (alumino)phosphates to give apatitic cements is well documents in dental literature (Chow 2000; Chow 1991; Dorozhkin 2009b; Dorozhkin 2009a; Ambard & Mueninghoff 2006). CAC has been shown to have suitable rheology for additive manufacture and has been used to produce models for bone reconstruction (Travitzky et al. 2014; Maier et al. 2011)

2.4.1 Nuclear waste encapsulation

More recently there has been a shift in focus towards applications that consider the environmental isolation of wastes either through immobilisation or encapsulation. CAC has been shown to exhibit favourable leaching properties when encapsulating toxic metals such as lead, zinc and copper, and to be a viable waste matrix for toxic waste management (Navarro-Blasco et al. 2013). The promise demonstrated has motivated further works including the use of CAC to immobilise toxic phosphate sludges, where the sludge is the acidic precursor for the acid-base setting mechanism of the system (Navarro-Blasco et al. 2015).

The use of CAC has been identified as a possible alternative to conventional cementing systems for ILW (Ojovan & Lee 2005; Toyohara et al. 2002). The phosphate modification of CAC adapted from the original system developed by Sugama and co-workers has been shown to potentially provide a suitable matrix for the encapsulation of reactive metal containing radioactive ILW, taking advantage of

the low pH of the system (Kinoshita et al. 2013; Swift et al. 2013; Ojovan & Lee 2005). This system, the focus of this thesis is discussed in detail in section 2.5.3.

The prime concern when processing radioactive waste, prior to its long term storage, is to minimise the release of radioactive material in to the environment for as long as possible. This migration or dispersion of radionuclides maybe limited by immobilisation of the wastes via "*solidification, embedding or encapsulation*" as per the International Atomic Energy Agency definition (Ojovan & Lee 2005). Radioactive waste generated and being stored in the UK is classified in to one of the following three categories: (1) Low Level Wastes (LLW) – "*Wastes having a radioactive content not exceeding 4 GBq ([3]) per tonne of alpha, or 12 GBq per tonne of beta/gamma activity*"; (2) Intermediate Level Wastes (ILW) – "*Wastes exceeding the upper boundaries for LLW, but which do not require heating to be taken into account in the design of storage or disposal facilities*"; and (3) High Level Wastes (HLW) – "*Wastes in which the temperature may rise significantly as a result of their radioactivity, so this factor has to be taken into account in the design of storage or disposal facilities*" (Nuclear Decommissioning Authority 2010).

For wastes deemed to satisfy the criteria of ILW, cementation presents a well-established route used to encapsulate and package the material. As a result of being readily available, inexpensive and benefitting from well documented and established materials development and deployment for application, cementation was quickly adopted for this use (Glasser 1997). In the UK a Portland cement composite system is preferred, where PFA and (GG)BFS are frequently used SCMs as the complementary composite components (Setiadi et al. 2006). These are particularly chosen as they can reduce the thermal parameters, such as heat of hydration, during mixing and the initial days of curing, without which the matrix would not satisfy the parameter envelopes (Zhou et al. 2006) for such a demanding application. The consideration of these parameters is vital in maintaining chemical and mechanical properties such that the wasteform is successful in immobilising the radionuclides from the environment, both

[3] The becquerel (Bq) is the SI unit of radioactivity, defined as the activity of a quantity of radioactive material in which one nucleus decays per second.

during processing and thereafter during storage and long-term disposal. The migration of some radionuclides is considerably reduced via the reduction of their solubility (and preferential precipitation as an hydroxide), which is the case in the high pH environments of the Portland cement composites (Glasser 1997; Atkins & Glasser 1992).

However, the pH of the matrix and its pore solution can contribute to corrosion of encapsulated reactive metals, such as magnesium and aluminium, both of which are primary metallic wastes found in the Magnox waste stream arising from fuel cladding used in reactors of the same name, primarily of concern for the UK where the reactor design was developed and all but 3 (of approximately 30) are/were located (Ojovan & Lee 2005).

The aluminum content is not only limited to that arising from the MAGNOX sheathing and cladding but considerable quantities from decommissioning activities and processing. This content is selected not only from neutron activation – resulting in ^{28}Al, ^{26}Al and ^{27}Mg, in addition to 'foreign' radionuclides as a result of contamination from other materials during decommissioning and service. The corrosion of aluminium in the wasteform results in the formation of corrosion products such as hydrogen, which is flammable and potentially explosive, qualities to be avoided when considering the long-term storage of ILW. Additionally the more inert corrosion products, aluminium hydroxides and the modified surrounding cement matrix result in regions of porosity and volume changes, which are both unattractive with respect to mechanical properties of the entire waste package and also its chemical integrity.

2.5 Modified calcium aluminate cements

As with the Portland cement system, a number of modifications to the CAC system are possible, to improve the material for application throughout curing and under various conditions, this can also include minor additions to adjust the kinetics of hydration and fresh state properties, incorporation of SCMs to reduce the clinker content and thus the embodied carbon and modifications to the binder/hydration chemistries to mitigate (the effects of) conversion.

2.5.1 Additives

Common additives for the retarding of hydration include sugars, small organic acids (including sodium citrate and citric acid), glycerine (Scrivener 2003), inorganic salts such as calcium chloride, and also hydroxylic organic compounds (Bensted & Barnes 2002). Common setting/hydration accelerators include $C_{12}A_7$ and alkali salts (Scrivener 2003) and alkali hydroxides (Bensted & Barnes 2002). Well known plasticisers, such as sodium citrate and lignosulphonate, have been reported to be perform well however may have retarding side-effects (Scrivener 2003). Some notable studies are listed in **Table 2-3**.

The general mechanism ascribed for retardation of setting of these CAC castables is the chelation or binding of the calcium ions in solution or gel phases (Bensted & Barnes 2002). These mechanisms result in a greater energetic barrier for the calcium (or aluminium ions) to overcome to form the conventional hydrates, either in solution or as a result of a gelatinous diffusion barrier.

Conversely, the acceleration of hydration is generally attributed to heterogeneous nucleation (Bensted & Barnes 2002). Work carried out to report the effect of various alkali chloride salts indicated that the degree of acceleration was a function of the ionic radius of the chloride cation (Ukrainczyk et al. 2012) and it was proposed that the alkali metals in solution precipitate hydrates rapidly, removing/reducing the nucleation barrier for the conventional CAC hydrates to form and providing a suitable substrate on which they can crystallise.

Table 2-3 Reported studies of various accelerators and retarders of CAC hydration.

CAC System	Additive	Function	Reference
Istra 40 CAC	Alkali metal chloride salts	Accelerators	(Ukrainczyk et al. 2012)
Giulio Revelante HAC	Alkali metal salts	Accelerators	(Matusinović & Vrbos 1993)
Secar 51 CAC + NaP	Citric acid	Retarder	(Sugama 2006b)
Unnamed commercial CAC	Glucuronic-6,3-lactone, gluconic acid, boric acid and sodium tetraborate decahydrate	Retarders	(Sugama, Carciello, et al. 1992)
Secar 80 CAC + sodium phosphate	Boric acid, sodium gluconate, lignosulphonate and glucose polymer	Retarders	(Allan & Kukacka 1995)
Ciments Molins CAC	Transition metal nitrates	Retarders	(Navarro-Blasco et al. 2013)
Secar 71 CAC	Acetic acid	Both depending on quantity	(Smith et al. 2005)
LaFarge Ciment Fondu	Citric acid and lithium salts	Accelerators	(Rodger & Double 1984)
Secar 51 CAC + sodium phosphate + fly ash	Boric acid	Retarder	(Swift 2013)

2.5.2 Adjusting hydration to minimise or avoid conversion

There is a clear motivation to reduce the negative effects on mechanical properties associated with the conversion process of CAC materials. This has been widely investigated and has been achieved to varying degrees of success via a number of methods. Minimising the degree to which conversion affects mechanical properties of the castable during its service, whilst not actually avoiding conversion itself, is arguably the one of the most common methods of dealing with this problem. This can be achieved by limiting the water to cement ratios such that the density change is limited in a smaller volume and is recommended as good practice (Bensted & Barnes 2002). Alternatively, preferentially initiating conversion early in the curing of CAC,

or indeed the direct precipitation of the stable hydrates by curing at elevated temperatures, is another route to minimising the effects of conversion on the performance of the materials during service (Pérez et al. 1984; Scrivener 2003; Hewlett 2004).

An alternative to high temperature curing, hydration of CAC in highly alkaline media has been reported by Fernández-Jiménez et al. (2011) to result in the direct precipitation of the stable CAC hydrates from the onset, avoiding the large density changes associated with conversion part way through hydration once the final set has already taken place. Their work also reported the precipitation of silicon-substituted katoite when CAC was hydrated in highly alkaline media and in the presence of soluble silica.

The presence of silica during hydration of CAC has also been shown to preferentially precipitate strätlingite (C_2ASH_8) either from the onset or in a pseudo-conversion process of the conventional metastable hydrates. Investigations by Ding et al. (1995) showed that conversion reactions in CAC in the presence of glassy silica and sodium sulphate were avoided; this built upon work by Midgley and Rao (1978) who reported that the minor strätlingite (C_2ASH_8) formation during conversion contributed strength development despite a net strength reduction. It has been reported by Ding et al. that in the presence of sodium ions there was promoted dissolution of silica, which then reacted with the hexagonal phases to form stable crystalline C_2ASH_8, preventing the formation of hydrogarnet and minimising gibbsite formation. This work looking at C_2ASH_8 formation was continued in a later study (Ding et al. 1996), where the effect of various sodium salts (including carbonates, sulphates, nitrates, phosphates and silicates) in forming C_2ASH_8 preferentially to hydrogarnet in the presence of a siliceous zeolite was reported. This preferential precipitation was generally independent of the anion type, amongst those investigated.

The hydration of CAC in the presence of silica is of particular interest, as SCMs such as fly ash (FA) and BFS have a high silica content and can be good candidates to perform the dual function of reducing the embodied carbon and alter the hydration pathway forming siliceous hydrates, as per the work of Ding et al. This is confirmed by Mostafa et al. (2012) who report that CAC/FA and silica fume (SF) blended systems preferentially precipitate C_2ASH_8 in place of conventional stable hydrates

from the silicon incorporation by the metastable phases, and that this effect is also more pronounced in the presence of sodium sulphate. Similar studies by Hidalgo et al. (2009) reported the formation of monocarboaluminate phases at early curing periods for the SF and FA blended CAC systems, in addition to silicon substituted katoite. BFS as an SCM blended with Secar 71 has also been reported to precipitate C_2ASH_8 in place of conventional stable hydrates, and these materials show even greater sulphate resistance (Majumdar & Singh 1992; Majumdar et al. 1990).

The modification of the hydration pathway is not only limited to the formation of siliceous hydrates as the primary precipitates. The calcium nitrate (CN) modification of the CAC system was proposed by Falzone et al. (2015) to precipitate a more thermodynamically favourable AFm hydrate. This was empirically verified in the same publication and the NO_3-AFm was detected with the absence of C_3AH_6.

The effect of alkalis on the hydration of CAC hydration may be equally important as the role of the conjugate base in solution. Investigations by Fernández-Jiménez et al. (Fernández-Jiménez et al. 2008) into the alkali activation of metakaolin and CAC blended systems with NaOH solutions indicate that the hydration of CAC is significantly altered, preventing the formation of any conventional hydrate phases. It was found that two aluminium-rich intermediate gel phases were formed, where the CAC was the source of the aluminium and calcium ions forming N-A-S-H and C-A-S-H products.

2.5.3 (Sodium) Phosphate-modified CAC

In addition to its use as an additive such as in the case of improving rhelogical properties of CAC slurries (Sokolar & Vodova 2014), the phosphate modification of CAC has also been shown to be a suitable method to adjust the hydration pathway of CAC. A number of previous studies have investigated the properties of the sodium phosphate-modified CAC system, however no conclusive understanding of its hydration has been presented. Studies have shown that it is possible to produce materials with up to twice the compressive strength and greater increases in flexural strength than CAC without phosphate modification (Ma & Brown 1992). Hydrothermal treatment improved carbonation properties and formed apatitic phases (Sugama, Allan, et al. 1992) analogous to those found in bone (Kelly 2012).

The modification of CAC with ammonium polyphosphate based fertiliser was investigated (Sugama & Carciello 1991) with the aim of producing carbonation resistant geothermal well cements. It was found that the major hydration product, and primary strength contributing phase, was an ammonium calcium pyrophosphate. Phase evolution was investigated using FTIR, XPS (X-ray photoelectron spectroscopy), XRD and EDS. Samples were subjected to hydrothermal treatment at various temperatures and significant conversion from amorphous ammonium pyrophosphate and CAC precursor to hydroxyapatite and anorthite was detected after treatment at 200°C for 20 hours.

A later study by Sugama and Allan (1992) reported that FTIR analysis of the hydration product showed no P-O-P linkages at ~720 cm^{-1}, hence by comparison to orthosphosphate and pyrophosphate reference samples it was concluded that the hydration product was an amorphous orthophosphate salt, $NH_4CaPO_4{\cdot}xH_2O$. The reactivity of the CAC with the phosphoric acid was investigated using isothermal DSC. The formation of hydrated alumina gel was proposed to take place on the surface of the calcium depleted cement grain at the interface with the ammonium phosphate-rich solution. This, in addition to the NH_3, a product of NH_4^+ reaction with hydroxyl ions from CAC, controls the rate of reaction for the synthesis of the amorphous orthophosphate salt binder phase.

A similar result was demonstrated in a paper by Sugama and Carciello (1995) using monobasic orthophosphate NaH_2PO_4 and $(Na_3PO_3)_n$ with the primary hydrate phase being sodium calcium orthophosphate hydrate salts ($NaCaPO_4{\cdot}xH_2O$), identified by FTIR analysis. Again Sugama characterises the absence of P-O-P vibrations at ~720 cm^{-1} as indicating the formation of an orthophosphate.

A subsequent investigation by Sugama et al. (1999), into the exposure of phosphate-modified CAC to hot sulphuric acid, identified the binding phase as amorphous $CaHPO_4{\cdot}xH_2O$ as a result of FTIR analysis. It was maintained as in previous studies that the calcium depleted CAC grains formed a layer of hydrated alumina, which was supported by the formation of anorthite during hydrothermal treatment. In addition, hot sulphuric acid attack resulted in the further decalcification of the unreacted CAC which was suggested to form a hydrated alumina layer similar to that found during the acid-base removal of calcium ions by the phosphate anions. IR bands associated with

the amorphous calcium orthophosphate phase that remained post-acid erosion indicated that this phase is resilient to such attack.

CAC modified with varying weight percentages of sodium polyphosphate, of different chain lengths, has been shown by Ma and Brown (1992) to produce high strength materials. It was reported that the PO_4 group and the phases for which it is responsible are analogous to the SiO_4 building block and its subsequent silicate compounds. The flexural strength and compressive strength were reported to be significantly greater than in the unmodified CAC cement as a result of the decrease in average pore diameter and porosity. No crystalline hydration products were reported up to a curing period of 10 months, in agreement with a similar investigation by Walter and Odler (1996) who also investigated the effect of chain length of phosphates on the hydration behaviour of CAC, but limited their investigation to the effects on setting time and compressive strength. A later study (Ma & Brown 1994) reported that the hydrated binder phase was characterised to be an amorphous C-A-P-H gel phase which is the primary contributor to strength development, and which offset the decrease in strength and integrity associated with conversion.

More recent investigations have focused on the application of phosphate-modified CAC materials as waste encapsulation and immobilisation matrices. Due to the lower pH pore solution of unmodified CAC (Macias et al. 1996) it was identified as a suitable encapsulant for low and intermediate level radioactive waste by Swift et al. (2013), with a focus upon a minimising corrosion of encapsulated metals and satisfying a parameter envelope set out by the nuclear industry. Having previously assessed the solidification/stabilization of toxic metals in calcium aluminate cement matrices (Navarro-Blasco et al. 2013), success in using the phosphate-modified CAC system for the incorporation of Pb, Cu and Zn from aqueous metal solutions has also been reported (Fernández et al. 2014). The same group has also verified the possibility of using phosphate containing wastes from the automotive industry in producing a phosphate-modified CAC for the immobilisation of hazardous sludges (Navarro-Blasco et al. 2015).

The incoherence in the literature regarding the characterisation of the main binder consititutes one of the largest barriers to the widescale adoption of the material by industrial. When considering demanding application such as radioactive waste

encapsulation, the long-term modelling of chemical and mechanochemical properties is important to assess the performance of a matrix inside a geological disposal facilty over many years. Hence if this system is to be considered for any demanding application further investigation of its binder chemistry is required.

Table 2-4 Summary of notable investigations into the phosphate modification of CAC

Reference	CAC system	Modification	Binding phase
(Sugama & Carciello 1991)	Lumnite CAC	Ammonium dihydrogen monobasic orthophosphate (40 wt%)	Ammonium calcium pyrophosphate (anorthite & hydroxyapatite under hydrothermal cond.)
(Sugama & Carciello 1992)	C_3A, CA, CA_2	Ammonium dihydrogen monobasic orthophosphate (40 wt%)	Ammonium calcium orthophosphate salts
(Sugama & Carciello 1992)	Refcon CAC, Lehigh Cement	Ammonium dihydrogen monobasic orthophosphate (40 wt%)	Anorthite & hydroxyapatite under hydrothermal conditions (170°C)
(Ma & Brown 1992)	Secar 71, Lafarge Aluminates	$(NaPO_3)_n$, $(NaPO_3)_n{\cdot}Na_2O$, $(NaPO_3)_3$	Non-crystalline hydrates, potentially aluminate-phosphate gel
(Ma & Brown 1994)	Secar 71, Lafarge Aluminates	$(NaPO_3)_n$, $(NaPO_3)_n{\cdot}Na_2O$, $(NaPO_3)_3$	C-A-P-H gel
(Allan & Kukacka 1995)	Secar 80, Lafarge Aluminates	$(NaHPO_3)_n$, $Na_5P_3O_{10}$, $(NaPO_3)_3$	n/a
(Sugama & Carciello 1995)	Refcon CAC, Lehigh Cement	NaH_2PO_4, $-(-NaPO_3-)-_n$	Amorphous sodium calcium orthophosphate salts and hydrated alumina gel
(Walter & Odler 1996)	Secar 51, Secar 71, Lafarge Aluminates	$Na_{n+2}{\cdot}P_n{\cdot}O_{3n+1}$; where n=4,7,28 and 30	X-ray amorphous binding phase
(Sugama et al. 1999)	Refcon CAC, Lehigh Cement	$-(-NaPO_3-)-_n$	Amorphous $Ca(HPO_4){\cdot}xH_2O$ and hydrated alumina gel
(Sugama et al. 2000)	Refcon CAC, Lehigh Cement	$-(-NaPO_3-)-_n$	Anorthite and hydroxyapatite under hydrothermal conditions (280°C)

(Sugama et al. 2002)	Secar 51, 60, 71 & 80, Lafarge Aluminates	-(-$NaPO_3$-)-$_n$	Secar 51 & 61 : $Ca_3(PO_4)_3(OH)$ and g-AlOOH; Secar 71 & 80 : $Ca(HPO_4)\cdot xH_2O$
(Sugama et al. 2005)	Secar 60, Lafarge Aluminates	-(-$NaPO_3$-)-$_n$	Hydrogarnet, g-AlOOH & hydroxyapatite under hydrothermal conditions (200°C)
(Morejón-Alonso 2009)	CA phase by Pechini method	Na_2HPO_4 2.5 wt./vol. %	Conventional CAC hydrates
(Swift et al. 2013)	Secar 51, Kerneos Aluminate Technologies	KH_2PO_4, $NH_4H_2PO_4$, -(-$NaPO_3$-)-$_n$, $(NaPO_3)_6$	Amorphous calcium phosphate and hydrated alumina gel
(Swift 2013)	Secar 51, Kerneos Aluminate Technologies	-(-$NaPO_3$-)-$_n$	Amorphous calcium phosphate and hydrated alumina gel
(Fernández et al. 2014)	Electroland, Ciment Molins	-(-$NaPO_3$-)-$_6$	Amorphous calcium phosphate and hydrated alumina gel
(Navarro-Blasco et al. 2015)	Electroland, Ciment Molins	Phosphate coating sludge from automotive industry	Amorphous calcium phosphate

2.5.4 Polymer - CAC composites

In addition to those systems identified in 2.5.3, there exist phosphate-CAC composites which are defined by having discrete (and relatively inert) components bound in a phosphate based matrix. The modification of CAC by addition of polymeric compounds has been reported to exhibit considerable improvements in the compressive and flexural strengths of the cured materials, whilst maintaining the refractory properties of the base CAC, making them suitable for high temperature high performance applications (Šoukal et al. 2013).

Polymer and CAC composite systems, known as macro defect free (MDF) cements, are well known for their high flexural strength, comparatively low porosity and subsequent high compressive strength (Donatello et al. 2009; Popoola 1991). MDF cement materials are commonly prepared using a conventional CAC clinker mixed with water (at a low w/c between 0.08 and 0.2), polymer and optional plasticiser (where the polymer may be either as a dry powder or solution). High shear mixing of

the batch results in a thick dough like material, which may be pressed or extruded (Donatello et al. 2009; Georgescu et al. 2002).

Although the same process has been performed using PC, PC/SAFB and SAC systems[4] mixed with various polymers (including BA/AN, Poly-P and PBA)[5], the most widely used configuration is the CAC-polyvinyl alcohol (PVA) system (Donatello et al. 2009). The PVA modification has been shown to improve the rheological properties of the material (during the early stages of hydration) and also delay the formation of the conventional CAC hydrate, hydrogarnet.

These materials are characterised by their composite nature, where there is a bulk polymer phase, unreacted cement grains and an interfacial region where there exists an amorphous polymeric cement hydrate compounds (Donatello et al. 2009). This third interfacial region has also been described as the interaction between the hydrated surface of cement grains and bulk polymer via chemical cross-linking (Alfani et al. 1999; Kalina et al. 2014). The interfacial region has been shown to be where conventional CAC hydrates, if precipitated, are observed (Popoola 1991).

2.6 Calcium phosphate cements

It is necessary to also consider an additional category of materials, calcium phosphate cements (CPCs), as they are particularly compatible in their chemistry with phosphate-modified CAC materials, susceptible to the same beneficial effects of some CAC additives and also able to incorporate CAC materials for reinforcement (Morejón-Alonso 2009). They have been developed for a number of applications since the late 1980s, especially in the field of biomaterials due to favourable in vivo resorption characteristics due to the low crystallinity and aqueous synthesis of the hydrate phases (Dorozhkin 2009a).

The phosphate-modified CAC systems discussed in 2.5.3 and listed in **Table 2-4** generally consider the formation of a calcium phosphate type binding phase, where

[4] SAC, sulfoaluminate cement; SAFB, sulfoaluminate-ferrite-belite.

[5] BA/AN, butylacrylate/acrylonitrile; Poly-P, polyphosphate; PBA, poly (butyl acrylate).

definitive characterisation is made difficult due to its lack of long range order. As such it is important to examine the wider subset of materials to which this binding phase may belong: phosphate bonded ceramics or cements.

2.6.1 Acid base reactions

The two step acid-base method of preparing ceramic like materials is an attractive one as it occurs in the liquid phase, at ambient temperatures and yields pH neutral products (Dorozhkin 2009a). The acid-base synthesis method, which is the attributed mechanism for phosphate-modified CAC, maybe generalised by the following equations (Sugama, Allan, et al. 1992), where MO is the proton accepting metal oxide and H_2A is the acid :

$$MO + H_2A \rightarrow MA + H_2O$$ Equation 2-10

$$MO \cdot xSiO_2 + H_2A \rightarrow MA + xSiO_2 + H_2O$$ Equation 2-11

In the case of phosphate cements, setting reactions may be generally categorised as either neutralisation of acid by base or the hydrolysis of a calcium phosphate. In the case of the former where lime is the basic powder from which cations are leached and a phosphate salt in solution gives an acid, the resultant salt product formed may be "*(a) an apatite ($Ca_{10-x}(HPO_4)_x(PO_4)_{6-x}(OH)_{2-x}$); (b) a dicalcium phosphate dihydrate (DCPD, $CaHPO_4 \cdot 2H_2O$); or (c) an amorphous calcium phosphate (ACP $Ca_3(PO_4)_2 \cdot nH_2O$, n = 3.0–4.5)*" (Barinov & Komlev 2011). The hydrolysis of this third type of product, ACP, can lead to the formation of hydroxyapatite, which is used to explain the detection of HOAp after curing under hydrothermal conditions by Sugama et al. (2002), and supports their characterisation of the binding phase as ACP.

The latter method, hydrolysis of a metastable calcium phosphate, an alternative to an acid-base reaction is the one step hydrolysis of reaction of a metastable phosphate phase, as follows :

$$3Ca_3(PO_4)_2 + H_2O \rightarrow Ca_9(HPO_4)(PO_4)_5OH$$ Equation 2-12

The one step process involves little change in pH as it is the dissolution of a metastable reagent in an aqueous solvent and the subsequent precipitation of a thermodynamically favourable stable phase, as a result the Ca/P ionic ratio remains constant (Dorozhkin 2009a). The setting behaviour of apatitic cements via this method is generally slower, with the apatite phases evolving slowly resulting in a viscous paste changing into a hard paste (Bohner 2007a).

The precipitation of hydroxyapatite in calcium phosphate cements is not only limited hydrolysis reactions. The acid base reaction, investigated by Brown and Chow, involving a basic tetracalcium phosphate (TTCP, hilgenstockite) and a slightly acidic dicalcium phosphate anhydrous (DCPA, monetite) has been reported to precipitate a poorly crystalline hydroxyapatite, which is slightly basic (Bohner 2007a). The through solution reaction is shown in Equation 2-13.

$$2Ca_4(PO_4)_2O + 2CaHPO_2 \rightarrow Ca_{10}(PO_4)_6(OH)_2$$ Equation 2-13

Relative to the hydrolysis induced setting reactions, brushitic cements, setting as a result of acid base neutralisation are generally fast setting, attaining hardness from a liquid state in upwards of ten seconds. Investigated by Lemaître et al. (1987), the slightly basic β-tricalcium phosphate (β-TCP) and the slightly acidic monocalcium phosphate monohydrate (MCPM) react to precipitate a neutral dicalcium phosphate dehydrate (DCPD, brushite) (Bohner 2007a), as shown in Equation 2-14.

$$Ca_3(PO_4)_2 + Ca(H_2PO_4)\cdot H_2O + 7H_2O \rightarrow 4CaHPO_4\cdot H_2O$$ Equation 2-14

It has been shown that MCPM maybe replaced with phosphoric acid (Bohner 2007b), and in the case of the reaction of MCPM and CaO in solution with varying content of phosphate buffer (Boudeville et al. 1999), it has been reported that the replacement of water solution with phosphate buffer solution decreases the setting time, which is in

agreement with its effect on the CAC system (Fernández et al. 1994; Chotard, Smith, et al. 2003; Sugama, Allan, et al. 1992; Sugama & Carciello 1991).

2.6.2 Phosphate chemistry

Phosphate ore deposits, the most important being calcium fluorophosphates, are mined and reacted with sulphuric acid to produce phosphoric acid, H_3PO_4 (Wagh 2004). Acid phosphates such as sodium phosphates are produced via an acid-base reaction between phosphoric acid and basic sodium compounds such as carbonate and hydroxide (U.S. Environmental Protection Agency 2000). When phosphoric acid is reacted with alkaline compounds, the phosphates synthesised can produce linear, cyclic and branch chain polymers (Wagh 2004). Linear phosphates are generalised by the following structure :

$$M_{(n+2)}(P_nO_{(3n+1)})_x \qquad \text{Equation 2-15}$$

Where x is the valency of the cation M, and nx is the chain length and the number of phosphorus atoms in the molecule. When n = 1 the phosphate is referred to as an orthophosphate and where n = 2 the phosphate is known as a pyrophosphate (Wagh 2004).

2.6.2.1 Phosphate dissolution and phase precipitation

Protonation occurs during hydrolysis of phosphate chains. Phosphates which can undergo more than one protonation are labelled as polybasic. The dissolution of acidic phosphates results in a pH decrease due to the release of protons into to the solution, whereas the dissolution of oxides and hydroxides result in the release of hydroxyl ions (by uptake of protons in the solution) thereby increasing the pH of the solution. The dissociation extent therefore depends greatly upon the pH of the solution and this can determine the solubility of a compound. Therefore the dominant species in solution differs depending upon the pH.

When metal oxides dissolve in a phosphate solution, they may then combine with the phosphate anions (Wagh 2004), and this has been exploited in a number of commercially viable water softening and purification applications for a number of

years (Gilmore 1937). The dominant phases will combine but minor dissociated components will also combine to produce minor phases during precipitation.

The ionisation/dissociation constant, pK_{so}, indicates to what extent and the rate at which acids or bases dissolve in water. The pK_{so} can be calculated experimentally using the molar concentrations of the dissociated cation and anion components in solution (Wagh 2004) :

$$pK_{so} = -\log[\langle M^{n+}\rangle\langle (H_2PO_4)^{n-}\rangle] \qquad \text{Equation 2-16}$$

The ionisation constants for phosphate salts can vary greatly. From the ionisation constants for each dissociation process it is possible to calculate the likelihood of the reaction occurring at a particular pH and thereby model the relative populations of various dissociated phases for a particular phosphate salt at different pH (Migneault & Force 1988). Full deprotonisation of phosphates in solutions begins at a pH between 9 and 11 (Migneault & Force 1988).

Altering the pH of a phosphate solution results in markedly different FTIR absorption spectra, as a result of the different protonation states of the ogliomers. Hence, this technique is widely used for the characterisation of phosphates in solution and in powder form. The increase in protonation of the anionic phosphate in solution results in a decrease for the ν_{as}(P-O) vibrations bands and an increase in the absorption of ν_{as}(P-OH), thereby also resulting in a frequency shift (Gong 2001).

2.7 Concluding remarks

Phosphate-modified calcium aluminate cement displays great potential as a material for applications where it exhibits properties that improve upon those belonging to existing neat CAC or Portland cement based solutions. These include use in vivo for biomedical applications due to high bioresorptivity, in composite materials for refractory and some niche structural applications, and as toxic/radioactive waste encapsulation matrices.

The acid-base reaction results in rapid hardening and formation of reaction product with a comparatively neutral pH, whilst minimising and potentially avoiding the conversion process and hence maintaining the strength profile of CAC materials. Hence this material, originally developed for geothermal well applications as it maintained high chemical and mechanical integrity under geothermal conditions, has more recently been proposed as a versatile waste encapsulation matrix. Intermediate level radioactive wastes often contain reactive metals such as magnesium and aluminium, which under high pH conditions, such as in Portland cement systems, may corrode rapidly and reduce the integrity of the wasteform.

Although there is some existing literature regarding the phosphate modification of the CAC system, an incomplete picture of the hydration behaviour exists in addition to there being an incoherence as to the binding phase characterisation. Specifically, there is disagreement in the literature regarding the characterisation of the chemical composition of the binding phase: whether it is a calcium orthophosphate hydrate or a C-A-P-H gel? When considering this material for specialised applications in vivo or encapsulating toxic/radioactive wastes, its performance over biological timescales or extended geological time periods cannot be anticipated without investigation of the hydration pathway and characterisation of the binding phases as a function of immediate time periods.

The precursor to this work, conducted by Swift (2013), examined the fresh state properties of a similar system, focusing on its suitability as a ILW encapsulation matrix, specifically looking at fresh state properties of the material and conformation to processing standards set out by industrial bodies immobilising such wastes. However the system chosen was complex with a number of additives and without a

experimental design to examine the effect of phosphate, hence it is difficult to determine the fundamental interaction between the phosphate and CAC during hydration and how to leverage this to improve materials properties. Fundamental investigation of the system is required before such materials can be considered for the applications to which it has been attributed, especially demanding ones such as ILW encapsulants. The following chapters examine the characterisation of the evolving system, assessing the fresh state behaviour and long term hydration of the system modified with phosphates – an area which is underrepresented in the existing body of literature – using conventional techniques and advanced NMR spectroscopy. In support of this additionally some complementary trialling of the system to assess the corrosivity of aluminium is required.

3 Experimental procedures

3.1 Materials

3.1.1 Calcium aluminate cement

The calcium aluminate cement used throughout this project was supplied by Kerneos Inc., from their SECAR range. SECAR 51, the trade name for the clinker selected for this work, was composed primarily of calcium aluminates with a very low iron content, as a result of its manufacture from white bauxite. The oxide composition as provided by the manufacturer is displayed in Table 3-1. Cement was stored in sealed plastic containers at 20°C in a dry environment.

Table 3-1 Oxide composition of Secar 51 from X-ray fluorescence analysis (Kerneos Inc 2006)

Raw Material	Chemical constituents (% as oxide)							
	Al_2O_3	CaO	SiO_2	Fe_2O_3	TiO_2	MgO	SO_3	K_2O + Na_2O
Secar 51	≥50.0	≤39.5	≤6.0	≤3.0	<4.0	<1.0	<0.4	<0.5

3.1.2 Phosphates

Two sodium phosphates were used in this project to elucidate their effect on hydration which has not been studied extensively (as discussed in Chapter 2), reagent grade sodium polyphosphate [$(NaPO_3)_n$, 97%, Acros Organics], sodium dihydrogen phosphate dihydrate (monophosphate, $NaH_2PO_4 \cdot 2H_2O$, 99%, Acros Organics).

3.1.3 Aluminium

Three different types of metallic aluminium were used in this study: aluminium plate with 3 mm thickness, grade 1050 (supplied by BNFL (now NNL), elemental composition shown in Appendix A), and cut to a desirable size, used for mass loss studies; aluminium wire (99.98 %) obtained from BDH Chemicals (UK) with a diameter of 0.75 mm was used for image analysis experiments; and fine aluminium

powder (general purpose grade) obtained from Fisher Scientific was used for all other corrosion experiments.

3.2 Sample synthesis

Samples were prepared following a two-step process: (stage 1) initial phosphate dissolution, followed by (stage 2) mixing of the phosphate solution with the anhydrous cement clinker.

Stage 1: Phosphate powders were weighed, mixed with distilled water, and mixed in airtight cylindrical containers on a roller mixer for 24 h at 20°C. When formulations required both monophosphate and polyphosphate, the powders were measured, mixed and then introduced to the distilled water simultaneously.

Stage 2: The mixing protocol depended on the quantity of slurry being prepared: (i) small batches of mass <50 g, were hand mixed. In this case, the cement powder was added to the mix water (with or without dissolved phosphates) during a period of 30 s during hand mixing with a steel spatula, and then stirred for a further 120 s; (ii) large batches of mass >500 g were shear mixed, with an initial 30 s of hand mixing of the solution with the anhydrous cement, followed by shear mixing using a Silverson L4RT high shear mixer for 120 seconds at 2500 rpm. Mixing was conducted at 20°C in a temperature-controlled environment.

3.2.1 Formulations

Formulations considered consist of those with either (i) only sodium polyphosphate modification, (ii) only sodium monophosphate modification, or (iii) modification by a combination of these phosphates. Sample names are indicative of their formulation and can be described by the general form "*P*p*M*m", where *P* and *M* are the polyphosphate and monophosphate to dry cement clinker ratios, defined on a mass basis, respectively. Precursor quantities for example formulations are shown in Table 3-2.

Table 3-2 Precursor quantities for example formulations

Formulation	Total Slurry amount, (g)	w/solid	p/cement	m/cement	Secar 51 (g)	Polyphosphate (g)	Monophosphate (g)	Water (g)
Neat CAC	1000	0.35	0	0	740.74	0.00	0.000	259.26
0.4p0m	1000	0.35	0.4	0	571.43	228.57	0.000	200.00
0.4p0.05m	1000	0.35	0.4	0.05	555.56	222.22	27.778	194.44
0p0.1m	1000	0.35	0	0.1	689.66	0.00	68.966	241.38

3.3 Analytical techniques applied to fresh pastes

3.3.1 Vicat penetration

The setting time of prepared slurries was determined by the Vicat needle penetration method ASTM Standard C807 – 08 (2008). Both the initial and final setting times of a paste can be determined using this method. The setting behaviour was characterised by the depth of penetration by a needle into the freshly prepared sample. As soon as reasonably possible after mixing, the slurry was cast into a lubricated smooth cylindrical mould, with inside diameter 60 ± 0.5 mm and depth of 40 ± 1 mm, resting on a flat surface. The mould was agitated to ensure the evacuation of any air bubbles and the exposed surface of cement was cut with a trowel such that the slurry was flush with the top of the mould. This was then placed on a rotating stage in the Vicat apparatus where a needle drops from above the exposed surface of the mould, penetrating the cement with each downwards motion, at regular intervals.

Sample testing was performed using a MASTRAD Vicat penetration apparatus. Needle penetrations were at least 10 mm apart from each other and tests were performed at 23 ± 5°C.

3.3.2 Isothermal calorimetry

Calorimetry is a versatile technique, which can be used to measure the heat flow between a material and its surrounding during either a reaction or thermal treatment (Ramachandran et al. 2002). This is particularly useful in cement chemistry, particular in characterising constituent phases in a complex multiphase material or to monitor the heat flow during the early stages of hydration. The heat flow between a material and its surroundings is a function of a number of properties, both physical and chemical, of the material itself or a process/reaction taking place.

Isothermal conduction calorimetry experiments, where a constant temperature inside the chamber is maintained during the experiment, are particular useful in monitoring the exothermic hydration of reactive minerals. Samples and references are housed in separate thermally insulated chambers and the difference in heat flow between the sample and reference to their respective surroundings is measured. Isothermal calorimetric studies of cement hydration were conducted using an eight channel TAM AIR Microcalorimeter. Temperatures were maintained at 25 ± 0.02 $^{\circ}$ C and fresh paste was mixed externally, weighed into a plastic ampoule, and immediately placed in the calorimeter. Care was taken to not contaminate the outer surface of the ampoules. The heat flow was recorded for the first 70 or 270 h of reaction, depending on the formulation. All values of heat release rate were normalised by the total mass of paste being studied. The instrument reference ampoules contained the same quantity of water as the samples being tested.

3.3.3 Fourier transform infrared spectroscopy

Fourier transform infrared (FTIR) spectroscopy is a powerful non-destructive technique assessing the bonding between atoms within a material. Bonded structures and molecules contain atoms connected by bonds (Schrader 1995) which can exist with different energy states. These bonds are free to vibrate and may be excited by incident radiation, the specific wavelength of which is a function of a number of internal structural variables. Photons of a specific energy, which satisfies the energetic transition from one quantised vibrational state to another, are absorbed, resulting in an absorption spectrum. As the energies required for the excitations are discrete and specific to the vibrational mode, the nuclides involved and the number of atoms in the mode (Siesler et al. 2008), the absorption lines in the spectrum are characteristic of the structure being studied. The vibrational modes induced may be stretching (oscillation of the bond length) or bending (oscillation of the bond angle between a wide maximum angle and a narrow minimum) and these may vibrate either in phase or in antiphase (referred to as symmetric and asymmetric respectively) (Theophanides 2012) . Hence the technique is particularly useful in extracting structural information as well as semi quantitative information.

Transmission FTIR experiments, parameters for which are described in section 3.4.4, pass an infrared beam through the sample at after which point the spectrum is detected. Although particularly useful for the study of materials in the solid state, this method requires that certain considerations be made during sample preparation (Griffiths & Haseth 2007), such as being able to produce thin samples; no band having too great an absorbance; grinding and pressing effects on the spectra; and the sample to be a solid mixed with a IR transparent matrix material such as potassium bromide. An alternative, attenuated total reflection (ATR) FTIR, is a method which requires the sample to be placed directly upon a crystal and maintain sufficient contact area with the crystal (Griffiths & Haseth 2007). As a result of the straightforward sample preparation, this technique has become increasingly attractive over transmission FTIR and is the preferred method when studying liquids. In the ATR case the broadband IR spectrum is directed through the crystal, propagating by one or more (user controlled parameter) total internal reflections achieved by striking the boundary of the crystal at an angle greater than the critical angle (which is a function of the interfacial boundary). The evanescent field of the radiation, created at the interface as a result of the totally internally reflected wave, penetrates the sample placed at the interface and is susceptible to the same absorption phenomena observed for conventional transmission FTIR (Schrader 1995). The obtained spectrum, post Fourier processing, resembles the transmission spectrum and its sensitivity may be adjusted by altering the number of reflections (Schrader 1995). The depth of penetration of the evanescent field is in the order of microns, depending upon the crystal used (Solé et al. 2005), and hence this is a common pseudo-bulk technique in surface analysis of solids.

For ATR FTIR experiments a PerkinElmer Spectrum 100 FTIR Spectrometer with Universal diamond crystal ATR accessory fitted was used. Spectra obtained for liquids were collected with a resolution of 4 cm^{-1}.

3.4 Analytical techniques applied to powdered raw materials and hardened pastes

3.4.1 Pre-conditioning of the specimens

Large batches of paste were prepared, and slurries were cast in airtight centrifuge tubes and cured in an environmental chamber that maintained a temperature of 20°C. After curing for the required duration, samples were demoulded and hydration was arrested.

Arresting hydration prior to any analysis was necessary to ensure that a defined degree of hydration is maintained for all samples (Zhang & Scherer 2011), so that data obtained from analysis techniques can be considered in the context of the extent of hydration/ curing period. This process attempts to maintain the phase assemblage, and induce minimum microstructural changes in the material, by removing unbound pore water, which facilitates further hydration. The removal of water can be achieved by the solvent exchange method, where the monolith is crushed and immersed in a bath of an organic liquid with low surface-tension properties (Knapen et al. 2009; Zhang & Scherer 2011) and negligible interaction with hydrate phases or the anhydrous clinker, which drives the replacement of water by the solvent.

Samples in this study were arrested by immersion in acetone for 48 h, following crushing. Excess acetone was drained and the cement was left to air dry for 24 h, after which samples were stored in a vacuum dessicator at ~50 Torr, to prevent reaction with the atmosphere, particularly carbonation. Prior to subjecting samples to any of the analytical techniques mentioned (unless otherwise noted), and after the hydration reaction was arrested, the samples were ground and sieved to pass a 53 μm sieve.

3.4.2 X-ray diffractometry

X-ray diffraction (XRD) was used to determine the crystalline phases present in the samples. XRD is a widely used non-destructive method to determine constituent crystalline phases from characteristic diffraction of incident monochromatic X-ray radiation. The distances between adjacent atoms within a lattice structure, the bond lengths, are similar in size to the wavelength (λ) of the radiation. This similarity of the two lengths results in the diffraction of the incident X-rays, with the regular repeating structure of the crystal acting as a diffraction grating (Clearfield et al. 2008). Figure 3-1 shows a schematic of the diffraction of three incident X-rays from three planes of a lattice in a crystal.

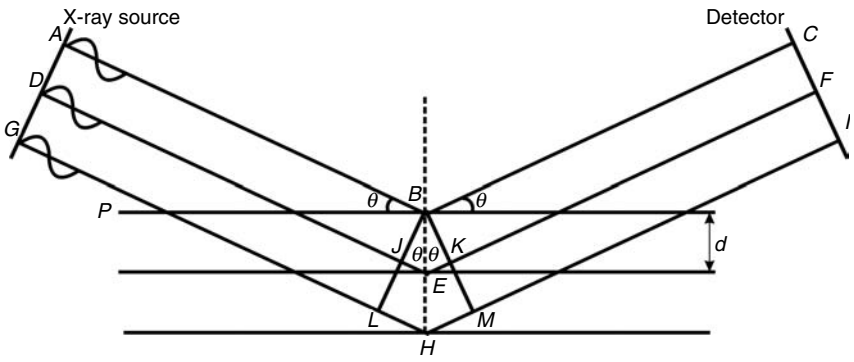

Figure 3-1 Bragg Diffraction of incident radiation from a set of parallel planes (Clearfield et al. 2008).

In this geometric arrangement the wavelets which penetrate to each subsequent plane, deeper into the crystal from the surface, travel further. For diffraction to occur the difference in path length between wavelets reflecting from different planes must be an integral number of wavelengths, such that the reflected wavelets are all in phase (Clearfield et al. 2008). When these are not in phase, destructive interference would result, thereby reducing the intensity. Conversely, coherent wavelets go on to constructively interfere. This is described by Bragg's law, Equation 3-1 , where *n* is an integer determined by the order of the interference, *d* is the interplanar distance and θ is the scattering angle.

$$2d \sin\theta = n\lambda \qquad \text{Equation 3-1}$$

The values of θ at which there is constructive interference are characteristic for each configuration of atoms in the unit cell. Hence, it is possible to identify the structure based upon these 'reflections', by cross-referencing with an index or database of characteristic diffraction data for known structures such as the Powder Diffraction File (PDF) developed and maintained by the International Centre for Diffraction Data (ICDD).

In the case of a finely ground powder, an ideal sample has a representative number of crystals of each constituent phase of the bulk specimen, with crystals randomly oriented. Such a large number of particles (>1 million) causes averaging effects (Clearfield et al. 2008). Certain preferred orientations can be induced by improper sample preparation, however this can be reduced by sample rotation during irradiation and data collection.

X-ray diffraction was performed using a Siemens D5000 Diffractometer using a copper source (Cu Kα, 0.15418 nm) from a fine focus sealed tube source running at 40 kV and generating at 40 mA. Scans were continuous in the 2θ range 5-55° with a step size of 0.02 and at a rate of 1°/min. These parameters were used for all experiments unless otherwise stated.

3.4.3 Thermogravimetric analysis

Thermal analysis techniques measure the change in a particular property of a material as a function of temperature as it undergoes thermal treatment (Ramachandran et al. 2002). These properties studied can include mass loss, heat flow, optical and acoustic properties. Thermal analytical techniques have been primarily utilised in this study to characterise and quantify phase assemblages through thermal decomposition processes.

Thermogravimetric analysis (TGA) is a technique which measures the mass loss of a sample as a function of the temperature of the sample. This is particular useful in identifying the dehydration or decomposition of phases. Mass losses as a result of dehydration or decomposition occur at characteristic temperatures depending on the way water or other functional groups such as hydroxyls, carbonates, sulphates, nitrates, among others, are incorporated into the specific structure of each of the phases forming in the system.

This is achieved by a configuration involving a microbalance inside a furnace (Ramachandran et al. 2002), from which data are logged as a function of temperature. Data are conventionally plotted with the percentage of the sample weight remaining as a function of temperature known as a TG curve or thermogram, however the first derivative of this curve, a DTG curve, is often plotted as well. The DTG curve is plotted in units of wt%/°C, and helps in distinguishing the mass losses due to dehydration/decomposition of a particular phase in a multiphase material. Depending on the crystallinity of the phase, and/or phase contamination, mass loss can occur over a wide temperature range with a Gaussian shaped peak (equivalent to a shallow slope in the TGA curve) (Gabbott 2008) centred about the characteristic temperature (which is the value quoted in discussions throughout this thesis) for the dehydration/decomposition process. Experimental parameters such as heating rate,

sample preparation and atmosphere used can affect either the rates or temperature ranges at which dehydration/decomposition processes occur, or can modify the chemistry of samples during testing.

In this thesis, TGA experiments were performed using a PerkinElmer TG Analyser, with a heating rate of 10°C/min starting at room temperature to a maximum temperature of 1000°C. The starting mass of sample being tested was kept at 40 mg for all experiments, and all were conducted under nitrogen flow (flow rate of 40 ml/s) with alumina crucibles/pans samples during heating and data collection.

3.4.4 Transmission FTIR spectroscopy

In addition to the ATR FTIR analysis of fresh pastes and liquids as described in section 3.3.3, transmission FTIR spectroscopy was also performed on powder samples to take advantage of the higher resolution achievable by this technique at low wavenumbers, as a result of a better signal to noise ratio.

The schematic configuration of a transmission FTIR spectrometer consists of a source emitting a continuous spectrum of infrared radiation, which as a beam passes through a Michelson interferometer. During the data collection the detector is adjusted such that the focal plane, where the maximum constructive interference occurs, moves relative to the detector (Solé et al. 2005). The resultant of this is the detection of a set of periodic maxima and minima, a sinusoidal function of the displacement of the interferometer, when considering a simple case of incident monochromatic radiation. The resultant interferogram, an interference pattern made up of periodic maxima and minima may be processed using Fourier mathematics to identify the frequencies present (Siesler et al. 2008). Absorptions at particular frequencies as a result of bonding within the sample are easier to identify once the Fourier processing has been completed, manifesting as intensity drops in the frequency resolved spectra.

Transmission FTIR experiments were performed using a PerkinElmer FTIR Spectrometer SPECTRUM 2000 with a wavenumber range of 400-7000 cm^{-1} and 4 scans per spectrum collection. Samples were prepared using ground and sieved cement powder mixed with potassium bromide (infrared transparent) in a mass ratio of 1:100 and total mass of 0.2 g, pressed into pellets with a pressure of 10 tonnes.

3.4.5 NMR spectroscopy : fundamental theory

Nuclear magnetic resonance (NMR) spectroscopy can be used to determine the structure of materials and the dynamics of processes occurring within them (MacKenzie & Smith 2002).

The resonance of nuclei at their characteristic frequencies is exploited in an NMR experiment. Nuclei have a quantum property, known as spin (I), which as with all quantum numbers has quantised value (in this case either integer or half-integer). This nuclear spin arises as a result of the spins associated with the constituent subatomic particles of a nucleus, and those nuclei with even mass number and even charge have zero spin and are not NMR active (MacKenzie & Smith 2002). The angular momentum or nuclear magnetic momentum, ($\mathbf{I} = \mathbf{I}_x + \mathbf{I}_y + \mathbf{I}_z$), of a nucleus is a function of the spin and the presence of a static magnetic field ($\mathbf{B}_0$). As a result of Zeeman splitting, shown in Figure 3-2, which occurs for a nucleus in a magnetic field, a set of non-degenerate nuclear energy levels are created (Smith & van Eck 1999), where the total number of energy levels, a function of the spin number, I, is 2I+1 states. In the presence of the magnetic field, the precessing vector $\mathbf{I}$ aligns either parallel or antiparallel to $\mathbf{B}_0$ (Engelhardt & Michel 1987).

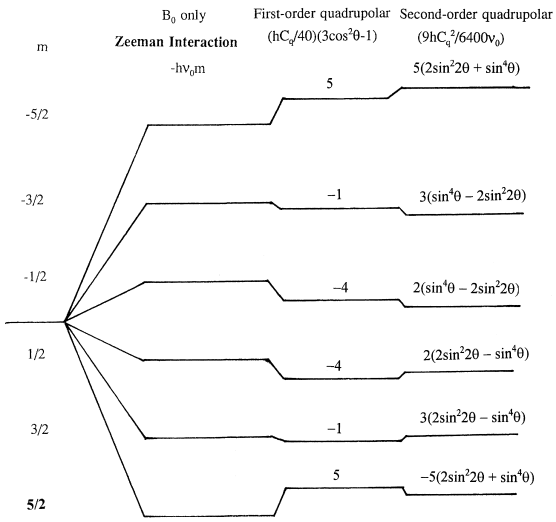

Figure 3-2 Nuclear energy level diagram showing the effect of a magnetic field and the quadrupolar interaction (Smith & van Eck 1999).

Nuclei may be excited to transit from one energy level to another, which is achieved by irradiation by an electromagnetic wave in the radiofrequency (RF) wavelength range. Electromagnetic waves consist of electrical and magnetic fields oscillating perpendicular to one another and it is the magnetic component of the RF irradiation, known as the applied magnetic field or $\mathbf{B}_1$, which interacts with the nuclear magnetic momentum vector (MacKenzie & Smith 2002). To affect **I**, the frequencies of precession of the momentum vector, known as the Larmor frequency (specific to the nuclide), and that of the RF wave must be matched (Aravamudhan n.d.).

The z-component of this momentum vector changes, and the x and y components become non-zero, as a result of the irradiation as shown in Figure 3-3. However I maintains its precession motion, describing a cone shaped volume whose radius is a function of the irradiation.

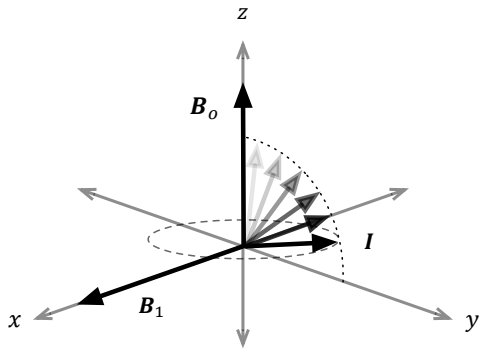

Figure 3-3 Effect of applied magnetic field upon the nuclear magnetic momentum vector, adapted from MacKenzie and Smith (MacKenzie & Smith 2002).

When the applied magnetic field pulse finishes, the spin vector continues to precess and simultaneously realign along the z direction, as it was before the RF irradiation; this period is the T_1 relaxation and is characteristic of the nuclide (MacKenzie & Smith 2002). The sample is housed in a sample holder encased with a coil, which is arranged such that any changes in magnetic field in the x-y plane result in a change of magnetic flux through the wire. This changing flux results in an induced electromotive force (emf), which when plotted as a function of time is known as a free induction decay (FID) (MacKenzie & Smith 2002). Multiple bonding environments of the detected nuclide present in a sample further complicate the FID. In this case during irradiation the momenta may be considered to be in phase,

however as the irradiation is halted, there is a period of dephasing as the vectors precess with different angular velocities, which is referred to as T_2 relaxation. Additionally, multiple contributions to the induced emf in the coil complicate the signal considerably.

To calculate the constituent frequencies of precession present in the spin ensemble contributing to the detected emf, Fourier mathematics can be adopted to plot the intensity as a function of frequency. This obtained spectral plot is the basis for displaying collected NMR data. However, the frequencies obtained are a function of the magnetic field strength of the spectrometer (the static field $\mathbf{B}_0$) (Keeler 2002), which is inconvenient when comparing with datasets obtained from different instruments at different field strengths. To remove this dependency upon the field strength, the data are normalised with respected to a reference sample using the relationship in Equation 3-2.

$$\delta = \frac{\upsilon - \upsilon_{ref}}{\upsilon_{ref}} \qquad \text{Equation 3-2}$$

Where δ is the chemical shift in units of parts per million (ppm) relative to the resonance frequency of the reference sample, and υ and υ_{ref} are the constituent frequencies and the frequency of the reference respectively (Keeler 2002).

3.4.5.1 Magic Angle Spinning (MAS)

The advent of the NMR technique attracted great application within the field of solution chemistry, where structurally informative spectra could be obtained with relative ease despite the technological limitations of the period (MacKenzie & Smith 2002).

The magnetic field experienced by a nucleus is described by the nuclear spin Hamiltonian, $\hat{H}$, that accounts for all mechanisms contributing to the total interaction energy, including both external and internal spin interactions. In the case of liquids, rapid atomic motion occurring faster than the interaction frequency of the nuclei results in the effect of some contributors to the spin Hamiltonian being nullified or minimised. The nuclear spin Hamiltonian is the sum of seven different interactions as described by Equation 3.3, where $\hat{H}_Z$ is the Zeeman interaction with $\mathbf{B}_0$; $\hat{H}_{RF}$ the interaction of the momentum with the $\mathbf{B}_1$ field; $\hat{H}_D$ is the dipolar interaction between two dipoles (through space spin-spin interaction); $\hat{H}_J$ is the electronically mediated spin-spin interactions; $\hat{H}_{CS}$ is the chemical shielding (resulting in effective $\mathbf{B}_0$ due to the effect of nearby electrons); and $\hat{H}_Q^{(1)} + \hat{H}_Q^{(2)}$ are the first and second order quadrupolar interactions (where the nuclide has spin I > ½ and charge distribution is not spherical) (Klinowski 1984; MacKenzie & Smith 2002).

$$\hat{H} = \hat{H}_Z + \hat{H}_{RF} + \hat{H}_D + \hat{H}_J + \hat{H}_{CS} + \hat{H}_Q^{(1)} + \hat{H}_Q^{(2)} \qquad \text{Equation 3-3}$$

The first two terms of the Hamiltonian, $\hat{H}_Z + \hat{H}_{RF}$, are dependent upon experimental parameters and are considered external interactions, whereas the remaining terms are termed internal interactions.

In the case of liquids, the limited internal interactions result in the nuclei in similar bonding environments experiencing the same effective magnetic field. The spectral consequence of this is sharp and well defined resonances, which are structurally informative and easier to discern as individual peaks. In the case of solid samples internal interactions dominate, resulting in broad-line spectra. The line shapes are broadened to such an extent that structural analysis is extremely difficult, limiting the utility of static solid state NMR, however a technique known as Magic Angle

Spinning can to a significant extent reduce the contribution of some of the internal interactions. Each of the $\hat{H}_D$, $\hat{H}_{CS}$ and $\hat{H}_Q^{(1)}$ averaged interactions have a $(3\cos^2\theta - 1)$ dependency (MacKenzie & Smith 2002), which can be reduced to zero by rapidly spinning the sample at an angle of $\theta_m = \arccos(1/3)^{1/2}$ (~54.736°) to the static magnetic field. Additionally, the second order quadrupolar interaction, $\hat{H}_Q^{(2)}$, is also partially reduced by spinning at this angle but not to the same extent as other internal interactions. This is due to a more complex spatial term, which results in a dependency upon two trigonometric functions (Equation 3-4 and Equation 3-5) of the same variable. The $P_2(\cos\theta)$ dependency is the same as that found in the internal interactions, however the solution to the $P_4(\cos\theta)$ dependency is θ = 30.6°, 70.1°. Hence there is no single angle to the magnetic field at which the rotor may be spun to remove all quadrupolar interactions (Frydman et al. 2002), .

$$P_2(\cos\theta) = \tfrac{1}{2}(3\cos^2\theta - 1) \qquad \text{Equation 3-4}$$

$$P_4(\cos\theta) = \tfrac{1}{8}(35\cos^4\theta - 30\cos^2\theta + 3) \qquad \text{Equation 3-5}$$

Figure 3-4 shows the effect of magic angle spinning on the line shape of the spectra collected. In addition to a reduction in broadening there are additional peaks, known as spinning sidebands; at low spinning frequency the averaging effect for the chemical shift anisotropy is incomplete, resulting in additional peaks equally spaced as a function of spinning speed (Andrew et al. 1958; MacKenzie & Smith 2002). Hence, high spinning speeds are used to ensure that these sidebands do not overlap the main transition, simplifying any subsequent analysis.

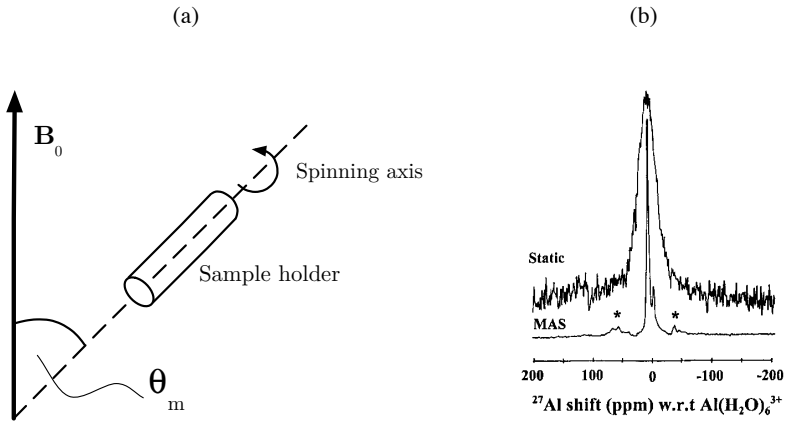

Figure 3-4 (a) Spinning axis oriented at the magic angle, and (b) effect of spinning at the magic angle upon observed line shape for a sintered alumina-yttria mixture(MacKenzie & Smith 2002).

MAS experiments were carried out a Varian VNMRS 200 spectrometer (operating with a 9.4 T field) using a CP/MAS probe with 4 mm o.d. zirconia (PSZ) rotors. Spectra collected for ^{27}Al, ^{23}Na and ^{31}P MAS, MAS NMR are referenced to external samples of 1.0 M aqueous solution of $AlCl_3 \cdot 6H_2O$, 1 M aqueous solution of NaCl and 85% H_3PO_4, respectively. This spectrometer, probe, rotors and references were used for all MAS experiments unless otherwise stated.

3.4.5.2 Cross polarisation (CP)

Rare nuclei such as ^{13}C and ^{15}N, so termed due to their low natural abundance, are difficult to study as a result of low signal intensities and low spin polarisation (Laws et al. 2002). The study of these nuclei has been greatly aided by a technique known as cross polarisation, where the spin polarisation may be transferred from easily polarisable nuclei to those of interest.

This is achieved by initial irradiation of the abundant nuclei, often ^{1}H, followed by irradiation by a second RF wave on the rare-nucleus channel. The transfer of magnetisation/spin polarisation is thermodynamically favourable, however to facilitate a more rapid transfer the two sets of nuclei have to be able to 'communicate' efficiently (MacKenzie & Smith 2002). Effective 'communication' and spin polarisation transfer is achieved by satisfying the Hartmann-Hahn condition, Equation 3-6, where I and S refer to the two nuclei and γ is the gyromagnetic ratio.

$$\gamma_I \mathbf{B}_{1I} = \gamma_S \mathbf{B}_{1S}$$ Equation 3-6

The mechanism of transfer is via the spatially dependent magnetic heteronuclear dipolar interaction (Kolodziejski & Klinowski 2002). However, the technique is often used in conjunction with magic-angle spinning, which averages the $\hat{H}_D$ interaction complications that would otherwise result in spectral distortion (MacKenzie & Smith 2002). This dipolar interaction is characterised by the internuclear distance and mobility of functional groups (Kolodziejski & Klinowski 2002), rather than being electronically mediated as is the $\hat{H}_J$ interaction, but nevertheless does provide substantial structural information. Specifically the connectivity between the nuclei may be assessed, in the field of cement chemistry this technique can be used in qualitatively assessing the degree of protonation of phases and thus identifying resonances associated with hydrate phases (Klinowski 1984).

CP experiments were carried out under MAS conditions using the same spectrometer, field strength and probe as the MAS experiments. CP/MAS data are referenced to the same standard reference compounds as in the MAS experiments.

3.4.5.3 REDOR/ REAPDOR

The multiple internal nuclear spin interactions that exist in a complex sample result in a large number of variables affecting the resonant frequency of a particular nucleus, other than just the general environment, resulting in broader peak shapes and fewer identifiable characteristic peaks. Hence for these powder samples it is important to collect spectra under MAS conditions, however the supressed internal interactions are functions of the structural properties of surrounding nuclei. These interactions may be selectively exploited to either facilitate more efficient experiments, as in CP/MAS, or to determine chemo-structural variables, which govern those interactions.

Double resonance experiments such as REDOR (rotational echo double resonance) and REAPDOR (rotational echo adiabatic passage double resonance) both take

advantage of the heteronuclear dipolar interaction, $\hat{H}_D$. Over a rotor period, under MAS conditions, the dipolar coupling function integrates to zero (Laws et al. 2002), however π pulses on the secondary (S) nucleus channel can change the sign of the dipolar coupling, as seen in Figure 3-5. This sign change is as a result of reversing spin polarisation of the S nuclei, and the resulting dipolar function does not average with time. With the recombinant dipolar coupling, the magnetisation of the I spin decays due to averaging effects (Frydman et al. 2002), whereas in the absence of the S channel irradiation there would be focusing of the signal after an integer number of rotor cycles.

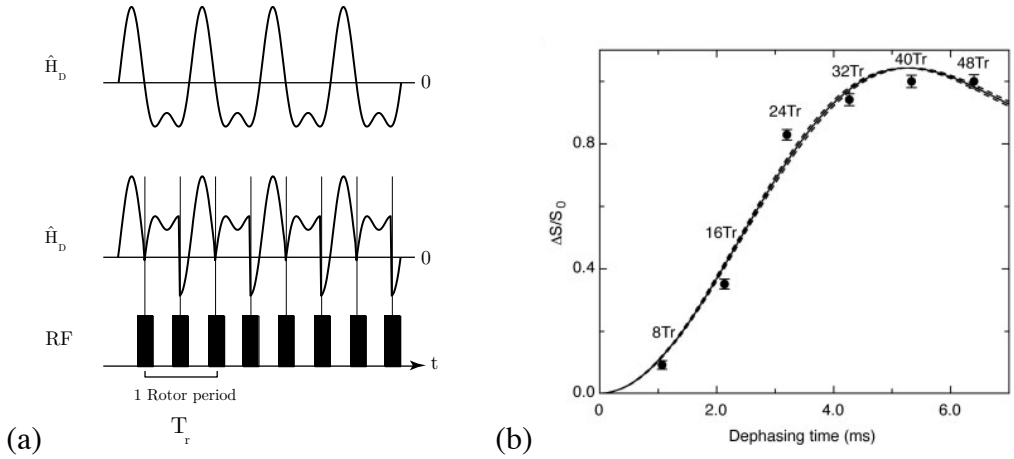

Figure 3-5 (a): Top: Heteronuclear dipolar coupling as a function of time; bottom: Heteronuclear dipolar coupling as a function of time with two π pulses per rotor. Adapted from Frydman et al. (Frydman et al. 2002). Right(b): an example of a typical REDOR dephasing curve (Kovacs & Fowler 2007).

The extent of the intensity decrease (Δ*S*) is a function of both external parameters, such as the pulse sequence, and internal factors characterised by the dipolar coupling constant (Equation 3-7).

$$D = \frac{1}{2\pi}\frac{\gamma_I\gamma_S}{r_{IS}^3}\cdot\frac{\mu_0}{4\pi} \qquad \text{Equation 3-7}$$

Internal interaction parameters may be calculated by calculating the REDOR fraction, ($\Delta S = S_0 - S$) , where S is the signal intensity under the same conditions without S dipolar recoupling. Multiple experiments are performed with increasing numbers of pulses (n) on the S channel, whilst maintaining the same time period between each pulse, thus increasing the dipolar dephasing effect on the collected spectra. REDOR fractions for each experiment can be calculated and ($\Delta S/S$) is plotted as a function of the S channel pulse scheme duration (nT_r), as shown in Figure 3-5 (b). The dephasing curve is a function of the dipolar coupling interaction and the pulse scheme parameters. The major objective of this type of experiment is to calculate the internuclear distance between the two nuclides involved in the interaction. This is achieved by fitting the dephasing curves to a universal dipolar dephasing curve (MacKenzie & Smith 2002):

$$\frac{\Delta S}{S} = 1 - \frac{1}{2\pi}\int_{0}^{\beta=2\pi}\int_{0}^{\alpha=\pi/2}\cos[2\sqrt{2}nT_r D\sin 2\beta\sin\alpha]\sin\beta\,d\alpha\,d\beta \qquad \text{Equation 3-8}$$

Where α and β are the azimuthal and polar angles defining the principal axis system of the dipolar tensor in the lab frame (the z axis is parallel to the rotational axis of the spinning rotor) (Pan et al. 1990; MacKenzie & Smith 2002). Gullion and Vega (2005) have reported a simplified version of Equation 3-8 and accounted for various S spin values ($\frac{1}{2} - \frac{7}{2}$).

The REDOR technique is particularly effective for spin ½ - ½ dipolar recoupling, however it is considerably more difficult for quadrupolar nuclei with spin I > ½. Applying a π pulse to a broad resonance is difficult and generally ineffective (Tannús & Garwood 1997), as a result of the dominating quadrupolar interaction, hence very few of the quadrupolar nuclei transit between spin states as desired (Gullion & Vega 2005). REAPDOR, a very similar experiment also utilising the dephasing dipolar effect, addresses this disadvantage of the REDOR technique by applying an adiabatic pulse to introduce the dipolar coupling (Hughes et al. 2002).

An adiabatic pulse, in contrast to π pulses, has a frequency that varies with time during the pulse (Tannús & Garwood 1997), and one pulse irradiates the quadrupolar nuclide channel as shown in Figure 3-6. Adiabatic pulses take advantage of the oscillations of the quadrupolar splitting (Gullion & Vega 2005; Tran 2011), which are present due to the time dependency introduced by magic angle spinning. Much like the REDOR technique, REAPDOR analysis plots the dephasing effect of the dipolar coupling as a function of the evolution period (a function of m in Figure 3-6)These dephasing curves are more complex than those obtained in the REDOR experiment. Two important considerations are: (i) not all spins will transit state, and (ii) spin state transitions that do occur change quantum state by either 2 or 1 ($\Delta m = \pm 1,2$ where m is the eigenvalue for the z component of the magnetisation vector $\mathbf{I}$, i.e. $\left|+\frac{5}{2}\right\rangle \rightarrow \left|+\frac{3}{2}\right\rangle$ and $\left|+\frac{5}{2}\right\rangle \rightarrow \left|+\frac{1}{2}\right\rangle$) (Gullion & Vega 2005).

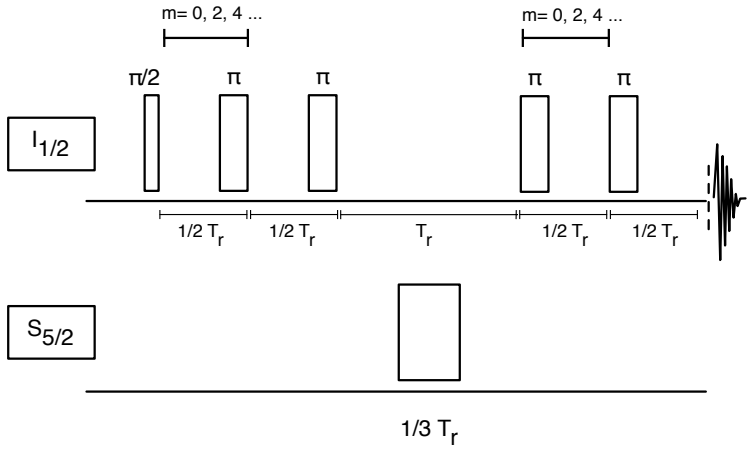

Figure 3-6 $^{31}P\{^{27}Al\}$ REAPDOR pulse scheme.

Both of these considerations affect the dephasing and hence the REAPDOR fraction (calculated using the same function as in REDOR). With the caveat that the adiabaticity population transfer satisfies a minimum requirement, Goldbourt et al. (2003) have reported a universal formula, Equation 3-9, this is limited for the case of a spin-$\frac{1}{2}$ and spin-$\frac{5}{2}$ system, where $\lambda = (2m+2)T_r D$ and m is the number of rotor cycles). Alternate spin pair systems are described by Gullion and Vega (2005)),

$$S^{REAP}_{1/2,5/2}(\lambda) = 0.63(1 - e^{-(3.0\lambda)^2}) + 0.2(1 - e^{-(0.7\lambda)^2}) \quad \text{Equation 3-9}$$

An important consideration to make here is that the universal functions (Equation 3-8 and Equation 3-9) used to describe the dipolar dephasing curves are functions of the two-spin dipolar coupling term (Equation 3-7). Hence, they are only directly applicable in the case of an isolated spin pair. Nonetheless, data obtained from a multi-spin system can still be informative. Other than qualitative data obtained from the shape of the dephasing curve, in conjunction with a structural model NMR modelling software internuclear distance calculations have been reported (Li, Feng, et al. 2013).

REAPDOR experiments reported here were also conducted using a Varian VNMRS 400 spectrometer (operating with a 9.4 T field) using a CP/MAS probe with 4 mm o.d. zirconia (PSZ) rotors. The pulse scheme shown in Figure 3-6 was used, but specific experimental parameters are discussed in the chapter in which the results are presented.

3.5 Analytical techniques assessing aluminium corrosion

A number of techniques were chosen to assess the corrosion of encapsulated aluminium as a function of time and encapsulant formulation. Depending on the type of metallic aluminium used, including plate, wire and powder (described in section 3.1.3), different techniques suitable for analysis with varying resolution and accuracy were identified.

3.5.1 Mass loss

The mass of metallic aluminium in a corrosive environment decreases with the formation of aluminous corrosion products, and hence can be indicative of the extent

of corrosion. Aluminium plate was cut into 25 x 10 x 2 mm pieces, and placed in 50 mL airtight plastic centrifuge tube cast with slurry. Care was taken to ensure that the aluminium pieces had a similar surface finish on all faces after cutting, to minimise the effect of the surface upon the rate of corrosion. The mass of the aluminium was recorded before encapsulation, and then upon demoulding and liberation from within the hardened cement. Corrosion products were removed from each of the surfaces of aluminium using a wire brush, taking care to minimise the amount of aluminium metal being removed.

3.5.2 Hydrogen collection

Time resolved measurements of the hydrogen gas corrosion product release have been shown to be a good measure of the extent of aluminium corrosion (Swift 2013; Kinoshita et al. 2013; Zhang et al. 2012). With an appropriate experimental setup, it is possible to monitor corrosion in situ on a lab scale. Two methods are employed and examined in this work, (i) water displacement, where evolved hydrogen is collected in an upturned water-filled container (decreasing the water level as a function of gas collected); and (ii) by the use of a mass spectrometer.

3.5.2.1 Water displacement

Aluminium content was set to 5 mass% of the total precursor mass before mixing. Slurries were prepared with aluminium powder mixed with the cement clinker prior to solution introduction. Containers were cast with 10 g of slurry and placed in glass vessels. Vessels consisted of two glass cups connected by ground glass joints, with a spout for gas to exit the vessel. Silicone vacuum grease was applied at the joint to prevent water leaking in and hydrogen escaping from anywhere other than the spout. Vessels were kept under water and positioned such that gas bubbles would rise into an upturned water filled measuring cylinder, as shown in Figure 3-7.Containers were glued to the inside base of the vessels to maintain the same position throughout the experiment.

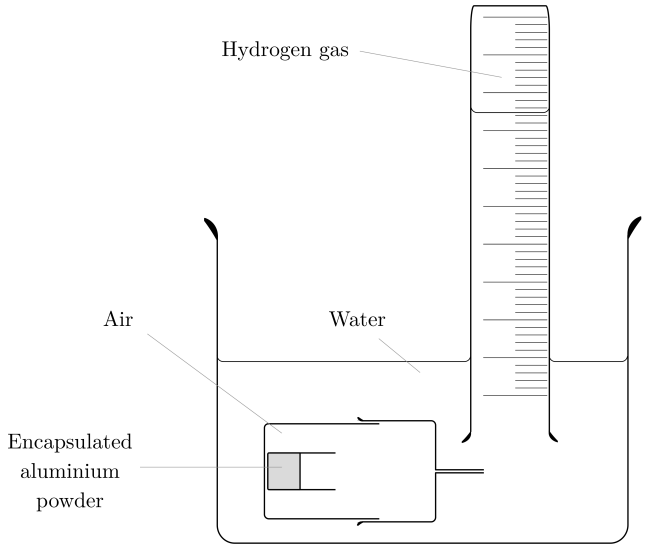

Figure 3-7 Apparatus for hydrogen gas collection by water displacement.

3.5.2.2 Mass spectrometry

Mass spectrometry is a technique that can be employed to detect the presence and quantity of gases. The technique relies on ionisation of the molecules by passing the gas through an electron beam and onwards into electric and/or magnetic fields to deviate the gas molecules path of motion as a function of its mass to charge ratio (Gauglitz & Vo-Dinh 2006). Upon successful divergence of the constituent ions they go on to strike to the surface of secondary electron multiplier (SEM) detectors, generating electrons from which a current can be measured and semiquantification of the initial gas content may be made.

Slurries with the same mass percentage of aluminium powder addition as used in the gas collection experiments were also prepared for mass spectrometry. Samples of mass 100 mg were cast in alumina crucibles and placed in a PerkinElmer TGA 4000 with an attached Hiden residual gas analyser (RGA) series mass spectrometer module. Samples were held isothermally at 20°C under a controlled nitrogen flow atmosphere (20 mL/s), and the mass loss and gas evolution from samples were measured as a function of time. To prevent excessive drying of the sample crucibles were covered with plastic paraffin film, however a small hole was made to enable the evolved hydrogen to easily escape.

3.5.3 Differential scanning calorimetry

Calorimetric thermal analysis devices have one of two basic schematic designs, either subjecting both the sample and an inert reference to the exact same thermal conditions by treating both with the same furnace, or by separate furnaces and maintaining the same temperature for both sample and reference. The latter, known as differential scanning calorimetry (DSC) is instead a measure of the power (or heatflow) required to maintain the same temperature for a sample as the reference, both of which are undergoing the same thermal by their respective furnaces (Gabbott 2008).

DSC was used to quantify the mass percentage of aluminium remaining in a sample at any point in time by ramping the temperature through a range centred about the melting point of metallic aluminium. The energy required to melt the metallic aluminium fraction was calculated from the DSC heat flow curve, where a difference in heat flow between the inert reference and the sample is observed over the melting temperature range of aluminium metal. Quantification of the remaining metallic aluminium indicates any decrease as a result of corrosion product formation.

DSC experiments were performed using a PerkinElmer STA 8000 instrument using an alumina crucible under a nitrogen environment (40 ml/min flow rate). The temperature was programmed to increase from room temperature to 580°C at a rate of 40°/min, followed by a slower ramp to 700°C at a rate of 5°/min. Post processing of the data to determine remnant aluminium quantitity is described in Chapter 7.

3.6 Concluding remarks

Identified in this chapter are methods for sample preparation, and the theory behind techniques used to characterise and test materials throughout the following chapters. The experimental procedures sections in subsequent chapters identify key parameters and processes specific to the experiments reported therein, where these are not discussed in this chapter.

4 Materials and fresh state properties

Note: Sections from this chapter are based on the paper "Phosphate modification of calcium aluminate cement to enhance stability for immobilisation of metallic wastes", by M.A. Chavda, H. Kinoshita, & J.L. Provis, Advances in Applied Ceramics, **2014**, 113(8), pp. 453–459.

4.1 Introduction

The term 'calcium aluminate cement' (CAC) refers to a broad category of cementitious materials with a high content of aluminium and lime and relatively little silica. So, any investigation aimed at preventing or avoiding the conversion processes associated with these materials, and subsequent optimisation for reactive metal encapsulation, requires detailed initial characterisation of the precursors to contextualise the investigation for the specific cement used. Furthermore, certain processing stages prior to the mixing of cement clinker and solution, and the thermal behaviour of the freshly mixed pastes, are investigated to better understand the effects of phosphate modification prior to examining phase precipitation in hardened formulations, the results of which are reported in subsequent chapters of this thesis.

The raw materials used throughout this body of work also require detailed characterisation to support results reported in subsequent chapters of this thesis, according to the experimental protocols described in Chapter 3. Attention is paid to the chemical and physical properties of the powders before mixing, by way of XRD, XRF, FTIR and TGA for phase characterisation; and laser particle size distribution measurement, respectively. Chemical analysis to determine the speciation of the phosphate ions in solutions was carried by a combination of liquid NMR measurements and solution-state FTIR. Fresh state properties in the hours immediately following mixing the CAC powder with the phosphate solution were investigated with both Vicat testing to determine setting time by penetration, and

isothermal calorimetry to evaluate the heat exchange between the formulations and the environment as a result of the hydration reactions. The calorimetric experiments build on the very limited data in the literature concerning sodium phosphate modification of CAC, assessing the effect of the type of phosphate (orthophosphate or polyphosphate), quantity of addition, and modification by the two types of phosphate in various ratios.

4.2 Experimental procedures

The experimental parameters used for the experiments not described in this section, such as the slurry preparation, particle size distribution, XRD, TGA and FTIR, are outlined in the Experimental Procedures chapter, Chapter 3.

Laser diffraction was conducted on raw precursors to assess the size distribution of the particles present. A Malvern Mastersizer 3000 with dry dispersion unit was used, with varying feed rate and air pressure depending on the powder studied. Measurements were obtained over 5 seconds, with a laser obscuration of between 0.5 and 6 % and after a 20 second background measurement.

XRF was conducted using a 1 g sample in 10 g of lithium tetraborate flux and performed on a wavelength dispersive Philips PW2440 sequential X-ray fluorescence spectrometer.

Liquid NMR was carried out on a Bruker Avance III HD 500 fitted with a 5 mm PABBO BB/19F-1H/D-GRD probe. A 1D pulse program sequence was run with a power-gated decoupling using a 30 degree flip angle. Samples were run at 300 K and phosphoric acid was used as a reference material.

Isothermal calorimetric studies of cement hydration were conducted using an eight channel TAM AIR Microcalorimeter. Temperatures were maintained at 25 ± 0.02 °C and fresh paste was mixed externally, weighed into a plastic ampoule, and immediately placed in the calorimeter. Care was taken to not contaminate the outer surface of the ampoules. The heat flow was recorded for the first 70 or 270 h of reaction, depending on the formulation. All values of heat release rate were

normalised by the total mass of paste being studied. The instrument reference ampoules contained the same quantity of water as the samples being tested.

4.3 Results and discussion

4.3.1 Materials

4.3.1.1 CAC

CAC powder was subjected to laser diffraction analysis to estimate the particle size distribution (PSD), shown in Figure 4-1. The shape of the continuous distribution, with lower and upper bounds of 0.2 and 200 μm respectively, indicates the superposition of two contributions, centred approximately at 8 and 30 microns. A number of CAC clinkers designed to have high alumina contents may have additions of α-Al_2O_3 after the firing stage during manufacture (Hewlett 2004), which would result in an evident change in the shape of the PSD (depending on the quantity added), however this is not the case for Secar 51. This PSD shape may be categorised as an artefact of the manufacturing process of the clinker. A pressure of 3 bar was set in the dry particle dispersion unit of the laser sizer during the experiments to reduce any agglomeration as a result of compaction or potential partial hydration during storage. Consequently, no contributions from material with particle size greater than 200 microns were registered.

Additionally experiments were carried out here with parameters suggested by the manufacturer, Malvern Instruments, for cement powders. Laser diffraction with a liquid dispersant was performed using isopropanol in the same instrument, however results were difficult to reproduce and agglomeration was more apparent in the spectra. Further supporting data are reported, as suggested by Ferraris & Garboczi (2013), in Appendix A.

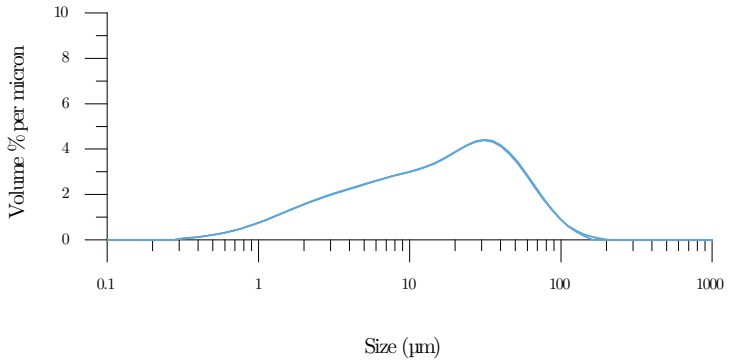

Figure 4-1 Particle size distribution of CAC.

Figure 4-2 shows the X-ray diffractogram obtained for CAC, which is dominated by the presence of CA (pattern diffraction file (PDF) #1-070-0134) and minor phases, C_2AS (PDF #35-755) and CT (PDF #1-075-0437). The sample exhibited high long-range order for all constituent phases. $C_{12}A_7$ (PDF #9-413) is expected to be present in quantities lower than the detection limit for XRD. This phase assemblage is consistent with manufacturer data (Kerneos Inc 2006). The XRF data obtained, shown in Figure 4-3, indicate that the oxide composition largely conforms to manufacturer-provided XRF results, with the exception of alkali oxide content, which is in excess of the manufacturer's tolerances for the particular cement, and which has previously been reported to be present in sodium and calcium aluminates ($NaAl_{11}O_{17}$, PDF #21-1096, and $K_{1.7}Al_{11}O_{17}$, PDF #84-380 (Guirado & Galí 2006)). In such small quantities these phases, mayenite, ferrite (PDF #30-226) and other minor phases require high-intensity radiation sources and high-resolution detectors in place of conventional laboratory X-ray instruments for phase identification by diffraction.

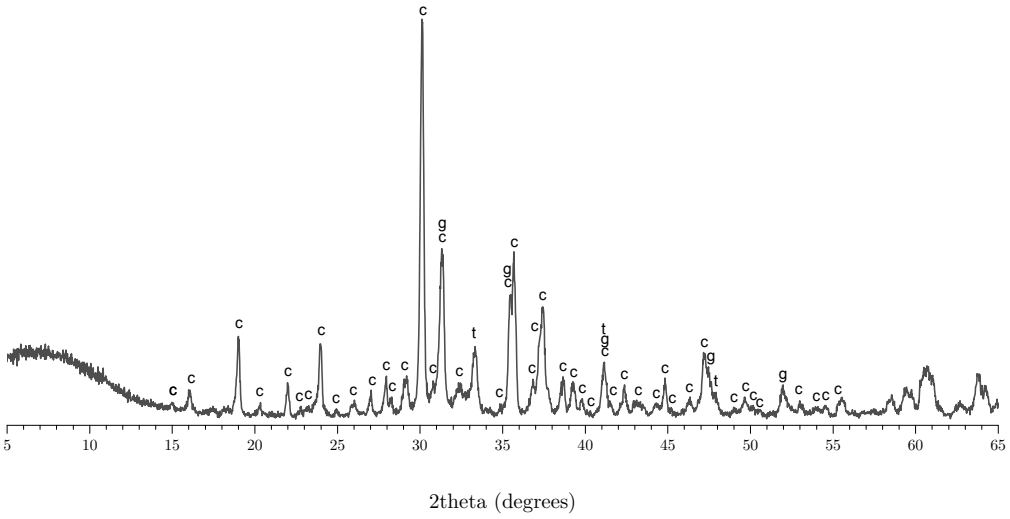

Figure 4-2 Diffractogram for anhydrous CAC. Letters indicate phases identified : monocalcium aluminate (CA, c), gehlenite (C_2AS, g), calcium titanate (CT, t).

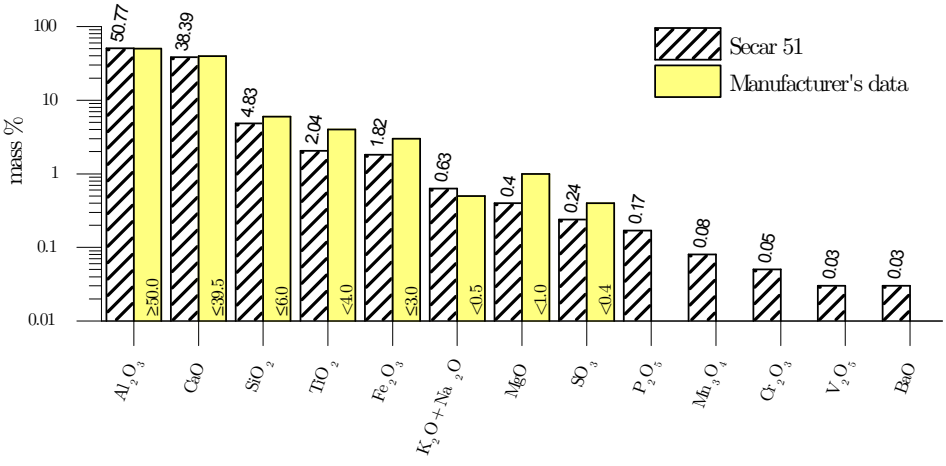

Figure 4-3 Oxide composition for CAC clinker obtained by XRF compared with data provided by the manufacturer.

The results of thermogravimetric (TG) analysis conducted on the CAC, and the first derivative (DTG) curve, are shown in Figure 4-4, indicated a small mass loss of less than 1 % during heating of the sample up to 1000°C. The first derivative of the TG data, Figure 4-4(b), resolves the mass losses into three events, however due to the very low mass losses involved, the limited signal to noise ratio is particularly noticeable in the first derivative of the data. This, coupled with the broad nature of the peaks, complicates the identification of the dehydration processes causing the mass losses.

The lowest temperature mass loss event centred about 100°C is typical for loosely bound water, however it is unlikely to be fully free water, considering the reactivity of the anhydrous clinker with water, as some degree of pre-hydration of the clinker is likely upon contact with the atmosphere. The dehydration of a hydrated alumina gel phase or metastable phases (Scrivener 2003) is well known to occur at these temperatures, however the featureless mass loss over a broad temperature is likely to indicate contributions from the dehydration of both the gel phase and metastable phases.

The assignment of gel and metastable phase dehydration is supported by the presence of a more defined mass loss at ca. 250°C that is indicative of the presence of AH_3, a conventional CAC hydrate, which is most likely to have formed due to partial hydration during storage. This intermediate temperature mass loss results from a two-step dehydration described by Balek et al. (2003a), involving proton migration towards the hydroxyls followed by a hydrothermal conversion to boehmite at the centre of the gibbsite crystals. However it must be noted that the two step dehydration described may not be clearly identifiable for fine grained gibbsite (Rivas Mercury et al. 2006) as smaller crystals cause a smaller pressure buildup in the gibbsite grains; this follows for poorly crystalline gibbsite which dehydrates at a lower temperature (Kloprogge et al. 2002).

The asymmetric high temperature mass loss event peaking at 650°C is tentatively assigned to the decomposition of calcite (Ramachandran et al. 2002), however in a study of many different CACs by Guirado & Gali (2006) a similar mass loss for the clinker most similar in composition to Secar 51 (labelled by the authors as C2) in the same temperature range was left uncharacterised.

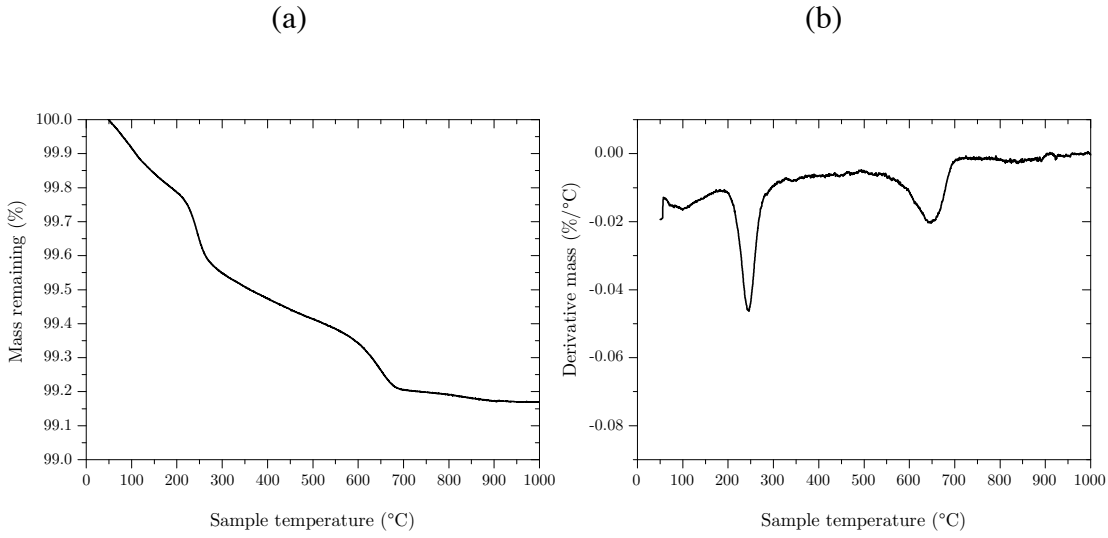

Figure 4-4 (a) TGA mass loss curve for CAC, and (b) corresponding first derivative.

FTIR spectra obtained from the CAC are shown in Figure 4-5. Five characteristic regions (i)-(v) are identified, where (i) is dominated by the presence of O-H stretching modes, from which the presence of conventional CAC hydrates may be verified (Torréns-Martín et al. 2013; Hidalgo et al. 2009); (ii) is characteristic of O-H bending modes in water (Hidalgo et al. 2009); (iii) is indicative of asymmetric stretching modes of carbonates (Gaki & Chrysafi 2006); (iv) contains characteristic Al-O vibrational modes (Tarte 1967; Gaki & Chrysafi 2006) and (v) is attributed to Ca-O vibrational modes. Tarte (1967) identifies particular ranges in region (iv) to be characteristic of particular aluminium environments, depending upon aluminium coordination and whether units are condensed or isolated. The absorptions in the range 700 – 400 cm^{-1} are in good agreement with the work of Gaki et al. (2006), who reported FTIR data for monocalcium aluminate synthesised by solid state sintering.

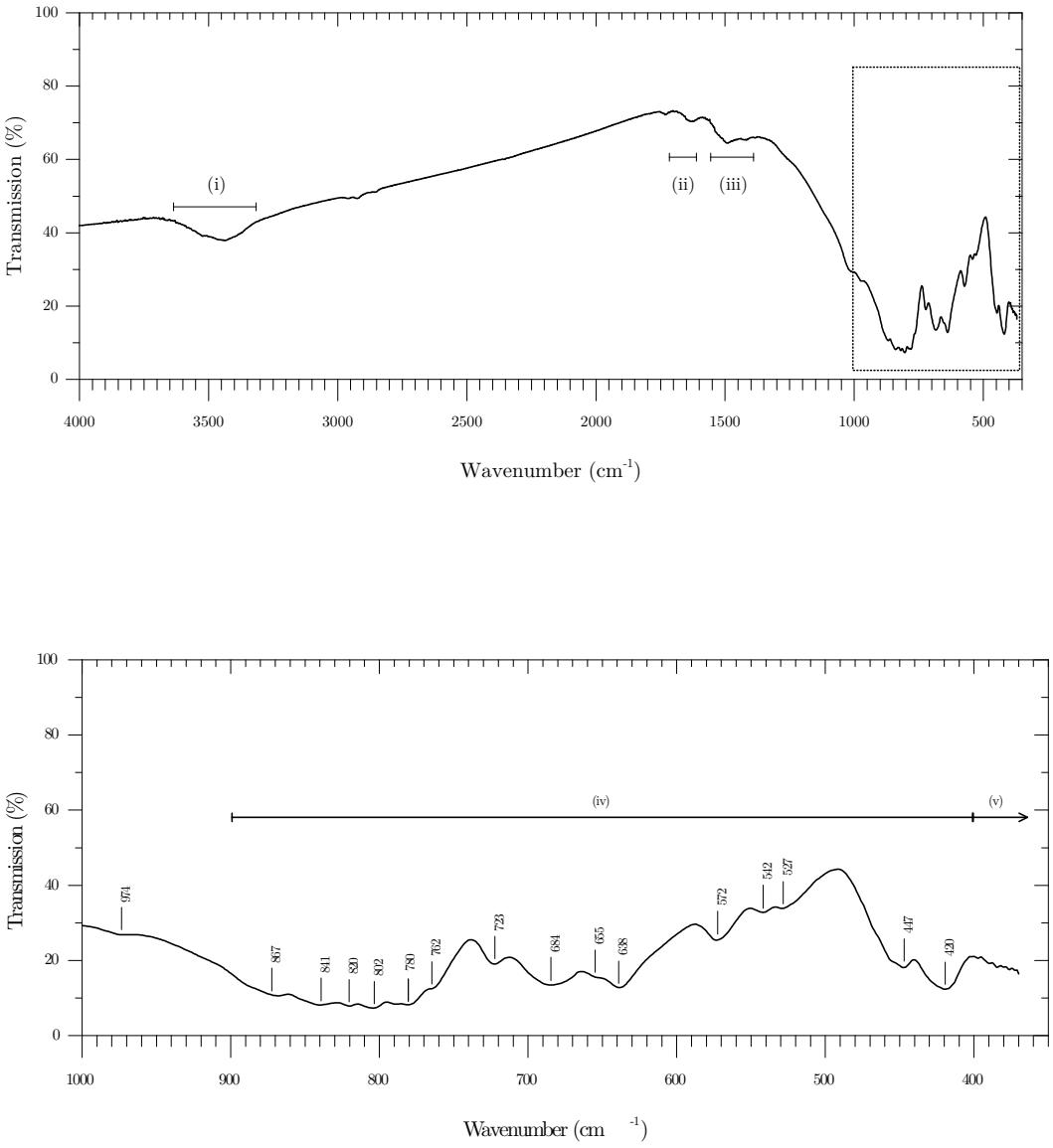

Figure 4-5 Full MIR spectrum for anhydrous CAC (top) and high-end MIR spectrum (bottom).

4.3.1.2 Phosphates

The particle size distributions measured for the sodium monophosphate and polyphosphate ($(NaPO_3)_n$) precursors, shown in Figure 4-6, indicate considerably different size ranges among the dry powders used in this project. The particle size distribution for monophosphate precursors was seen to vary considerably between successive scans, however this may be attributed to a smaller number of particles diffracting light for each scan as a result of their much larger particle size and maintaining the same obscuration criterion for all experiments. This variation between replicate scans was not observed for the CAC or polyphosphate samples, which both

had considerably smaller particle sizes whereas the monophosphate powder straddles the upper detection limit, further affecting the distribution calculated by the diffraction algorithms used.

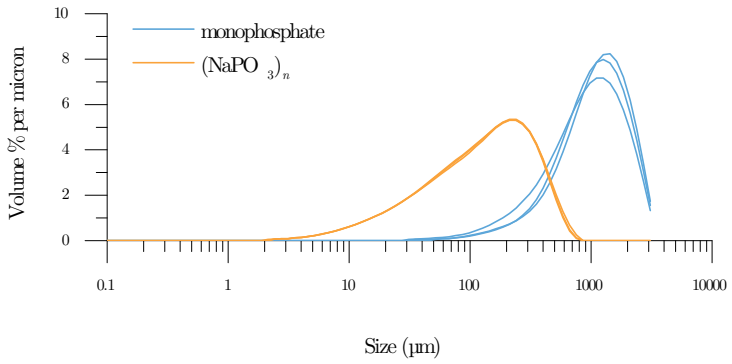

Figure 4-6 Particle size distributions for phosphate precursor powders.

X-ray diffractograms obtained for phosphate precursor powders, plotted in Figure 4-7, show the crystalline phase assemblage for both. The $(NaPO_3)_n$ diffraction data shows an absence of defined reflections and is dominated by a region of diffuse scattering resulting from one or more phases with little long range order. In contrast, the monophosphate powder diffractogram displays clear sharp reflections relating to sodium dihydrogen phosphate monohydrate and dihydrate, $NaH_2PO_4{\cdot}H_2O$ (PDF #11-065) and $NaH_2PO_4{\cdot}2H_2O$ (PDF #10-198) respectively. This was contradictory to information provided by the supplier, which identified the dihydrate as the primary phases, indicating a dehydration of the phosphate, may be during storage. This was considered to be of little significance as the monophosphate was to be dissolved in water prior to mixing, however attention was paid to ensuring that the dissolution was complete before introducing the cement clinker as the rates of dissolution of these powders were significantly different. It was noted that a duration of 24 hours on a roller mixer was more than sufficient to dissolve all the phosphate, however solutions with considerable phosphate dissolved and left for longer periods (>365 days) were observed to precipitate large crystals.

Phosphate precursors were subjected to thermogravimetric analysis; the mass loss and first derivative mass loss curves are shown in Figure 4-8(a) and (b) respectively. The

polyphosphate powder exhibits very little mass loss, less than 2 mass %, across the temperature range. The fastest rate of mass loss is identified at ca. 50°C, likely to be due to adsorbed water, however higher temperature mass loss events are most likely to be the decomposition of hydrated phosphate chains. Monophosphate powder, as a result of its considerably higher degree of hydration, exhibited a number of large mass loss events. The dehydration may be split into three dominant processes, which occur below ca. 120°C, between 120 and 250°C, and a final stage between 250 and 350°C. The dehydration behaviour closely resembles that reported by De Jager et al. (2001), who describe the dehydration of sodium dihydrogen phosphate hydrate as occurring in three steps: (1) removal of crystalline water, which is complete at a temperature of 120°C, occurring in two stages indicating the presence of two distinct sites for crystalline water; (2) above 120 and below 250 degrees, the removal of constitutional water during the condensation of adjacent PO_4 tetrahedra resulting in the formation of pyrophosphate ($(P_2O_7)^{4-}$) anion; and (3) above 300°C, where adjacent pyrophosphate anions condense to form longer chain cyclical metaphosphates releasing water in two steps (at 310 and 345°C).

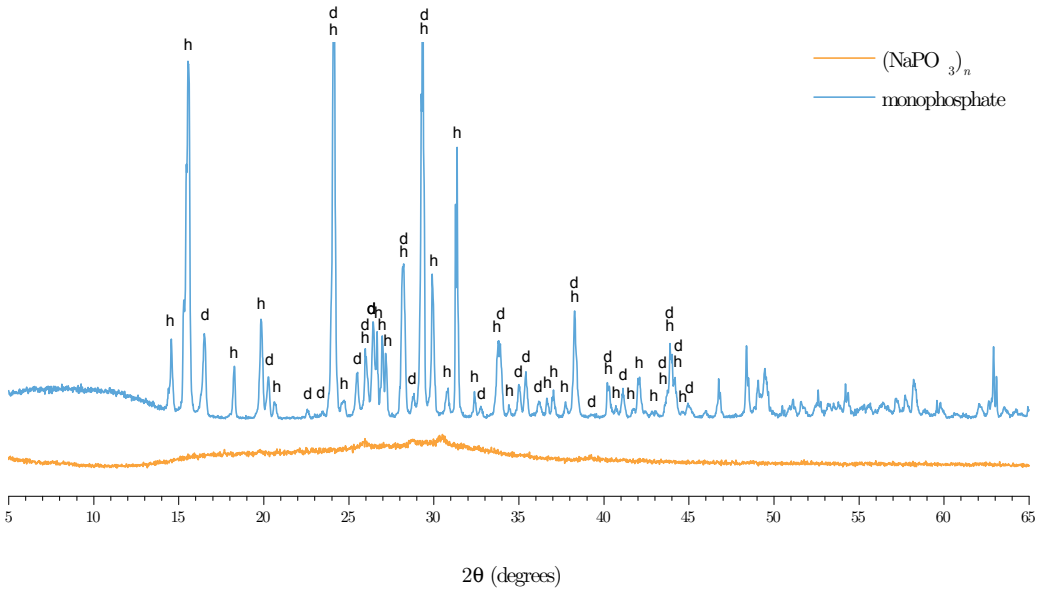

Figure 4-7 X-ray diffractograms for phosphate precursors, where h and d denote the presence of $NaH_2PO_4 \cdot H_2O$ and $NaH_2PO_4 \cdot 2H_2O$ respectively.

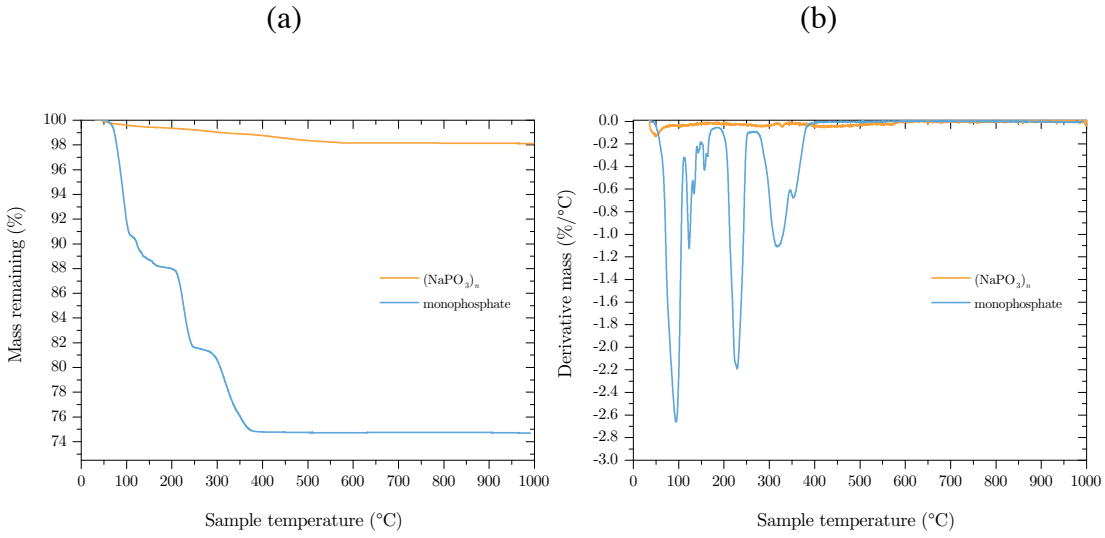

Figure 4-8 (a) TGA mass loss curve and respective (b) first derivative data, for phosphate precursors.

Figure 4-9 shows solution-state FTIR data obtained for phosphate solutions prepared for cement formulations with the same sample names, this solution FTIR experiments were conducted on the phosphate solutions prior to mixing with cement clinker. The spectrum obtained for the 0p0m formulation solutions, with no dissolved phosphate at all, is as expected, typical for water. It consisted of two characteristic absorptions, one broad feature at approximately 3250 cm^{-1} and another at 1700 cm^{-1}, both of which are as a result of O-H vibrational modes (Contreras et al. 2006). Solutions containing only monophosphate exhibited the same absorptions, in addition to vibrational modes all associated with the $H_2PO_4^-$ orthophosphate ion (Gong 2001; Arai & Sparks 2001), which is the conjugate base of H_3PO_4 acid. The responses at 1155 and 1740 cm^{-1} are due to the asymmetric and symmetric modes of P-O bonds respectively, whereas the responses at 941 and 876 cm^{-1} are due to the symmetric and asymmetric vibrational modes of the P-OH bond (Gong 2001). These are typical of aqueous orthophosphates and with increasing dissolved monophosphate content, the responses for these absorptions increased.

Spectra obtained for the phosphate solutions prepared by dissolution of only polyphosphate, also shown in Figure 4-9, resulted in different spectra. The peak at 1250 cm^{-1}, characteristic of asymmetric stretching of bridging PO_2^{2-} (-O-P(O^-)$_2$-O-) bonds (Gong 2001; Michelmore et al. 2000) was observed, showing the presence of phosphate chains in solution and was absent in solutions only prepared with

monophosphate. A large absorbance at 1076 cm^{-1} is the complementary symmetric stretching of the PO_2^{2-} bond and absorptions at the lowest wavenumbers are attributed to antisymmetric stretching of P-O-P bonds (Michelmore et al. 2000). Additionally, there is a weak shoulder at 1150 cm^{-1} which is attributed to antisymmetric stretch of the terminal PO_3 group (Michelmore et al. 2000). Of the spectra shown in Figure 4-9, none exhibited absorptions in the regions associated with cyclic phosphates, which would be observed at 1258, 1295 and 1312 cm^{-1} (Gong 2001), implying that the condensed phosphate ions detected in solution were linear.

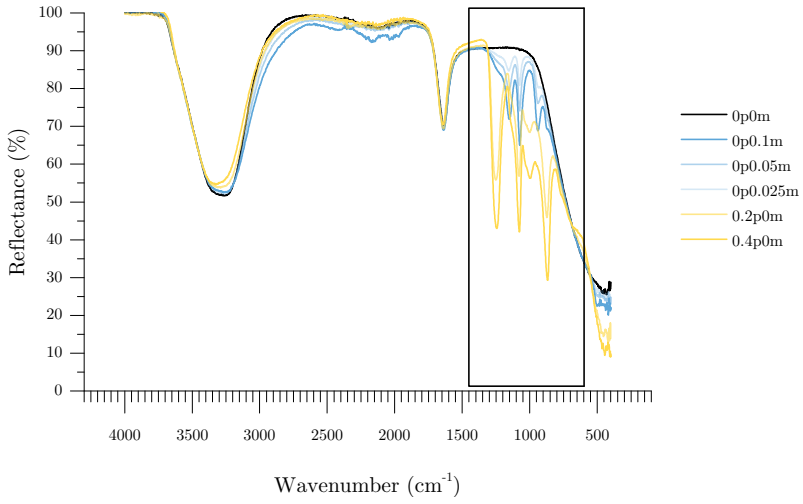

(a)

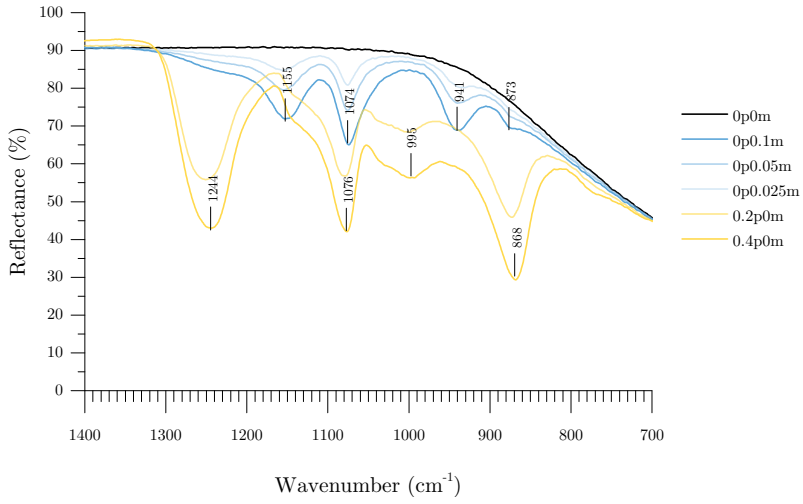

(b)

Figure 4-9 (a) ATR FTIR spectra obtained from phosphate solutions prepared for formulations, prior to mixing with cement clinker, with modification by a single phosphate, and (b) expanded region of the dataset. Additional information identifying the phosphate mass loadings for solutions are presented in the appendix.

Figures 4-10 and 4-11 show the ATR FTIR spectra obtained for phosphate solutions prepared by the dissolution of both mono- and polyphosphate in combinations for formulations in the 0.2p*x*m and 0.4p*x*m series with the same names. As with the spectra in Figure 4-9, showing phosphate solutions prepared by dissolution of only a single phosphate, the spectra in Figures 4-10 and 4-11 also show no responses at wavenumbers indicative of cyclic phosphate ions. Both figures showed similar lineshapes and responses as a result of increasing the dissolved content of monophosphate.

Apart from the response at ca. 1250 cm^{-1}, due to the stretching of the bridging PO_2^{2-} bonds, the absorptions all increased in intensity with increasing dissolved monophosphate content. This is likely to be due to the fact that the remaining absorptions due to polyphosphate ions overlap with absorptions due to orthophosphate ions. The PO_2^{2-} resonance shows a decrease in intensity and a shift in peak position to higher wavenumbers, indicating a decrease in both the quantity of bridging bonds and the average chain lengths of the dissolved polymers (Michelmore et al. 2000). The peak at 1074 cm^{-1} increases in intensity despite there being a decrease in average chain length; this is due to overlapping with the P-O vibrations of the orthophosphate ions as a result of the monophosphate content, which also results in a shift of the peak to lower wavenumbers. Similarly for the highest frequency absorption, there is an increase despite its assignment to P-O-P stretching, as the decrease in the chain length offsets the increasing absorption due to P-OH vibrations of the orthophosphate ions as a result of the dissolved monophosphate. Despite showing clear trends for these peaks, the changes in peak intensity are relatively small due to the competing changes in contributing absorptions, however in the case of the responses at 940 and 1150 cm^{-1} this is not the case. The former is due to the presence of asymmetric P-OH vibrations of the orthophosphate ions, hence with increasing monophosphate this absorption also increases, and as the peak does not overlap with any others (which are decreasing) the increase is considerable. The latter shows an increase in absorption due to the increase in orthophosphate ions with increasing dissolved monophosphate content, however additionally the reduction in chain length of the polyphosphate ions results in an increase in terminal PO_3 vibrations, hence

considerably more absorption is observed in this peak with increasing dissolved monophosphate content.

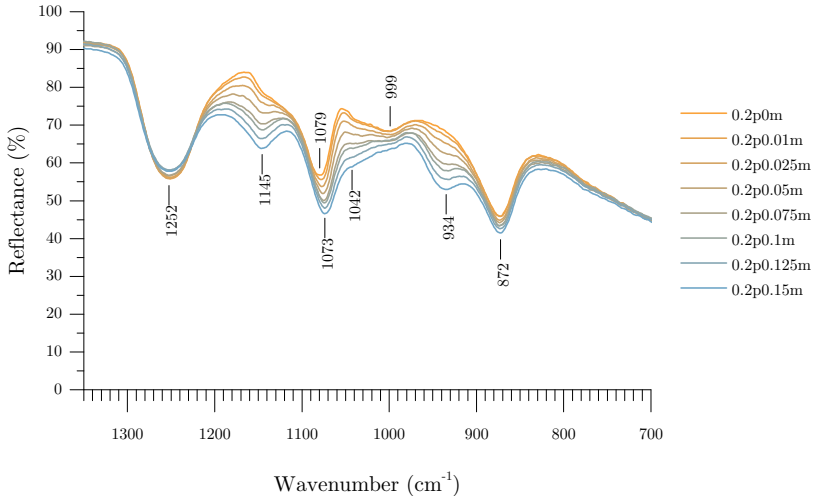

Figure 4-10 ATR FTIR spectra obtained from phosphate solutions, prior to mixing with cement clinker, prepared for 0.2p series formulations. Additional information identifying the phosphate mass loadings for solutions are presented in the appendix.

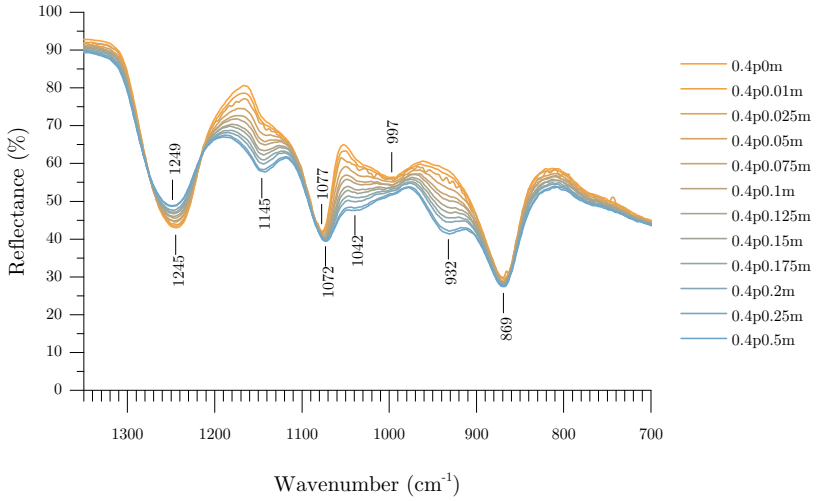

Figure 4-11 ATR FTIR spectra obtained from phosphate solutions, prior to mixing with cement clinker, prepared for 0.4p series formulations. Additional information identifying the phosphate mass loadings for solutions are presented in the appendix.

Figure 4-12 shows the ^{31}P NMR data obtained for selected phosphate solutions prepared for cement formulations of the same label, for the 0p0.1m, 0.4p0m and 0.4p0.05m formulations. Three distinct regions of resonance can be seen focused about 0, -8 and -22 ppm, which are coincident with those reported for Q^0, Q^1 and Q^2 environments respectively (Brow et al. 1993; Döhler et al. 2015), where Q^n is a general notation referring to a phosphate structural unit with *n* bridging P-O-P bonds. The solution prepared for 0p0.1m, with only monophosphate addition, exhibited one resonance indicating only the presence of orthophosphate ions, and all of the phosphorus nuclei were in this configuration. The 0.4p0m and 0.4p0.05m formulations exhibited resonances in each of the three characteristic regions, however the resonance for orthophosphate ions in the 0.4p0m was small.

Table 4-1 shows the relative proportions of the resonances regions constituting the total resonance response for each of the solutions. From these data it is possible to identify that the ratio of bridging Q^2 units to terminal Q^1 units decreases in the case where there is monophosphate dissolved in addition to the polyphosphate, resulting in a decrease in average chain length.

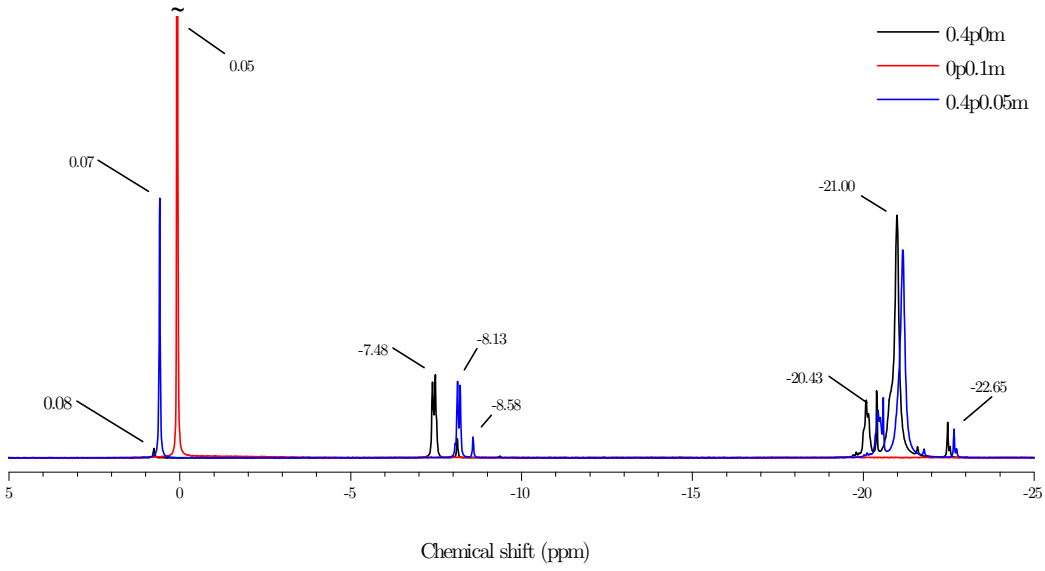

Figure 4-12 ^{31}P solution NMR data obtained from phosphate solutions, prior to mixing with cement clinker, prepared for 0.4p0m, 0p0.1m and 0.4p0.05m formulations. The orthophosphate peak at 0.05 ppm marked with the tilde symbol (~) is approximately ten times greater than the vertical scale shown. Additional information identifying the phosphate mass loadings for solutions are presented in the appendix.

Table 4-1 Integral values as a fraction of total resonance intensity for each of the three different phosphate environments

Solution	Q^0 (0 to 1 ppm)	Q^1 (-7 to -9 ppm)	Q^2 (-20 to -23 ppm)
0p0.1m	1.00	0	0
0.4p0m	<0.01	0.14	0.86
0.4p0.05m	0.16	0.12	0.72

Measurements of the pH of phosphate solutions, 24 h after mixing but prior to mixing with cement clinker, shown in Figure 4-13, indicated an increase in the acidity of the solution with increasing dissolved monophosphate content. This decrease in the pH results in the acceleration of hydrolysis of the longer chains (Bell 1947), and coupled with the direct dissolution of the orthophosphate, results in a large resonance in the orthophosphate region and a decrease in the average chain length of the condensed phosphate ions. Data collected one week after mixing, Figure 4-14, the phosphate solutions showed very a slight increase in pH across all solution formulations in the 0.4p*x*m series, indicating the hydrolysis of the chains (Dorozhkin 2009b).

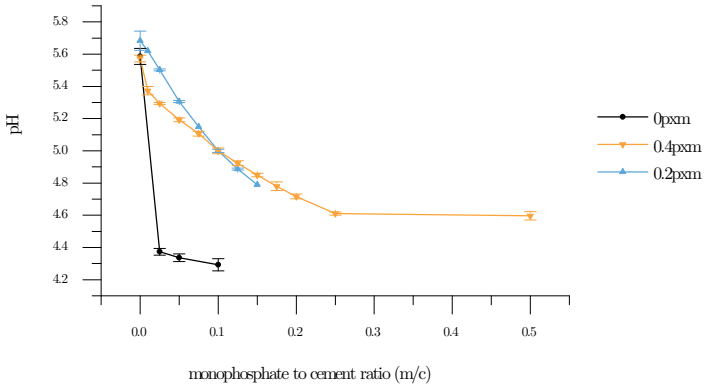

Figure 4-13 pH measurements obtained from phosphate solutions, prior to mixing with cement clinker, prepared for the 0p*x*m, 0.2p*x*m and 0.4p*x*m formulations. Additional information identifying the phosphate mass loadings for solutions are presented in the appendix.

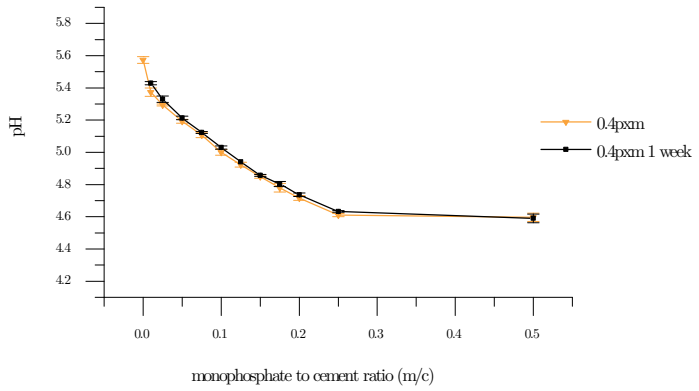

Figure 4-14 Comparison of pH measurements obtained from phosphate solutions, prior to mixing with cement clinker, values for 0.4p*x*m formulations solutions 24 hours and 7 days after solution preparation. Additional information identifying the phosphate mass loadings for solutions are presented in the appendix.

The purpose of these initial characterisation experiments was to examine the precursors chosen for this investigation. The laser diffraction particle size analysis was used to compare fineness of various precursors and a disparity between the size distributions obtained prompted attention to be paid to the methodology and protocols used when combining these materials. Consequently it was decided to add phosphate to the distilled water prior to mixing with the cement, as opposed to premixing the dry precursors together and then adding water, to ensure that the widely differing dissolution rates of the phosphates (due to specific surface areas) did not affect the modification of the conventional CAC hydration. A mixing duration of 24 hours was observed to ensure complete phosphate dissolution and speciation stabilisation, as the respective pHs of the solutions remained very close to stable for up to 7 days. TG and XRD analysis of the CAC indicated negligible hydration during storage and hence no preconditioning steps were applied to this material. The mixing parameters and curing conditions are described in Chapter 3.

4.3.2 Fresh state properties

4.3.2.1 Vicat study

Setting time data determined by Vicat analysis shown in Figure 4-15 were obtained following the ASTM Standard C807 – 08 (2008). All samples with addition of mixed mono- and polyphosphates hardened, however the formulations in the 0p*x*m series did not exhibit hardening in the first 48 hours, in line with results reported by Sugama and Carciello (1995), who studied the addition of monophosphate to a similar CAC. Both the initial and final setting times depend strongly on the monophosphate content, but the effect was not monotonic. The 0.2p*x*m series generally had much shorter initial and final setting times than 0.4p*x*m. The use of sodium monophosphate as a setting retarder for CAC has been documented previously (Holmgren & Bearden 1965), but it is seen here that excess doses of this additive cause the loss of this retarding effect. The maximum initial and final setting times were achieved at slightly different m/c (monophosphate to cement mass ratio) ratios in the two series. For the 0.2p*x*m series, m/c ratios of 0.075 and 0.1 were identified as giving the maximum initial and final setting times respectively, whereas ratios of 0.05 and 0.075 were identified as giving these maxima for the 0.4p*x*m series. The greatest extent of retardation of the initial or final sets for the two series did not occur at the same m/c ratio, but the ratio between mono- and polyphosphates (m/p) at the longest setting time for the 0.2p*x*m series coincides with the second retardation peak for the 0.4p*x*m series, suggesting that the retardation may be related to some extent to the interaction between mono- and polyphosphates.

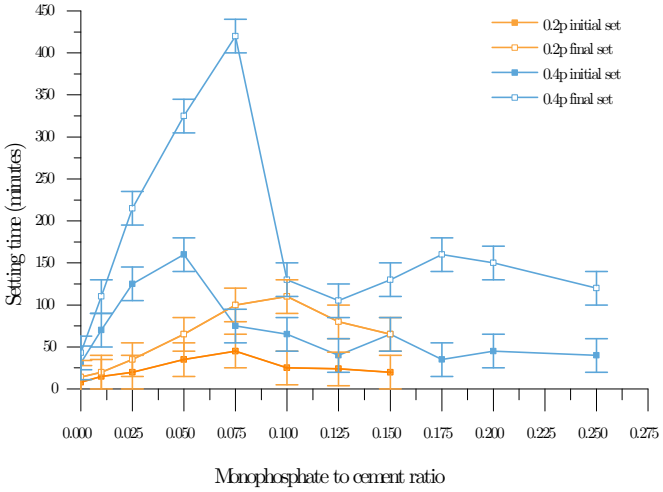

Figure 4-15 Vicat setting time data for 0.2p and 0.4p series.

4.3.2.2 Isothermal calorimetry

Calorimetric data obtained for 0p*x*m (including neat CAC paste), *x*p0m, 0.2p*x*m and 0.4p*x*m formulations are depicted in Figures 4-16, 17, 18 and 19. The convention for such data is to plot time resolved heat flow and cumulative heat flow. However, due to the relative rapid heat evolution of the formulations investigated it is clear that a linear time axis (plotted against in sub plots (a) and (b) in all calorimetry data figures) does not display data in the most useful way. As such, in addition to linear-scale plots (a) and (b) for Figures 4-16, 17, 18 and 19 the same data have been plotted with a logarithmic time scale, in sub plots (c) and (d) for the same data. This enables clearer discernment of the line shape soon after data collection begins, where it is changing considerably more rapidly, and to identify subtle behaviours and trends over longer periods at points tens of hours after data collection begins, where the heat evolution is more stable. Without displaying the data in such a way it very conceivable that the complex heat flow response detected may be simplified to a single heat evolution event. Similarly, events occurring over durations that are magnitudes greater are at risk of not being noted at all.

The heat flow curve obtained for neat CAC was characteristic of the hydration of calcium aluminate cements, consisting of an initial brief exotherm followed by an induction period until a large exotherm after circa 10 hours. The first heat release,

detected from the beginning of data collection, relates to the wetting period where rapid dissolution of the clinker takes place during and shortly after mixing (Guan et al. 2009). This is followed by an induction period where very little heat is released until 10 hours after the initial mixing has elapsed, which is characterised by a large exothermic event, as a result of the precipitation of hydrates (Ukrainczyk & Šipušić 2008). This exothermic event after approximately 10 hours curing period is the only event after the initial wetting period and this is characteristic of the heat evolution during CAC hydration, primarily due to the process being dominated by one very reactive phase, CA.

The calorimetric study carried out by Brown & Ma (1994), investigating the effects of various condensed sodium phosphates in reducing post-hydration strength regression of calcium aluminate cement, represents the entirety of the published literature on the calorimetry of sodium phosphate modified calcium aluminate cements. Isothermal calorimetry, measuring the heat exchange of a material with its environment as it undergoes a chemical reaction process, can provide considerable information about the kinetics of the hydration of a cementitious material. Brown & Ma reported that the condensed phosphates investigated substantially accelerated the initial hydration of the CAC, regardless of the composition of the phosphate. The characteristic calorimetry curve lineshape observed for the hydration of CAC materials consists of an initial exothermic event as a result of the wetting of the cement during mixing, followed by an induction period where there is little heat release. Approximately 10 to 16 hours after initial mixing the induction period is ended by an exothermic event corresponding to the precipitation of CAC hydrates (Ukrainczyk & Šipušić 2008). The results reported by Brown & Ma indicate that the addition of sodium polyphosphates resulted in hydration without a discernable incubation period, as the exothermic precipitation event began before the event associated with the wetting of the cement was completed. To clarify this behaviour, and to add to the limited body of available data, calorimetric monitoring of the hydration reactions of phosphate-modified CAC will be a major theme of this chapter.

Formulations in the 0p*x*m series, those with monophosphate addition, showed no typical lineshape, either for either heat flow or cumulative heat flow data, shown in Figure 4-16 (c) and (d). All formulations showed higher initial heat release during

wetting than the neat CAC, and generally increasing monophosphate addition in this single phosphate series resulted in an increasing heat release being detected throughout the reaction process. For all the formulations other than that with the lowest monophosphate content, exothermic events were detected after hydration periods far greater than the duration at which the neat CAC sample stopped exhibiting exothermic events. All formulations in this series exhibited subsequent heat release events, the complexity of which increased with increasing monophosphate content, as can be seen in Figure 4-16 (c), where a change in the slope of the graph indicates a thermal event. It is difficult, from the data obtained, to determine whether these are different exothermic events and that the hydration pathway has been considerably altered, or whether the reactions are similar but the kinetics of conventional hydration are being affected.

Data collected for the *x*p0m series of formulations are shown in Figure 4-17. With polyphosphate modification, an additional exothermic event was observed early in the hydration of the samples, similar to the behaviour observed when >1% additions of lithium carbonate are made to the same CAC system (Niziurska et al. 2015). With low polyphosphate to cement ratios, there was considerable overlap between the peak due to wetting and this new event, however with increasing polyphosphate content the event occurred after increasingly greater curing periods. The characteristic neat CAC hydration peak, usually observed about 10 hours after initial mixing, is maintained at low polyphosphate to cement ratios, however at ratios of greater than 0.1 its presence is difficult to determine. After 64 hours of hydration all formulations in this series reach a low and steady rate of heat evolution, considerably sooner than those studied in the 0p*x*m series. The difference between total heat evolved over the period studied for the formulations in the *x*p0m series and the neat CAC sample was considerably less than the difference observed between the 0p*x*m formulations and the neat CAC.

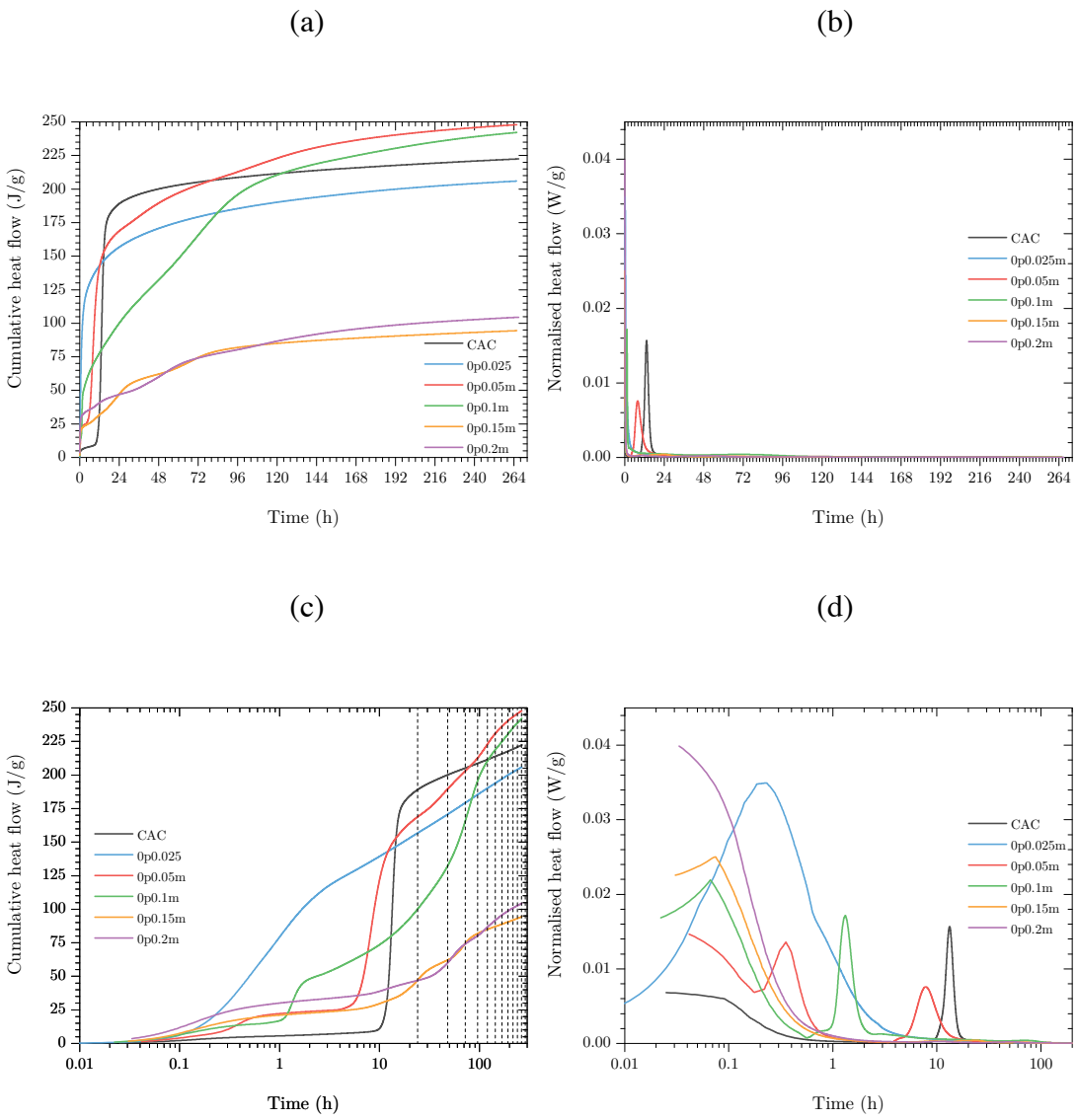

Figure 4-16 (a) Cumulative heat evolution and (b) rate of heat flow for neat CAC and 0p*x*m formulations over the first 264 hours, and the same data plotted with a logarithmic time axis ((c) and (d) respectively).

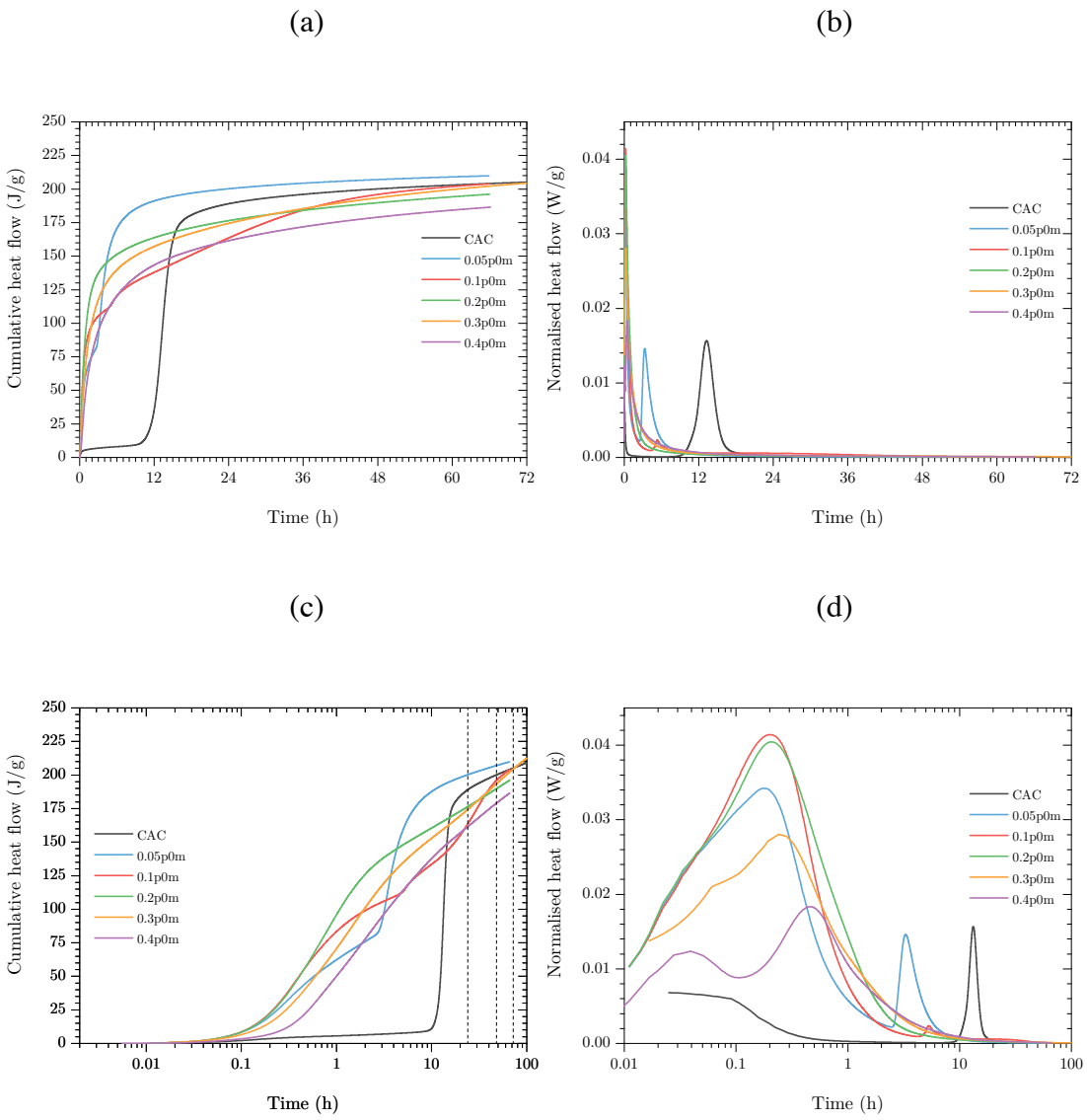

Figure 4-17 (a) Cumulative heat evolution and (b) rate of heat flow for neat CAC and *x*p0m formulations over the first 64 hours, and the same data plotted with a logarithmic time axis ((c) and (d) respectively).

Figure 4-18 shows the total heat evolution over the first 60 hours following mixing, plotted as a function of the total phosphate to cement mass ratio for the two single phosphate formulation series, 0p*x*m and *x*p0m. Errors were calculated as the standard deviation from the mean for replicate experiments for neat CAC, obtaining a value of 9 J/g, this is taken as a modest estimate of the errors associated with this technique. However any future experiments must be performed in replicate for each sample studied. Both types of modification result in the decrease of total heat evolution during this period, however the effect from monophosphate addition is considerably greater. It must be noted that the contributions to this cumulative heat release throughout the time period studied were all exothermic events, and for the 0p*x*m series some formulations continued to exhibit fluctuating heat release. While the neat CAC formulation and those in the *x*p0m series exhibit slow ongoing heat release behaviour 60 hours after mixing, the 0p*x*m formulations did not. This may be interpreted as indicating either a retarding effect on the hydration of the CAC, or alteration of the hydration pathway significantly and in a complex manner such that the complexity of the hydration pathway is a function of the degree of monophosphate addition.

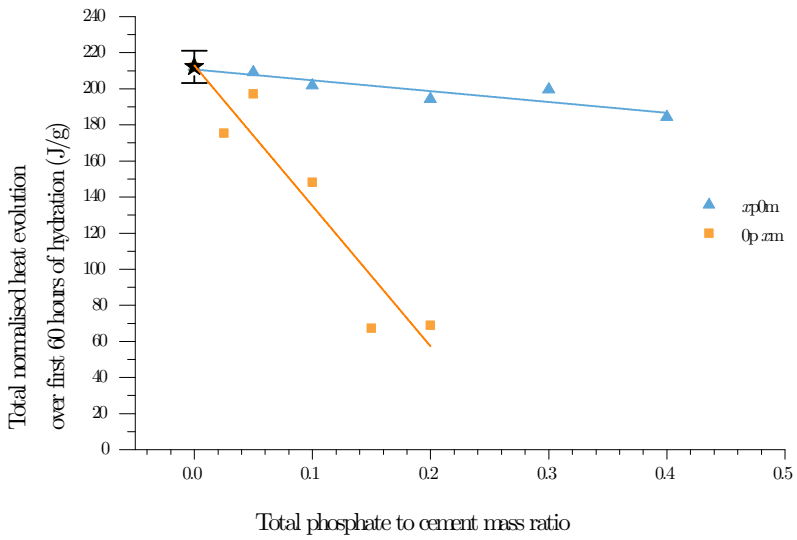

Figure 4-18 Cumulative heat evolution over the first 60 hours as a function of total phosphate content.

Calorimetry data obtained for the 0.2p*x*m and 0.4p*x*m series are shown in Figures 4-19 and 4-20 respectively. The cumulative heat flow curves plotted as a function of the hydration period, shown in subfigures (b) in both graphics, exhibit distinct lineshapes for both formulation series and for neat CAC, being that of a wetting event followed by another main event. Unlike the 0p*x*m formulation series, the complexity of the calorimetric signal did not change at all; all formulations in these series exhibited only two exothermic events.

All the formulations belonging to the 0.2p*x*m series exhibit a wetting event considerably higher than that observed for the neat CAC sample. With small addition of monophosphate the maximum heat release rate during this wetting period decreases, however at greater monophosphate contents this trend reverses with greater rates during the wetting period observed than even the 0.2p0m formulation. In the case of the 0.4p*x*m series the monophosphate content generally increased the maximum rate observed during wetting.

Both series of formulations exhibited two exothermic events, including the wetting event. With increasing monophosphate content the time period between the wetting period, which occurs immediately after mixing, and the beginning of the second exothermic event increased; this was also true for both series. In the case of the 0.2p0m formulation, the second exothermic event begins during the wetting period itself, however can be delayed with monophosphate addition to at least two hours after mixing. The time of the second exothermic event in the case of the 0.4p*x*m series was shown to be delayed up to 5 hours after initial mixing, as in the case of the 0.4p0.2m formulation. As a result of both of these effects, there is a positive correlation between the cumulative heats evolved from the point of mixing until the times of the second events with increasing monophosphate content.

Similar analysis to that depicted in Figure 4-18 is shown in Figure 4-21 for the 0.2p*x*m and 0.4p*x*m formulation series. It can be seen that there is a trend of increasing cumulative heat evolution 60 hours after mixing, with increasing monophosphate content and decreasing polyphosphate content. The former of these observations is particularly interesting, as the formulations with no polyphosphate and only monophosphate addition exhibit a large decrease with increasing monophosphate

content, indicating that the effects of the two phosphates used in combination are more complex than just additive.

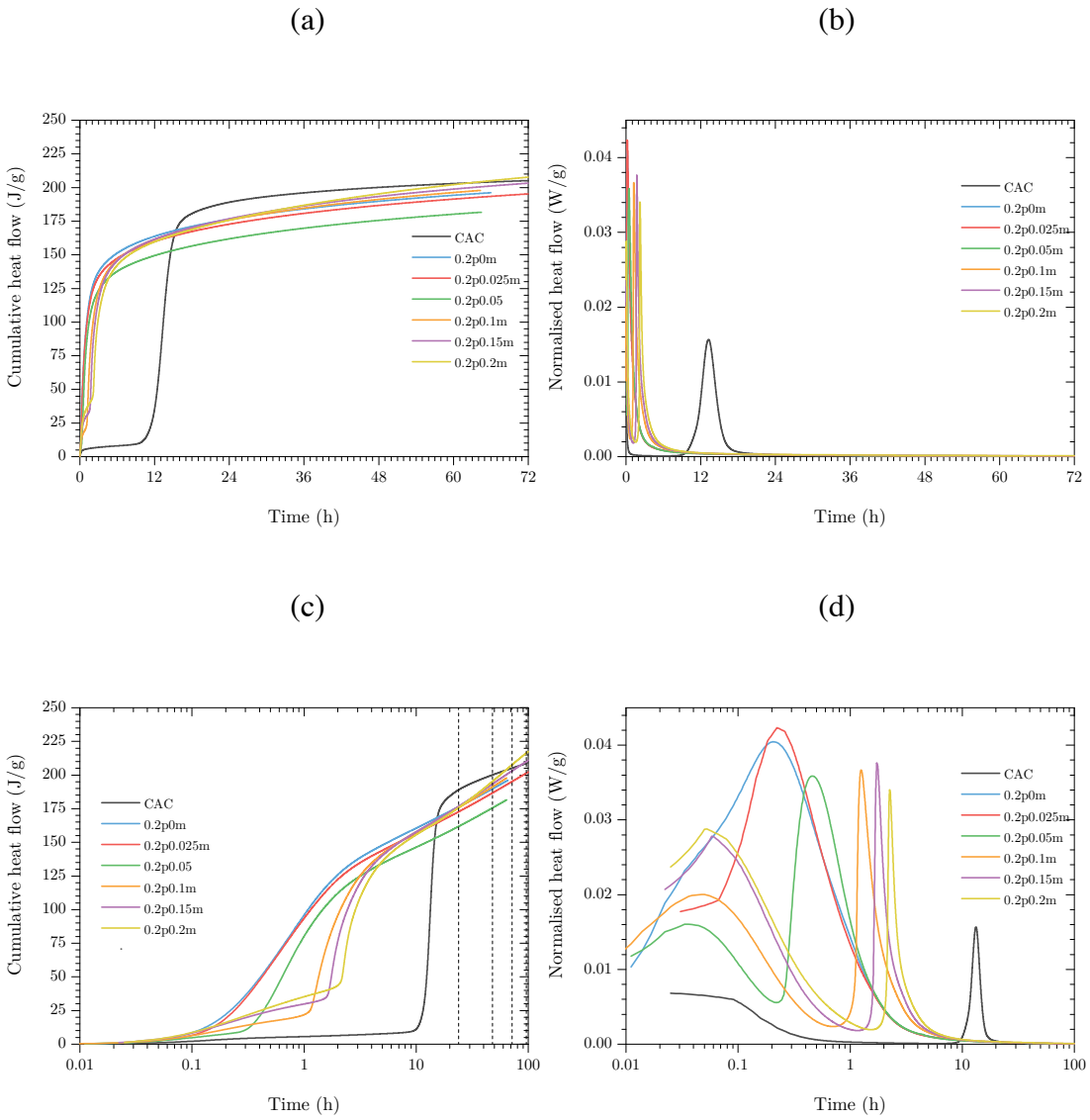

Figure 4-19 (a) Cumulative heat evolution and (b) rate of heat flow for neat CAC and 0.2p*x*m formulations over the first 264 hours, and the same data plotted with a logarithmic time axis ((c) and (d) respectively).

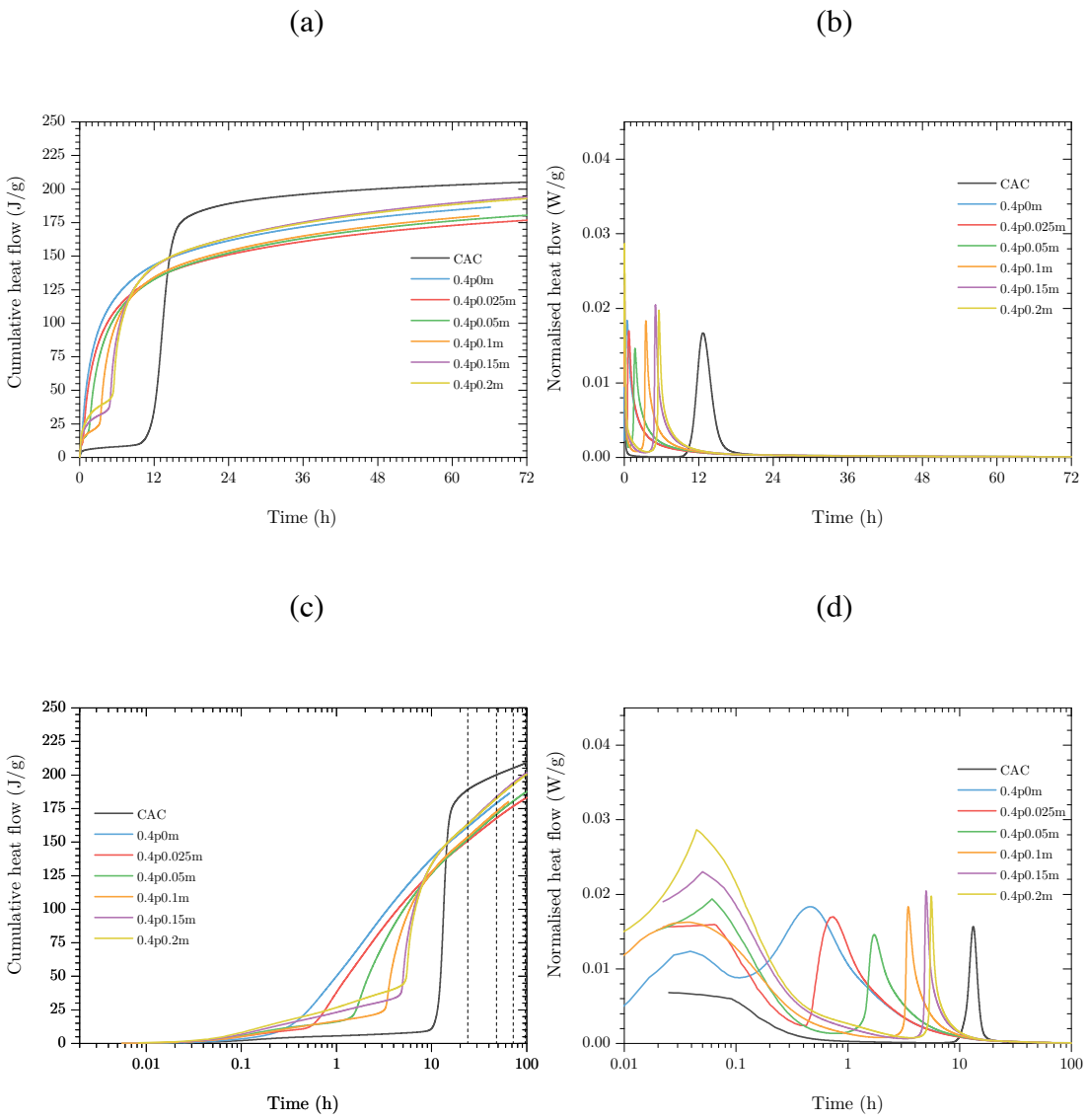

Figure 4-20 (a) Cumulative heat evolution and (b) rate of heat flow for neat CAC and 0.4p*x*m formulations over the first 264 hours, and the same data plotted with a logarithmic time axis ((c) and (d) respectively).

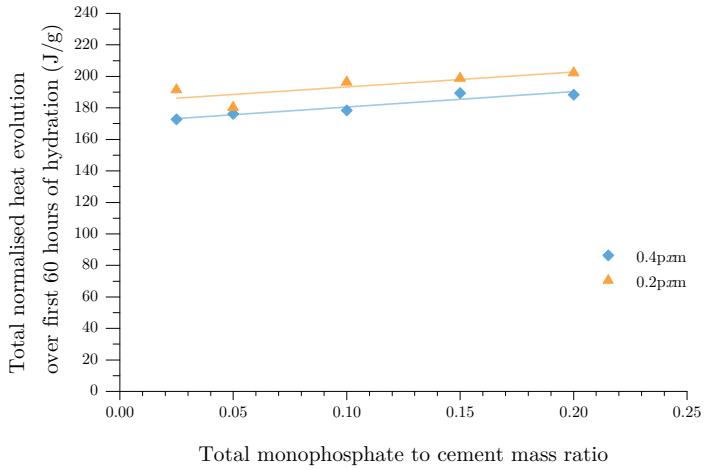

Figure 4-21 Cumulative heat evolution, for the 0.4pxm over the first 60 hours as a function of monophosphate content.

4.4 Conclusions

This chapter examined the raw precursor materials, phosphate solutions and the fresh state setting and heat evolution properties. The particle size distribution of the CAC and phosphate powders indicated considerably different average particle sizes ranging from approximately 20 to 1000 microns. To minimise the effect of the specific surface area of the powders on their dissolution, the phosphate powders were dissolved in the distilled water 24 hours prior to clinker dissolution. The XRF and XRD data obtained for the CAC clinker confirmed the primary crystalline phases to be CA, C_2AS and CT. TGA data for the CAC clinker showed partial pre-hydration and potential calcite content, however the combined mass loss for both of these event was less than 1 wt%.

FTIR and NMR spectroscopic analysis of phosphate solutions indicated that in the monophosphate solution, the phosphate speciation was limited to orthophosphate ions. Polyphosphate solution exhibited less than 1% of the phosphate environments orthophosphate units (Q^0) whereas a significant majority (86%) and the remainder were Q^1 and Q^2 units respectively. In the mixed phosphate solutions the ratio of Q^2 to

Q^1 decreased, indicating a shorter chain length for those non-orthophosphate ions in solution.

Vicat results showed that the 0p*x*m series exhibited setting times considerably longer than 48 hours, and as such they were not measurable by the Vicat method. Although the initial and final setting times were shorter than the neat CAC in 0.2p*x*m and 0.4p*x*m series, additional increase in the monophosphate to cement ratio in the mixed phosphate formulations was found to be able to increase the setting time at a specific range of monophosphate content.

The 0p*x*m and *x*p0m series exhibited higher heat evolution during the initial wetting period than the neat CAC. The 0p*x*m series, with increasing monophosphate to cement ratio, exhibited a considerable decrease in the total heat evolution in the first 60 hours of hydration, the nature of which appeared to be complex (i.e. number of contributing thermal events). The *x*p0m series also indicated a milder decrease in the total heat evolution during the initial 60 hours, with increasing polyphosphate content. Formulations in the mixed phosphate series all exhibited a characteristic lineshape, consisting of a wetting event followed by a second exothermic event, with the monophosphate content determining the dormancy period between the two. The total heat evolution over the initial 60 hours of hydration in these two series increased with with increasing monophosphate content implying that the effect of modification with a combination of mono- and polyphosphates, is not additive and that the mechanism is more complex.

The data in this chapter identify that the average chain length of the phosphate ions can considerably alter the fresh state of the cement slurries prepared, and presents a possible tool to tune these properties. The following chapter examines the phase evolution of the formulations in this system to determine the effect of phosphate modification in single and mixed phosphate series at longer curing periods, with the aim of determining the hydration pathway and the occurrence of conversion.

5 Structural evolution of phosphate-modified CAC under ambient and hydrothermal conditions

Note: Sections from this chapter are based on the findings from the manuscripts *"Phosphate modification of calcium aluminate cement to enhance stability for immobilisation of metallic wastes"*, by M.A. Chavda, H. Kinoshita, & J.L. Provis, *Advances in Applied Ceramics*, **2014**, 113(8), pp. 453–459, and *"Modification of low-pH calcium aluminate cement to enhance stability for immobilisation of metallic wastes"*, by M.A. Chavda, H. Kinoshita, & J.L. Provis, *Proceedings of the 32nd Cement and Concrete Science Conference (CCS 2012)*, **2012**, *Belfast, UK*.

5.1 Introduction

Calcium aluminate cements (CAC) are well known for their rapid hardening, early strength development and resistance to chemical attack (Scrivener 2003). These properties have made them suitable for use in several key applications (Juenger et al. 2011), including as a biomaterial for bone and dental repairs (Kraft & Hermansson 2003), in refractory concretes (Bensted & Barnes 2002; Hewlett 2004), specialised mortars for structural applications (Scrivener 2003) and carbonation resistant geothermal well applications, (Sugama 2006a). More recently, as a result of their lower pore solution pH relative to Portland cement (Macias et al. 1996), they have also been developed for waste encapsulation purposes, specifically immobilisation of metallic radioactive wastes (Swift et al. 2013; Kinoshita et al. 2013; Milestone 2006; Ojovan & Lee 2005) and solutions containing toxic metals (Fernández et al. 2014).

The high early-age strength development of calcium aluminate cements is a result of the reactivity of monocalcium aluminate and the subsequent precipitation of the metastable hydrate phases, CAH_{10} and C_2AH_8. The dissolution of these metastable phases and subsequent re-precipitation as stable phases, C_3AH_6 and AH_3, which is known as conversion, has associated disadvantages. As a result of 'converting' from metastable phases to denser stable hydrates, there is an increase in porosity via the considerable loss of solid volume fraction within the hardened material, leading to a loss in strength (Scrivener 2003; Bensted & Barnes 2002; Bradbury et al. 1976; Hewlett 2004). There have been a number of well-documented structural failures of CAC concretes, which has resulted in the prohibition of the use of this material for structural applications in a number of countries worldwide (Neville 2009a).

The process of conversion is well documented in the literature, as the presence of the various crystalline hydrate phases is easily detected through the use of XRD and thermal analysis techniques such as TGA (Pacewska & Nowacka 2014; Bushnell-Watson & Sharp 1992) and DTA (Bradbury et al. 1976). In addition to the four primary hydrate phases listed above, an amorphous gel phase is also formed as part of the conventional CAC hydration process, however there is little agreement in the literature as to the chemistry of this gel, either being a hydrated alumina gel (Bensted & Barnes 2002; Hewlett 2004) or a C-A-H gel (Edmonds & Majumdar 1988; F. Guirado et al. 1998).

A number of investigations have targeted the modification of the neat CAC system to avoid the disadvantageous development in properties as a result of the conversion process. Chemical modification of CAC has been conducted using highly alkaline solutions, including sodium hydroxide and sodium silicates (Fernández-Jiménez et al. 2011), favouring the direct precipitation of C_3AH_6 or Si-substituted katoite as main reaction products respectively, and hence avoiding the volume changes associated with the precipitation of the intermediate metastable phases. Inclusion of supplementary siliceous cementitious materials such as silica fume (Mostafa et al. 2012; Hidalgo et al. 2009), fly ash (Mostafa et al. 2012; Hidalgo et al. 2009; Fernández-Carrasco & Vázquez 2009), and blast furnace slag (Majumdar & Singh 1992), has also been demonstrated to be an effective pathway to limit deleterious

conversion, through promoting the formation of secondary products such as strätlingite (C_2ASH_8) and calcium silicate hydrate (C-S-H).

The phosphate modification of CAC materials has been shown to affect the hydration of CAC materials considerably. Initial investigations of phosphate modification of CAC carried out by Sugama and co-workers (Sugama & Carciello 1991; 1992a; Sugama & Carciello 1992; Sugama & Carciello 1993; Sugama & Wetzel 1994), assessed the effect of ammonium polyphosphate fertiliser upon the hydration of CAC. This work built upon previous investigations synthesising magnesium phosphate cement via the acid-base reaction between dead burnt magnesium and the same polyphosphate fertiliser (Sugama & Kukacka 1983). All these studies report the precipitation of an amorphous phosphate hydrate phase, in place of conventional CAC hydrates, and identify this as responsible for the setting and strength development. Earlier publications (Sugama & Carciello 1991; Sugama & Carciello 1992) in the series indicate that this hydrate is an amorphous ammonium calcium pyrophosphate whereas in later studies (Sugama, Allan, et al. 1992; Sugama & Carciello 1993; Sugama & Wetzel 1994; Sugama & Taylor 1994) it is revised to be described as an orthophosphate due to the absence of absorptions in the FTIR spectra for P-O-P linkages. Due to environmental concerns the acidic component of the system was changed to sodium phosphate for subsequent studies, and in the case of modification with sodium polyphosphate the resultant hydrate phase was analogous to that observed for the ammonium polyphosphate system, sodium calcium orthophosphate salts. This was further revised to be described as amorphous calcium phosphate and hydrated alumina gel, in a later study (1995) with sodium phosphate modification of CAC and fly ash blends. A similar modification of the CAC system by Brown & Ma (1992; 1994) was also reported to prevent conventional CAC hydrate precipitation, however the amorphous phase was characterised to be a C-A-P-H gel with greater variability in stoichiometry. More recent investigation of this system, carried out by Swift et al. (2013) to examine the possibility of further investigation of the system as an alternative encapsulation matrix for intermediate level radioactive waste, concluded that the primary hydrate phase consisted of an amorphous calcium phosphate and hydrated alumina gel.

There is thus limited coherence in the literature concerning the hydration of sodium phosphate modified CAC, furthermore there is little information reported regarding the phase assemblage after extended hydration periods. The calorimetry and Vicat data discussed in the previous chapter indicate that the kinetics of the hydration process, and hence the setting of the cement, may be finely controlled through the simultaneous modification of the CAC by sodium monophosphate and polyphosphate. Such control can be advantageous when developing materials for challenging time sensitive applications, such as for dental reconstructive cements and rapid setting structural repair cements. However, reports of investigations into these 'mixed phosphate' systems do not exist in the literature. Of the systems reported in the literature, only Brown & Ma report phase assemblage analysis after curing periods of greater than 7 days (30 months), and hence it is evident that further study on the long-term hydration is required.

To better understand the roles of sodium monophosphate and polyphosphate in the longer term hydration of CAC, both independently and in combination with one another, three series of formulations were prepared: (i) 0p*x*m, (ii) 0.2p*x*m, and (iii) 0.4p*x*m. The 0p*x*m series comprised of two additional formulations in addition to neat CAC ($x = 0$), which were $x = 0.025$ and 0.1. These were chosen on the basis of the calorimetry data obtained in the previous chapter, which indicated that with low levels of monophosphate addition in this series there was no induction period observed, whereas when the m/c (monophosphate to cement ratio, x) ratio was 0.1 an induction period was observed. In the case of the 0.2p*x*m formulation series a similar approach was taken, by examining formulations where $x = 0$, $x = 0.025$ and $x = 0.1$; the latter two values being chosen as they indicate levels of monophosphate addition which have ($x = 0.025$) no induction period due to low level modification, and ($x = 0.1$) a distinct induction period due to greater alteration of the reaction mechanism. Additionally, these values straddle the peak for setting times of this series as determined by Vicat analysis, also reported in the previous chapter. A similar rationale was used to select the formulations for further investigation, however additionally a formulation with a very high monophosphate to cement ratio (0.25) was chosen as well. Samples were subjected to analysis by XRD and TGA to determine the hydrate phase development as a function of curing duration. The longer-term behaviour of the 0.4p0.05m composition was examined by XRD as this formulation

exhibited the most favourable setting behaviour as reported in the previous chapter. This was also the formulation chosen to investigate the influence of hydrothermal treatment.

5.2 Experimental procedures

The experimental parameters used for the experiments not described in this section, such as the slurry preparation, sample casting, curing and demoulding, in addition to analytical techniques such as XRD, TGA, are outlined in the Experimental Procedures chapter.

Formulations selected for hydrothermal treatment were prepared and cast in Teflon containers and placed in steel vessels, shown in Figure 5-1, which were closed using a Teflon washer and steel cap. The steel cap and vessel were secured using a bracket with a screw and placed in a furnace at 180°C for various durations. Vessels removed from the furnace were opened once they had cooled to room temperature.

Figure 5-1 Steel vessel (centre), Teflon insert (right) and fastening bracket (left) used for hydrothermal treatment.

Compressive strength measurements for the 0.4p0m and 0p0.1m formulations were carried out using a Zwick Roell testing instrument using demoulded samples but without the hydration arrested, as such the testing was performed at the specified age. Cylindrical samples with diameter 14 mm were cut to lengths of 28 mm, the ends polished flat and parallel, and tested to failure. Compressive strength values were calculated using the maximum load per unit area of the contact face. Care was taken to ensure that the contact faces were polished flat and perpendicular to the length axis of the cylinders. Samples were tested in triplicate and the error bars on plots of the strengths represent the standard deviation of the set of measurements.

5.3 Results and discussion

5.3.1 Long term hydration

5.3.1.1 XRD

All the samples examined in this chapter hardened and developed strength. Diffraction data for the neat CAC, 0p0.025m and 0p0.1m formulations after 28, 120 and 180 days of curing at 20°C are shown in Figure 5-2. The neat CAC samples show limited reflections from the clinker phases such as monocalcium aluminate (CA, Powder Diffraction File (PDF) #01-070-0134), when compared with the CAC anhydrous clinker. Strong reflections for the hydrate phases hydrogarnet (C_3AH_6, PDF #00-024-0217) and gibbsite (AH_3, PDF #00-012-0401) are observed. This is typical of conventional CAC hydration, where there is considerable CA dissolution and precipitation of the stable hydrate phases and the absence of metastable phases such as CAH_{10} (PDF #00-012-0408) and C_2AH_8 (PDF #00-045-0564) after 28 days under these curing conditions. This, in addition to the fact that there are only small differences between the diffractograms obtained for samples cured for 28 and 180 days, indicates that the majority of hydration of these samples occurs within the first 28 days, followed by slow ongoing hydration thereafter.

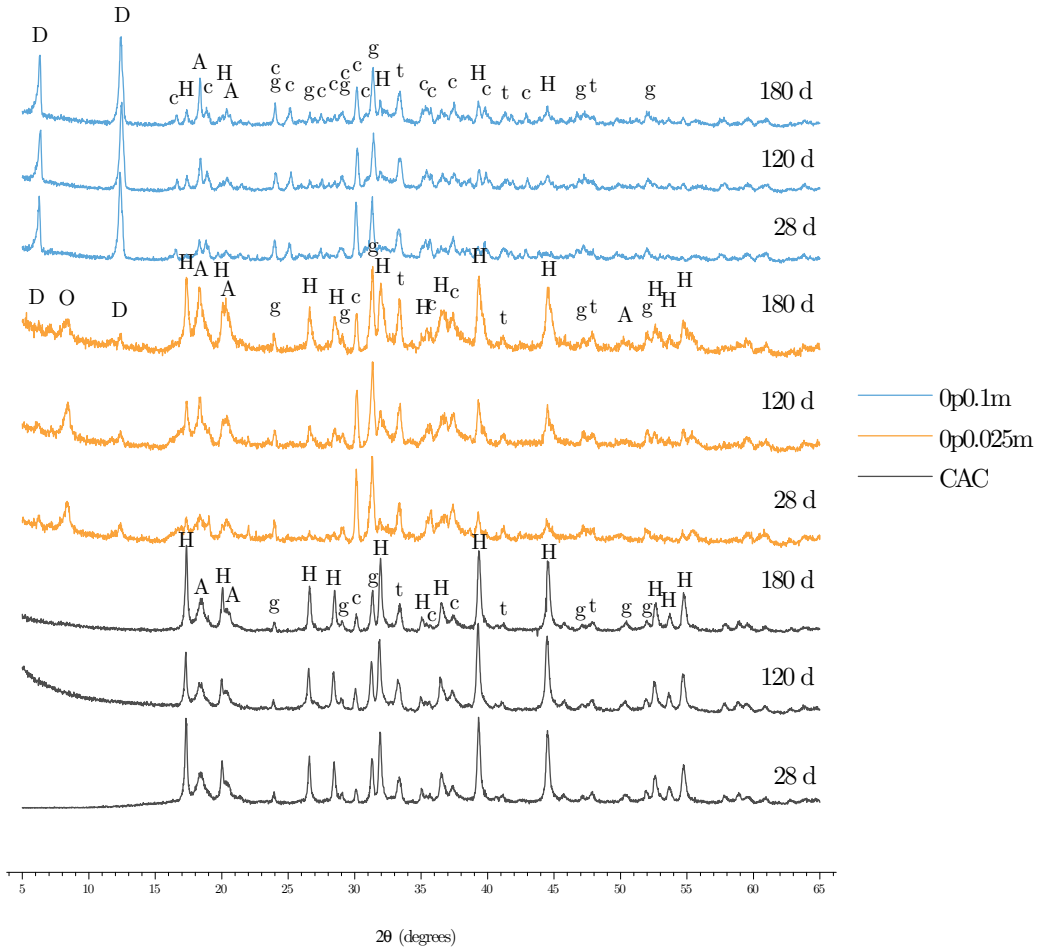

Figure 5-2 X-ray diffractograms obtained for CAC, 0p0.025m and 0p0.1m formulations, at 28, 120 and 180 days of curing: letters indicate monocalcium aluminate (CA, c), gehlenite (C_2AS, g), calcium titanate (CT, t) and CAC hydration phases CAH_{10} (D), C_2AH_8 (O), hydrogarnet (C_3AH_6, H) and gibbsite (AH_3, A).

The effects of a small addition of monophosphate can be seen from the diffractograms shown in Figure 5-2 for the 0p0.025m formulation. For each of the three curing periods all hydrate phases, including both stable and metastable, are observed. With increasing curing period there is a decrease in the intensity of reflections belonging to clinker phases and an increase in the intensity for reflections belonging to the stable hydrates, gibbsite and hydrogarnet. At greater levels of monophosphate addition, as in

the 0p0.1m samples, for which XRD data are shown in Figure 5-2, greater unreacted clinker content is observed at each of the three curing durations when compared with the neat CAC and 0p0.025m formulations. In addition the presence of C_2AH_8 is not detected, however reflections for CAH_{10} dominate the diffractograms and this phase persists even after 180 days curing. However, reflections belonging to gibbsite and hydrogarnet are clearly identifiable. The presence of C_2AH_8 is not required in conventional hydration, but this phase will usually form due to 'ease of nucleation' (Scrivener 2003), however as can be seen in the previous chapter, the heat of hydration for this formulation is very low, and as such this also does not favour the precipitation of this metastable phase (Bushnell-Watson & Sharp 1990). The persistence of the monocalcium aluminate decahydrate phase up to 180 days after slurry preparation is noteworthy, as in conventional CAC hydration at room temperature this phase is generally not observed after a few days. It may be that this phase is formed as a result of crystallisation from the C-A-H gel as described by Bushnell-Watson and Sharp (1992).

Figure 5-3 displays three sets of diffractograms obtained for the 0.2p*x*m series of formulations, specifically 0.2p0m, 0.2p0.025m and 0.2p0.1m samples. In the case of the 0.2p0m formulation, the phosphate addition results in only unreacted clinker phases being identified after 28 and 120 days of curing, without the formation of crystalline hydration products, although the binder had hardened and developed significant strength (section 5.3.1.3) by this point in time. However, after 180 days of hydration, the precipitation of CAH_{10}, gibbsite and hydrogarnet is observed.

The relative peak height ratio of the CA reflection at approximately 30° to a gehlenite peak, such as that found at 31° 2θ, is useful as a semi-quantitative measure to determine the extent of clinker dissolution of systems, as gehlenite is considered inert at these stages of hydration in this system with the w/c at 0.4. Although the through solution hydration (Hewlett 2004) of gehlenite is possible reported instances have occurred at very long curing periods , presumably after the anhydrous CAC is consumed and conversion has taken place. Specifically, this ratio is useful in determining the extent of hydration of the clinker itself. For these systems, this is a useful metric in determining the extent of hydration, as considerable unreacted clinker remains at long curing periods. This ratio is plotted as a function of the curing period

for the 0p*x*m and 0.2p*x*m formulation series in Figure 5-4, from which it is possible to see that the 0.2p*x*m formulations have considerably less clinker dissolution in the initial 28 days than the 0p*x*m formulations.

The mixed phosphate formulation, 0.2p0.025m, exhibits interesting hydration behaviour, in that gibbsite precipitation is observed at 28 days hydration, and after 120 days curing the extent of hydration (as measured by clinker consumption) surpasses that achieved by the 0.2p0m formulation after 180 days. At 180 days of hydration there is considerable gibbsite and hydrogarnet precipitation, however no presence metastable hydrate phases is detected at any of the ages at which analysis was performed. With greater monophosphate content and in the presence of polyphosphate, such as in 0.2p0.1m, the precipitation of stable hydrate phases is slower, and at 180 days the presence of CAH_{10} is detected. Across the three formulations studied and the three curing durations it is possible to discern regions of diffuse scattering, one centred at 30° 2θ and another at higher angles around 50° 2θ. These regions are indicative of structures with little regular long-range order and hence the angles of the reflections vary, as such positive identification of these phases by diffraction analysis is difficult.

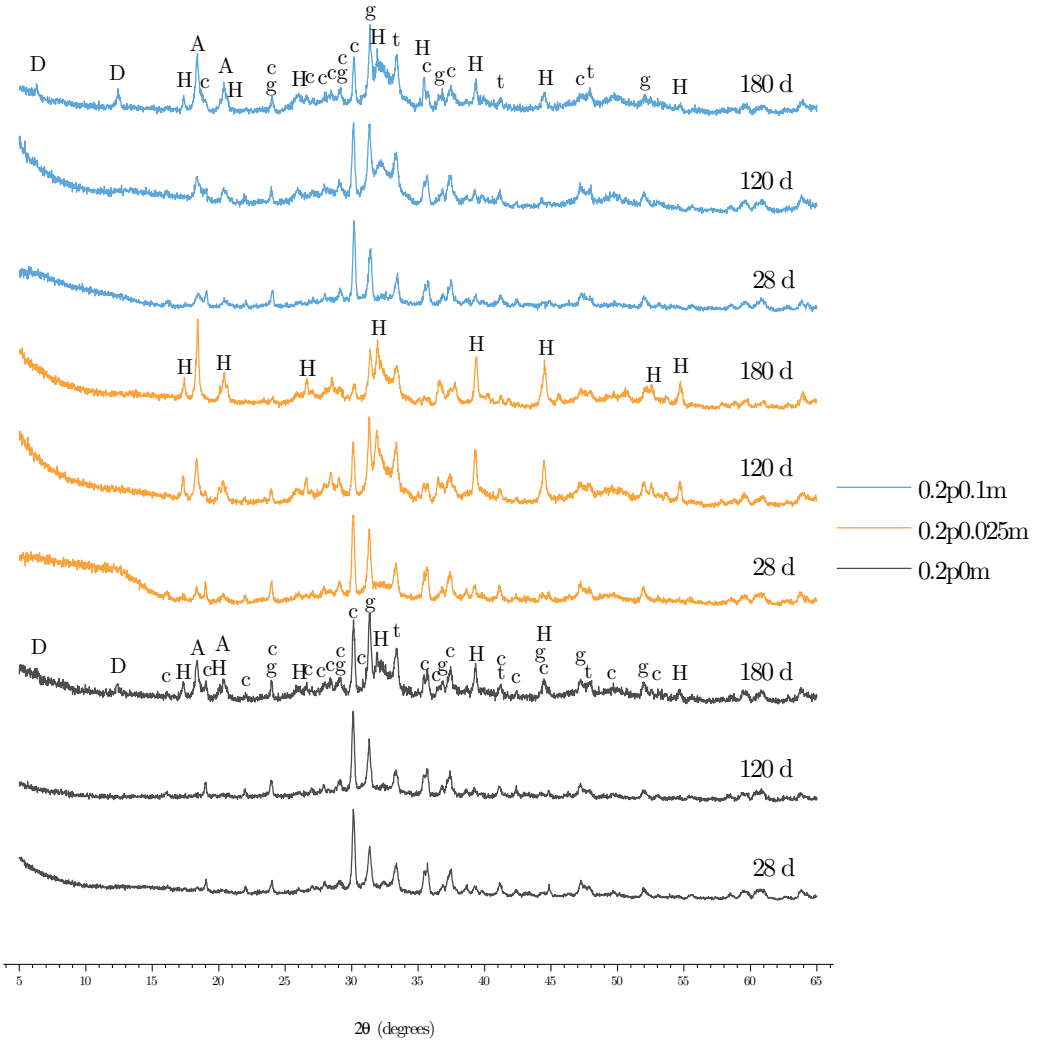

Figure 5-3 X-ray diffractograms obtained for 0.2p0m, 0.2p0.025m and 0.2p0.1m formulations, at 28, 120 and 180 days of curing: letters indicate monocalcium aluminate (CA, c), gehlenite (C_2AS, g), calcium titanate (CT, t) and CAC hydration phases CAH_{10} (D), C_2AH_8 (O), hydrogarnet (C_3AH_6, H) and gibbsite (AH_3, A).

Increasing monophosphate addition can be seen to retard the dissolution of the reactive clinker phase, CA, for both series. In the case of the 0.2p*x*m system, all three formulations seem to show an increase in the rate of clinker consumption after 120 days. In the absence of monophosphate, the 0.2p0m formulation exhibits little CA consumption. However, for the mixed phosphate formulations in this series, at low monophosphate addition the clinker consumption after 180 days surpasses those of the formulations in the 0p*x*m series, and for greater monophosphate additions exhibits an intermediate clinker consumption compared to the other two 0.2p*x*m formulations.

Hence the effect of monophosphate content, in mixed phosphate formulations, upon hydration/clinker consumption is not linear.

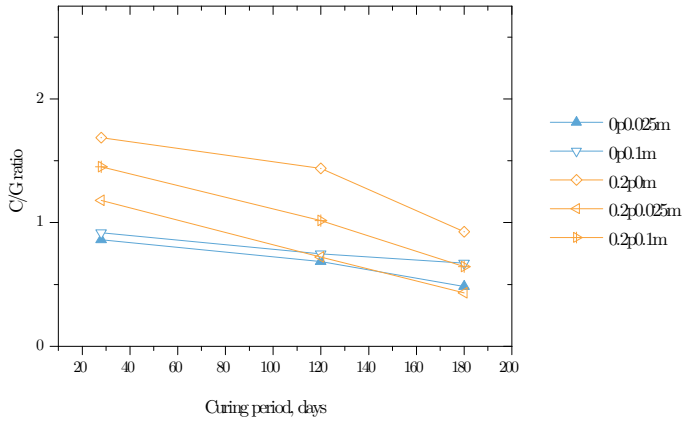

Figure 5-4 Ratio of gehlenite (31°) to CA (30°) reflection peak heights as a function of curing period, for 0.2p*x*m and 0p*x*m series formulations.

Four samples were studied in the 0.4p*x*m formulation series, 0.4p0m, 0.4p0.075m, 0.4p0.175m and 0.4p0.25m, and the diffraction data for these samples at 28, 120 and 180 days hydration are shown in Figure 5-5. The crystalline phase assemblage for these samples was consistent across formulation and curing period; no reflections for crystalline phases other than unreacted clinker phases were observed. As the samples in this series hardened, developed strength and no crystalline phases other than those found in the clinker have been detected, the hydrate phase(s) must be present with little long-range order. The regions of diffuse scattering centred about 30° 2θ support this, and are especially clear in the diffractograms for this formulation series. Interestingly there is only one such region observed in the 0.4p*x*m formulation series, unlike the 0.2p*x*m formulation series, which exhibited another at higher scattering angles. The clinker consumption as a function of time was minimal, and similar analysis to that shown in Figure 5-4 was not meaningful as the changes in the intensities were dwarfed by the noise in the dataset. However the clinker consumption for all the formulations over the entire range of curing periods studied was less than that calculated for 0.2p0m.

Figure 5-6 displays the diffractograms obtained for the 0.4p0.05m sample, which was studied for extended curing periods of up to 1080 days. The sample can be seen to exhibit the same absence of any crystalline hydrate phase precipitation as the rest of the 0.4p*x*m series, and this persists up to the longest curing period studied. In the case of the study by Swift (2013), a considerable 'conversion' from the amorphous binding phase to crystalline hydroxyapatite and a zeolitic phase was observed within 360 days of curing, whereas in this case either the binding phase is stable, or the conversion is considerably reduced or delayed.

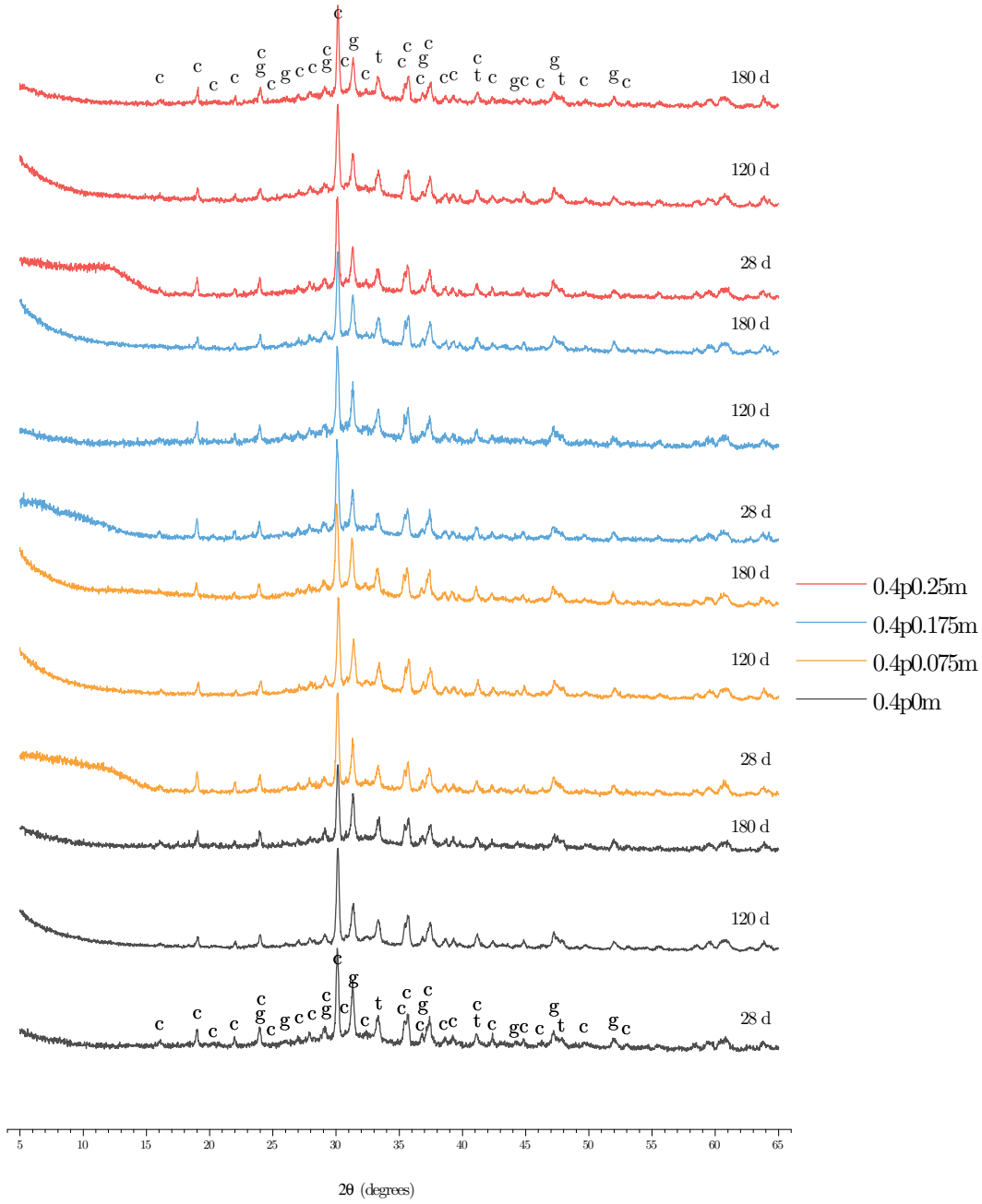

Figure 5-5 X-ray diffractograms obtained for 0.4p0m, 0.4p0.075m, 0.4p0.175m and 0.4p0.25m formulations, at 28, 120 and 180 days of curing: letters indicate monocalcium aluminate (CA, c), gehlenite (C_2AS, g), calcium titanate (CT, t).

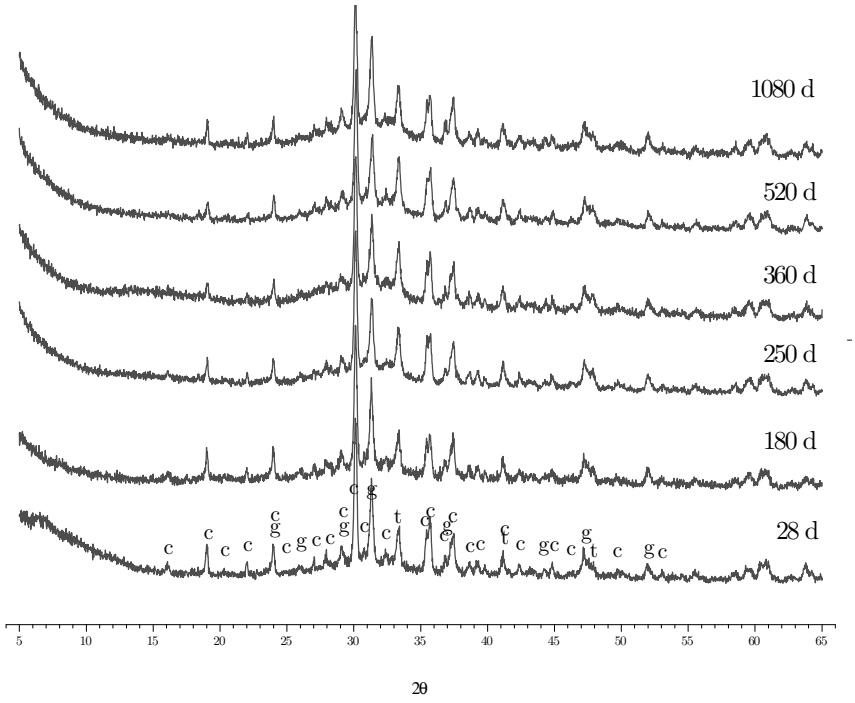

Figure 5-6 X-ray diffractograms obtained for the 0.4p0.05m formulation cured for various time periods: letters indicate monocalcium aluminate (CA, c), gehlenite (C_2AS, g), calcium titanate (CT, t).

5.3.1.2 TGA

TGA was performed to better understand the phase assemblage, through measuring the mass loss of a sample as a function of temperature during heating. Figure 5-7 shows data obtained for formulations in the 0p*x*m series at three different ages: parts (a), (c) and (e) show the mass as a function of temperature, while parts (b), (d) and (f) show the first derivative thermogravimetric (DTG) data, enabling better distinction between multiple mass loss events. A wide range of dehydration temperatures for CAC hydrates have been reported in the literature, however the sequence in which they dehydrate is consistent, with mass losses at higher temperatures being associated with the loss of structural water from the more thermodynamically favourable hydrates, and the systematic nature of this experiment makes use of this to aid characterisation.

Data obtained for the neat CAC samples shows two principal regions of mass loss, one at low temperatures below 150 °C, indicative of loosely bound water, and another between 200 and 350 °C. After 28 days of curing, the derivative data in this second region exhibit two distinct overlapping mass loss events, resulting in a primary peak

at 273 °C with a pronounced shoulder at 295 °C, typical of the principal dehydration temperatures of gibbsite (Balek et al. 2003b) and hydrogarnet (Ramachandran et al. 2002) respectively. After 120 days of hydration the hydrogarnet peak dominates the mass loss over the higher temperature range, resulting in the gibbsite peak becoming the shoulder to it.

After 180 days, greater quantities of the two stable hydrates are detected, and the combined peak width of the mass loss events for gibbsite and hydrogarnet dehydration also decreases, indicating an increase in the crystallinity of the two phases. The absence of any metastable phases after each of the three curing periods investigated, and the presence of considerable quantities of gibbsite and hydrogarnet is consistent with the conclusions drawn from the XRD data as discussed above. A broad mass loss centred about 700 °C is indicative of calcite decomposition (Ramachandran et al. 2002), perhaps due to minor carbonation during storage or analysis.

With monophosphate addition, the dehydration of metastable phases is detectable by TGA. At low levels of monophosphate addition, as in 0p0.025m, there are a number of mass loss events. Centred about 100 °C is a mass loss event which may be characterised as being due to poorly bound water or a gel phase associated with the hydration of CAC (Scrivener 2003), possibly a C-A-H type gel (Bushnell-Watson & Sharp 1992; F. Guirado et al. 1998; Ramachandran et al. 2002) or a hydrated alumina gel (Fujii et al. 1986; Skibsted et al. 1993). However in the presence of monophosphate this gel may additionally contain phosphorous. With increasing monophosphate content the mass lost from this dehydration event increases, supporting the likelihood that the chemistry and kinetics of formation of this phase is strongly linked with the phosphate addition, alternatively this may be as a result of additional free water in the less reacted samples. The absence of a significant mass loss at this temperature for the neat CAC indicates that the material has reached a stage of slow ongoing hydration post-conversion, where the large quantity of metastable phases formed early in the hydration process have converted to stable phases and are no longer present, with the liberated free water continuing to hydrate clinker at a much slower rate.

(a) (b)

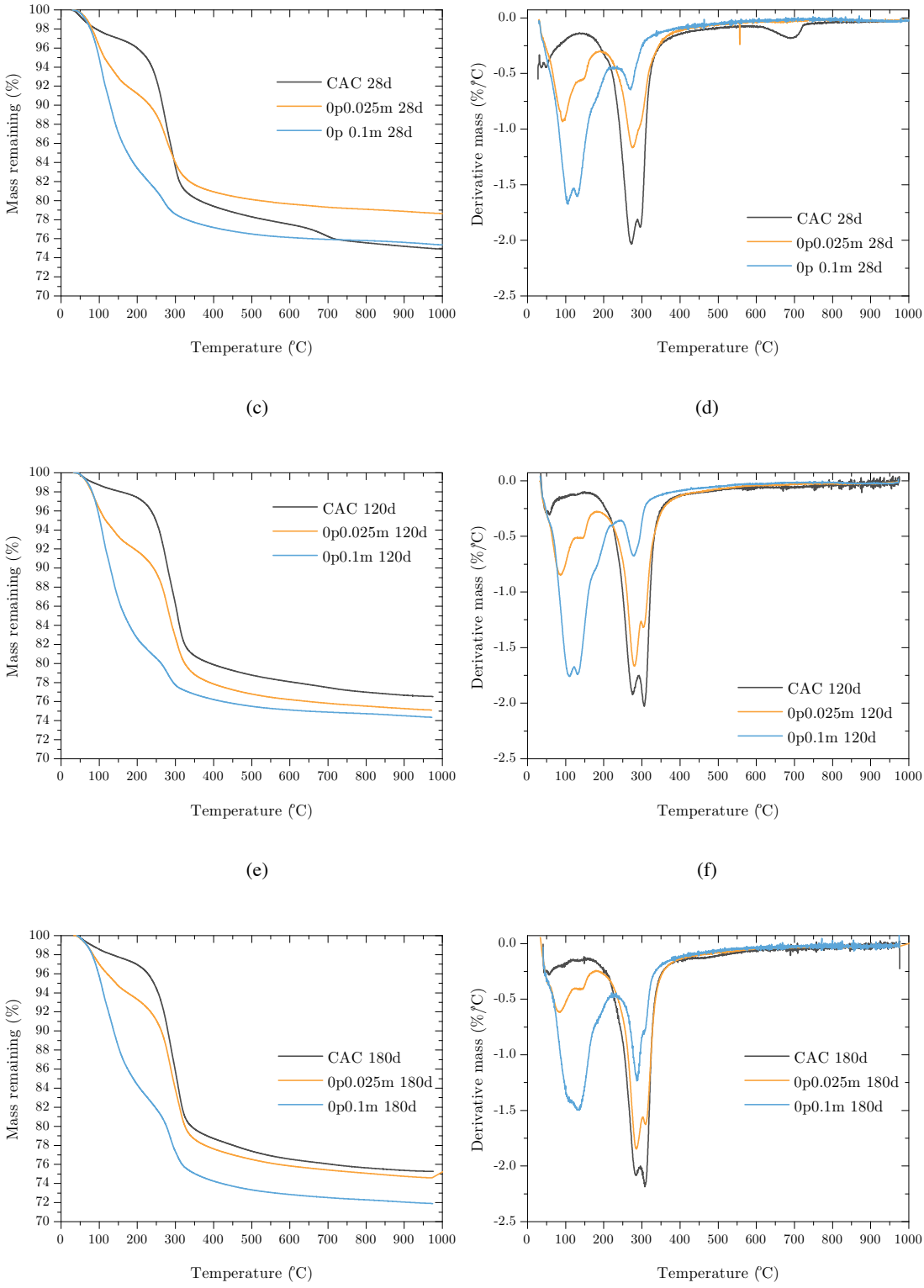

Figure 5-7 Thermogravimetric analysis of formulations in the 0p*x*m series after 28, 120 and 180 days of curing. Parts (a), (c) and (e) show TGA mass loss data, and the respective first derivative data are plotted in (b), (d) and (f).

In the case of the 0p0.1m sample, this gel phase dehydration overlaps the mass loss associated with the dehydration of CAH_{10}, as such there is a prominent shoulder

visible at 132 °C, in agreement with the detection of this phase by XRD. Additionally there is a weak shoulder observed in the DTG for the 0p0.1m formulations, indicating the presence of C_2AH_8. However the absence of this phase from the diffraction data indicates either that the amount present is limited and below the detection limit of the technique, or that it is poorly crystalline, or possibly a combination of both. There is a more defined mass loss associated with the 0p0.025m formulation, which may be solely attributed to the dehydration of C_2AH_8, however the line shape of the first derivative displays a very flat shoulder, perhaps due to the superposition of a neighbouring mass loss from the presence of a smaller quantity of CAH_{10}.

At higher temperatures, a mass loss due to the presence of gibbsite and a shoulder due to hydrogarnet are observed, however the rate of mass loss indicates considerably lower quantities than are detected for the neat CAC after a 28 day curing period. In this higher temperature region only a small peak due to the dehydration of gibbsite is observed for the 0p0.1m sample, consistent with the XRD diffractogram.

With increasing curing period the neat CAC sample exhibited an increase in the intensity of the dehydration peak attributed to hydrogarnet, due to an increased content of this phase as per conventional advanced CAC hydration. The gel phase and metastable phase content of the 0p0.025m sample decrease with curing period, accompanied by a consistent increase in the gibbsite and hydrogarnet contents. The 0p0.1m sample exhibits a consistent increase in the stable phase content as a function of curing period. Also, an increase in the gel and CAH_{10} content between 28 and 120 days of hydration can be seen, however this decreased in the case of samples cured to 180 days, indicating that the rate of dissolution of the clinker reduces to be significantly below the rate of conversion of metastable and gel phases to stable hydrates, after 120 days of curing.

Figure 5-8 shows data obtained for the 0.2p*x*m series. All samples show a low temperature mass loss event, relating to the gel phase dehydration. In the case of the 0.2p0.025m, the addition of a little monophosphate to a polyphosphate rich system results in the acceleration of the conventional hydration in the longer term, relative to the 0.2p0m formulation. As with the 0p*x*m series, there seems to be a conversion process whereby the hydrate phases detected at low temperatures are consumed in the process leading to the precipitation of the stable hydrates. The presence of gibbsite is

detected for each of the three formulations at 28 days; dehydration of hydrogarnet is detected after 120 days of hydration in the case of the 0.2p0.025m formulation, whereas this is only detected at 180 days for the 0.2p0m and 0.2p0.1m samples. Additionally, the quantities of the stable hydrates detected in 0.2p0.025m were greater than for the other formulations in the 0.2p*x*m series at each curing period examined.

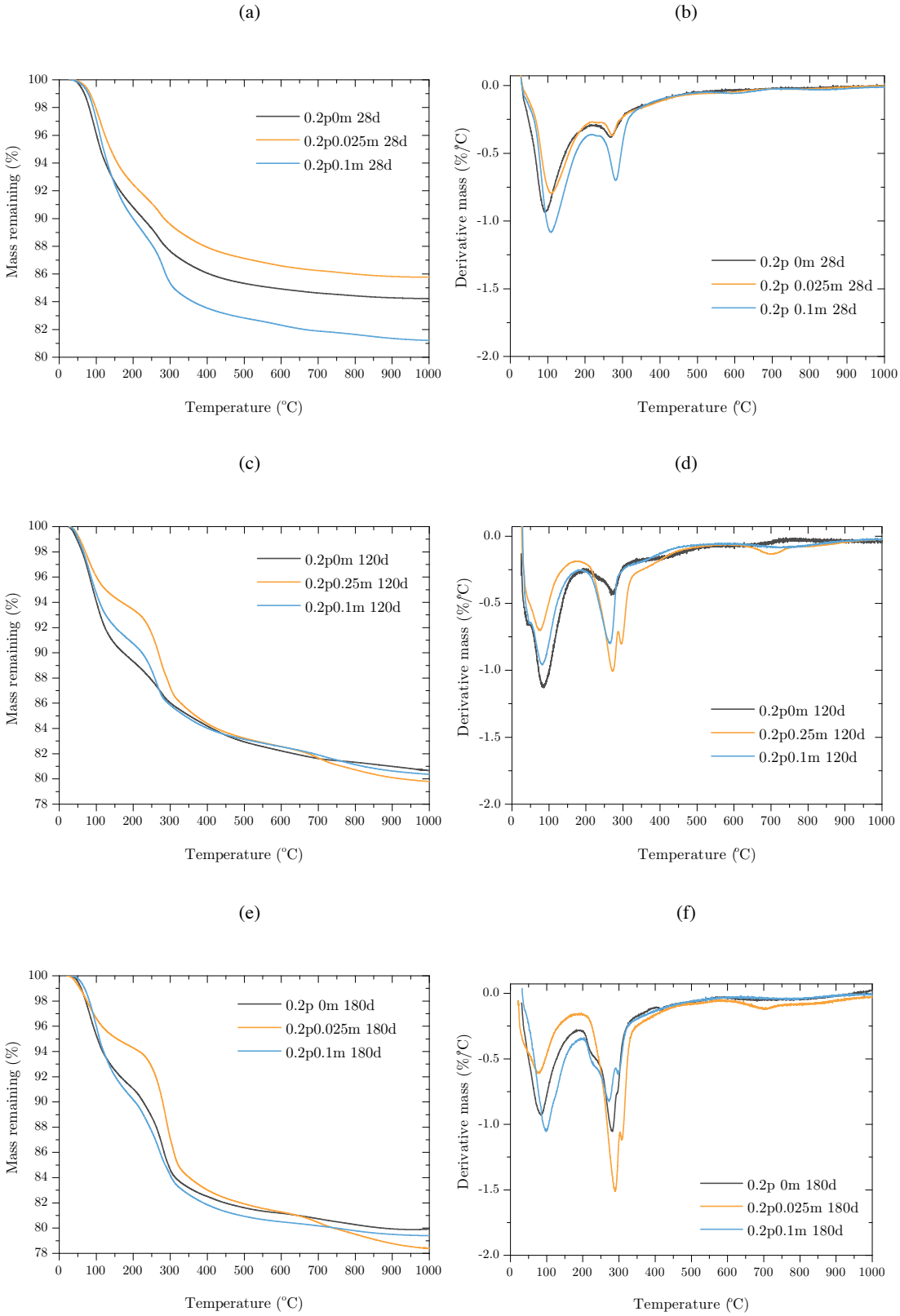

Figure 5-8 Thermogravimetric analysis of formulations in the 0.2p*x*m series after 28, 120 and 180 days of curing. Parts (a), (c) and (e) show TGA mass loss data, and the respective first derivative data are plotted in (b), (d) and (f).

At 180 days, a broad shoulder at 225 °C is observed for both the 0.2p0m and 0.2p0.1m formulations. This is similar to that observed for the formulations in 0.4p*x*m series, data for which are shown in Figure 5-9.

The formulations in the 0.4p*x*m series exhibit three main mass loss events at 90, 230 and just below 300 °C. Each of these mass loss events can occur over a broad temperature range indicating the loss of non-crystalline water (F. Guirado et al. 1998). This is in agreement with the diffraction data obtained for this series of formulations, which showed the absence of any crystalline hydrate phase precipitation.

The lowest temperature dehydration event in the case of 0.4p*x*m series formulations is attributed to the gel phase, which is least developed for the 0.4p0m formulation at each of the curing periods relative to the other formulations within the series. This mass loss event progressively increases across the series with curing period up to 180 days, implying continuous dissolution of the clinker throughout this period. A very broad mass loss event centred below 250 °C is also observed at 28 days curing. After 120 days this event is less broad, but nevertheless indicates the dehydration of a phase with very little long range order, followed by mass loss events related to the heating of the products of the intermediate mass loss, analogous to that described by Guirado et al. (1998). Guirado et al. (1998) describe the dehydration of CAH_{10} as being characterised by four different mass loss events, two low temperature events (often overlapping) occur as a result of crystalline CAH_{10} dehydrating and later collapsing, followed by a very broad peak generally appearing as a plateau between the low temperature events and a more defined peak at approximately 260-280 °C. The higher temperature mass losses are of particular interest as they relate to the decomposition of the amorphous portion of CAH_{10}, and Guirado et al. suggest that this dehydration results in the formation of cryptocrystalline gibbsite which then undergoes its own dehydration at 280 °C. This effect is reduced after 180 days, and the intermediate and higher temperature mass loss events occur at more similar temperatures across formulations in the series, this may be as a result of a more narrow variability in the chemistry of this amorphous phase as its maturity increases.

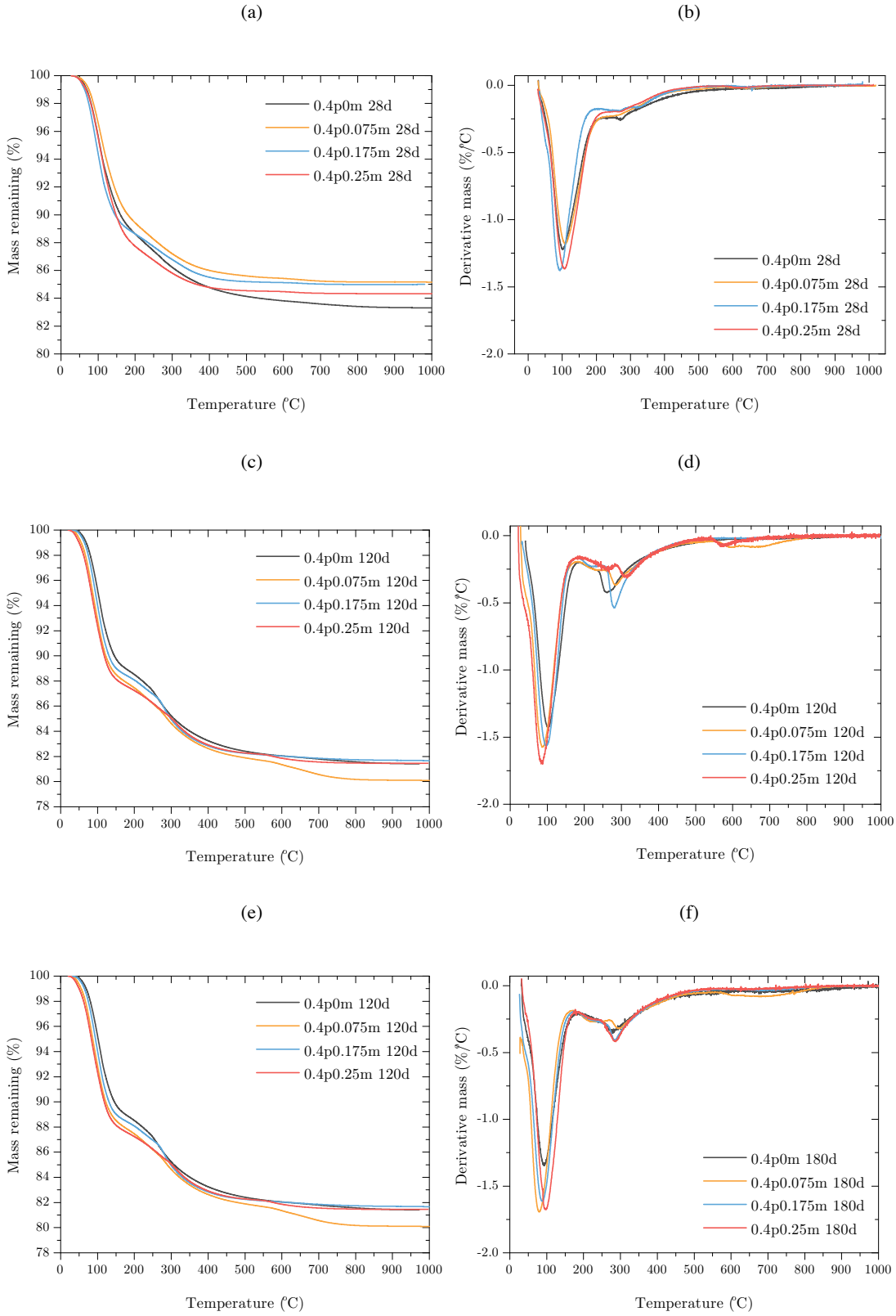

Figure 5-9 Thermogravimetric analysis of formulations in the 0.4p*x*m series after 28, 120 and 180 days of curing. Parts (a), (c) and (e) show TGA mass loss data, and the respective first derivative data are plotted in (b), (d) and (f).

5.3.1.3 Compressive strength

The evolution of compressive strength as a function of curing period was determined for the 0.4p0m, 0p0.1m and neat CAC samples, as shown in Figure 5-10. For the neat CAC formulation, 31 MPa was reached after 48 hours of curing, which is typical for such high alumina cementitious materials and also forms the basis of its use as an additive to OPC based systems for the control of the setting behaviour (Zhang et al. 1997). A local maximum in strength of 60 MPa was observed after 4 days of curing, however this reduces thereafter, followed by a steady increase in strength after 7 days. This sudden increase upon early hydration is attributed to the metastable phases, such as CAH_{10} and C_2AH_8, dominating the hydrate phase assemblage and contributing to the strength development. However as hydration proceeds these metastable phases dissolve and the more stable hydrate phases steadily precipitate, hence the observation of a considerable drop in compressive strength followed by a gradual increase, which is typical for CAC cured at this temperature with a water to cement ratio in the region of 0.4 (Scrivener 2003). As the setting behaviour of the 0p0.1m could not be determined within the first 24 hours via Vicat testing, as explained in the previous chapter, and as such, the low strength observed for the 0p0.1m formulation at short curing durations was expected. However, this increases steadily, whilst consistently exhibiting strengths lower than those obtained for the neat CAC and 0.4p0m formulations. For the 0.4p0m formulation it is observed that during the first few days of curing the compressive strengths exhibited were characteristically high (31 MPa after 48 hours), as expected from CAC materials (Taylor 1990), however this increases with curing period (to a maximum of 72 MPa after 360 days), which is higher than the strength exhibited by the neat CAC at each of the curing periods studied after 4 days. The early strengths obtained are in good agreement with those obtained by Sugama et al. (1991), but less than the 77 MPa reported by Swift et al. (2013). This difference in compressive strength is attributed to a higher water to cement ratio (Scrivener 2003) and different phosphate to cement ratio used here, both of which affect the rate of reaction, phase assemblage and porosity development.

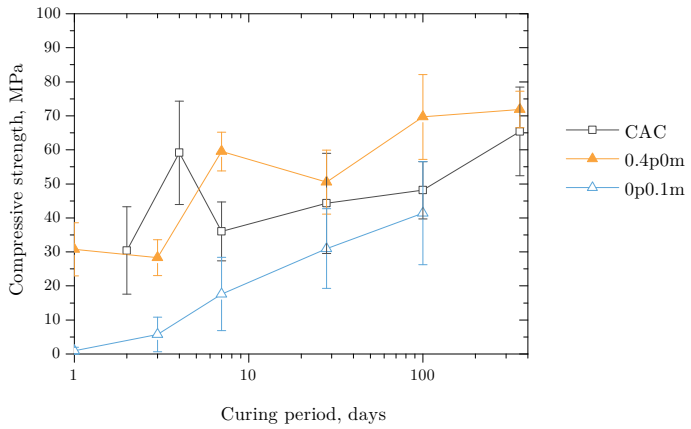

Figure 5-10 Compressive strength values determined for neat CAC, 0.4p0m and 0p0.1m samples, as a function of curing period.

5.3.1.4 Discussion

The addition of monophosphate to the CAC system results in the persistence of metastable phases up to at least 180 days of age, with a considerable reduction in the rate of clinker dissolution. Whereas with lower monophosphate addition there is persistence of the C_2AH_8, in the case of the greater monophosphate quantities only the decahydrate metastable phase is observed with very prominent reflections. The content of stable hydrates for this series of samples does not reach the level observed for the neat CAC samples, at any point during the first 180 days of hydration. With both TGA and XRD analysis, a clear conversion process can be observed for the 0p*x*m series whereby the metastable phases, which undergo low temperature dehydration events and exhibit low angle 2θ reflections, reduce whilst the contents of stable phases such as gibbsite and hydrogarnet increase. With increasing monophosphate content this retardation of the hydration process is even more prominent, with the rate of stable phase precipitation (and clinker phase dissolution) decreasing relative to the neat CAC and 0p0.025m formulations.

The polyphosphate modified CAC formulations, 0.2p0m and 0.4p0m, show a deviation away from the conventional hydration behaviour. Both exhibit large mass loss events at low temperatures associated with the dehydration of an amorphous gel phase with low long-range order, and no detection of conventional hydrate phases at 28 days of curing by TGA or XRD analysis. If the characterisation of the quantity of this low temperature mass loss being a function of the phosphate content is correct,

then in the absence of detecting any other mass losses it is reasonable to propose that this amorphous gel phase is likely to be a phosphate-containing binding phase, and similar to the C-A-P-H gel described by Ma and Brown (1994), which can act as a diffusion barrier, whilst also complexing the calcium (Chughtai et al. 1968) and/or aluminium ions (Hsu 1968).

In the case of the 0.4p0m formulation, the absence of conventional crystalline phases persists to the maximum curing period duration studied. For the 0.2p0m formulation, with time, conventional stable hydrate phases are observed, however it is unclear whether these precipitated via the amorphous gel phase as an intermediate. For the formulations in the 0.2p*x*m series it can be seen that the precipitation of the stable hydrates is at the expense of the amorphous phase, implying that it is an intermediate metastable phase similar to CAH_{10} and C_2AH_8. Within the 0.2p*x*m series it is clear that a non-linear relationship between the phase evolution and the increasing monophosphate content is observed. At low levels of monophosphate addition there is an elevated rate of stable hydrate precipitation with respect to the 0.2p0m. However with greater monophosphate modification, such as in the 0.2p0.1m formulation, this is not the case, and the rate of stable hydrate precipitation reduces relative to the 0.2p0.025m sample, but still maintains a rate greater than that observed for the 0.2p0m formulation. A similar effect is seen for the dissolution of the clinker phases. The effect of the minor monophosphate content can be seen to decrease the average chain length of the phosphate ions in solution, as identified from the solution NMR and FTIR data presented in the previous chapter. As such, although it is not discernable from the data collected, it is possible that the C-A-P-H gel is a single amorphous phase with a variable composition/stoichiometry with low levels of monophosphate addition, however as this increases two phases are observed which may result in a smaller diffusion barrier for the precipitation of CAC hydrates. Such a secondary amorphous phase may dehydrate at a similar temperature to that of the primary amorphous phase, to which the low temperature mass loss event is attributed, and hence mass losses may be overlapping and subsequently difficult to determine.

In the case of the 0.4p*x*m series, it is observed that there is no crystalline phase precipitation at any point in the hydration period studied for any of the samples. An amorphous phase is detected, likely also to be a C-A-P-H phase, similar to that

observed for the 0.2p*x*m series, which dehydrates at low temperatures. However, the stoichiometry of these phases is likely to be different, changing over time and dependent on the monophosphate content. What is seen, however, is that the effect of polyphosphate dominates over that of the monophosphate, in the quantities investigated. There seems to only be one 2θ range over which diffuse scattering is observed, centred about 32 degrees, whereas in the case of the 0.2p*x*m there is an additional region of diffuse scattering observed at a higher angle range.

5.3.2 Hydrothermal treatment

The 0.4p0.05m formulation was hydrothermally treated at 180 °C for 4, 6, 24 and 120 hours, and the diffraction data obtained for each of these samples are shown in Figure 5-11. It was observed that up to 4 hours of hydrothermal treatment did not result in any crystalline phase precipitation; this is indicated by the absence of any reflections other than those belonging to the clinker phases. This is the same as was found for 0.4p0.05m cured without hydrothermal treatment, complete with a region of diffuse scattering centred about 30° 2θ indicating the presence of a phase with low long range order. After 6 hours of treatment, reflections for the clinker phases disappear, indicating the full dissolution of this phases, replaced by strong and defined reflections for hydroxyapatite (HA, $Ca_5(PO_4)_3(OH)$, PDF #01-084-1998) in addition to the presence of two regions of diffuse scattering at just below 15° and 38° 2θ. With increasing treatment duration, the peaks for HA become even more defined and increase in intensity, whilst sharp reflections begin to emerge from the regions of diffuse scattering. From the diffractograms alone it is not possible to positively identify the phases responsible for these reflections, however it may be inferred that there is more than one phase in addition to HA, primarily due to the presence of a well defined peak at 24° 2θ (not belonging to HA) and the presence of a region of diffuse scattering assumed to belong to neither HA or the aforementioned well defined reflection. In addition to the peak at 24° 2θ the powder diffraction file card for HA in the range 27-30° 2θ shows a higher intensity for the (210) reflection at 29° than for the (102) reflection at 28°, which is not observed for the diffractogram plotted in Figure 5-11. It is suggested that the two additional phases may be boemite (γ-AlO(OH), PDF #01-076-1871) and a hydroxysodalite type feldspathoid (zeolite-like) phase ($Na_2O{\cdot}Al_2O_3{\cdot}1.68SiO_2{\cdot}1.73H_2O$, PDF #00-031-1270). Assignment of the

HA and boehmite reflections was in line with the findings of Sugama et al. (2000) who reported that the hydrothermal treatment of a sodium phosphate modified fly ash / CAC blended cement resulted in the formation of HA and analcime ($NaAlSi_2O{\cdot}H_2O$), similar in composition to the phases detected in these samples, as primary crystalline phases with boehmite as a minor phase. The formation of these phases under hydrothermal conditions has also been attributed with reduced carbonation rates (Sugama & Carciello 1993).

The hydroxysodalite type phase has also been reported by Grutzeck and Siemer (1998) who combined a fly ash with a sodium aluminate slurry at elevated temperatures. Both of these systems, in addition to the CAP system investigated by Swift (Swift 2013), who looked at the single phosphate modification of CAC and PFA or BFS blends (without hydrothermal treatment), all had considerable silicon contents. Swift noted that the formation of the sodium-containing zeolitic phase coincided with the dissolution of the gehlenite phase, whose reaction became significant after the complete dissolution of CA in the system, whereas in the formulations considered here this was only observed after hydrothermal treatment and was not observed for any sample during the curing periods studied and in the case of the 0.4p0.05m sample this was not observed during the 1050 days for which it was studied. The varying silicon contents of the systems reported and the different parameters of synthesis are responsible for the different phases being formed. What is clear is that the formation of HA is consistent for all the systems, and that this generally occurs before the sodium containing zeolitic phase precipitation. The presence of the hydroxysodalite type phase is particularly interesting for the encapsulation of radioactive waste due to its zeolite-like structure, which has the capacity to accommodate various ions of radiological and environmental interest, either through in situ incorporation or via ion exchange (Grutzeck & Siemer 1998).

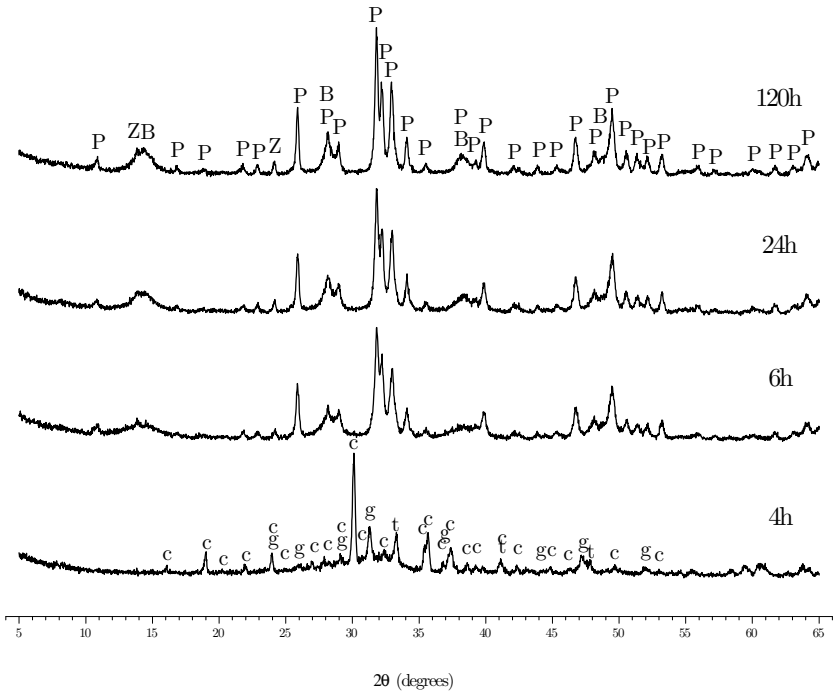

Figure 5-11 X-ray diffraction data obtained for the 0.4p0.05m formulation subjected to hydrothermal treatment at 180 °C for 4, 6, 24 and 120 hours: letters indicate monocalcium aluminate (c), gehlenite (g), calcium titanate (t), hydroxyapatite (P), boehmite (B) and hydroxysodalite type zeolite (Z).

TGA was performed on these samples. Mass loss data for the formulation hydrothermally treated at 180 °C for 1, 2, 4, 6, 8, 24 and 120 hours are shown in Figure 5-12 and their respective first derivatives are plotted in Figure 5-13. After 1 hour of treatment a thermogram typical for the 0.4p*x*m series after 28 days of curing is observed, and three characteristic mass loss events can be observed. The largest occurs at low temperature and corresponds to the amorphous hydrate phase, followed by the two-step dehydration of the secondary gel phase. With increasing hydrothermal treatment duration the amorphous phase content decreases rapidly, to the point where after 4 hours the three different mass losses are not overlapping and are clearly distinguishable. This is aligned with the absence of an apparent difference in the XRD reflections for these samples (the diffractogram obtained after 4 hours of hydrothermal treatment in Figure 5-11 shows no dissimilarities with those plotted in Figure 5-13). After 6h of treatment, a mass loss at approximately 500°C and an increase in the low temperature mass loss region are observed, and similarly at 24

hours or more of hydrothermal treatment, and additional mass loss events are resolved at 450 and 120°C. The assignment of these is made difficult due to the limited data available for the zeolite type phase. However, the the boehmite to alumina transition has been reported to be in the region of 350-450°C (Alphonse & Courty 2005; Perry 2011), coupled to the absence of dehydration behaviour of hydroxyapatite below 1000°C (Wang & Li 2007), supports the assignment of the 450°C mass loss event to the dehydration of boehmite to form corundum, and the broader higher temperature event to the zeolite type phase. With the presence of the boehmite, an additional peak is observed at 275°C which is assigned to the two step dehydration process of any remnant binder phase, with a small peak width that reflects the more homogeneous chemistry of this remnant after the formation of large quantities of more thermodynamically stable products.

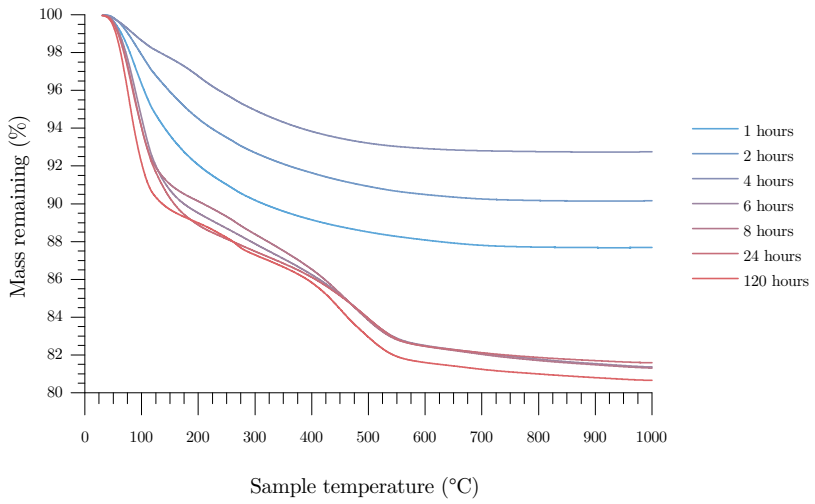

Figure 5-12 Thermogravimetric mass loss data obtained for 0.4p0.05m subjected to hydrothermal thermal treatment at 180 °C for increasing time periods up to a maximum of 120 hours.

The phase evolution with hydrothermal treatment is important for a number of reasons. From a waste packaging perspective the current cement encapsulation routes for ILW require the casting of the slurry into steel drums. Hence, if these were exposed to higher temperatures either intentionally as in hot isostatic pressing processes (although these are as of now limited to other radioactive waste packages)

or in the case of extreme conditions as a result of an accident, understanding the phase assemblage is an important cornerstone of modelling its chemical and mechanical integrity. Hydrothermal conditions are also encountered when considering materials for geothermal well applications, the application for which phosphate-modified CAC was originally developed by Sugama and co-workers.

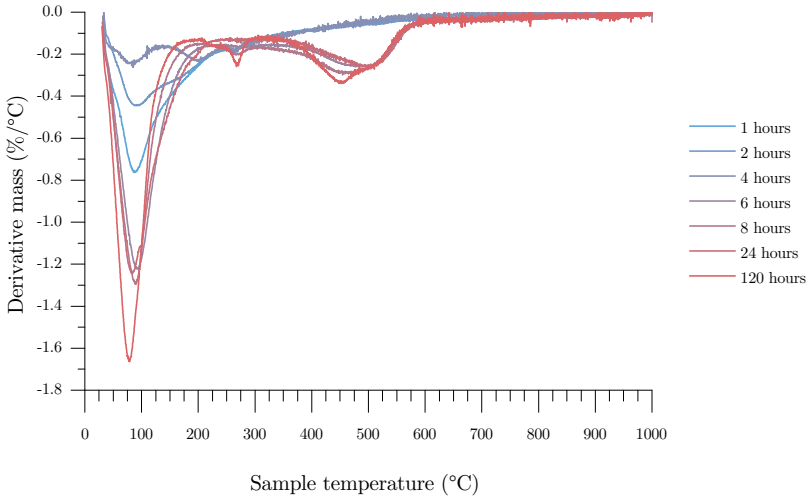

Figure 5-13 First derivative of TG mass loss data, showing the rate of loss of mass as a function of temperature, obtained for the 0.4p0.05m subjected to hydrothermal thermal treatment at 180 °C for increasing time periods up to a maximum of 120 hours.

5.4 Conclusions

Monophosphate modification of the CAC system, i.e. the development of formulations in the 0p*x*m series, results in a change of the kinetics of the hydration process, resulting in the persistence of metastable phases for up to 180 days. There exists a linear relationship between the extent of retardation of the hydration process, both in terms of clinker dissolution and the precipitation of hydrates, and the monophosphate content in 0p*x*m in the range studied.

Polyphosphate modification of the system results in the decrease of the rate of clinker dissolution and therefore limits the formation of conventional hydrates. In the case of the 0.2p*x*m system, low monophosphate content increases the rate of dissolution of the clinker, however greater monophosphate content results in the decrease of this dissolution. All the samples in the 0.2p*x*m and 0.4p*x*m series exhibited the presence of a hydrate phase with low long-range order, suspected to be a C-A-P-H phase, which dehydrates at approximately 100 °C. In the case of the 0.2p*x*m samples this phase could be an intermediate metastable phase via which the stable hydrates form. At high polyphosphate contents, as in the 0.4p*x*m series, the effect of polyphosphate dominates and no conventional hydrate phase precipitation is detected at all of the curing periods studied. In the case of the 0.4p0.05m no crystalline hydrate phases are detected up to a maximum curing period of 1080 days, with no 'conversion' to crystalline hydroxyapatite or zeolitic phases as seen by Swift (2013). Compressive strength of the 0.4p0m formulation develops early in its hydration (31 MPa at 48 hours) and consistently exceeds that of the neat CAC after the initial week of hydration, with a maximum determined value of 71 MPa after 360 days. The compromise of mechanical properties as a result of the conversion process was observed after 4 days for the neat CAC formulation, however this was avoided in 0.4p0m.

Hydrothermal treatment of the 0.4p0.05m formulation results in the formation of hydroxyapatite as the primary phase and the probable formation of secondary phases: boehmite and a hydroxysodalite type zeolite phase, similar to that reported in the literature for systems with a similar chemistry (Sugama et al. 2000; Grutzeck & Siemer 1998; Swift 2013). Among these, the HA and boehmite are documented as

advantageous phases when considering radioactive waste encapsulation applications (Grutzeck & Siemer 1998) and also minimising carbonation rates at hydrothermal temperatures (Sugama & Carciello 1993).

The 0.4p0m formulation was identified as a promising formulation to investigate further as it both inhibited the precipitation of conventional hydrate phases up to 180 days and exhibited improvements in compressive strength over the neat CAC samples. The focus of the following chapter is to better characterise the amorphous hydrate phase, which in this chapter is proposed to be a C-A-P-H gel phase.

6 NMR study of hydrate phases

Note: this chapter is in large part taken from the papers *"Identification of the hydrate gel phases present in phosphate-modified calcium aluminate binders"*, by M.A. Chavda, S.A. Bernal, D.C. Apperley, H. Kinoshita, & J.L. Provis, *Cement and Concrete Research,* **2015**, 70, pp. 21-28, and *"An NMR study of the hydration phases of sodium polyphosphate-modified calcium aluminate cement"* by M.A. Chavda, S.A. Bernal, D.C. Apperley, H. Kinoshita, & J.L. Provis, "*1st International Conference on the Chemistry of Construction Materials"*, **2013**, Berlin, Germany. Some minor modifications and revisions have been made for inclusion in this thesis.

6.1 Introduction

The phosphate modification of CAC has been investigated over the past decades, with the aim of preventing the conversion process, which can lead to unfavourable developments in the properties of the hardened material. The sodium phosphate modification of CAC has indeed been shown to be effective in altering the hydration of CAC, both in the literature (Sugama & Carciello 1995; Ma & Brown 1994; Swift et al. 2013) and in the previous chapters, with the latter focusing on extended curing periods of up to 180 days and the role of modification by phosphates and monophosphates simultaneously. The phosphate modification of CAC yields a complex hydrate phase, which has little long-range order and hence has been difficult to positively identify, resulting in an incoherence within the reported literature of the phase characterisation.

The clear discrepancies in the open literature regarding the gel chemistry of phosphate-modified CAC, as detailed in Chapter 5, elucidate that there is not a good existing understanding of the chemistry or mechanism of formation of the key binding phases in this binding system. Although these materials can be attractive in niche applications from a commercial point of view as a consequence of their moderate pH compared with conventional Portland cements, and so have been proposed for carbonation resistant geothermal well applications and as immobilisation matrices for

metallic radioactive wastes, this lack of understanding is currently restricting their deployment.

Solid-state nuclear magnetic resonance (NMR) spectroscopy has been used successfully in studying hydration of complex cement hydration processes due to its sensitivity to disordered as well as crystalline phases (Taylor 1990), including in the analysis of CACs (Skibsted et al. 1993; Cong & Kirkpatrick 1993; Müller et al. 1981; Rettel et al. 1997). Magic angle spinning (MAS) NMR spectroscopy has been widely used in cement hydration studies to probe local environments of aluminium and silicon nuclei. Nuclei such as ^{31}P have not been exploited to the same extent in the context of cement chemistry, despite favourable NMR properties; some notable investigations appear in the field of biocompatible dental cements (Legrand et al. 2009; Stamboulis et al. 2006) and the study of Portland cement (Poulsen et al. 2010). In the phosphate-modified CAC systems studied here, this is a key nucleus, which has not previously been examined through the use of advanced NMR techniques in phosphate-modified CAC, and so provides an obvious target for analysis here.

Therefore, this study seeks to better understand the phase chemistry in phosphate-modified calcium aluminate cements, and specifically to characterise the poorly-understood amorphous binding phase and gain further insight into its formation. Unmodified CAC, and CAC with sodium phosphate modification (where the sodium polyphosphate to cement ratio was maintained at 0.4), are assessed using XRD, TGA, and solid state NMR spectroscopic techniques including ^{29}Si MAS, ^{27}Al MAS, ^{31}P MAS, ^{31}P{^{1}H} CP/MAS, and ^{31}P/^{27}Al REAPDOR NMR. The phosphate content was selected based on long term phase development behaviour assessed in the previous chapter, where it is reported that a polyphosphate to cement ratio of 0.4 was shown to inhibit crystallisation of conventional CAC hydrates (the metastable of which are prone to conversion). No monophosphate was added to minimise the complexity of the chemistry for this investigation.

6.2 Experimental procedures

Cement pastes were formulated with a water to cement ratio of 0.35. Samples were mixed and cast in centrifuge tubes, sealed and kept at a temperature of 20°C and 100% relative humidity for 7, 180 and 360 days.

Hydration reactions were arrested and the materials subjected to XRD, TGA and NMR. The former two techniques were performed with the parameters outlined in Chapter 3.

All NMR experiments described in this chapter were performed on a Varian VNMRS 400 spectrometer (9.4 T), using a CP/MAS probe with 4 mm o.d. zirconia (PSZ) rotors.

a. ^{27}Al MAS NMR spectra were collected at 104.199 MHz and spinning speed 14.0 kHz (without proton decoupling), using a pulse delay of 0.2 s, a pulse width of 1.0 ms and an acquisition time of 10 ms, for 10,000 repetitions.
b. ^{31}P MAS were collected at 161.87 MHz and spinning speed 12.0 kHz, using a pulse delay of 60 s, a pulse width of 3.8 ms and an acquisition time of 30 ms, for 30 to 40 repetitions. ^{31}P{^{1}H} CP/MAS spectra were collected at the same spinning speed as ^{31}P MAS NMR, and at the same frequency, but with a pulse delay of 30 s, a pulse width of 1.0 ms and an acquisition time of 30 ms. A two pulse phase modulation (TPPM) decoupling frequency of 87.1 kHz was used in the initial ^{1}H 90° pulse and ^{1}H decoupling.

The chemical shifts of ^{27}Al and ^{31}P were referenced to external samples of 1.0 M aqueous solution of $AlCl_3 \cdot 6H_2O$ and 85% H_3PO_4, respectively.

For collection of ^{31}P{^{27}Al} REAPDOR spectra, the spin rate was fixed at 10 kHz with a 60 s recycle delay. An initial π pulse of duration 8.3 μs on the ^{31}P channel was followed by an adiabatic pulse on the secondary ^{27}Al channel for 33.3 μs (one third of a rotor period). The I{S} REAPDOR pulse sequence used is shown in Figure 6-1.

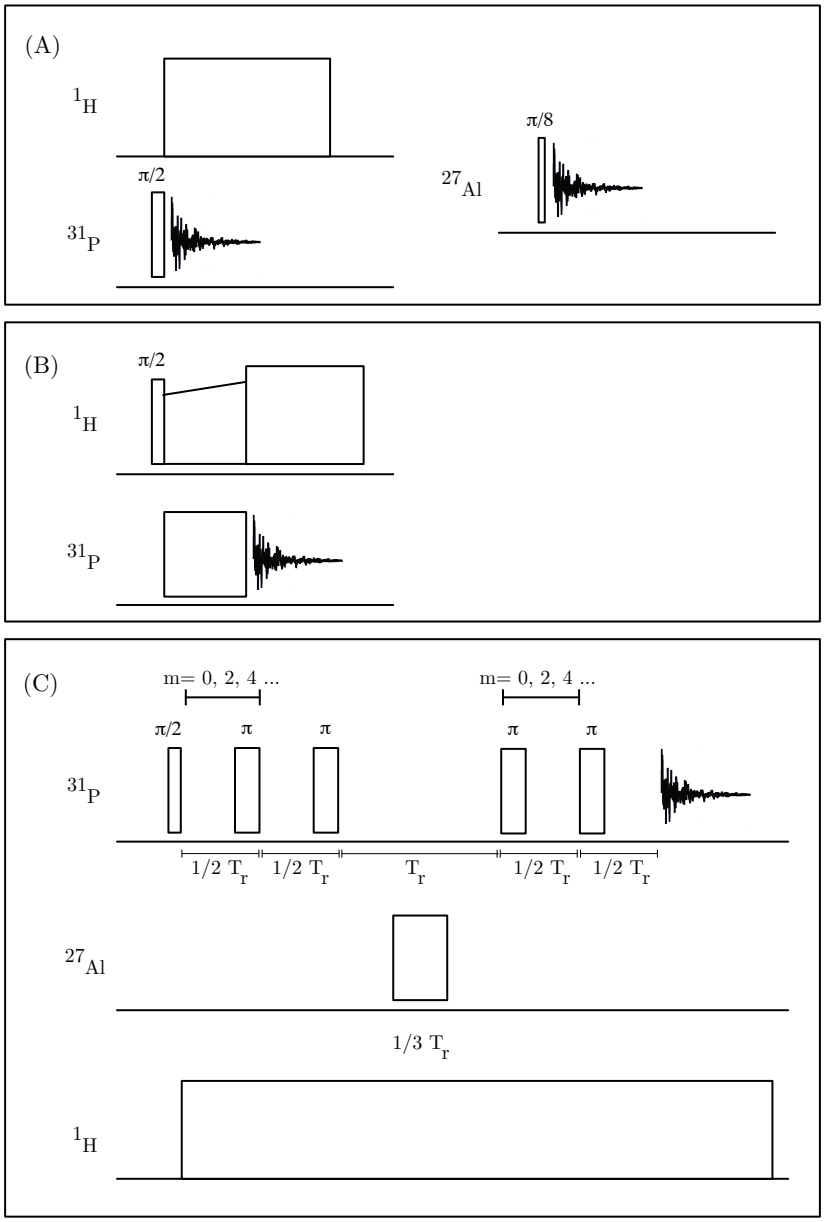

Figure 6-1 The NMR pulse sequences used for (A) ^{27}Al and ^{31}P MAS, (B) ^{31}P{^{1}H} CP/MAS and (C) ^{27}Al{^{31}P} REAPDOR experiments.

6.3 Results and discussion

6.3.1 X-ray diffractometry

Figure 6-2 displays the diffractograms for all samples prepared. Well-defined and intense reflections of the crystalline calcium aluminate clinker phases, including monocalcium aluminate ($CaAl_2O_4$, powder diffraction file (PDF) #01-070-0134), calcium titanate ($CaTiO_3$, PDF #01-075-2100) and gehlenite ($Ca_2Al_2SiO_7$, PDF #00-035-0755) are observed in the diffractogram of the anhydrous CAC (Figure 6-2). After 7 days of hydration of the CAC, formation of both metastable CAH_{10} ($CaO{\cdot}Al_2O_3{\cdot}10H_2O$, PDF #00-012-0408) and C_2AH_8 ($2CaO{\cdot}Al_2O_3{\cdot}8H_2O$, PDF #00-045-0564), and stable hydrate phases including hydrogarnet C_3AH_6 ($3CaO{\cdot}Al_2O_3{\cdot}6H_2O$, PDF #00-024-0217) and gibbsite ($Al(OH)_3$, PDF #00-012-0401), is observed. At extended times of curing (180 days) the characteristic low-angle reflections of the metastable CAH_{10} (~12° 2θ) and C_2AH_8 (~7° 2θ) are not identified, and instead a significant increase in the intensity of the reflections assigned to the stable hydrates hydrogarnet and gibbsite is observed. This suggests that the metastable phases have completely dissolved and re-precipitated as cubic hydrates after 180 days of curing. No significant changes in the intensity of the gehlenite and calcium titanate reflections are detected between 7 and 180 days of curing, indicating the low reactivity of these components upon hydration.

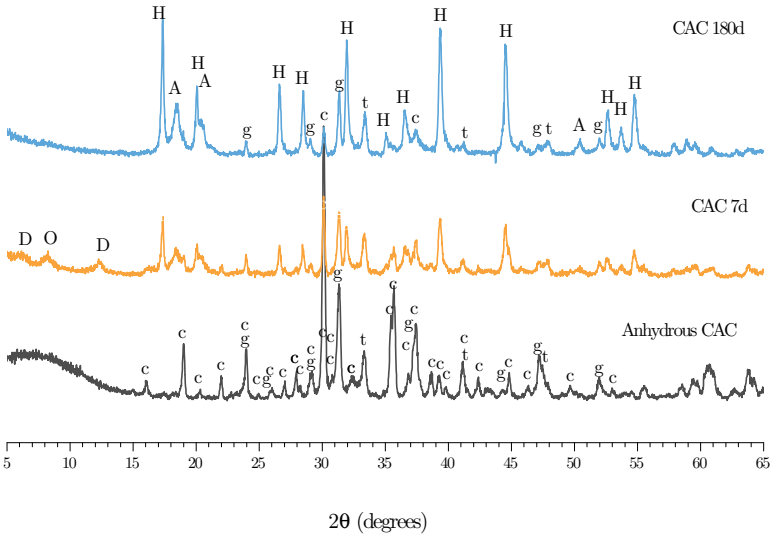

Figure 6-2 X-ray diffractograms of anhydrous CAC, $(NaPO_3)_n$ and neat CAC samples at 7 and 180 days of curing. Letters indicate phases identified, lowercase for clinker phases monocalcium aluminate (CA, c), gehlenite (C_2AS, g), calcium titanate (CT, t) and capitals for hydration products CAH_{10} (D), C_2AH_8 (O), hydrogarnet (C_3AH_6, H) and gibbsite (AH_3, A)

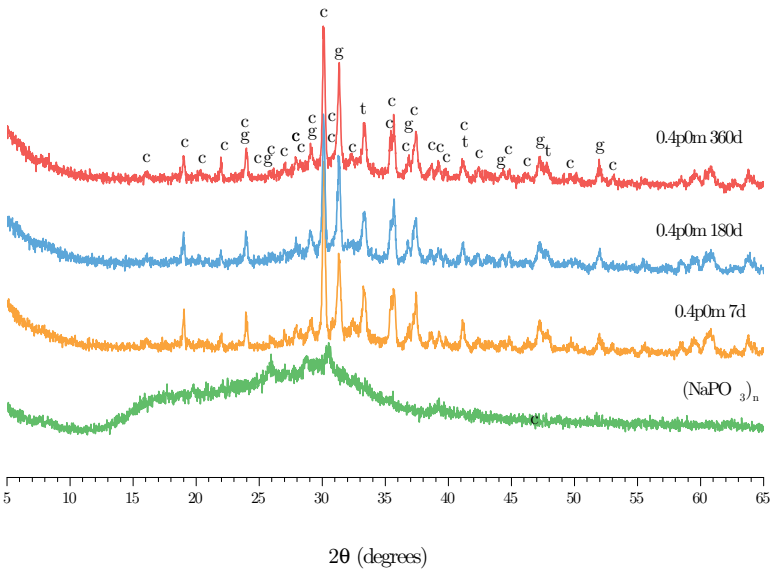

Figure 6-3 X-ray diffractograms of polyphosphate modified CAC formulation (0.4p0m) after 7, 180 and 360 days of curing. Letters indicate phases identified, lowercase for clinker phases monocalcium aluminate (CA, c), gehlenite (C_2AS, g) and calcium titanate (CT, t).

The diffractograms of the phosphate-modified CAC, Figure 6-3, show no reflections for either the conventional hydrate products observed in hydrated CAC (Figure 6-2) or any crystalline phases other than the anhydrous cement phases, whose intensity reduces as a function of curing period indicating dissolution. The only new feature observed is a broad diffuse scattering peak, centred at 30° 2θ, in all the polyphosphate modified samples, indicating that the precipitation of a phase with limited long-range order is occurring. This is the same as was observed in chapter 5. The phosphate modification is inhibiting the precipitation of conventional crystalline CAC hydrates, even at advanced times of curing, mitigating any potential issues surrounding conversion throughout the one year curing period considered in this study.

6.3.2 Thermogravimetry

The mass loss of CAC samples as a function of the sample temperature, as measured by thermogravimetry, is shown in Figure 6-4. The conventional CAC hydrates exhibit characteristic weight losses during heating as a result of dehydration reactions. Unmodified CAC samples cured for 7 days show two regions of weight loss. The low temperature region exhibits a primary weight loss at 90°C with a secondary shoulder at 132°C, which indicate the presence of CAH_{10} and C_2AH_8 respectively (Bushnell-Watson & Sharp 1992), consistent with the phases observed (Figure 6-2) by XRD. The assignment of these peaks is complicated by the effect of sample preparation, sample holder geometry and heating regime, and hence a wide range of dehydration temperatures are reported for these phases in the literature (Ukrainczyk et al. 2007), however the sequence in which these phases dehydrate remains the same (Bushnell-Watson & Sharp 1992). The formation of a gel type phase which dehydrates over a broad temperature range, partially overlapping that of the decahydrate of monocalcium aluminate, further complicates the peak assignment (Scrivener 2003). The composition of this gel type phase even in the neat CAC system is not fully understood, as it remains unclear whether this phase is a hydrated alumina gel (AH_n) (Skibsted et al. 1993; Fujii et al. 1986) or a calcium aluminium hydrate (C-A-H) (Bushnell-Watson & Sharp 1992; F. Guirado et al. 1998; Ramachandran et al. 2002) type gel.

Mass losses at higher temperatures are associated with the loss of structural water from the more thermodynamically favourable hydrates. Overlapping peaks for the dehydration of γ-gibbsite (Balek et al. 2003a) and hydrogarnet (Ramachandran et al. 2002), in the ranges 275–300°C and 300–315°C respectively, are observed in the unmodified CAC thermogravimetric data. In CAC samples cured for 180 days, weight losses corresponding to dehydration/decomposition of the hexagonal metastable phases are not identified, and instead the peaks corresponding to dehydration of AH_3 and C_3AH_6 are considerably more intense compared with those observed in specimens cured for 7 days. In agreement with the diffraction data, this indicates that the conversion of CAH_{10} and C_2AH_8 is essentially complete after 180 days of curing. The residual mass loss in the low temperature range (below 200°C) for the 180 day cured sample can be assigned to the alumina-rich gel phase produced as a by-product of conversion.

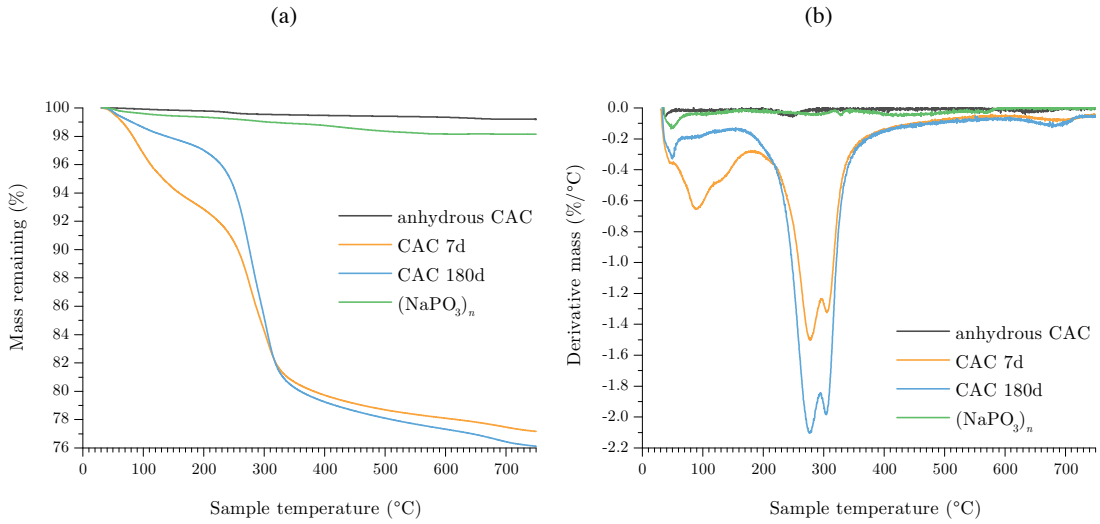

Figure 6-4 (a) Thermograms and (b) differential thermograms of sodium polyphosphate, anhydrous CAC clinker, and CAC samples hydrated for 7 and 180 days.

The thermograms for the phosphate-modified calcium aluminate samples (Figure 6-5), show considerably different behaviour from the neat CAC samples (Figure 6-4). Broader peaks consistent with non-crystalline water environments (F. Guirado et al. 1998) are observed in these samples, in agreement with the XRD results (Figure 6-3)

which did not show the formation of any crystalline hydrates in phosphate-modified calcium aluminate cements. These samples exhibit three main weight losses, at ~90, 230 and 280°C. Generally, weight losses below 100°C indicate the dehydration of phases with loosely-bound water, and the evaporation of free water. In the case of the phosphate-modified CAC the largest weight, below 100°C, may be attributed to the dehydration of the amorphous phase(s) forming in these systems, as indicated by XRD (Figure 6-3).

The weight loss at higher temperature (centred at ~300°C) is assigned to dehydroxylation of poorly crystalline gibbsite (AH_3). The broad temperature range over which this weight loss takes place suggests low crystallinity, which is why this phase was not detected by XRD. The intermediate temperature weight loss (centered at ~220°C) is difficult to characterize. Guirado et al. (1998) identified that dehydration of CAH_{10} occurs in several stages, including a mass loss at 225°C associated with the dehydration of the amorphous portion (denoted CAH_y by those authors) which results from the partial dehydroxylation and structural disruption of the initial crystalline hydrate phase. Therefore it is possible that the mass loss observed in this temperature range in the phosphate-modified CAC may be analogous to that described by Guirado et al. (1998), but resulting from an initially disordered rather than crystalline room-temperature phase. An extended curing period does not seem to affect the phase assemblage of the material according to either XRD or TGA, but there is an increase in the intensity of the mass loss attributed to AH_3 between 7 and 180 days curing, and a significant increase in mass loss in the region assigned to the amorphous gel type phase between 180 and 360 days curing, in Figure 6-5.

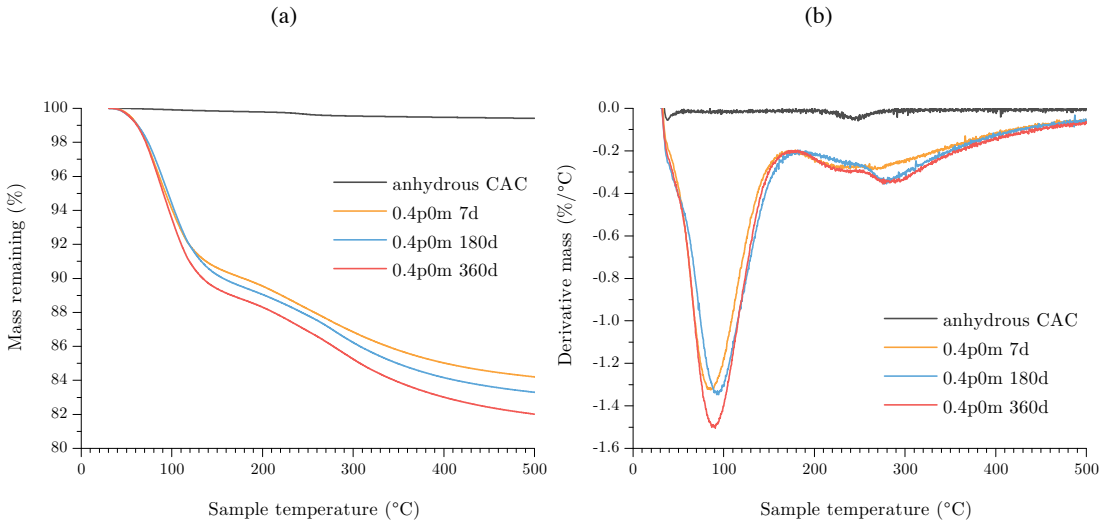

Figure 6-5 (a) TGA and (b) derivative TGA data for anhydrous CAC clinker and polyphosphate modified CAC samples hydrated for 7, 180 and 360 days.

6.3.3 Solid-state nuclear magnetic resonance spectroscopy

6.3.3.1 ^{27}Al MAS NMR

^{27}Al MAS NMR spectra of anhydrous CAC and hydrated samples are shown in Figure 6-6. Distinct aluminium co-ordination environments (Al^{IV}, Al^{V} and Al^{VI}), are typically located at chemical shifts between 52 to 80 ppm, 30 to 40 ppm, and -10 to 20 ppm, respectively (Müller et al. 1981; Skibsted et al. 1993). The spectrum of the anhydrous CAC is dominated by a large resonance at 78 ppm, due to the tetrahedral aluminium in the monocalcium aluminate present in the CAC (Cong & Kirkpatrick 1993), in addition to a very small response at 9 ppm indicative of the partial hydration of the materials during storage and consistent with the ~1% mass loss in the clinker during TGA experiments in Figure 6-5.

Hydrated CAC samples, Figure 6-6, show reduced resonances in the Al^{IV} region as a result of the dissolution of clinker phases during hydration, and an increase in the Al^{VI} region as a result of precipitation of hexagonal and cubic hydrate phases. With increasing curing duration, the unmodified CAC samples exhibit less intense resonances for tetrahedral aluminium, as hydration nears completion after 180 days. However, a considerable change in the line shape in the Al(VI) region is observed after 7 days of curing as a result of the conversion of CAH_{10} and C_2AH_8. The resulting

resonances, at 8 and 12 ppm, can be attributed to the presence of AH_3 and C_3AH_6 respectively (Müller et al. 1984), consistent with the phases identified by X-ray diffraction (Figure 6-2) and thermogravimetry (Figure 6-4). In the absence of the metastable phases after 180 days of curing, as observed by other analytical techniques, a defined shoulder due to gibbsite (8 ppm) is identifiable.

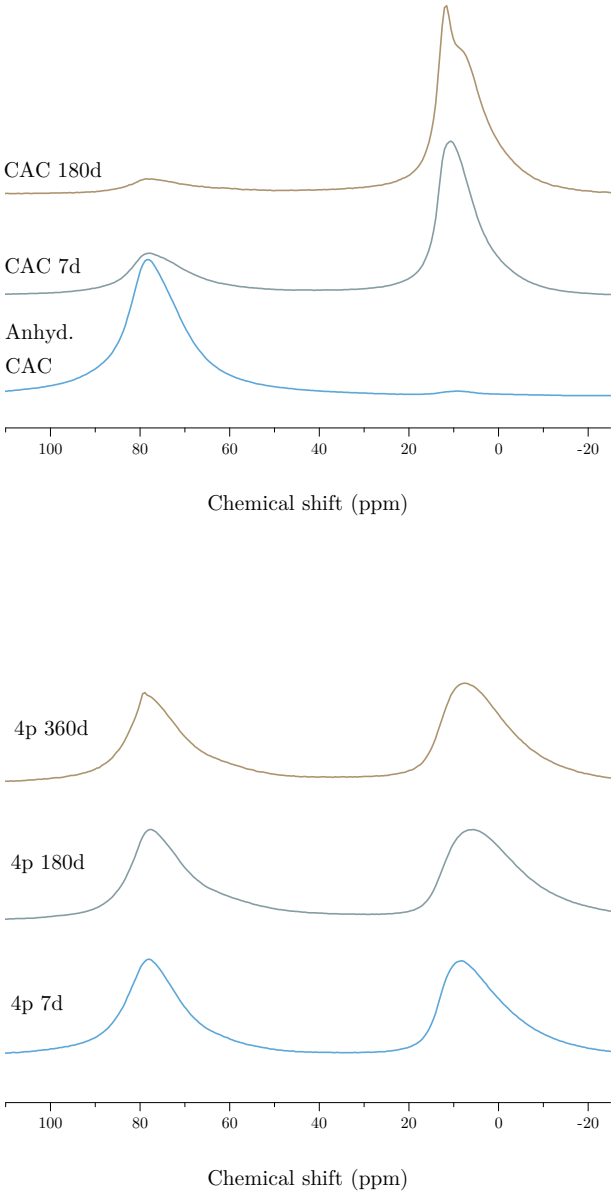

Figure 6-6 ^{27}Al MAS NMR spectra for (top) anhydrous CAC and CAC hydrated for 7 and 180 days, and (bottom) polyphosphate modified CAC samples (0.4p0m) hydrated for 7, 180 and 360 days.

Phosphate modified CAC samples (Figure 6-6 (bottom)), exhibit spectra, which are considerably different spectra from those obtained for neat CAC samples. Resonances in regions associated with both Al^{IV} and Al^{VI} coordinated environments are present. With increasing curing period, the diffraction data indicate a higher extent of dissolution of CAC phases, which are typically identified in the tetrahedral region of ^{27}Al MAS NMR spectra; however, significant changes are not observed in the downfield response, indicating that this band may not be attributed solely to Al environments present in the remaining unreacted CAC, and may also include contributions from a secondary phase forming in these systems.

The line shape and intensity of the two main bands identified in both the tetrahedrally and octahedrally coordinated regions of the spectra in Figure 6-6 bottom seem to be similar after 7 days of curing; however, with increasing curing duration there is a small increase in the octahedrally coordinated aluminium band. The upfield peak for phosphate modified samples at all curing periods exhibited large peak widths (Full width half maxima (FWHM) of 16.3, 19.4, 17.5 ppm for 7, 180 and 360 day cured samples respectively) that could be assigned to either one phase with limited long range order, or the combination of a number of distinct contributions. This resonance is largely attributed to the presence of the gibbsite identified by thermogravimetry (**Error! Reference source not found.**6-5), although contributions from C-A-H or C-A-P-H gel may not be discounted as it could also hold aluminium in octahedral co-ordination. The formation of such a gel cannot be ruled out considering the potential identification of this phase by thermogravimentry (peak at 225°C in Figure 6-5) and its very low long range order. However the precise identification of this gel necessitates the use of the phosphorus nucleus as a structural probe, and also the application of more advanced NMR techniques, as discussed below.

6.3.3.2 ^{31}P MAS and $^{31}P\{^{1}H\}$ CP/MAS NMR

Cross polarisation (CP) NMR experiments are a powerful probe of interatomic correlations, whereby a primary nucleus, often ^{1}H, is initially irradiated, followed by a pulse on a secondary nucleus. Once both are excited and coupling has been achieved, they may be decoupled by a further pulse on the primary channel, followed by data collection on the secondary channel. The resultant spectrum is comparable to a conventional MAS spectrum but with additional structural information: there is an

added dependence upon proximity between the two nuclei for each environment (MacKenzie & Smith 2002), which enables selective analysis of secondary nucleus sites which are closely interacting with an atom of the primary nucleus. Here, the application of $^{31}P\{^{1}H\}$ CP/MAS NMR provides the possibility to distinguish whether phosphate environments are related to hydrogen atoms, which is essential in accurately characterising the gel phase present in the phosphate-modified CAC binder.

The ^{31}P MAS and $^{31}P\{^{1}H\}$ CP/MAS spectra, Figure 6-7 (top) and (bottom) respectively, show very little change in the coordination environment of the phosphorus as a function of curing duration, for the phosphate-modified CAC samples. A change in the chemical shift in a ^{31}P spectrum can be indicative of changing connectivity of the phosphate units and/or the electronegativity of next-nearest-neighbours (NNNs) (Turner et al. 1987). The MAS spectrum for the polyphosphate precursor shows three broad responses at 1, -7 and -20 ppm attributed to Q^0, Q^1 and Q^2 structural units respectively (Turner et al. 1987; Belloque et al. 2000; Brow et al. 1993). The dissolution of the phosphate, prior to slurry preparation, results in a reduction in the concentration of the Q^2 units as a result of hydrolysis.

In both sets of spectra (MAS and CP/MAS) for the hydration products of the phosphate-modified CAC, two broad main bands are identifiable at 1.1 (shoulder) and -4.1 ppm (main peak), indicate the presence of multiple relatively disordered hydrated phosphorus environments. The line shapes of the ^{31}P MAS and ^{31}P CP/MAS spectra are comparable, indicating that all of the phosphorus environments in these samples are protonated to some extent, and thus they likely relate to hydrate phases forming in these binders. This is consistent with suggestions by Swift et al. (2013) and the findings of the previous chapter, where the weight loss identified by thermogravimetry below 200°C was assigned to an amorphous phosphate hydrate phase.

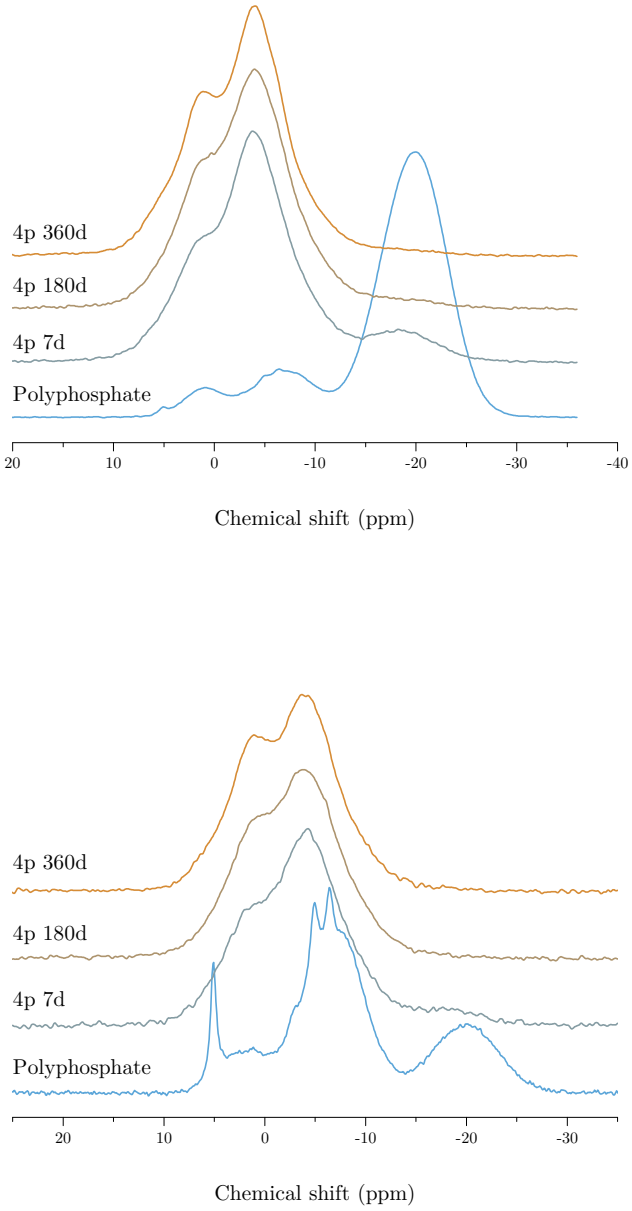

Figure 6-7 (top) ^{31}P MAS NMR spectra and (bottom) ^{1}H{^{31}P} cross polarisation MAS spectra, for polyphosphate modified CAC samples and the sodium polyphosphate precursor.

The resonance positions straddle the region for crystalline calcium phosphates (He et al. 2007; Miquel et al. 1990; Pourpoint et al. 2007; Legrand et al. 2009) and the downfield limit reported for crystalline aluminophosphates (Fedotov et al. 1987; Bleam et al. 1989), which are generally minerals holding aluminium in octahedral coordination (Kim & Kirkpatrick 2004), such as brazilianite $NaAl_3(PO_4)_2(OH)_4$. On

the other hand, calcium aluminophosphates such as crandallite $CaAl_3(PO_4)_2(OH)_5(H_2O)$ have been reported to have intermediate ^{31}P chemical shifts (-1.81 (Williams et al. 1981) and -5.2 (Bleam et al. 1989) ppm), although little information regarding chemical shifts is available in the literature for these phases. From the ^{31}P MAS NMR data alone, it is very difficult to discern whether the resonances identified in phosphate modified CACs relate to calcium phosphate, aluminophosphate or C-A-P-H type phases.

Similar chemical shifts (1.5 – 2.0 ppm depending on the Na/P ratio), to those observed in Figure 6-7, have been reported (Brow et al. 1990) for sodium phosphate glasses, and assigned to Q^1 environments. In studies of Ca-free sodium aluminophosphate glasses, Zhang and Eckert (Zhang & Eckert 2006) reported ^{31}P chemical shifts of ~1.6 and -4.6 ppm, which they also assigned to Q^1 units, with 0 and 1 bonded aluminium units respectively; this also in agreement with the results of Lang et al. (Lang et al. 2001).

The formation of aluminophosphate complexes as a result of the interaction of phosphate with aluminium oxides and hydroxides has been reported by a number of investigators (Van Emmerik et al. 2007; Li et al. 2010; 2013; Lookman et al. 1997); particularly, corundum was reported (Li, Pierre-Louis, et al. 2013) to form inner sphere surface complexes and surface precipitates with phosphates. The surface complexes resonate at far more negative chemical shifts, < -11 ppm, than the sites identified here, but the chemical shifts at which the resonances occur for the phosphate modified CAC samples lie within the region identified as characteristic for inner sphere surface complexes (Li, Pierre-Louis, et al. 2013). Investigations by Van Emmerik et al. (2007) into phosphate sorption onto gibbsite also reported the formation of a number of different aluminium-containing phosphate environments, with inner sphere complexes dominating at pH 8, which is within 1-2 pH units of conditions in the modified CAC systems studied here. Kim and Kirkpatrick (2004), examining phosphate adsorption onto aluminium oxyhydroxide, also identified surface adsorbed phosphate in inner-sphere complexes whose abundance increased with increasing pH, whilst the precipitation of crystalline aluminophosphates decreased. The formation of such complexes here would result in a diffusion barrier forming around the unreacted cement particles, inhibiting or significantly retarding

further cement hydration, consistent with the reduced degree of reaction identified in the phosphate modified CACs by X-ray diffraction (Figure 6-3) compared with unmodified CACs. A similar mechanism was suggested by Rettel et al. (1997) who investigated the acid-base reaction within the sodium citrate modified CAC system.

6.3.3.3 ^{31}P{27Al} REAPDOR NMR

Further quantitative structural information can be obtained from REAPDOR NMR experiments, such as the interatomic distance between two nuclei. This experiment introduces dipolar coupling between the nuclei of primary interest, ^{31}P here, and a second nuclear species, in this case ^{27}Al. This is introduced by irradiation on the ^{31}P channel, followed by an adiabatic pulse on the ^{27}Al channel. The effects of this on the spectrum obtained from the ^{31}P channel result in a decrease of the response intensity with increasing contact time, interatomic distance, nuclei probed and pulse scheme factors (Goldbourt et al. 2003). REAPDOR experiments are very similar to the more common REDOR (rotational-echo double resonance) pulse schemes, but more suitable to improve spin transitions of quadrupolar secondary nuclei (Hughes et al. 2002).

The primary application of this type of experiment is to measure the dipolar coupling of the two nuclei, $\hbar\gamma_I\gamma_S/2\pi r^3$ (where $\hbar$ is Planck's constant divided by 2π, γ is the gyromagnetic ratio and r is the internuclear separating distance), and thus for the case of an isolated spin pair it is possible to calculate the internuclear distance. Multiple spectra are collected with varying dipolar evolution times and signal intensities from a reference spectrum S_0 (where no dephasing adiabatic is used) and from spectra with varying dipolar evolution times, S, are calculated. The REAPDOR fraction, ΔS, for each spectrum is calculated as the intensity ratio $((S-S_0)/S_0)$, which when plotted against the evolution time results in a dataset which is a function of the rotor dynamics and the dipolar coupling.

The aluminium-phosphorus atomic interaction in the phosphate-modified samples cured for 360 days was investigated by REAPDOR NMR. Figure 6-8 shows the spectra collected on the phosphorus channel after various dipolar evolution periods, along with a reference S_0 spectrum collected with no irradiation on the aluminum channel. The dephasing, a decrease of resonance intensities, indicates intimate

coordination between the aluminium and phosphorus nuclei, especially those associated with the peak at -4.1 ppm.

The REAPDOR fraction ΔS was plotted against the dipolar evolution time, as shown in Figure 6-9. Each dataset is fitted with a universal REAPDOR equation, Eq. 1, for spin-1/2 and spin-5/2 nuclei, as reported by Goldbourt et al. (Goldbourt et al. 2003). The universal fitting curve is a function of λ, $\lambda=(2m+2)T_rD$, where *m* is the number of rotor cycles, T_r the rotor period and D is the dipolar coupling.

$$S_{\frac{1}{2},\frac{5}{2}}^{REAP}c(\lambda) = 0.63\left(1 - e^{-(3.0\lambda)^2}\right) + 0.2\left(1 - e^{-(0.7\lambda)^2}\right) \quad (1)$$

The fitting of the REAPDOR data collected for phosphate modified CACs yielded Al-P internuclear distances of 3.0 and 3.6 Å for the -4.1 and 1.1 ppm peaks respectively. It is noted that the universal curve is specifically defined for an isolated spin pair, and hence is at best an approximation to the exact bond lengths for bidentate structures such as the Q^2 environment identified here, where multiple interactions complicate the dipolar coupling. On purely geometric grounds, the Al-P interaction distances identified here seem rather short, and the bidentate nature of some of the complexes may be the reason for this. Nonetheless, it is clear that the -4.1 ppm peak corresponds to a shorter Al-P interaction distance than the 1.1 ppm peak.

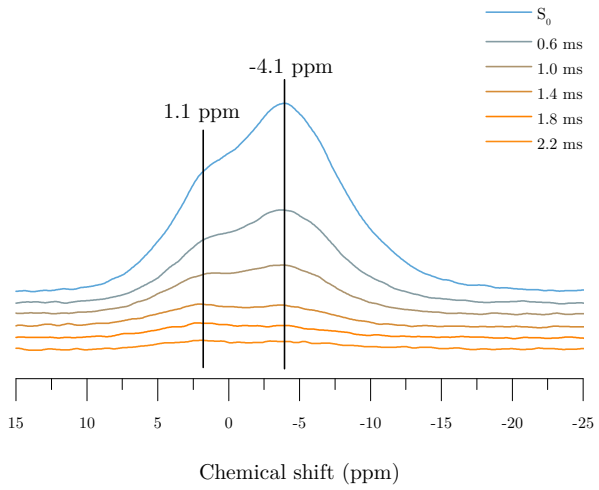

Figure 6-8 ^{27}Al {^{31}P } REAPDOR NMR analysis of the polyphosphate-modified CAC sample cured for 360 day showing the reference S_0 spectrum, and spectra with ^{27}Al irradiation at various dipolar evolution times.

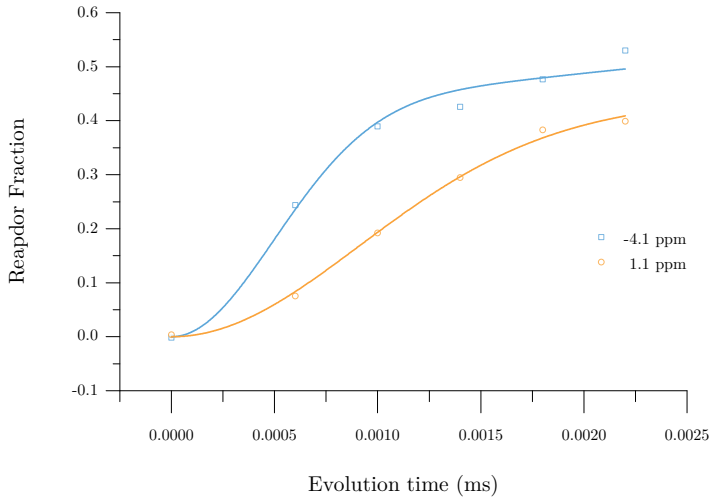

Figure 6-9 Peak-resolved dephasing curves for ^{31}P/^{27}Al REAPDOR NMR analysis of the polyphosphate-modified CAC sample cured for 360 days.

At higher evolution times, longer-range interactions can contribute to the dephasing, resulting in a poorer fit with Eq. 1, hence the dipolar evolution time was limited to 2.2 ms. As a result of a convoluted signal, where some contributions are from environments without aluminium-phosphorus interactions, even at greater evolution periods some residual response is present in the spectra despite the adiabatic

dephasing pulse on the secondary channel, and hence the REAPDOR fractions do not reach unity. To account for this residual response, Eq. 1 was modified by a scaling factor.

Investigations of the dipolar coupling between aluminium and phosphorus in the samples indicate a fair degree of intimacy between the two, as seen by the dephasing of the signal, and provide evidence that previous explanations of the hydrate chemistry which did not consider alumino-phosphate phases do not fully describe this system. The resonant frequencies of the bands identified in the ^{31}P spectra, and the shielding effects of calcium and aluminium on chemical shift, suggest the possibility of a C-A-P-H phase with little long-range order. Due to the broad peak widths, the presence of a calcium orthophosphate as suggested by Sugama et al. (1999) cannot be entirely discounted from the data presented in this chapter, but it appears much more likely that the phosphate sites in the disordered component are intimately intermixed with aluminate species rather than forming a well-defined phosphate phase.

6.4 Conclusions

The phosphate modification of calcium aluminate cement results in a significant deviation away from the conventional hydration behaviour of calcium aluminate cement. None of the conventional crystalline calcium aluminate hydrates were detected in phosphate-modified samples, either by XRD or by thermal analysis, during a curing period of one year. The inhibition of conventional crystalline phase precipitation by phosphate modification has thus been shown to be effective in preventing the calcium aluminate hydrate conversion process, at least for the curing periods studied.

The understanding of the hydration mechanism and phase assemblage of phosphate modified CAC is challenging due to the difficulty in characterising the very poorly crystalline hydrates forming. The weight loss identified by thermogravimetry below 200°C is difficult to resolve, however it is likely that that in the absence of any conventional crystalline hydrates precipitating, a calcium aluminate hydrate-based gel is forming in addition to the poorly crystalline gibbsite detected by the same method. The formation of phosphate complexes at phosphate-aluminium hydroxide interfaces

is well established in the literature, and therefore, it is possible that a similar mechanism is resulting in the formation of phosphate complexes at the interface with amorphous gibbsite.

The phosphate-modified CAC systems are also seen by REAPDOR NMR to contain considerable dipolar interactions between aluminium and phosphorus, supporting the identification of aluminophosphate type phases. The ^{31}P MAS NMR spectra are consistent with the presence of calcium within these phases, and CP/MAS NMR shows that they are hydrous, resulting in the final identification of the key binding phase as a disordered C-A-P-H type gel. These complex gels would be the primary reason for the deviation from conventional hydrate phase formation, and also the prevention of further hydration of the unreacted CAC particles at extended times of curing.

7 Application of phosphate-modified CAC as an encapsulant for aluminium

7.1 Introduction

The CAC system has been identified as a promising alternative encapsulant for ILW (Ojovan & Lee 2005; Toyohara et al. 2002) and more recently for other wastes such as toxic metals (Navarro-Blasco et al. 2013) and hazardous sludges (Navarro-Blasco et al. 2015). The attractiveness of CAC for the encapsulation of MAGNOX ILW encapsulation, over the use of the existing PC-based system, arises from its lower pore solution pH which may reduce the corrosion of aluminium, a major constituent of several important waste streams. Lower pH environments, relative to the pH of 11-13 found in PC, result in the less rapid dissolution of the passivating alumina layer on the surface of the encapsulated aluminium. CAC provides such conditions, and in the case of the phosphate-modified CAC system developed by Sugama & co-workers (1991), further reduce the pH closer to neutral, which is able to approach the passivation region of the Pourbaix diagram for aluminium, shown in Figure 2-10. Work by Toyohara et al. (2002) has shown the CAC system to be effective in reducing the mobility of the especially toxic ^{129}I radionuclide, through sorption on to calcium aluminate hydrates.

The phosphate modification of the CAC system, as investigated by Swift (2013) for the encapsulation of aluminium, did show a process of 'conversion' analogous to the conventional conversion of unmodified CAC, where there was a precipitation of crystalline hydroxyapatite and a zeolite phase at the expense of the amorphous binding phase. This non-conventional conversion was thought to be the cause of delayed '*latent*' aluminium corrosion, which was observed during trials of encapsulation of aluminum in that formulation, as a result of the liberation of free

water during the conversion. It was observed that the phosphate modified formulations initially evolved little hydrogen in comparison with PC/BFS and PC/PFA composite formulations. However, after longer hydration periods this was not the case, and cumulatively the phosphate modified CAC formulations evolved greater amounts of hydrogen in total, indicating more aluminium corrosion.

As discussed in Chapter 5, analysis of the highly workable 0.4p0.05m formulation showed that even after 1050 days of curing no such conversion process was observed. Hence this formulation is still a possible alternative for ILW encapsulations, and in addition to the 0.4p0m, 0p0.1m, 0.2p0m and the neat CAC formulations, it is trialled in this chapter to study performance with encapsulated aluminium.

Few studies in the literature examine the corrosion potential of aluminium in cement matrices. Table 2-2 lists notable studies, which consider the corrosion of encapsulated metals within CAC systems, and/or reactive ILW metals encapsulated within cementitious matrices. The method used by Swift (Kinoshita et al. 2013; Swift 2013) to monitor the rates of corrosion was the quantification of hydrogen evolution by water displacement, and a similar technique was also used by Zhang et al. (Zhang et al. 2012). This method is suitable to monitor the hydrogen generation of the waste package, however this is not a direct measurement of the corrosion process itself, and the hydrogen dissolution in water and transport through the matrix both complicate the mechanism. In addition to this method, DSC, image analysis and mass loss measurement methods are also used to determine the remaining aluminium quantities by alternate means.

This chapter examines the relative performance neat CAC and four phosphate modified CAC formulations: (i) 0p0.1m, (ii) 0.2p0m, (iii) 0.4p0m, and (iv) 0.4p0.05m, with respect to encapsulated aluminium corrosion.

7.2 Experimental procedures

Formulations were prepared as per the mixing protocol outlined in the Experimental Procedures, Chapter 3. XRD analysis of the precursors and hardened binders is also described therein.

Laser diffraction was conducted on the aluminium powder (general purpose grade) which was used as a waste simulant, to determine the size distribution of the particles present. A Malvern Mastersizer 3000 with dry dispersion unit was used. Measurements were obtained over 5 seconds, with a laser obscuration of between 0.5 and 6.0 % and after a 20 second background measurement.

Assessment of the extent of aluminium corrosion was undertaken using a number of methods: (i) hydrogen evolution, (ii) differential scanning calorimetry, (iii) image analysis, and (iv) mass loss; each of which is described in the Experimental Procedures chapter.

Samples used to examine hydrogen evolution by the water displacement method, as described in 3.5.2.1, were prepared in the same manner as described in section 5.2, however in this case they also included 5 wt.% aluminium powder. Samples of 10 g mass were cast in centrifuge tubes cut to the appropriate size.

Where hydrogen evolution was studied by mass spectrometry, hand mixed samples of 10 g were prepared with 5 wt.% aluminium powder. 130 mg samples were cast in alumina crucibles and tested as described in 3.5.2.2.

The remaining content of aluminium in selected samples was determined by DSC, using 40 mg samples retrieved from larger 10 g samples prepared as described in section 5.2, whilst maintaining a 5 wt.% addition of aluminium powder. The remaining quantity of aluminium (and hence the corrosion rate) may be calculated by integrating the DSC peak at 660°C which is attributed to its melting. Peak area was calculated in the temperature limits 640 to 680°C, by calculating the difference between the integrals of a linear baseline fit across this temperature range, using the Perkin Elmer Thermal Analysis software Pyris version 11.0.3. The peak area

represents the energy required to melt the remaining aluminium, from which the remaining percentage of aluminium in the sample may be calculated.

Scanning electron microscopy was conducted using a TM3030 Hitachi benchtop SEM with an accelerating voltage of 15 kV. Sample preparation included cutting of cross sections using a diamond blade saw, followed by manual grinding with silicon carbide grinding paper of 240, 400, 1200 and 2500 grit.

7.2.1 Materials

Data presented in sections 7.3.1 and 7.3.2 were obtained with the addition of aluminium in a fine (high surface area) powdered form, which was chosen to ensure that the levels of aluminium corrosion were within the sensitivity ranges of the methods being used to characterise them. The particle size distribution of aluminium as determined by laser diffraction is shown in Figure 7-1. The results indicated that the powder had a single modal diameter of approximately 35 µm, with all particles smaller than 200 µm and greater than 3 mm. The X-ray diffraction data for this material, shown in Figure 7-2, indicated highly crystalline aluminium powder, as expected, with no detectable contamination from other phases including alumina.

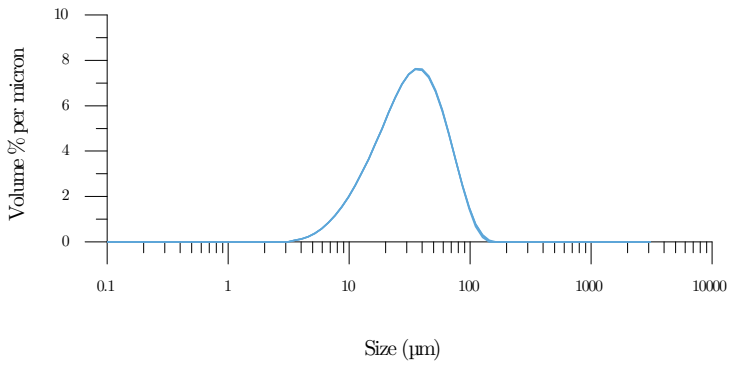

Figure 7-1 Particle size distribution of aluminium powder.

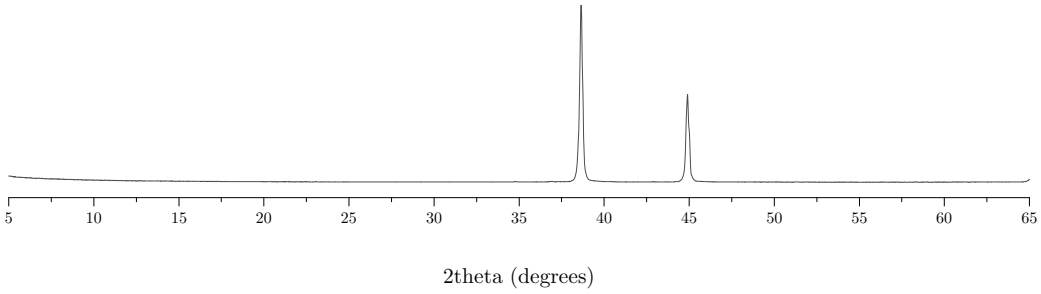

Figure 7-2 X-ray diffractogram for aluminium powder.

Data presented in sections 7.3.3 and 7.3.4 were obtained using aluminium wire and plate respectively. These were chosen as they were more suited to the corrosion quantification methods employed in their respective experiments, additionally the existing literature only considers encapsulated monolithic aluminium.

For PC based formulations, CEM I provided by Hanson Ribblesdale was used in combination with BFS from Redcar steel works for the BFS/PC blended system, at a mass ratio of 9:1 BFS:PC. XRF data for the BFS and PC are shown in Appendix A. Mixing and curing of these formulations was performed to the same protocol as for the mixes based on CAC.

7.3 Results and discussion

7.3.1 Hydrogen evolution

7.3.1.1 Water displacement

The evolution of the hydrogen gas corrosion product is a direct indicator of the corrosion of the encapsulated aluminium metal. Figure 7-3 shows the data obtained for water displacement experiments where the hydrogen gas was collected in an upturned measuring cylinder, and the volumetric displacement of the water by evolved hydrogen was measured as a function of time. The data indicate that there is a rapid corrosion of the metal within the initial 24 hours after mixing and casting, which

is then followed by a steady and relatively slower rate of corrosion through to the end of the time period studied. All of the phosphate modified formulations showed a reduction in total cumulative hydrogen evolution over the period studied, relative to the neat CAC formulation. The monophosphate-only formulation 0p0.1m exhibits the smallest improvement in hydrogen evolution relative to the neat CAC of all the phosphate modified formulations.

Figure 7-4 displays the same data as a function of log time, which shows that each of the formulations exhibit a distinct point at which there is considerable corrosion early after casting, in agreement with other investigations using the water displacement method (Swift 2013; Zhang et al. 2012). The 0p0.1m formulation delays the point at which the maximum rate of corrosion is observed to be later than that of the neat CAC sample, whereas the polyphosphate formulations advance this to earlier than in the neat CAC sample. The polyphosphate modification results in a reduction of hydrogen evolution (of the neat CAC system) by 50% in the case of the 0.2p0m formulation, and as much as 77% for the 0.4p*x*m series of formulations.

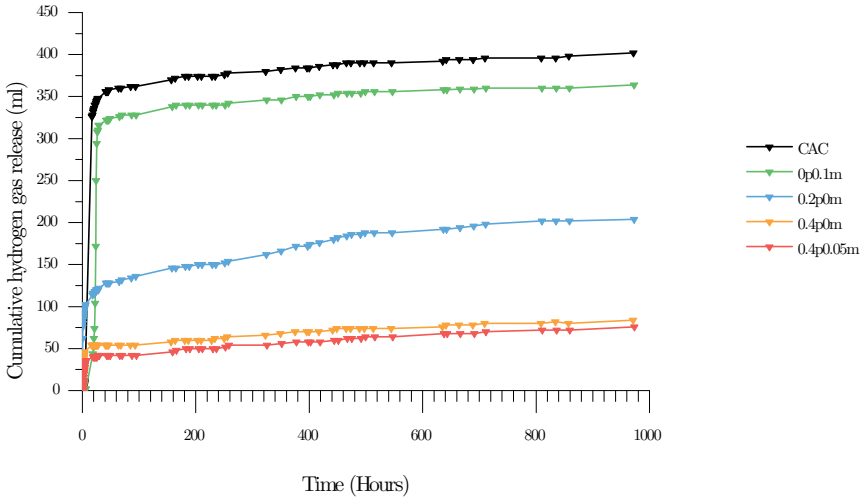

Figure 7-3 Cumulative hydrogen release as a function of time. Temperature was recorded to be 20 ± 2°C throughout the period studied.

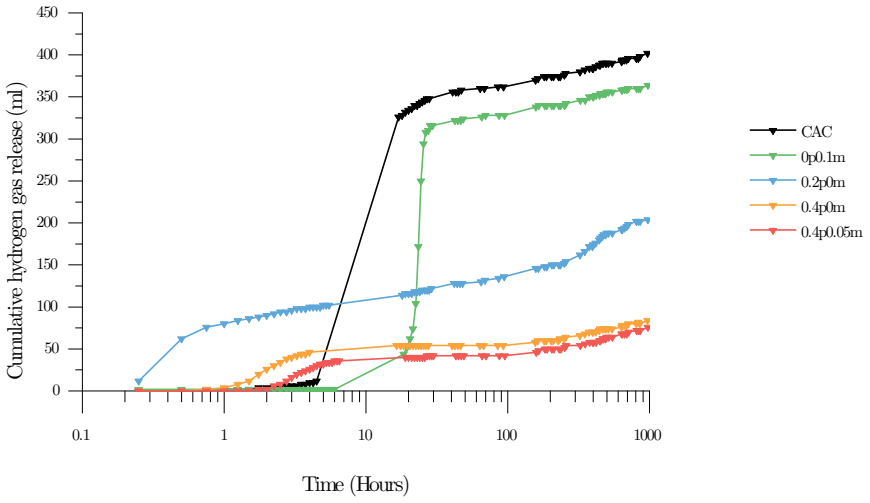

Figure 7-4 Cumulative hydrogen release as a function of time, on a logarithmic scale. Temperature was recorded to be 20 ± 2°C throughout the period studied.

The period of rapid initial corrosion can be seen to be a function of both phosphate content and phosphate chain length. Monophosphate delays the rapid corrosion event, whereas at low polyphosphate modification, as in the 0.2p0m formulation, this occurs from the start of the experiment, resulting in the evolution of hydrogen in quantities in excess of the neat CAC formulation in the early stages of the process. At higher levels of polyphosphate modification, for the 0.4p*x*m samples, this is delayed to 1 hour after mixing in the case of the polyphosphate only sample and delayed to 2 hours for the 0.4p0.05m sample. This may be correlated to the early age hydration as studied by calorimetry in Chapter 4, where the quantity of polyphosphate modification determines the time at which the characteristic exothermic event associated with hydration is observed – which is increasingly delayed with increasing polyphosphate content. A similar effect upon the time at which maximum corrosion rates were observed. The order in which peak corrosion rates are observed for the formulations is the same as that observed for the peak heat flow plotted in section 4.3.2.2 : (i) 0.2p0m, (ii) 0.4p0m, (iii) 0.4p0.05m, followed by (iv) CAC. The 0p0.1m sample is the exception to this trend. It must be noted that data could not be collected at the usual frequency for the CAC, however the line shape of the rate of hydrogen release for this formulation is most likely to be similar to that observed for the other formulations and would have a well defined peak between 5 and 17 hours.

At the conclusion of the water displacement experiment, the samples were removed from the hydrogen collection apparatus. It was observed that the hardened cements were very porous, as a result of the corrosion of aluminium soon after mixing and before the cement had hardened. These cements are quick-setting and viscous, hence the bubbles introduced by hydrogen evolution and the voids left by corroded aluminium were retained in the microstructure. This is the same mechanism by which air-entrained concretes can be produced, using chemical admixtures which evolve gas before complete hardening of the matrix; these include calcium carbide, sodium percarbonate and (most commonly) aluminium powder (Narayanan & Ramamurthy 2000).

Error! Reference source not found. 7-5 shows the diffraction data obtained for the samples prepared for the water displacement experiment, 40 days after mixing (i.e. at the conclusion of the hydrogen evolution measurement). The peaks associated with aluminium metal are clear and distinct in the formulations, which evolved little hydrogen gas, 0.4p0m and 0.4p0.05m. Conversely, the 0.p0.1m and CAC samples showed no presence of aluminium metal, implying that it had all been consumed via corrosion during the 40-day period of measurement. Using the ideal gas equation it is possible to calculate the number of moles of hydrogen generated and hence the mass of aluminium which has corroded to evolve this amount of hydrogen, as a further verification of the effectiveness of the water displacement method. The 402 ml of hydrogen recorded 972 hours (40.5 days) after mixing equates to approximately 0.45 g of corroded aluminium metal, which is very closely comparable to the 0.5 g encapsulated by a 10 g sample with 5 wt.% loading of aluminium.

The diffraction data for the 0.2p0m sample showed the presence of remaining aluminium metal in the matrix, as expected due to the intermediate volume of hydrogen evolved during the course of the experiment. The phase development of these formulations was similar to that observed in Chapter 5, for each of the formulations apart from the neat CAC sample, which showed additional peaks which have been attributed to the presence of strätlingite, C_2ASH_8 (PDF #00-029-285) and a considerable reduction in the intensity of the reflections associated with gehlenite. The latter is the only source of silicon in the system and it is proposed that the precipitation of C_2ASH_8 is as a result of the slight reactivity of the gehlenite, which

has been shown to hydrate at very long curing periods (Bensted & Barnes 2002). This is especially likely in the case that the CAC hydrates are present as highly stable hydrogarnet and gibbsite with little unreacted clinker remaining. The precipitation of C_2ASH_8 is in line with the reported products formed during hydration with simultaneous corrosion of encapsulated aluminium, both in BFS/PC systems (Setiadi et al. 2006) and in phosphate modified CAC with PFA addition (Swift 2013). However, in the latter case it was unclear whether this precipitation is as a result of gehlenite hydration or from the dissolution of silica from the PFA additions. However this is most likely due to the SCM incorporation as the XRD data shown in Figure 7-5 reveals that for the phosphate modified formulations in this study without any such siliceous SCM addition, there was no C_2ASH_8 precipitation. Obtaining diffraction data for the material after it has been studied for hydrogen gas release is useful in determining whether the assessment of hydrogen evolution is reliable. An alternate method to achieve the same may be DSC as per section 7.3.2, where the energy required to melt the remnant aluminium may be calculated from the thermogram, and hence its mass estimated. The technique has provided data which are indicative of the absolute aluminium corrosion over a long period with reasonable accuracy.

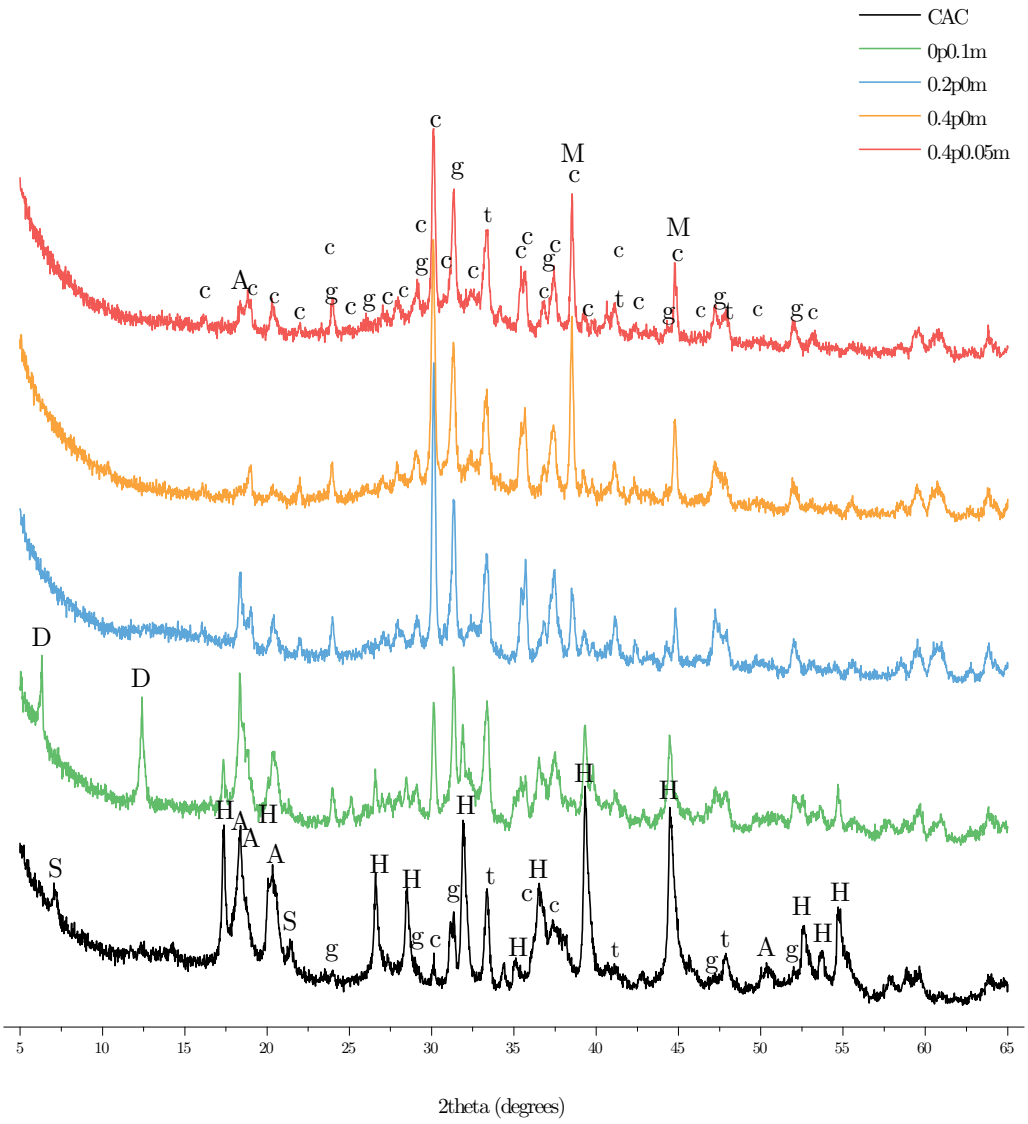

Figure 7-5 Diffractograms obtained from the samples 40 days after casting, after the water displacement experiment: letters indicate monocalcium aluminate (CA, c), gehlenite (C_2AS, g), calcium titanate (CT, t) and CAC hydration phases CAH_{10} (D), C_2AH_8 (O), hydrogarnet (C_3AH_6, H), gibbsite (AH_3, A) , strätlingite (C_2ASH_8, S) and aluminium metal (Al, M).

7.3.1.2 Mass spectrometry

The results of in situ detection of hydrogen evolution by mass spectrometry (MS) are shown in Figure 7-7, and revealed similar behaviour to that determined by the water displacement method. The higher sensitivity of the technique relative to the water displacement method is evident in the data shown in Figure 7-6, where the MS response showed that the hydrogen was not released continuously at a constant rate,

but rather that the lineshape was jagged. This indicates that the corrosion was taking place via a more complicated staged mechanism, most probably via multiple cycles of precipitation and dissolution of passivating phases at the interface of the aluminium metal, limiting the corrosion. This is particularly evident for the CAC and 0p0.1m formulations, whose corrosion behaviour could be identified to be constituted of multiple events, whereas this was less clear for the 0.4p0.05m formulation. In the case of this formulation, which showed very little relative hydrogen evolution, this may be indicative of a simpler mechanism where there was an initial period of corrosion followed by corrosion inhibition by a relatively stable reaction product (passivation) layer.

The technique was used qualitatively to determine the times at which corrosion rates were highest, and it can be seen that with low level of polyphosphate modification highest rates of corrosion were seen earlier, in agreement with the conclusions drawn by the water displacement method (which has a much lower time resolution). Higher polyphosphate contents exhibited this peak in corrosion rate later, but nevertheless before that which was observed for the neat CAC samples. Both observations again are in agreement with the deviation (relative to the neat CAC) of the times at which exothermic events were observed in the isothermal calorimetry data presented in Chapter 4. Hence, the early hydration reactions have a considerable effect on the corrosion of the encapsulated metal, potentially as a result of the increased temperatures, availability of free water, and the dynamic phase assemblage.

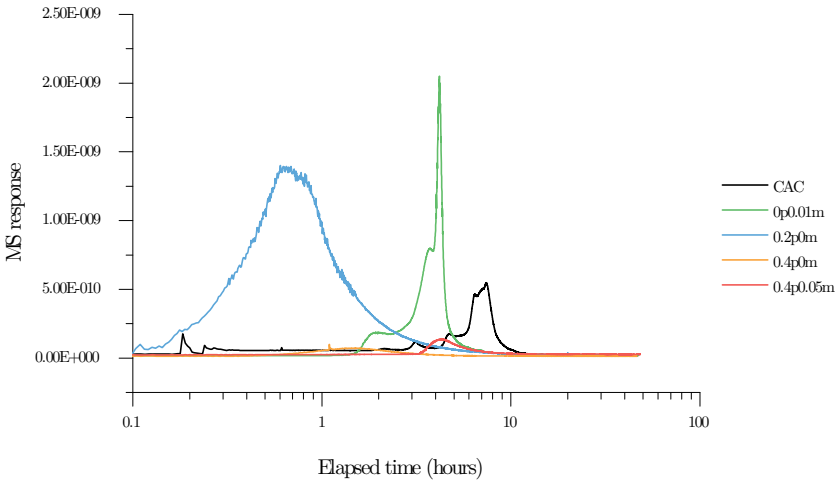

Figure 7-6 Mass spectrometry responses for hydrogen evolution as a function of time for encapsulated fine aluminium powder.

The cumulative mass spectrometry responses for each of the formulations are shown in Figure 7-7, which indicate that over the 50 hours the samples were monitored, the CAC and 0p0.1m samples evolved considerably more hydrogen than the other formulations, in line with the results from the water displacement method. However with this technique it must be noted that the ionisation of water molecules in the mass spectrometer contributes to these measurements, and as such there is a background associated with the measurements. Hence, without calibration to account for this, involving cross calibration against a sample gas with known hydrogen content and flowrate, it is not possible to determine the absolute rate of hydrogen evolution.

The technique itself was a valuable tool in determining the relative corrosion rates over the duration of the immediate period after mixing and the technique is more sensitive to hydrogen detection than possible by the water displacement method. The resulting data is also higher resolution, in the case of the data presented in this chapter it was possible to determine that the corrosion processes for samples other than those in the 0.4p*x*m series were more likely to be comprised of precipitation/dissolution/corrosion repeating cycles. Achieving the same insight with the low resolution and sensitivity of the water displacement method would not have been possible.

However the benefits are less when considering long term experiments or more complex and larger sample geometries. The apparatus used for the water displacements is easily scalable to accommodate larger samples and those encapsulating monolithic aluminium, however in the case of the MS a bespoke reactor vessel would be required. Additionally for longer-term samples it would not be cost effective or good value to run samples in parallel for durations in the order of months with multiple spectrometers. The two methods are complementary and it would be used to conduct both when seeking to assess hydrogen evolution to assess corrosion of an encapsulated metal.

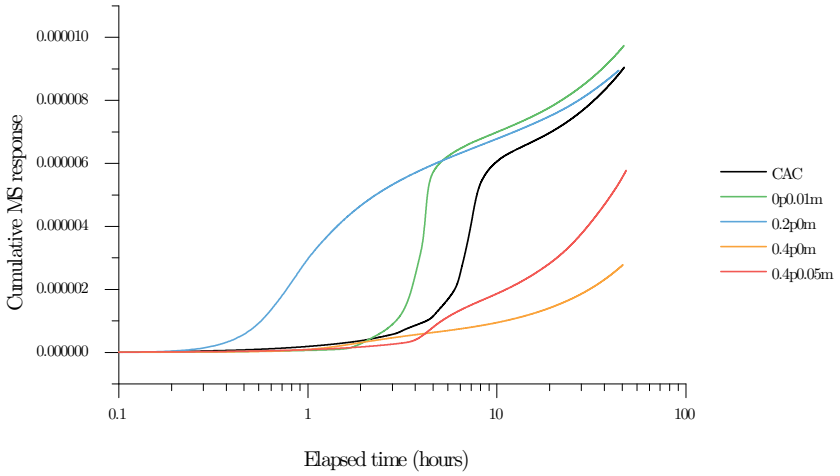

Figure 7-7 Data shown in **Error! Reference source not found.**7-6 displayed as a cumulative total as a function of time.

7.3.2 Differential scanning calorimetry analysis

Samples cast for DSC experiments exhibited severe symptoms of aluminium corrosion, in comparison with smaller samples. Figure 7-8 shows eruption of the plastic centrifuge tubes in which samples were cast, as a result of three factors: (i) hydrogen generation, (ii) considerable self-heating of the sample, and (iii) expansion of the monolith as a result of corrosion product growth. It is thought that this was due to the larger volumes being cast with encapsulated Al powder, whereas in other

experiments either smaller quantities were used, or the aluminium being encapsulated had a lower surface area to volume ratio, thus reducing its reactivity. Where possible, samples taken for DSC analysis were retrieved from centrifuge tubes that had not ruptured, to ensure that the relative humidity and CO_2-free environment had been maintained.

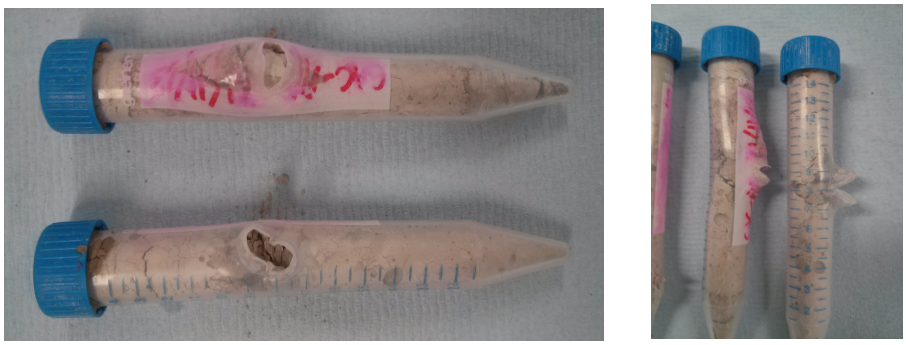

Figure 7-8 Typical examples of ruptured 10 mL sample tubes as a result of corrosion of powdered aluminium in a CAC matrix.

Figure 7-9 shows the differential scanning calorimetry data obtained for each of the five formulations studied, at 1, 3 and 7 days after mixing. These data were used to determine the energy required to melt the remaining aluminium in the sample, using the endothermic latent heat of melting peak centred about 660°C, as determined by a reference sample, which was normalised by mass and plotted as a function of curing time in Figure 7-10. This temperature range can also be associated with the decomposition of calcite (Šauman 1971), however the formulations investigated showed no calcite formation at any of the ages studied, this was expected considering the intrinsic carbonation resistance of the binder system (Scrivener 2003) and the care taken during curing. Using the latent heat of melting for aluminium, 321 kJ/kg (Perry 2011), as a conversion factor it is possible to determine the mass percentage of aluminium remaining in each sample, which is displayed on the vertical axis of **Error! Reference source not found.** 7-10. Each of the formulations exhibit a higher rate of aluminium corrosion in the first 3 days of curing. Each of the phosphate modified formulations, apart from 0p0.1m, show a decrease in aluminium corrosion compared to the neat CAC sample at each of the ages examined. The 0p0.1m sample

contains no remaining aluminium after 7 days, indicating the complete consumption of the metal by corrosion, in agreement with the XRD data obtained for samples after 40 days in the water displacement experiment. For the 0.4p*x*m series of formulations, at least 3.8 wt.% aluminium, 76% of the quantity initially added, remains after 7 days, whereas for the neat CAC this figure was nearly three times smaller at 1.3 wt.% Al (26% of the initially added material), representing a considerable improvement in corrosion behaviour during the first seven days of curing.

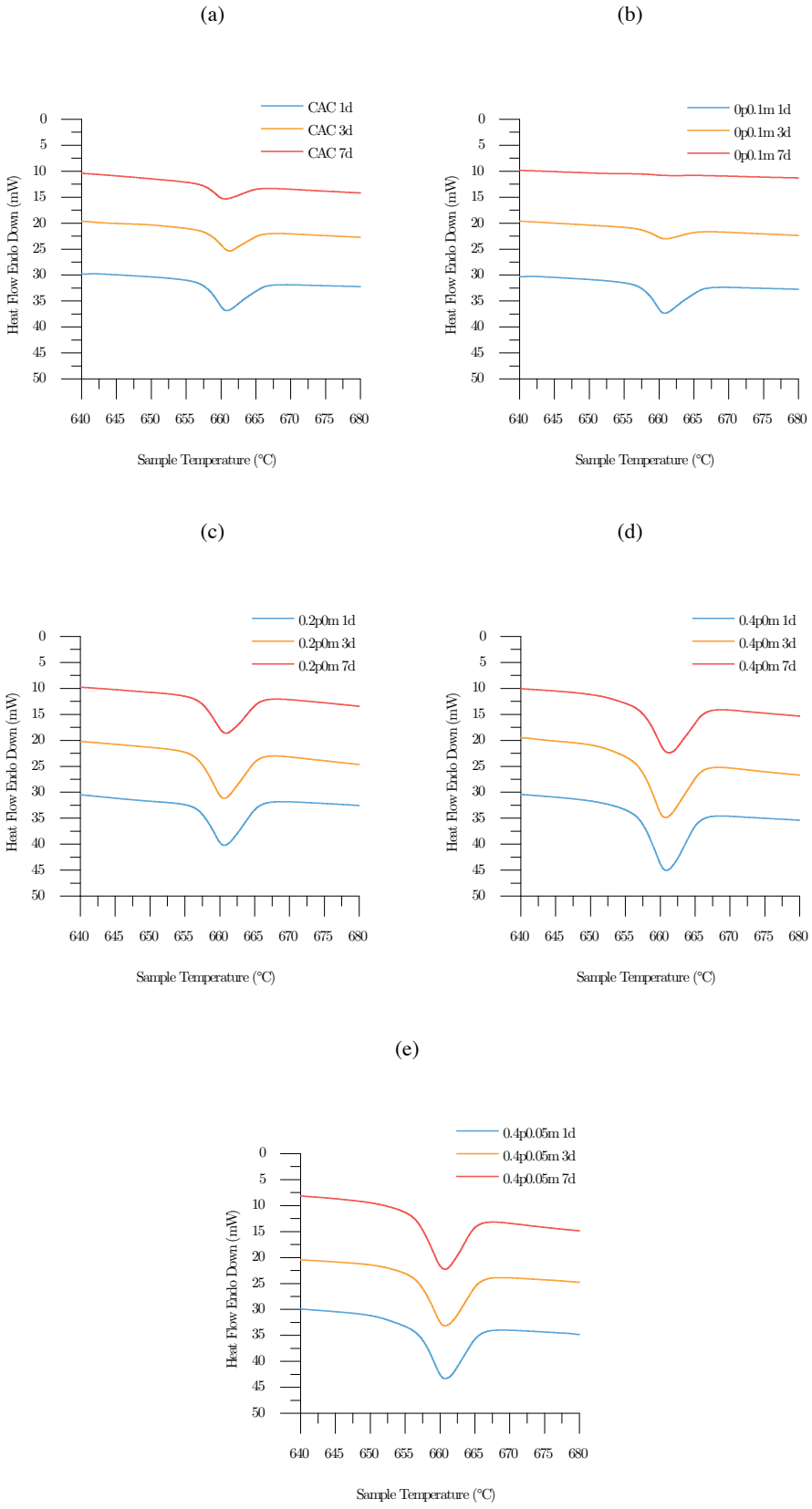

Figure 7-9 DSC thermograms obtained for (a) CAC, (b) 0p0.1m, (c) 0.2p0m, (d) 0.4p0m and (e) 0.4p0.05m formulations with 5 wt% encapsulated aluminium powder, showing the latent heat of melting of the remaining aluminium metal. Successive data sets in each plot are offset vertically by 10 mW for clarity.

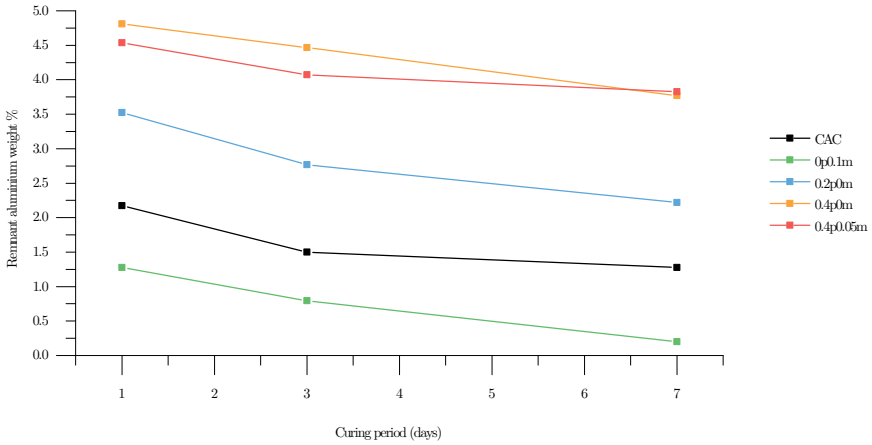

Figure 7-10 The wt.% of aluminium in each sample identified by DSC, as a function of curing period.

The relative performance of each of the formulations in terms of aluminium corrosion is similar to that observed by the mass spectrometry and water displacement methods. However, of these three methods, the DSC approach demonstrates the most simple and reliable measurement to determine absolute corrosion of the aluminium within the cement matrix at a given point in time, although its time resolution is the lowest of the three approaches because the measurements are not continuous. A considerable drawback for both the DSC and mass spectrometry methods is that they require a (representative) sample to fit into an appropriately sized crucible (approximately 70 µL). This requires the aluminium to be powdered, and hence any rates of corrosion determined are functions of this particle geometry and may not directly model the corrosion behaviour of large monolithic aluminium pieces. For the aluminium contained in ILW waste streams, the morphology is determined by the processes taking place during decommissioning, specifically the stripping of the fuel cladding and sheathing, hence there may be considerable variety in paticle size and shape within the material, ranging from powder fines to swarf, or larger monolithic aluminium elements with a much lower surface area to volume ratio.

7.3.3 Microscopy

Corrosion of monolithic aluminium in the cement systems of interest was investigated by scanning electron microscopy, using aluminium metal wire around which the cement formulations were cast. Cross sectional SEM micrographs of the specimens after 1, 7 and 100 days are shown in Figure 7-11. Samples with neat CAC were not examined, as after 1 day there was considerable aluminium corrosion resulting in the encapsulated aluminium wire no longer being in contact with the surrounding matrix. The high rate of corrosion in this cement led to the formation of a much larger interfacial region with higher porosity that was much weaker than the cement matrix and the aluminium wire and did not maintain adhesion. As a result it broke away, liberating the remnant corroded wire from the system and no longer encapsulating it.

The 0p0.1m formulation, in comparison to the CAC, encapsulated the wire effectively throughout the 100 days studied. It is thought that CAC encapsulated material corroded rapidly during the conversion of the hydrates, as a result of the increased free water availability during the process. However in the case of 0p0.1m this process is much slower, as it was reported in Chapter 4 that the metastable phases CAH_{10} and C_2AH_8 persist up to 180 days of curing, whereas for the neat CAC system these are seen in limited quantities after 7 days but not after 28 days of curing. Nevertheless considerable corrosion occurs, with a distinct layer of corrosion product visible in the SEM images in Fig 7-12a.

In the case of the 0.2p0m formulation (Fig 7-12b) there exists an interfacial corrosion product layer, which maintains good contact with both the encapsulated metal and the cement matrix, however this also indicates considerable corrosion of the metal itself. Conversely in the cases of 0.4p0m (Fig 7-12c) and 0.4p0.05m (Fig 7-12d) it is unclear how much of an interface exists between the metal and the matrix, after the initial hardening of the cements.

(a) 0p0.1m

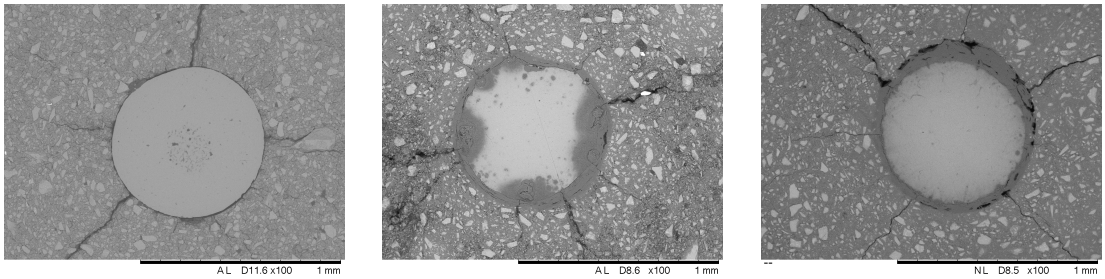

(b) 0.2p0m

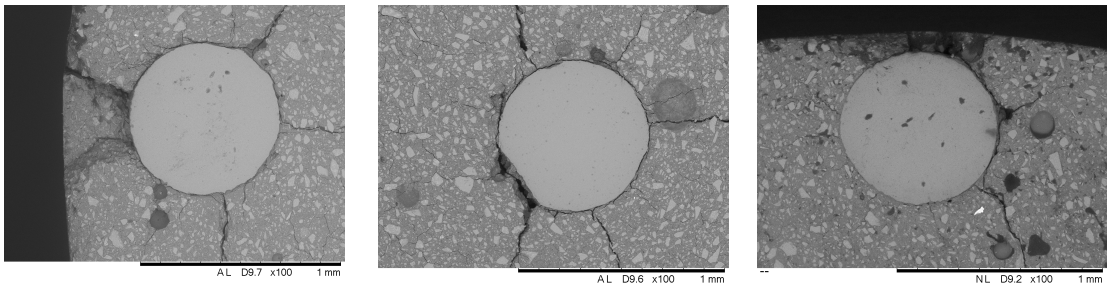

(c) 0.4p0m

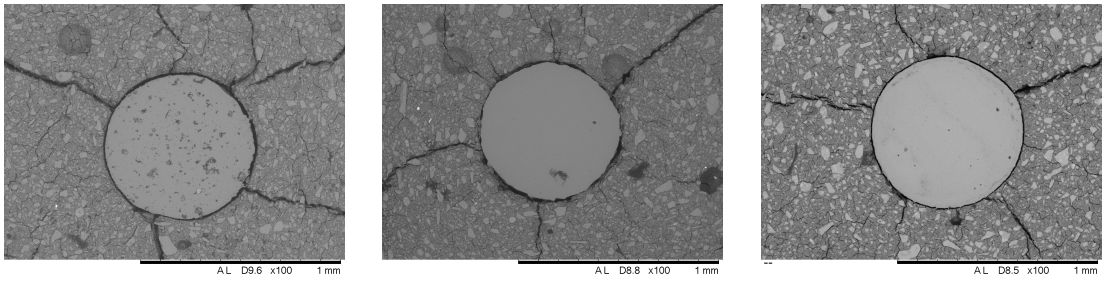

(d) 0.4p0.05m

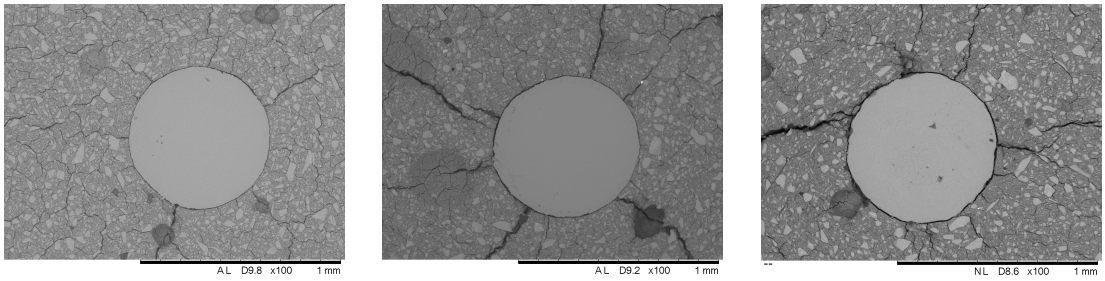

Figure 7-11 Scanning electron microscopy images obtained, showing cross sections of aluminium wire encapsulated in each of the 5 formulations investigated, after 24 hours, 7 days and 100 days of curing (left, centre and right images respectively).

The hetrogeneous nature of the cement-metal interface results in non-uniform corrosion of the encapsulated metal. In all the samples studied, certain regions along the circumference of the aluminium exhibited higher levels of corrosion as a result of localised pitting. As such, application of image analysis to SEM micrographs to determine the remaining cross sectional area of the aluminium metal was not meaningful, as the variability of this area along the length of the aluminium wire was not uniform and hence no good quantitative indication of the corrosion rate could be onntained. Although it was possible to isolate the aluminium metal from the matrix and the corrosion layer surrounding it, optical profilometry was also not suitable for determining the corrosion rate by calculating the cross sectional area of the aluminium wire, for the same reasons related to non-uniform pitting corrosion.

7.3.4 Aluminium plate encapsulation

In addition to the encapsulation of aluminium wire, monolithic aluminium plates were also encapsulated and studied over a longer period. In addition to the neat CAC and phosphate modified CAC formulations, PC and BFS/PC composite formulations were also studied. The results obtained for mass loss as a function of curing time for encapsulated aluminium plates in each of the formulations are shown in Figure 7-12. Mass loss was determined by extracting the plate from the cement, removing the corrosion products by brushing, and weighing. These values were compared to individual masses obtained for each of the plates prior to encapsulation.

Of the CAC based formulations, the neat CAC and 0.4p0.05m performed well and showed improvement over the PC based formulations. However this was not the case with the 0p0.1m and 0.2p0.075m formulations, which both exhibited considerable levels of corrosion and expansion of the matrix, resulting in the rupture of the centrifuge tubes in which they were cast, shown in Figure 7-13. In contrast to the samples shown in Figure, there is a considerably lower rate of corrosion as a result of using monolithic aluminium, as such this rupture occurs primarily due to volume expansion of the cements rather than due to hydrogen release during early curing.

Interestingly, despite exhibiting large mass losses due to corrosion, the PC and PC/BFS composite formulations showed little volume expansion and so the containers of these formulations were intact. It appears that the longer setting times associated with these materials allow for the incorporation of the products from the corrosion process, that occurs during early curing, into the cement itself. However, for these samples it was often observed that there was disruption to the matrix itself due to high rates of corrosion early in the hydration process, as seen in Figure 7-14 where the path of the hydrogen evolved has resulted in formation of a channel from the uppermost face to the encapsulated aluminium.

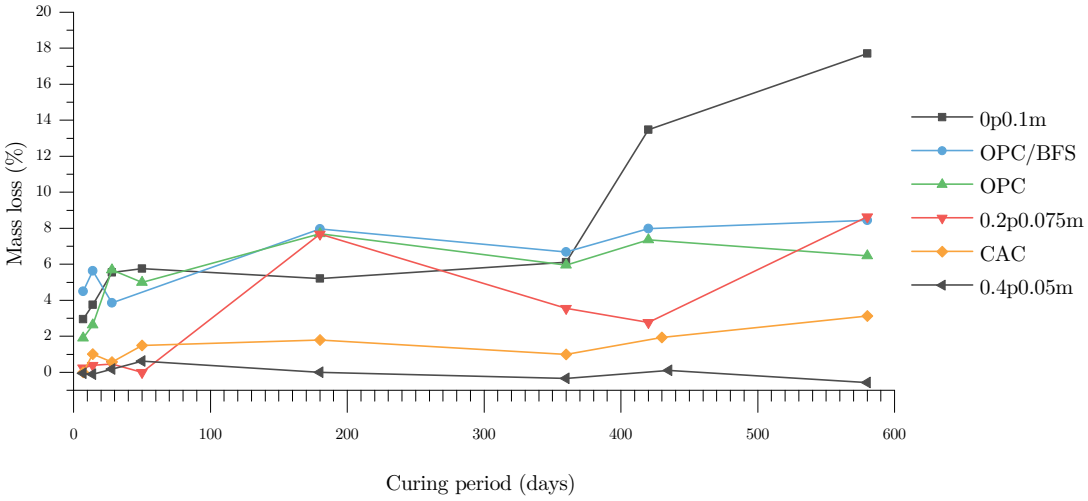

Figure 7-12 Mass loss of encapsulated aluminium plate, due to corrosion, as a function of curing/encapsulation period. Each individual point represents a distinct sample, and so the apparent negative corrosion rates in some time periods are related to experimental scatter rather than the actual reversal of the mass loss process.

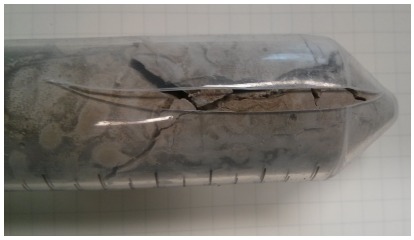

Figure 7-13 0p0.1m formulation with encapsulated aluminium plate after 420 days curing.

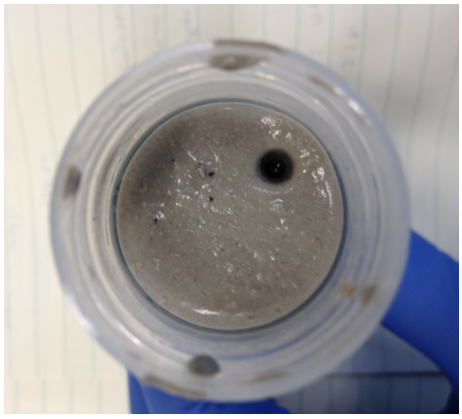

Figure 7-14 Typical voids observed for PC and PC/BFS composite formulations as a result of hydrogen release during early curing.

The encapsulated aluminium in the CAC matrix was accompanied by a discoloration and increased porosity in the surrounding material relative to the bulk of the matrix; these two distinct layers are visible in Figure 7-15. While the phosphate-modified CAC formulations with siliceous SCM addition studied by Swift (2013) showed C_2ASH_8 in the surrounding matrix material, in the neat CAC formulations here it was determined that the colour change in the matrix near the interface was not due to the same reason. Diffraction data for this region and the surrounding unaffected matrix material are shown in Figure 7-16, with the only difference between the two being the presence of a region of diffuse scattering centred about 13° 2θ. From this alone it is unclear to characterise this phase. There seems to be little reduction in the gehlenite reflections (as found in the materials tested in the water displacement experiment), however this may be due to increased levels of aluminium corrosion. It should be noted that no such colour difference or segmentation of the surrounding matrix material was observed in any of the phosphate modified CAC formulations.

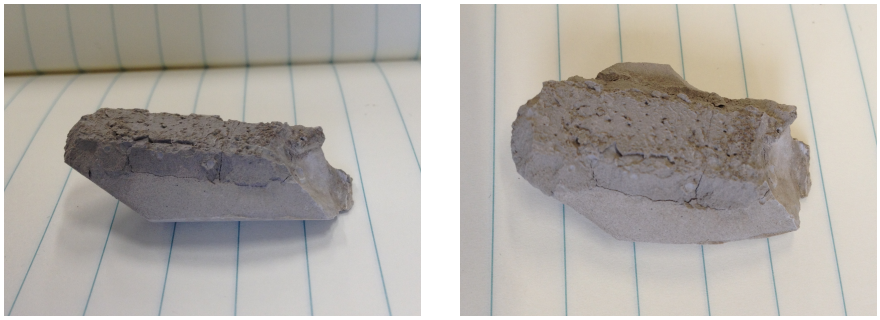

Figure 7-15 A sample of neat CAC cleaved from the interface with an encapsulated aluminium plate, exhibited is a clear region affected by corrosion of adjacent aluminium resulting in discolouration and increased porosity.

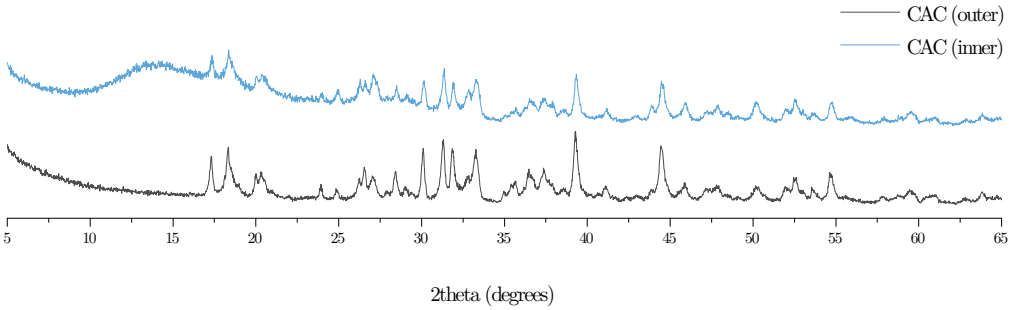

Figure 7-16 Diffractograms obtained for the 'inner' material nearer the interface with the aluminium and 'outer' material further away, both shown in **Error! Reference source not found.**.

In addition to casting the 0.4p0.05m formulation in a centrifuge tube, another sample with encapsulated aluminium was cast into a hydrothermal vessel and subjected to heat treatment at 180°C for 24 hours. Figure 7-17 shows a cross section of the sample, which shows the precipitation of a dense corrosion product and considerable cracking that looks to have grown from the vertices of the cross-sectional face of the aluminium plate.

Figure 7-18 shows the aluminium plate during removal from each specimen at 420 days of age, immediately after demoulding. The surface finish of the aluminium was only maintained in the sample demoulded from the 0.4p0.05m formulation. All other formulations showed considerably corrosion product growth on the surface of the

encapsulated metals, coupled with expansion induced tensile cracking and in the majority of cases also the cracking of their containers.

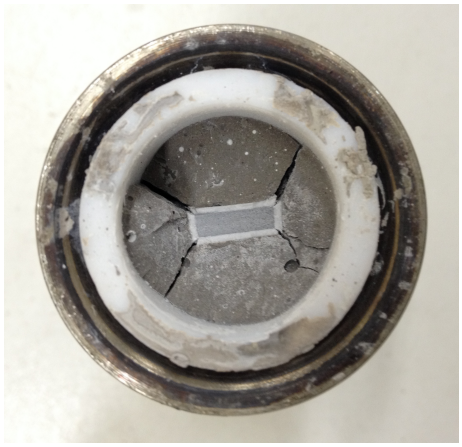

Figure 7-17 Aluminium plate encapsulated in 0.4p0.05m, after undergoing hydrothermal treatment.

(a) (b) (c)

(d) (e) (f)

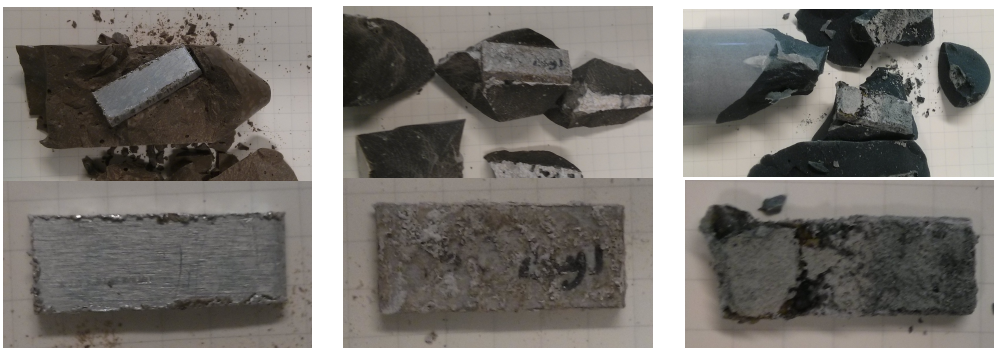

Figure 7-18 Images of aluminium plates demoulded after 420 days encapsulation in the following formulations: (a) CAC, (b) 0p0.1m, (c) 0.2p0.075m, (d) 0.4p0.05m, (e) PC, and (f) BFS/PC.

7.4 Discussion and implications

This chapter examines two different encapsulated aluminium metals, a powder and monolithic aluminium either as a plate or wire. With increased surface area to volume ratio, the powder exhibits a different corrosion rate when encapsulated. As such high corrosion rates are seen at different times after the initial mixing of the slurries. Of the techniques chosen to examine the corrosion of the encapsulated metals, all proved useful in determining the corrosion as a function of curing period.

The direct measurement of aluminium corrosion by DSC was accurate and effective but was limited to samples encapsulating powder metal. Similarly the evolution of hydrogen gas by water displacement and mass spectroscopy was accurate and generally the results from all three techniques were in good agreement. Whereas the mass spectroscopy gave very accurate semi quantitative data (without using a reference gas and calibrating) the DSC and water displacement methods could estimate the remnant aluminium wt.% loading of the samples effectively, although the water displacement method is the only one which may be easily adapted to larger samples with monolithic aluminium encapsulated. Conducting all three in combination is effective in determining the corrosion at early age curing with high accuracy using MS, long term monitoring by water displacement and verification of the latter by DSC and XRD once hydration and corrosion has been halted.

The data obtained from studies examining the encapsulation of monolithic aluminium indicate that the use of a more reactive powder fundamentally changes the relative performance of formulations in minimising corrosion, in the case that the formulations exhibit reasonable corrosion (0.4p*x*m formulations did not in either set of experiments). Whereas in the powder experiments it was observed that the 0.2p*x*m and 0p*x*m formulations performed comparably to the neat CAC, in the case of the monolithic plate encapsulation experiments they performed considerably worse. This indicates that in the phosphate modified system the slower, more progressive corrosion, and not that which occurs rapidly during early hydration, is more damaging to the 'waste package' – i.e. greater volume expansion and loss of mechanical integrity. The higher level of aluminium corrosion may tentatively be appropriated to the longer curing periods over which the 0p*x*m and 0.2p*x*m formulation begin to

precipitate greater quantities of conventional CAC hydrates, perhaps liberating free water available for corrosion and also an adjustment in the pH of the pore solution.`

The phase changes seen in the phosphate-modified CAC/PFA composite, investigated by Swift (2013), are held responsible for the 'latent' corrosion of the encapsulated aluminium at curing periods which coincide with this phase change. Hence as the phase assemblage in the 0.4p0.05m sample is stable from mixing until a minimum of 1050 d thereafter, as reported in Chapter 5, and the corrosion of encapsulated aluminium has been determined to be minimised relative to other formulations, there remains much promise in this system to be investigated further for encapsulation applications.

7.5 Conclusions

In the investigations conducted to examine the encapsulation of aluminium powder to study hydrogen evolution, phosphate modification of the CAC cements reduced the cumulative aluminium corrosion relative to the neat CAC formulation. The time of curing at which the maximum rate of hydrogen evolution occurs is dependent upon the formulation used to encapsulate the aluminium. This was similar to the dependence upon the formulation for the times at which the exothermic hydration events take place during early curing; indeed, it may be that the elevated corrosion is intimately linked to this. As a result of the encapsulated aluminium having high surface area to volume ratio, relatively high rates of aluminium corrosion were observed. In the case of the CAC this was accompanied by the precipitation of strätlingite, which is thought to be as a result of the hydration of gehlenite – the only source of silicon in the system. However, this was not observed in any phosphate modified CAC formulations, even 0p0.1m which maintains the conventional CAC hydration pathway (albeit slowly). With the more sensitive and higher resolution detection of hydrogen by mass spectrometry it was possible to determine a lineshape which was indicative of a more complex multistep mechanism of precipitation/dissolution/corrosion repeating cycles. This was the case for all the formulations studied apart from the 0.4p0.05m, which also exhibited the least aluminium corrosion in these experiments with powdered Al. Quantification of remaining aluminium in the cement matrix by DSC was successful, and observations

were aligned with the relative performances of the formulations determined by techniques used to measure the hydrogen evolution. Importantly, this method was the only technique among the powder encapsulation experiments which enabled examination of the aluminium directly for determination of corrosion rates.

Of the studies with monolithic aluminium, examination of encapsulated aluminium wire revealed that within the CAC matrix the breakdown of the porous corrosion product region that grew at the interface resulted in ineffective encapsulation of the wire. The 0p0.1m and 0.2p0m formulations exhibited corrosion and clearly identifiable corrosion layers. Conversely, the 0.4p*x*m exhibited less corrosion and the interface with the aluminium was difficult to identify.

Generally it was found that the greater the polyphosphate content of the formulation the better it was in minimising the aluminium corrosion, hence the 0.4p*x*m formulations performed better than the 0.2p0m formulations which improved upon the 0p0.1m formulation, The performance of the 0.4p0.05m formulation consistently outperformed the neat CAC formulation in minimising corrosion. However it must be noted that the relative performances between the CAC and the other phosphate modified formulations was dependent upon the analytical technique used to assess corrosion. In the case of rapid corrosion of aluminium powder soon after mixing the the performance of these formulations were comparable, conversely where corrosion was over a longer period (i.e. aluminium plate encapsulation) the CAC outperformed all phosphate modified formulations other than those in the 0.4p*x*m series.

The chemical stability of the phase assemblage of the 0.4p0.05m formulation, observed for up to 1050 days as reported in Chapter 5, and the considerable improvements upon the corrosion behaviour of encapsulated aluminium supports the requirement for further research in to this system for encapsulation of aluminium containing wastes.

8 Conclusions and recommendations

8.1 Conclusions

It was determined, from the work presented in this thesis that the phosphate modification of CAC can radically affect its hydration and thus properties. Varying the phosphate modification of CAC has been shown to a tool to tune the fresh state properties, reducing conversion issues by either changing hydration kinetics or changing the hydration pathway entirely, and optimised phosphate modified CAC formulation are suggested as waste encapsulation matrices as they were shown to maintain stability up to a minimum of 1080 days and developed little corrosion of aluminium metal during trials. A summary of conclusions drawn from the work presented in this thesis:

(i) Average chain length of phosphate ions in solution prior to mixing determines the fresh state properties of the slurry.
   a. The phosphate modification of CAC, using combinations of sodium polyphosphate and monophosphate in varying ratios can be used to tune the setting time of cement and control the exothermic heat flow during hydration reactions immediately after mixing.

(ii) The phosphate modification of CAC alters the hydration of the system considerably.
   a. The modification by sodium monophosphate alone adjusts the kinetics of hydration, maintaining metastable presence in the system for up to 180 days.
   b. Modification by polyphosphate, and by combinations of both phosphates, radically alters the hydration pathway of the system, resulting in the precipitation of a disordered binding phase. For lower levels of polyphosphate modification, as in the 0.2p*x*m series, over time precipitation of the conventional CAC hydrates can be observed,

Conversely, for the 0.4p*x*m series no conventional CAC hydrates are observed throughout the period studied, and for the 0.4p0.05m this extended to a minimum of 1050 days. Hydrothermal treatment of this sample resulted in the formation of hydroxyapatite, boehmite and a zeolite phase.

c. Samples in the 0.4p*x*m series consistently exhibited elevated compressive strengths relative to neat CAC, reaching up to 71 MPa after 360 days.

(iii) REAPDOR NMR experiments probing the binding phase of the 0.4p0m formulation showed the presence of strong interaction between aluminium and phosphorus, which in combination with ^{31}P CP/MAS experiments indicated the presence of a disordered C-A-P-H binding phase. This phase is identified to form on the surface of the clinker grains, acting as a diffusion barrier preventing conventional CAC hydration.

(iv) Phosphate content had a large influence on the ability of a formulation to minimise the corrosion of encapsulated aluminium.

a. Novel techniques were successfully trialled in determining encapsulated aluminium corrosion, by determining remnant aluminium metal or the formation of corrosion products.

b. The nature of phosphate modification can determine the time at which maximum aluminium corrosion rates occur.

c. The 0.4p*x*m formulations consistently outperformed all other formulations studied in both powder and plate encapsulation experiments.

(v) The 0.4p0.05m formulation shows a stable phase assemblage up to a minimum of 1050 days that exhibits the ability to encapsulate aluminium metal with minimal corrosion, and should be considered for further investigation as an ILW encapsulation matrix.

8.2 Recommendations for future work

Despite the development of CAC materials over 200 years ago, little work regarding the phosphate modification of this system is available. The work undertaken in this

thesis builds upon a limited body of literature describing the phosphate modified CAC system, as such further work is required before these materials are adopted for the demanding industrial applications for which they have been identified. Hence multiple directions for future works are discussed below for the development of this system to better understand their underlying chemistry and develop the supporting materials science such that they are more attractive from an industrial perspective.

Calorimetric studies in this thesis identify that the hydration reactions of CAC during the first 24 hours after mixing are considerably affected by the addition of sodium phosphates, however further work surrounding the specific mechanism, possibly elucidated by in situ ATR-FTIR study, would be useful in determining how to further capitalise on this mechanism for applications that require very specific fresh state properties. Further in depth studies of these hydration reactions and the binder phase would provide supporting data when modelling how these materials would behave in severe and demanding environments. This would also benefit from further probing with NMR techniques, examining the calcium environments as a function of curing and resolving broad aluminium spectra by performing two-dimensional MQMAS experiments. Although in this thesis the 0.4p0.05m formulation has been studied to 1050 days after curing, with the conclusion that the phase assemblage is stable over this period, further examination is desirable to define whether under ambient conditions this assemblage is thermodynamically stable in the very long term.

The focus of Chapter 7, trialling the formulations with aluminium encapsulation, considers a particular demanding application, for which the existing preferred cementing solution (PC/SCM composite) benefits from a richer body of literature and service track record. Much further work is required for the phosphate-modified CAC system to gain favour. As per Wilding's (1992) considerations, the qualities required for cements to be used in encapsulation of waste may be split into the following themes: (i) strength and mechanical properties, (ii) maintaining a solid mass, (iii) activity release under optimistic and pessimistic storage conditions. The system requires examination with respect to each of these and the processing parameters envelope associated with the waste packaging process at a processing site. The immobilisation of the activity of the encapsulated waste is a particularly important aspect to consider, standardised leachability testing of the samples with simulant

wastes after exposure to a variety of curing conditions would be useful to frame the performance of the matrix in the context of the better understood PC composite systems.

In addition to the corrosion of aluminium metal resulting in degradation of the wasteform and possible accelerated leaching behaviour, the corrosion behaviour of other present metals such as magnesium and uranium require examination. Resistance based testing of continuous encapsulated monolithic metal would be useful as an alternative technique to study its time resolved in situ corrosion. This may be either by a simple measurement of the increase in resistance as a result of a smaller volume of encapsulated metal, or by use of electrochemical techniques such as linear polarisation resistance.

9 References

Alfani, R., Colombet, P., Rizzo, N. & Nicolais, L., **1999**. Effect of temperature on thermo-mechanical properties of Macro-Defect-Free cement-polymer composite. *Journal of Materials Science*, (32), pp.5683–5687.

Allan, M. & Kukacka, L., **1995**. Calcium phosphate cements for lost circulation control in geothermal drilling. *Geothermics*, 24(2), pp.269–282.

Alphonse, P. & Courty, M., **2005**. Structure and thermal behavior of nanocrystalline boehmite. *Thermochimica Acta*, 425(1-2), pp.75–89.

Ambard, A.J. & Mueninghoff, L., **2006**. Calcium phosphate cement: review of mechanical and biological properties. *Journal of Prosthodontics*, 15(5), pp.321–8.

Andrew, E., Bradbury, A. & Eades, R., **1958**. Nuclear Magnetic Resonance spectra from a Crystal rotated at High Speed. *Nature*, 182, p.1659.

Ann, K.Y. & Cho, C.G., **2014**. Corrosion resistance of calcium aluminate cement concrete exposed to a chloride environment. *Materials*, 7(2), pp.887–898.

Ann, K.Y., Kim, T.-S., Kim, J.H. & Kim, S.-H., **2010**. The resistance of high alumina cement against corrosion of steel in concrete. *Construction and Building Materials*, 24(8), pp.1502–1510.

Arai, Y. & Sparks, D.L., **2001**. ATR–FTIR Spectroscopic investigation on phosphate adsorption mechanisms at the ferrihydrite-water interface. *Journal of Colloid and Interface Science*, 241(2), pp.317–326.

Aravamudhan, S., *NMR as a Tool for Structure Determination*.

ASTM Standard C807 - 08, **2008**. Standard test method for time of setting of hydraulic cement mortar by modified vicat needle. *ASTM International,West Conshohocken, PA*.

Atkins, M. & Glasser, F.P., **1992**. Application of portland cement-based materials to radioactive waste immobilization. *Waste Management*, 12(2-3), pp.105–131.

Balek, V., Šubrt, J., Rouquerol, J., Llewellyn, P., Zeleňák, V., Bountsewa, I.M., Beckman, I.N., et al., **2003a**. Emanation thermal analysis study of synthetic gibbsite. *Journal of Thermal Analysis and Calorimetry*, 71, pp.773–782.

Balek, V., Šubrt, J., Rouquerol, J., Llewellyn, P., Zeleňák, V., Bountsewa, I.M., Beckman, I.N., et al., **2003b**. Emanation thermal analysis study of synthetic gibbsite. *Journal of Thermal Analysis and Calorimetry*, 71, pp.773–782.

Barinov, S.M. & Komlev, V.S., **2011**. Calcium phosphate bone cements. *Inorganic Materials*, 47(13), pp.1470–1485.

Bell, R., **1947**. Hydrolysis of dehydrated sodium phosphates. *Industrial & Engineering Chemistry*, 39(2), pp.136–140.

Belloque, J., De La Fuente, M.A. & Ramos, M., **2000**. Qualitative and quantitative analysis of phosphorylated compounds in milk by means of ^{31}P-NMR. *The Journal of Dairy Research*, 67(4), pp.529–39.

Bensted, J. & Barnes, P. eds., **2002**. *Structure and Performance of Cements* 2nd ed., London: Spon Press.

Bleam, W.F., Pfeffer, P.E. & Frye, J.S., **1989**. ^{31}P solid-state nuclear magnetic resonance spectroscopy of aluminum phosphate minerals. *Physics and Chemistry of Minerals*, 16, pp.455–464.

Bohner, M., **2007a**. Reactivity of calcium phosphate cements. *Journal of Materials Chemistry*, 17, pp.3980–3986.

Bohner, M., **2007b**. Reactivity of calcium phosphate cements. *Journal of Materials Chemistry*, 17(38), p.3980.

Boudeville, P., Serraj, S., Leloup, J.M., Margerit, J., Pauvert, B. & Terol, A., **1999**. Physical properties and self-setting mechanism of calcium phosphate cements from calcium bis-dihydrogenophosphate monohydrate and calcium oxide. *Journal of Materials Science. Materials in Medicine*, 10, pp.99–109.

Bradbury, C., Callaway, P. & Double, D.D., **1976**. The conversion of high alumina cement/concrete. *Materials Science and Engineering*, 23, pp.43–53.

Brow, R.K., Kirkpatrick, R.J. & Turner, G.L., **1990**. Local structure of $xAl_2O_3{\cdot}(1-x)NaPO_3$ glasses: an NMR and XPS study. *Journal of the American Ceramic Society*, 73(8), pp.2293–300.

Brow, R.K., Kirkpatrick, R.J. & Turner, G.L., **1993**. Nature of alumina in phosphate glass: II, structure of sodium aluminophosphate glass. *Journal of the American Ceramic Society*, 76(4), pp.919–28.

Bushnell-Watson, S.M. & Sharp, J.H., **1990**. On the cause of the anomalous setting behaviour with respect to temperature of calcium aluminate cements. *Cement and Concrete Research*, 20, pp.677–686.

Bushnell-Watson, S.M. & Sharp, J.H., **1992**. The application of thermal analysis to the hydration and conversion reactions of calcium aluminate cements. *Materiales de Construccion*, 42(228), pp.13–32.

Cardoso, F. a., Innocentini, M.D.M., Akiyoshi, M.M. & Pandolfelli, V.C., **2004**. Effect of curing time on the properties of CAC bonded refractory castables. *Journal of the European Ceramic Society*, 24(7), pp.2073–2078.

Chotard, T.J., Boncoeur, M.., Smith, a, Dupuy, J.. & Gault, C., **2003**. Application of X-ray computed tomography to characterise the early hydration of calcium aluminate cement. *Cement and Concrete Composites*, 25(1), pp.145–152.

Chotard, T.J., Gimet-Breart, N. & Smith, A., **2001**. Application of ultrasonic testing to describe the hydration of calcium aluminate cement at the early age. *Cement and Concrete Research*, 30, pp.405–412.

Chotard, T.J., Smith, a., Rotureau, D., Fargeot, D. & Gault, C., **2003**. Acoustic emission characterisation of calcium aluminate cement hydration at an early stage. *Journal of the European Ceramic Society*, 23(3), pp.387–398.

Chow, L.C., **2000**. Calcium phosphate cements: chemistry, properties, and applications. *Materials Research Society Symposium Proceedings*, 599, pp.27–37.

Chow, L.C., **1991**. Development of self-setting calcium phosphate cements. *Journal of The Ceramic Society of Japan*, 99(10), pp.954–964.

Christensen, A.N., Jensen, T.R., Lebech, B., Hanson, J.C., Jakobsen, H.J. & Skibsted, J., **2008**. Thermal decomposition of monocalcium aluminate decahydrate (CaAl2O4.10H2O) investigated by in-situ synchrotron X-ray powder diffraction, thermal analysis and ^{27}Al, ^{1}H MAS NMR spectroscopy. *Dalton transactions (Cambridge, England : 2003)*, 2(4), pp.455–62.

Christensen, A.N. & Lehmann, M.S., **1984**. Rate of reactions between D_2O and CaxAlyOz. *Journal of Solid State Chemistry*, 51(2), pp.196–204.

Chughtai, A., Marshall, R. & Nancollas, G.H., **1968**. Complexes in calcium phosphate solutions. *The Journal of Physical Chemistry*, 72(1), pp.208–211.

Clearfield, A., Reibenspies, J.H. & Bhuvanesh, N. eds., **2008**. *Principles and Applications of Powder Diffraction*, Chichester: John Wiley & Sons, Ltd.

Collier, N.C., **2010**. Immobilisation matrices for intermediate level nuclear wastes using sulphate activated BFS/OPC and PFA/OPC composite cements. *Advances in Applied Ceramics*, 109(5), pp.269–274.

Comité Européen de Normalisation, **2005**. EN 14647 : Calcium aluminate cement - Composition, specifications and conformity criteria.

Cong, X. & Kirkpatrick, R.J., **1993**. Hydration of Calcium Aluminate Cements: A Solid-State ^{27}Al NMR Study. *Journal of the American Ceramic Society*, 76(2), pp.409–16.

Contreras, C.A., Sugita, S. & Ramos, E., **2006**. Preparation of sodium aluminate from basic aluminium sulfate. *AZo Journal of Materials Online*, 2, pp.1–13.

Das, S., Mitra, A. & Poddar, P., **1996**. Thermal analysis of hydrated calcium aluminates. *Journal of Thermal Analysis*, 47, pp.765–774.

Ding, J., Fu, Y. & Beaudoin, J.J., **1996**. Effect of different inorganic salts/alkali on conversion-prevention in high alumina cement products. *Advanced Cement Based Materials*, 7355(96).

Ding, J., Fu, Y. & Beaudoin, J.J., **1995**. Strätlingite formation in high alumina

cement-silica fume systems: significance of sodium ions. *Cement and Concrete Research*, 25(6), pp.1311–1319.

Döhler, F., Mandlule, A., van Wüllen, L., Friedrich, M. & Brauer, D.S., **2015**. 31P NMR characterisation of phosphate fragments during dissolution of calcium sodium phosphate glasses. *Journal of Materials Chemistry B*, 3, pp.1125–1134.

Donatello, S., Tyrer, M. & Cheeseman, C.R., **2009**. Recent developments in macro-defect-free (MDF) cements. *Construction and Building Materials*, 23(5), pp.1761–1767.

Dorozhkin, S. V., **2009a**. Calcium orthophosphate cements and concretes. *Materials*, 2(1), pp.221–291.

Dorozhkin, S. V., **2009b**. Calcium orthophosphates in nature, biology and medicine. *Materials*, 2, pp.399–498.

Edmonds, R.N. & Majumdar, A.J., **1988**. The hydration of monocalcium aluminate at different temperatures. *Cement and Concrete Research*, 18(c), pp.311–320.

Van Emmerik, T.J., Sandström, D.E., Antzutkin, O.N., Angove, M.J. & Johnson, B.B., **2007**. ^{31}P solid-state nuclear magnetic resonance study of the sorption of phosphate onto gibbsite and kaolinite. *Langmuir*, 23(6), pp.3205–13.

Engelhardt, G. & Michel, D., **1987**. *High-resolution solid-state NMR of silicates and zeolites*, Chichester: John Wiley & Sons.

Falzone, G., Balonis, M. & Sant, G., **2015**. X-AFm stabilization as a mechanism of bypassing conversion phenomena in calcium aluminate cements. *Cement and Concrete Research*, 72, pp.54–68.

Fedotov, M.A., Mudrakovskii, I.L., Mastikhin, V.M., Shmachkova, V.P. & Kotsarenko, N.S., **1987**. Dependence of the ^{27}Al and ^{31}P NMR chemical shifts in alumophosphates on the composition of the second coordination sphere. *Bulletin of the Academy of Sciences of the USSR*, 36(10), pp.2169–71.

Fernández, E., Boltong, M. & Ginebra, M., **1994**. Common ion effect on some calcium phosphate cements. *Clinical Materials*, 16, pp.99–103.

Fernández, J.M., Navarro-Blasco, I., Duran, A., Sirera, R. & Alvarez, J.I., **2014**. Treatment of toxic metal aqueous solutions: encapsulation in a phosphate-calcium aluminate matrix. *Journal of Environmental Management*, 140, pp.1–13.

Fernández-Carrasco, L. & Vázquez, E., **2009**. Reactions of fly ash with calcium aluminate cement and calcium sulphate. *Fuel*, 88(9), pp.1533–1538.

Fernández-Jiménez, A., Palomo, Á., Vazquez, T., Vallepu, R., Terai, T. & Ikeda, K., **2008**. Alkaline Activation of blends of metakaolin and calcium aluminate. *Journal of the American Ceramic Society*, 91(4), pp.1231–1236.

Fernández-Jiménez, A., Vázquez, T. & Palomo, Á., **2011**. Effect of Sodium Silicate on Calcium Aluminate Cement Hydration in Highly Alkaline Media: A

Microstructural Characterization. *Journal of the American Ceramic Society*, 94(4), pp.1297–1303.

Ferraris, C. & Garboczi, E., **2013**. Identifying improved standardized tests for measuring cement particle size and surface area. *Transportation Research Record: Journal of the Transportation Research Board*, (2342), pp.10–16.

Frydman, L., Grant, D.M. & Harris, R.K., **2002**. Fundamentals of multiple-quantum magic-angle spinning NMR on half-integer quadrupolar nuclei magic-angle spinning NMR on half-integer quadrupolar nuclei. In *Encyclopedia of Nuclear Magnetic Resonance. Volume 9: Advances in NMR*. Chichester, UK: John Wiley & Sons, pp. 262–274.

Fujii, K., Kondo, W. & Ueno, H., **1986**. Kinetics of hydration of monocalcium aluminate. *Journal of the American Ceramic Society*, 64(4), pp.361–364.

Gabbott, P., **2008**. *Principles and applications of thermal analysis* P. Gabbott, ed., Oxford: Blackwell Publishing.

Gaki, A. & Chrysafi, R., **2006**. Synthesis of calcium aluminates through the polymeric precursor route. *Chemical Industry and Chemical Engineering Quarterly*, 12(2), pp.137–140.

Gauglitz, G. & Vo-Dinh, T. eds., **2006**. *Handbook of spectroscopy*, Weinheim: Wiley-VCH Verlag GmbH.

Georgescu, M., Puri, A., Coarna, M., Voicu, G. & Voinitchi, D., **2002**. Thermoanalytical and infrared spectroscopy investigations of some mineral pastes containing organic polymers. *Cement and Concrete Research*, 32(8), pp.1269–1275.

Gilmore, B.H., **1937**. Prevention of calcium deposits in process waters. *Industrial & Engineering Chemistry*, 29(5), pp.584–590.

Glasser, F.P., **1997**. Fundamental aspects of cement solidification and stabilisation. *Journal of Hazardous Materials*, 52(2-3), pp.151–170.

Goldbourt, A., Vega, S., Gullion, T. & Vega, A.J., **2003**. Interatomic distance measurement in solid-state NMR between a spin- 1/2 and a spin- 5/2 using a universal REAPDOR curve. *Journal of the American Chemical Society*, 125(37), pp.11194–5.

Gong, W., **2001**. A real time in situ ATR-FTIR spectroscopic study of linear phosphate adsorption on titania surfaces. *International Journal of Mineral Processing*, 63(3), pp.147–165.

Goñi, S., Andrade, C. & Page, C., **1991**. Corrosion behavior of steel in high alumina cement mortar samples: Effect of chloride. *Cement and Concrete Research*, 21(c), pp.635–646.

Gosselin, C., **2009**. *Microstructural Development of Calcium Aluminate Cement Based Systems with and without Supplementary Cementitious Materials*. Ecole

Polytechnique Fédérale de Lausanne.

Griffiths, P. & Haseth, J. De, **2007**. *Fourier transform infrared spectrometry* 2nd ed., New Jersey: John Wiley & Sons.

Grutzeck, M.W. & Siemer, D.D., **1998**. 98/00360 Zeolites synthesized from class F fly ash and sodium aluminate slurry. *Fuel and Energy Abstracts*, 39(1), p.29.

Guan, B., Lou, W., Ye, Q., Fu, H. & Wu, Z., **2009**. Calorimetric study of calcium aluminate cement blended with flue gas desulfurization gypsum. *Journal of Thermal Analysis and Calorimetry*, 98(3), pp.737–742.

Guirado, F. & Galí, S., **2006**. Quantitative Rietveld analysis of CAC clinker phases using synchrotron radiation. *Cement and Concrete Research*, 36(11), pp.2021–2032.

Guirado, F., Galí, S. & Chinchón, J.S., **1998**. Thermal Decomposition of Hydrated Alumina Cement (CAH10). *Cement and Concrete Research*, 28(3), pp.381–390.

Guirado, F., Galí, S., Chinchon, S. & Rius, J., **1998**. Crystal Structure Solution of Hydrated High-Alumina Cement from X-ray Powder Diffraction Data. *Angewandte Chemie International Edition*, 37(1/2), pp.72–75.

Gullion, T. & Vega, A.J., **2005**. Measuring heteronuclear dipolar couplings for I=1/2, S>1/2 spin pairs by REDOR and REAPDOR NMR. *Progress in Nuclear Magnetic Resonance Spectroscopy*, 47(3-4), pp.123–136.

El Hafiane, Y., Smith, a., Abouliatim, Y., Chartier, T., Nibou, L. & Bonnet, J.P., **2014**. Calcium aluminate cement tapes - Part I: Structural and microstructural characterizations. *Journal of the European Ceramic Society*, 34(4), pp.1017–1023.

He, Z., Honeycutt, C.W., Xing, B., McDowel, R.W., Pellechia, P.J. & Zhang, T., **2007**. Solid-state Fourier transform infrared and ^{31}P nuclear magnetic resonance spectral features of phosphate compounds. *Soil Science*, 172(7), pp.501–15.

Hewlett, P.C. ed., **2004**. *Lea's Chemistry of Cement and Concrete* 4th ed., Oxford: Elsevier Science & Technology Books.

Hidalgo, A., García, J.L., Cruz Alonso, M., Fernández, L. & Andrade, C., **2009**. Microstructure development in mixes of calcium aluminate cement with silica fume or fly ash. *Journal of Thermal Analysis and Calorimetry*, 96(2), pp.335–345.

Holmgren, C.R. & Bearden, W.G., **1965**. High temperature well cement, Patent no 3,180,748. , pp.1–3.

Hsu, P., **1968**. Interaction Between Aluminum and Phosphate in Aqueous Solution. In *Trace Inorganics In Water*. Advances in Chemistry. American Chemical Society, pp. 115–127.

Hughes, E., Gullion, T., Goldbourt, A., Vega, S. & Vega, A.J., **2002**. Internuclear

distance determination of S=1, I=1/2 spin pairs using REAPDOR NMR. *Journal of Magnetic Resonance*, 156(2), pp.230–241.

de Jager, H.-J. & Prinsloo, L.C., **2001**. The dehydration of phosphates monitored by DSC/TGA and in situ Raman spectroscopy. *Thermochimica Acta*, 376(2), pp.187–196.

Juenger, M.C.G., Winnefeld, F., Provis, J.L. & Ideker, J.H., **2011**. Advances in alternative cementitious binders. *Cement and Concrete Research*, 41(12), pp.1232–1243.

Kalina, L., Másilko, J., Koplík, J. & Šoukal, F., **2014**. XPS characterization of polymer–monocalcium aluminate interface. *Cement and Concrete Research*, 66, pp.110–114.

Keeler, J., **2002**. *Understanding NMR spectroscopy*,

Kelly, S., **2012**. *Fabrication of polymer composites as potential bone replacement materials*. University of Glasgow.

Kerneos Inc, **2006**. *Secar 51 Product data sheet, reference PDS-US-S51-8/06*, Chesapeake.

Kim, Y. & Kirkpatrick, R.J., **2004**. An investigation of phosphate adsorbed on aluminium oxyhydroxide and oxide phases by nuclear magnetic resonance. *European Journal of Soil Science*, 55(2), pp.243–251.

Kinoshita, H., Swift, P.D., Utton, C.A., Carro-Mateo, B., Marchand, G., Collier, N.C. & Milestone, N.B., **2013**. Corrosion of aluminium metal in OPC- and CAC-based cement matrices. *Cement and Concrete Research*, 50, pp.11–18.

Kirca, Ö., **2006**. *Temperature effect on calcium aluminate cement based composite binders*. Middle East Technical University.

Klinowski, J., **1984**. Nuclear magnetic resonance studies of zeolites. *Progress in Nuclear Magnetic Resonance Spectroscopy*, 16, pp.237–309.

Kloprogge, J., Ruan, H. & Frost, R.L., **2002**. Thermal decomposition of bauxite minerals: infrared emission spectroscopy of gibbsite, boehmite and diaspore. *Journal of Materials Science*, 37(6), pp.1–21.

Knapen, E., Cizer, O., Van Balen, K. & Van Gemert, D., **2009**. Effect of free water removal from early-age hydrated cement pastes on thermal analysis. *Construction and Building Materials*, 23(11), pp.3431–3438.

Kolodziejski, W. & Klinowski, J., **2002**. Kinetics of cross-polarization in solid-state NMR: a guide for chemists. *Chemical reviews*, 102(3), pp.613–28.

Kovacs, F. & Fowler, D., **2007**. A practical guide for solid-state NMR distance measurements in proteins. *Magnetic Resonance Part A*, 30A(1), pp.21–39.

Kraft, L. & Hermansson, L., **2003**. Dimension Stable Binding Agent Systems for

Dental Application, US Patent No. US6620232 B1.

Lamour, V., Monteiro, P.J.M., Scrivener, K.L. & Fryda, H., **2001**. Mechanical properties of calcium aluminate cement in concretes. In R. J. Mangabhai & F. P. Glasser, eds. *Calcium Aluminate Cements 2001: Proceedings of the International Conference on Calcium Aluminate Cements (CAC)*. London: IOM Communications, pp. 199–213.

Lang, D.P., Alam, T.M. & Bencoe, D.N., **2001**. Solid-state 31P/27Al and 31P/23Na TRAPDOR NMR investigations of the phosphorus environments in sodium aluminophosphate glasses. *Chemistry of Materials*, 13(2), pp.420–428.

Laws, D., Bitter, H. & Jerschow, A., **2002**. Solid-State NMR Spectroscopic Methods in Chemistry. *Angewandte Chemie International Edition*, 41, pp.3096–3129.

Legrand, A.P., Sfihi, H., Lequeux, N. & Lemaître, J., **2009**. ^{31}P Solid-State NMR study of the chemical setting process of a dual-paste injectable brushite cements. *Journal of Biomedical Materials Research. Part B: Applied Biomaterials*, 91(1), pp.46–54.

Lemaître, J., Mirtchi, A.A. & Mortier, A., **1987**. Calcium phosphate cements for medical use: state of the art and perspectives of development. *Silicates Industriels*, (9-10).

Li, W., Feng, J., Kwon, K.D., Kubicki, J.D. & Phillips, B.L., **2010**. Surface speciation of phosphate on boehmite (gamma-AlOOH) determined from NMR spectroscopy. *Langmuir*, 26(7), pp.4753–61.

Li, W., Feng, X., Yan, Y., Sparks, D.L. & Phillips, B.L., **2013**. Solid-state NMR spectroscopic study of phosphate sorption mechanisms on aluminum (hydr)oxides. *Environmental Science & Technology*, 47(15), pp.8308–15.

Li, W., Pierre-Louis, A.-M., Kwon, K.D., Kubicki, J.D., Strongin, D.R. & Phillips, B.L., **2013**. Molecular level investigations of phosphate sorption on corundum (α-Al2O3) by 31P solid state NMR, ATR-FTIR and quantum chemical calculation. *Geochimica et Cosmochimica Acta*, 107, pp.252–266.

Lookman, R., Grobet, P., Merckx, R. & Van Riemsdijk, W.H., **1997**. Application of 31P and 27Al MAS NMR for phosphate speciation studies in soil and aluminium hydroxides: promises and constraints. *Geoderma*, 80, pp.369–388.

Luz, a. P. & Pandolfelli, V.C., **2011**. Halting the calcium aluminate cement hydration process. *Ceramics International*, 37(8), pp.3789–3793.

Ma, W. & Brown, P.W., **1994**. Hydration of sodium phosphate-modified high alumina cement. *Journal of Materials Research*, 9(5), pp.1291–1297.

Ma, W. & Brown, P.W., **1992**. Mechanical behavior and microstructural development in phosphate modified high alumina cement. *Cement and Concrete Research*, 22(6), pp.1192–1200.

Macias, A., Kindness, A. & Glasser, F.P., **1996**. Corrosion behaviour of steel in high

alumina cement mortar cured at 5, 25 and 55° C: chemical and physical factors. *Journal of Materials Science*, 31, pp.2279–2289.

MacKenzie, K.J.D. & Smith, M.E., **2002**. *Multinuclear Solid State NMR of Inorganic Materials, 2002*, Oxford: Pergamon.

Maier, A.K., Dezmirean, L., Will, J. & Greil, P., **2011**. Three-dimensional printing of flash-setting calcium aluminate cement. *Journal of Materials Science*, 46(9), pp.2947–2954.

Majumdar, A.J., Edmonds, R.N. & Singh, B., **1990**. Hydration of secar 71 aluminous cement in presence of granulated blast furnace slag. *Cement and Concrete Research*, 20, pp.7–14.

Majumdar, A.J. & Singh, B., **1992**. Properties of some blended high-alumina cements. *Cement and Concrete Research*, 22(6), pp.1101–1114.

Matsuo, T., Nishi, T., Matsuda, M. & Izumida, T., **1995**. $LiNO_3$ addition to prevent hydrogen gas generation from cement-solidified aluminium wastes. *Journal of Nuclear Science and Technology*, 32(9), pp.912–920.

Matusinović, T. & Vrbos, N., **1993**. Alkali metal salts as set accelerators for high alumina cement. *Cement and Concrete research*, 23, pp.177–186.

McHardy, W.J., **1971**. Conditions for the formation of bayerite and gibbsite. *Mineralogical Magazine*, 38(295), pp.358–368.

Michelmore, A., Gong, W., Jenkins, P. & Ralston, J., **2000**. The interaction of linear polyphosphates with titanium dioxide surfaces. *Physical Chemistry Chemical Physics*, 2(13), pp.2985–2992.

Midgley, H.G. & Bhaskara Rao, P., **1978**. Formation of stratlingite, 2CaO.SiO2.Al2O3.8H2O, in relation to the hydration of high alumina cement. *Cement and Concrete Research*, 8(2), pp.169–172.

Migneault, D.R. & Force, R.K., **1988**. Dissociation constants of phosphoric acid at 25 C and the ion pairing of sodium with orthophosphate ligands at 25 C. *Journal of Solution Chemistry*, 17(10), pp.987–997.

Milestone, N.B., **2006**. Reactions in cement encapsulated nuclear wastes: need for toolbox of different cement types. *Advances in Applied Ceramics*, 44(6), pp.3–10.

Miquel, J.L., Facchini, L., Legrand, A.P., Rey, C. & Lemaître, J., **1990**. Solid state NMR to study calcium phosphate ceramics. *Colloids and Surfaces*, 45, pp.427–433.

Morejón-Alonso, L., **2009**. Influence of mixing liquid on the properties of calcium aluminate cement. *Key Engineering Materials*, 396-398, pp.241–244.

Mostafa, N.Y., Zaki, Z.I. & Abd Elkader, O.H., **2012**. Chemical activation of calcium aluminate cement composites cured at elevated temperature. *Cement and Concrete Composites*, 34(10), pp.1187–1193.

Müller, D., Gessner, W., Behrens, H.-J. & Scheler, G., **1981**. Determination of the aluminium coordination in aluminium-oxygen compounds by solid-state high-resolution ^{27}AI NMR. *Chemical Physics Letters*, 79(1), pp.59–62.

Müller, D., Rettel, A., Gessner, W. & Scheler, G., **1984**. An application of solid-state magic-angle spinning ^{27}Al NMR to the study of cement hydration. *Journal of Magnetic Resonance*, 57, pp.152–156.

Narayanan, N. & Ramamurthy, K., **2000**. Structure and properties of aerated concrete: A review. *Cement and Concrete Composites*, 22(5), pp.321–329.

Navarro-Blasco, I., Duran, a., Sirera, R., Fernández, J.M. & Alvarez, J.I., **2013**. Solidification/stabilization of toxic metals in calcium aluminate cement matrices. *Journal of Hazardous Materials*, 260, pp.89–103.

Navarro-Blasco, I., Duran, A., Pérez-Nicolás, M., Fernández, J.M., Sirera, R. & Alvarez, J.I., **2015**. A safer disposal of hazardous phosphate coating sludge by formation of an amorphous calcium phosphate matrix. *Journal of Environmental Management*, 159, pp.288–300.

Neville, A.M., **2009a**. History of high-alumina cement. Part 1: Problems and the Stone report. *Proceedings of the ICE-Engineering History and Heritage*, 162(EH2), pp.81–91.

Neville, A.M., **2009b**. History of high-alumina cement. Part 2: Background to issues. *Proceedings of the ICE-Engineering History and Heritage*, 162(EH2), pp.93–101.

Neville, A.M. & Brooks, J.J., **1987**. *Concrete technology* 2nd ed., Harlow: Pearson Education.

Niziurska, M., Małolepszy, J. & Malata, G., **2015**. The influence of lithium carbonate on phase composition of calcium aluminate cement paste. *Procedia Engineering*, 108, pp.363–370.

Nobes, R.., Akhmatskaya, E.., Milman, V., Winkler, B. & Pickard, C.., **2000**. Structure and properties of aluminosilicate garnets and katoite: an ab initio study. *Computational Materials Science*, 17(2-4), pp.141–145.

Nuclear Decommissioning Authority, **2010**. *Geological disposal: radionuclide behaviour status report*,

Ojovan, M.I. & Lee, W.E., **2005**. *An Introduction to Nuclear Waste Immobilisation*, Oxford: Elsevier.

Oliveira, I.R., Pandolfelli, V.C. & Jacobovitz, M., **2010**. Chemical, physical and mechanical properties of a novel calcium aluminate endodontic cement. *International Endodontic Journal*, 43, pp.1069–76.

Pacewska, B. & Nowacka, M., **2014**. Studies of conversion progress of calcium aluminate cement hydrates by thermal analysis method. *Journal of Thermal Analysis and Calorimetry*, (117), pp.653–660.

Pan, Y., Gullion, T. & Schaefer, J., **1990**. Determination of C-N internuclear distances by rotational-echo double-resonance NMR of solids. *Journal of Magnetic Resonance (1969)*, 90(2), pp.330–340.

Parr, C., **2008**. *Calcium aluminate cement - what happens when things go wrong?, reference TP-GB-RE-LAF-071*,

Pérez, M., Vázquez, T. & Triviño, F., **1984**. Study of stabilized phases in high alumina cement mortars part II effect of $CaCO_3$ added to high alumina cement mortar subjected to elevated temperature curing and carbonation. *Cement and Concrete Research*, 14(1), pp.1–10.

Perry, D., **2011**. *Handbook of inorganic compounds*, Boca Raton: CRC Press.

Popoola, O., **1991**. Microstructural and microchemical characterization of a calcium aluminate—polymer composite (MDF cement). *Journal of the American Ceramics Society*, 74(8), pp.1928–1933.

Poulsen, S.L., Jakobsen, H.J. & Skibsted, J., **2010**. Incorporation of phosphorus guest ions in the calcium silicate phases of Portland cement from ^{31}P MAS NMR spectroscopy. *Inorganic Chemistry*, 49(12), pp.5522–9.

Pourpoint, F., Gervais, C., Bonhomme, C., Azaïs, T., Coelho, C., Mauri, F., Alonso, B., et al., **2007**. Calcium Phosphates and Hydroxyapatite: Solid-State NMR Experiments and First-Principles Calculations. *Applied Magnetic Resonance*, 32(4), pp.435–457.

Prodjosantoso, A.K. & Kennedy, B.J., **2006**. Solubility of $SrAl_2O_4$ in $CaAl_2O_4$-a high resolution powder diffraction study. *Materials Research Bulletin*, 38(2003).

Ramachandran, V.S., Paroli, R.M., Beaudoin, J.J. & Delgado, A.H., **2002**. *Handbook of thermal analysis of construction materials*, New York: Noyes Publications.

Rashid, S., Barnes, P., Bensted, J. & Turrillas, X., **1994**. Conversion of calcium aluminate cement hydrates re-examined with synchrotron energy-dispersive diffraction. *Journal of Materials Science Letters*, 13(17), pp.1232–1234.

Rashid, S. & Turrillas, X., **1997**. Hydration kinetics of $CaAl_2O_4$ using synchrotron energy-dispersive diffraction. *Thermochimica Acta*, 302, pp.25–34.

Rettel, A., Damidot, D., Müller, D. & Gessner, W., **1997**. A NMR study of gels formed during the hydration of calcium aluminate cement in the presence of citrate or gluconate. In *10th International Congress on the Chemistry of Cement. Vol. 3*. pp. 3–7.

Rivas Mercury, J.M., Pena, P., de Aza, A.H., Sheptyakov, D. & Turrillas, X., **2006**. On the decomposition of synthetic gibbsite studied by neutron thermodiffractometry. *Journal of the American Ceramic Society*, 89(12), pp.3728–3733.

Rodger, S. a. & Double, D.D., **1984**. The chemistry of hydration of high alumina cement in the presence of accelerating and retarding admixtures. *Cement and*

Concrete Research, 14(1), pp.73–82.

Roemhildt, M.L., Wagner, S.D. & McGee, T.D., **2006**. Characterization of a novel calcium phosphate composite bone cement: Flow, setting, and aging properties. In *Journal of Materials Science: Materials in Medicine*. pp. 1127–1132.

Šauman, Z., **1971**. Carbonization of porous concrete and its main binding components. *Cement and Concrete Research*, 1(6), pp.645–662.

Schrader, B. ed., **1995**. *Infrared and Raman Spectroscopy*, Weinheim: Wiley-VCH Verlag GmbH.

Scrivener, K.L., **2003**. Calcium Aluminate Cements. In *Advanced Concrete Technology*. Oxford: Elsevier.

Scrivener, K.L., Cabiron, J.-L. & Letourneux, R., **1999**. High-performance concretes from calcium aluminate cements. *Cement and Concrete Research*, 29(8), pp.1215–1223.

Setiadi, A., **2006**. *Corrosion of Metals in Composite Cements*. University of Sheffield.

Setiadi, A., Hill, J. & Milestone, N.B., **2003**. Corrosion of Metals in Composite Cements. In *Cement and Concrete Science*. Leeds.

Setiadi, A., Milestone, N.B. & Hayes, M., **2004**. Corrosion of aluminium in composite cements. In *Cement and Concrete Science*. Warwick.

Setiadi, A., Milestone, N.B., Hill, J. & Hayes, M., **2006**. Corrosion of aluminium and magnesium in BFS composite cements. *Advances in Applied Ceramics*, 105(4), pp.191–196.

Siesler, H., Ozaki, Y., Kawata, S. & Heise, H. eds., **2008**. *Near-infrared spectroscopy: principles, instruments, applications*, Weinheim: Wiley-VCH Verlag GmbH.

Skibsted, J., Henderson, E. & Jakobsen, H.J., **1993**. Characterization of calcium aluminate phases in cements by ^{27}Al MAS NMR spectroscopy. *Inorganic Chemistry*, 32(6), pp.1013–1027.

Smith, a., El Hafiane, Y., Bonnet, J.P., Quintard, P. & Tanouti, B., **2005**. Role of a Small Addition of Acetic Acid on the Setting Behavior and on the Microstructure of a Calcium Aluminate Cement. *Journal of the American Ceramic Society*, 88(8), pp.2079–2084.

Smith, M.E. & van Eck, E.R.H., **1999**. Recent advances in experimental solid state NMR methodology for half-integer spin quadrupolar nuclei. *Progress in Nuclear Magnetic Resonance Spectroscopy*, 34, pp.159–201.

Sokolar, R. & Vodova, L., **2014**. Hexametaphosphate as deflocculation agent for calcium aluminate cements in porcelain body. *Advanced Materials Research*, 897, pp.30–33.

Solé, J., Bausa, L. & Jaque, D., **2005**. *An introduction to the optical spectroscopy of inorganic solids*, Chichester: John Wiley & Sons.

Soro, J., Smith, A. & Gault, C., **2006**. Thermomechanical characteristics of calcium aluminate cement and sand tapes prepared by tape casting. *Journal of the European Ceramic Society*, 26(16), pp.3799–3807.

Šoukal, F., Ptáček, P., Másilko, J., Opravil, T., Havlica, J. & Drdlová, M., **2013**. High temperature properties of MDF composite based on calcium aluminate cement and polyvinyl alcohol. *Journal of Thermal Analysis and Calorimetry*, 115(2), pp.1245–1252.

Stamboulis, A., Matsuya, S., Hill, R.G., Law, R. V, Udoh, K., Nakagawa, M. & Matsuya, Y., **2006**. MAS-NMR spectroscopy studies in the setting reaction of glass ionomer cements. *Journal of Dentistry*, 34(8), pp.574–81.

Sugama, T., **2006a**. Advanced cements for geothermal wells,. In *Brookhaven National Laboratory Report BNL-77901-2007-IR*. New York.

Sugama, T., **2006b**. Citric acid as a set retarder for calcium aluminate phosphate cements. *Advances in Cement Research*, (2), pp.47–57.

Sugama, T., Allan, M. & Hill, J.M., **1992**. Calcium phosphate cements prepared by acid–base reaction. *Journal of the American Ceramic Society*, 75(8), pp.2076–2087.

Sugama, T., Brothers, L.E. & de Putte, T.R. Van, **2005**. Air-foamed calcium aluminate phosphate cement for geothermal wells. *Cement and Concrete Composites*, 27(7-8), pp.758–768.

Sugama, T., Brothers, L.E. & Weber, L., **2002**. Calcium aluminate cements in fly ash/calcium aluminate blend phosphate cement systems: Their role in inhibiting carbonation and acid corrosion at a low hydrothermal temperature of 90◦C. *Journal of Materials Science*, 7, pp.3163–3173.

Sugama, T. & Carciello, N.R., **1993**. Carbonation of calcium phosphate cements after long-term exposure to Na_2CO_3-laden water at 250° C. *Cement and Concrete Research*, 23, pp.1409–1417.

Sugama, T. & Carciello, N.R., **1992**. Carbonation of hydrothermally treated phosphate-bonded calcium aluminate cements. *Cement and Concrete Research*, 22, pp.783–792.

Sugama, T. & Carciello, N.R., **1995**. Sodium phosphate-derived calcium phosphate cements. *Cement and Concrete Research*, 25(1), pp.91–101.

Sugama, T. & Carciello, N.R., **1991**. Strength development in phosphate-bonded calcium aluminate cements. *Journal of the American Ceramic Society*, 74(5), pp.1023–30.

Sugama, T., Carciello, N.R. & Gray, G., **1992**. Alkali carbonation of calcium aluminate cements: influence of set-retarding admixtures under hydrothermal

conditions. *Journal of Materials Science*, 27, pp.4909–4916.

Sugama, T. & Kukacka, L.E., **1983**. Magnesium monophosphate cements derived from diammonium phosphate solutions. *Cement and Concrete Research*, 13(3), pp.407–416.

Sugama, T. & Taylor, M., **1994**. Interfacial and mechanical behavior of fiber-reinforced calcium phosphate cement composites. *Cement and Concrete Composites*, 16(2), pp.93–106.

Sugama, T., Weber, L. & Brothers, L.E., **1999**. Resistance of sodium polyphosphate-modified fly ash/calcium aluminate blend cements to hot H_2SO_4 solution. *Cement and Concrete Research*, 29, pp.1969–1976.

Sugama, T., Weber, L. & Brothers, L.E., **2000**. Sodium-polyphosphate-modified fly ash/calcium aluminate blend cement: durability in wet, harsh geothermal environments. *Materials Letters*, (44), pp.45–53.

Sugama, T. & Wetzel, E., **1994**. Microsphere-filled lightweight calcium phosphate cements. *Journal of Materials Science*, 29(19), pp.5165–5176.

Swift, P., **2013**. *The development of calcium aluminate phosphate cement for radioactive waste encapsulation*. University of Sheffield.

Swift, P.D., Kinoshita, H., Collier, N.C. & Utton, C.A., **2013**. Phosphate modified calcium aluminate cement for radioactive waste encapsulation. *Advances in Applied Ceramics*, 112(1), pp.1–8.

Tannús, A. & Garwood, M., **1997**. Adiabatic pulses. *NMR in Biomedicine*, 10(8), pp.423–34.

Tarte, P., **1967**. Infra-red spectra of inorganic aluminates and characteristic vibrational frequencies of AlO_4 tetrahedra and AlO_6 octahedra. *Spectrochimica Acta Part A: Molecular Spectroscopy*, 23(1963), pp.2127–2143.

Taylor, H.F.W., **1990**. *Cement Chemistry*, London: Academic Press.

Theophanides, T. ed., **2012**. *Infrared spectroscopy – materials science, engineering and technology*, Rijeka: InTech.

Torréns-Martín, D., Fernández-Carrasco, L. & Martínez-Ramírez, S., **2013**. Hydration of calcium aluminates and calcium sulfoaluminate studied by Raman spectroscopy. *Cement and Concrete Research*, 47, pp.43–50.

Toyohara, M., Kaneko, M., Mitsutsuka, N., Fujihara, H., Saito, N. & Murase, T., **2002**. Contribution to Understanding Iodine Sorption Mechanism onto Mixed Solid Alumina Cement and Calcium Compounds. *Journal of Nuclear Science and Technology*, 39(9), pp.950–956.

Tran, T.T., **2011**. *Fluoride Mineralization of Portland cement*.

Travitzky, N., Bonet, A., Dermeik, B., Fey, T., Filbert-Demut, I., Schlier, L., Schlordt,

T., et al., **2014**. Additive manufacturing of ceramic-based materials. *Advanced Engineering Materials*, 16(6), pp.729–754.

Turner, G.L., Kirkpatrick, R.J., Risbud, S.H. & Oldfield, E., **1987**. Multinuclear magic-angle sample-spinning nuclear magnetic resonance spectroscopic studies of crystalline and amorphous ceramic materials. *American Ceramics Society Bulletin*, 66(4), pp.656–63.

U.S. Environmental Protection Agency, **2000**. *Sodium phosphate listing background document for the inorganic chemical listing determination*,

Ukrainczyk, N., Matusinović, T., Kurajica, S., Zimmermann, B. & Sipusic, J., **2007**. Dehydration of a layered double hydroxide—C2AH8. *Thermochimica Acta*, 464(1-2), pp.7–15.

Ukrainczyk, N. & Šipušić, J., **2008**. Microcalorimetric study on calcium aluminate cement. In *MATRIB 2008 International Conference on Materials, Tribology, Recycling*. Zagreb, pp. 382–388.

Ukrainczyk, N., Vrbos, N. & Šipušić, J., **2012**. Influence of metal chloride salts on calcium aluminate cement hydration. *Advances in Cement Research*, 24(5), pp.249–262.

Vargel, C., **2004**. *The corrosion of aluminium*, Oxford: Elsevier.

Wagh, A., **2004**. *Chemically bonded phosphate ceramics*, Oxford: Elsevier.

Walter, D. & Odler, I., **1996**. Investigation of MgO and CaO/Al_2O_3 polyphosphate cements. *Advances in Cement Research*, 8(29), pp.41–46.

Wang, L. & Li, C., **2007**. Preparation and physicochemical properties of a novel hydroxyapatite/chitosan-silk fibroin composite. *Carbohydrate Polymers*, 68(4), pp.740–745.

Wilding, C.R., **1992**. The performance of cement based systems. *Cement and Concrete Research*, 22, pp.299–310.

Williams, R.J.P., Giles, R.G.F. & Posner, A.M., **1981**. Solid state phosphorus NMR spectroscopy of minerals and soils. *Journal of the Chemical Society, Chemical Communications*, (20), pp.1051–2.

Yang, Q., Zhu, B. & Wu, X., **2000**. Characteristics and durability test of magnesium phosphate cement-based material for rapid repair of concrete. *Materials and Structures*, 33(4), pp.229–234.

Zhang, J. & Scherer, G.W., **2011**. Comparison of methods for arresting hydration of cement. *Cement and Concrete Research*, 41(10), pp.1024–1036.

Zhang, L. & Eckert, H., **2006**. Short- and medium-range order in sodium aluminophosphate glasses: new insights from high-resolution dipolar solid-state NMR spectroscopy. *The Journal of Physical Chemistry B*, 110(18), pp.8946–58.

Zhang, T., Vandeperre, L.J. & Cheeseman, C.R., **2012**. Magnesium-silicate-hydrate cements for encapsulating problematic aluminium containing wastes. *Journal of Sustainable Cement-Based Materials*, 1(1-2), pp.34–45.

Zhang, X., Yang, Y. & Ong, C.K., **1997**. Study of early hydration of OPC-HAC blends by microwave and calorimetry technique. *Cement and Concrete Research*, 27(9), pp.1419–1428.

Zhou, Q., Milestone, N.B. & Hayes, M., **2006**. An alternative to portland cement for waste encapsulation--the calcium sulfoaluminate cement system. *Journal of Hazardous Materials*, 136, pp.120–129.

APPENDIX (A)

Table A-1 Laser diffraction data obtained for studied samples, shown in Chapter 4.

Mass fraction	Largest particle diameter in given mass fraction, microns			
	CAC	Aluminium powder	Sodium polyphosphate	Sodium monophosphate
d_{10}	2	11	350	342
d_{50}	13	31	127	999
d_{90}	54	68	24	2050

Table A-2 Oxide composition of BFS and PC materials used for comparative formulations in aluminium encapsulation trials, Chapter 7.

Components as oxides	BFS	PC
CaO	38.8	65.4
SiO_2	35.5	20.0
Al_2O_3	13.4	4.6
Fe_2O_3	0.9	3.1
MgO	7.6	2.1
K_2O	0.4	0.7
Na_2O	0.3	0.3
SO_3	0.7	3.2
Loss on ignition	0.9	1.7
Others	1.5	0.6

Table A-3 Elemental composition for BNFL supplied 1350 Aluminium materials used for plate encapsulation experiments in Chapter 7.

Element	Amount (%)
Al	> 99.50
Si	< 0.10
Fe	< 0.40
Cu	< 0.05
Mn	0.01
Zn	0.05
Ga	< 0.03
B	< 0.05
V & Ti	< 0.02
Others	< 0.10

Table A-4 Precursor contents for formulations and wt% loadings of phosphates for corresponding phosphate solutions prior to mixing with cement clinker

Formulation	Total Slurry amount, (g)	w/solid	p/cement	m/cement	Secar 51 (g)	Polyphosphate (g)	Monophosphate (g)	Water (g)	% monophosphate in solution	% polyphosphate in solution
Neat CAC	1000	0.35	0	0	740.74	0.00	0.000	259.26	0.00	0.00
0.4p0m	1000	0.35	0.4	0	571.43	228.57	0.000	200.00	0.00	53.33
0.4p0.05m	1000	0.35	0.4	0.05	555.56	222.22	27.778	194.44	6.25	50.00
0p0.1m	1000	0.35	0	0.1	689.66	0.00	68.966	241.38	22.22	0.00
0p0m	1000	0.35	0	0	740.74	0.00	0.000	259.26	0.00	0.00
0p0.1m	1000	0.35	0	0.1	689.66	0.00	68.966	241.38	22.22	0.00
0p0.05m	1000	0.35	0	0.05	714.29	0.00	35.714	250.00	12.50	0.00
0p0.025m	1000	0.35	0	0.025	727.27	0.00	18.182	254.55	6.67	0.00
0.2p0m	1000	0.35	0.2	0	645.16	129.03	0.000	225.81	0.00	36.36
0.4p0m	1000	0.35	0.4	0	571.43	228.57	0.000	200.00	0.00	53.33
0.2p0m	1000	0.35	0.2	0	645.16	129.03	0.000	225.81	0.00	36.36
0.2p0.01m	1000	0.35	0.2	0.01	641.03	128.21	6.410	224.36	1.79	35.71
0.2p0.025m	1000	0.35	0.2	0.025	634.92	126.98	15.873	222.22	4.35	34.78
0.2p0.05m	1000	0.35	0.2	0.05	625.00	125.00	31.250	218.75	8.33	33.33
0.2p0.075m	1000	0.35	0.2	0.075	615.38	123.08	46.154	215.38	12.00	32.00
0.2p0.1m	1000	0.35	0.2	0.1	606.06	121.21	60.606	212.12	15.38	30.77
0.2p0.125m	1000	0.35	0.2	0.125	597.01	119.40	74.627	208.96	18.52	29.63
0.2p0.15m	1000	0.35	0.2	0.15	588.24	117.65	88.235	205.88	21.43	28.57
0.4p0m	1000	0.35	0.4	0	571.43	228.57	0.000	200.00	0.00	53.33
0.4p0.01m	1000	0.35	0.4	0.01	568.18	227.27	5.682	198.86	1.32	52.63
0.4p0.025m	1000	0.35	0.4	0.025	563.38	225.35	14.085	197.18	3.23	51.61
0.4p0.05m	1000	0.35	0.4	0.05	555.56	222.22	27.778	194.44	6.25	50.00
0.4p0.075m	1000	0.35	0.4	0.075	547.95	219.18	41.096	191.78	9.09	48.48
0.4p0.1m	1000	0.35	0.4	0.1	540.54	216.22	54.054	189.19	11.76	47.06
0.4p0.125m	1000	0.35	0.4	0.125	533.33	213.33	66.667	186.67	14.29	45.71
0.4p0.15m	1000	0.35	0.4	0.15	526.32	210.53	78.947	184.21	16.67	44.44
0.4p0.175m	1000	0.35	0.4	0.175	519.48	207.79	90.909	181.82	18.92	43.24
0.4p0.2m	1000	0.35	0.4	0.2	512.82	205.13	102.564	179.49	21.05	42.11
0.4p0.25m	1000	0.35	0.4	0.25	500.00	200.00	125.000	175.00	25.00	40.00
0.4p0.5m	1000	0.35	0.4	0.5	444.44	177.78	222.222	155.56	40.00	32.00